New developments of a scaling analysis methodology for nuclear reactors complex thermal-hydraulic transients with calculation of the distortion associated with the full-scale transposition

Antoine Ciechocki

université PARIS-SACLAY

New developments of a scaling analysis methodology for nuclear reactors complex thermal-hydraulic transients with calculation of the distortion associated with the full-scale transposition.

Nouveaux développements d'une méthodologie d'analyse d'échelle pour des transitoires complexes de thermohydraulique de réacteurs nucléaires avec calcul de la distorsion associée à la transposition d'échelle.

Thèse de doctorat de l'université Paris-Saclay

École doctorale n° 579 : Sciences Mécaniques et Energétiques, Matériaux et Géosciences (SMEMaG)
Spécialité de doctorat : Mécanique des fluides
Graduate School : Sciences de l'Ingénierie et des Systèmes (SIS),
Référent : CentraleSupélec

Thèse préparée dans l'unité de recherche **Service de Thermo-hydraulique et de Mécanique des Fluides (STMF)** (Université Paris-Saclay, CEA), sous la direction de **Lionel ROSSI**, directeur de recherche au CEA, de la co-encadrante **Sofia CARNEVALI**, ingénieure-chercheuse au CEA, du co-encadrant **Dominique BESTION**, consultant scientifique au CEA

Thèse soutenue à Paris-Saclay, le 31 mars 2023, par

Antoine CIECHOCKI

Composition du jury

Membres du jury avec voix délibérative

Uwe HAMPEL Professeur, Université de Dresde	Président
Alexandre LABERGUE Maître de conférences, Université de Lorraine	Rapporteur & Examinateur
Francesco SAVERIO D'AURIA Professeur, Université de Pise	Rapporteur & Examinateur
Jean-Luc VACHER Ingénieur Senior, EDF	Examinateur
Rafael MACIÁN-JUAN Professeur, Université technique de Munich	Examinateur

THESE DE DOCTORAT
NNT : 2023UPAST037

À mes parents et mon frère.

To my parents and my brother.

Acknowledgements

C'est au terme de trois enthousiasmantes années de thèse que s'écrivent ces lignes, achevant un travail mené avec engouement. Trois intenses années semées d'écueils mais qui furent toujours franchis, non sans l'aide et l'encouragement des personnes qui m'ont entourées. Je tiens donc à exprimer ici mes remerciements à l'égard de ceux qui ont contribué à l'aboutissement de ma thèse.

Je remercie sincèrement mes rapporteurs, Alexandre Labergue et Francesco Saverio D'Auria, pour leur précieuse expertise et leur temps accordé pour évaluer mon travail de recherche. Je remercie également le président de mon jury Uwe Hampel, pour son attention, ses commentaires et sa bienveillance, ainsi que mes examinateurs Rafael Macián-Juan et Jean-Luc Vacher, pour nos échanges constructifs. Votre présence lors de ma soutenance fût un honneur pour moi, et je vous suis profondément reconnaissant.

J'adresse toute ma gratitude à mon directeur de thèse, Lionel Rossi. Merci pour tous nos échanges de qualité et pour ton encadrement tout au long de cette thèse. Ton soutien, ton encouragement indéfectible ainsi que tes précieux conseils m'ont permis de mener à bien ce travail.

Je remercie chaleureusement mon encadrante de thèse, Sofia Carnevali, sans qui cette thèse n'aurait pu voir le jour. En tant que ton premier doctorant, j'ai été témoin de ton engagement envers la recherche et de ta passion pour enseigner et transmettre ton savoir. Tu as été constamment disponible, toujours prête à répondre à mes questions, à m'écouter et à me conseiller. Ta bienveillance et ta patience ont été une source de réconfort pour moi, en particulier lors des moments difficiles. Mais plus que tout, tu es devenue une amie très chère, toujours de bonne humeur, toujours prête à partager tes expériences et ton optimisme. Ta confiance en moi et tes encouragements ont été des facteurs clés dans la réussite de ma thèse. Je suis honoré d'avoir eu la chance de travailler avec toi et je te serai toujours reconnaissant pour ton soutien et ta gentillesse. Grazie di cuore.

Je remercie sincèrement Dominique Bestion, pour son co-encadrement. Merci énormément pour tous les enseignements scientifiques que vous avez pu m'apporter. Votre expertise, votre patience ainsi que votre disponibilité ont été inestimables pour moi, et j'ai appris énormément de vous. Vous avez su me guider avec bienveillance tout en me laissant l'autonomie nécessaire pour développer mes idées. Vos conseils et vos remarques m'ont permis d'aller au-delà de mes limites et de réaliser des progrès significatifs dans mes recherches.

Je tiens à remercier tous mes collègues et amis qui ont été à mes côtés tout au long de ce parcours. Merci pour tous nos enrichissants échanges du quotidien et pour l'aide que vous m'avez apporté, mais également pour tous les moments de convivialité au sein du laboratoire. Vous avez été une source de soutien et d'encouragement tout au long de ma thèse. Votre présence et votre amitié ont été essentiels pour maintenir ma motivation et me donner la force de persévérer. Je suis honoré d'avoir travaillé avec vous, et je sais que nos liens perdureront. Aussi, je remercie en particulier Kim-Claire Le Thanh et son successeur Anouar Mekkas pour m'avoir accueilli dans leur laboratoire.

Merci à ma famille pour le soutien inconditionnel que vous m'avez apporté durant ces trois années, et plus généralement au cours de l'ensemble de mes études. Vous m'avez toujours encouragé à poursuivre mes rêves et à persévérer dans mes ambitions. Je suis conscient que je n'aurais pas pu arriver jusqu'ici sans votre amour et votre soutien. Je vous en suis extrêmement reconnaissant et des mots ne suffiraient à exprimer ma gratitude. Merci Maman, merci Papa, merci Romain.

Merci enfin Tigrette pour ton réconfort pendant ces longues semaines de confinement.

Contents

List of Figures

List of Tables

Nomenclature

Acronyms

Symbol	Description
AIS	Accumulator Injection System
AoC	Agent of Change
ATLAS	Advanced Thermalhydraulic Test Loop for Accident Simulation
BETHSY	Boucle d'Etude ThermoHydraulique SYstème
BWR	Boiling Water Reactor
CATHARE	Code Avancé de ThermoHydraulique pour les Accidents de Réacteurs à Eau
CEA	Commissariat à l'Energie Atomique et aux énergies alternatives
CL	Cold Leg
CSAU	Code Scaling and Applicability and Uncertainty
CSNI	Committee on the Safety of Nuclear Installations
DBA	Design Basis Accidents
DSS	Dynamical System Scaling
ECCS	Emergency Core Cooling System
EDF	Electricité De France
EXP	EXPerimental results
FHFP	Full-Height, Full-Pressure
FoM	Figure of Merit
FRC	Fractional Rate of Change
FSA	Fractional Scaling Analysis
H2TS	Hierarchical Two-Tiered Scaling
HL	Hot Leg
HPIS	High Pressure Injection System
HQMD	High-Quality Mixture Discharge
IB-LOCA	Intermediate-Break Loss Of Coolant Accident
IET	Integral Effect Test
IL	Intermediate Leg
IRSN	Institut de Radioprotection et de Sûreté Nucléaire
ITF	Integral Test Facility
JAERI	Japan Atomic Energy Research Institute
KAERI	Korea Atomic Energy Research Institute
LB-LOCA	Large-Break Loss Of Coolant Accident
LOCA	Loss Of Coolant Accident
LPIS	Low Pressure Injection System
LSC	Loop Seal Clearing

Symbol	Description
LSP	Loop Seal Plugging
LSTF	Large Scale Test Facility
NC	Natural Circulation
NEA	Nuclear Energy Agency
NPP	Nuclear Power Plant
OECD	Organization for Economic Cooperation and Development
PCT	Peak Clad Temperature
PIRT	Process Identification and Ranking Table
PoI	Parameter of Interest
PRZ	Pressurizer
PWR	Pressurized Water Reactor
RCM	Reflux Condenser Mode
RHRP	Reduced-Height, Reduced-Pressure
ROSA	Rig Of Safety Assessment program
RPV	Reactor Pressure Vessel
RR	Reactor Refilling
SB-LOCA	Small-Break Loss Of Coolant Accident
SBD	Subcooled BlowDown
SCRAM	Safety Control Rod Axe Man
SET	Separate Effect Test
SETF	Separate Effect Test Facility
SG	Steam Generator
SMEMaG	Sciences Mécaniques et Energétiques, Matériaux et Géosciences
STMF	Service de Thermo-hydraulique et de Mécanique des Fluides
TPD	Two-Phase Discharge
TRACE	TRAC/RELAP Advanced Computational Engine
UPV	Universidad Politecnica de Valencia
USNRC	United States Nuclear Regulatory Commission
V&V	Verification and Validation
VRC	Volume Rate of Change

Roman Symbols

Symbol	Description	Unit
A	Area, cross section	m^2
C_k	Friction coefficient (CATHARE closure term)	$-$
e	Specific internal energy	$\mathrm{J} \cdot \mathrm{kg}^{-1}$
g	Gravitational acceleration	$\mathrm{m} \cdot \mathrm{s}^{-2}$
$\vec{F}$	Force vector	N
G_{cr}	Critical flow rate (CATHARE closure term)	$\mathrm{kg} \cdot \mathrm{s}^{-1}$
h	Local specific enthalpy	$\mathrm{J} \cdot \mathrm{kg}^{-1}$
H	Volume averaged specific enthalpy	$\mathrm{J} \cdot \mathrm{kg}^{-1}$
$h'_{ks,p}$	Derivative of h_{ks} with respect to pressure	$\mathrm{m}^3 \cdot \mathrm{kg}^{-1}$
K	Global expansion coefficient	$\mathrm{m}^3 \cdot \mathrm{Pa}^{-1}$
M	Mass	kg
$\dot{M}$	Mass flow rate	$\mathrm{kg} \cdot \mathrm{s}^{-1}$
$\vec{n}$	Unit normal vector	$-$
p	Local pressure	Pa
P	Pressure in a control volume	Pa
$\dot{P}$	Rate of pressure change	$\mathrm{Pa} \cdot \mathrm{s}^{-1}$
q	Power source	W
Q	Volume Rate of Change	$\mathrm{m}^3 \cdot \mathrm{s}^{-1}$
R	Stratification rate	$-$
S	Mass source term	$\mathrm{kg} \cdot \mathrm{m}^{-1} \cdot \mathrm{s}^{-1}$
SE	Energy source term	$\mathrm{W} \cdot \mathrm{m}^{-1}$
SM	Momentum source term	$\mathrm{N} \cdot \mathrm{m}^{-1}$
t	Time	s
T	Temperature	$^\circ\mathrm{C}$
$\bar{\bar{T}}$	Stress tensor	$\mathrm{N} \cdot \mathrm{m}^{-2}$
u	Velocity	$\mathrm{m} \cdot \mathrm{s}^{-1}$
V	Control volume	m^3
Y	Thermophysical property	$-$
W	Power	W
Z	Altitude	m

Greek Symbols

Symbol	Description	Unit
α	Void fraction	$-$
β	Added/virtual mass coefficient (CATHARE closure term)	$-$
γ	Expansion coefficient	$-$
Γ	Mass transfer between phases	$\mathrm{kg} \cdot \mathrm{m}^{-3} \cdot \mathrm{s}^{-1}$
δ	Droplet diameter (CATHARE closure term)	m
ν	Specific volume	$\mathrm{m}^3 \cdot \mathrm{kg}^{-1}$
$\nu'_{k,p}$	Partial derivative of ν_k with respect to pressure	$\mathrm{m}^4 \cdot \mathrm{s}^2 \cdot \mathrm{kg}^{-2}$
$\nu'_{k,h}$	Partial derivative of ν_k with respect to enthalpy	$\mathrm{m} \cdot \mathrm{s}^2 \cdot \mathrm{kg}^{-1}$
$\nu'_{ks,p}$	Derivative of ν_{ks} with respect to pressure	$\mathrm{m}^4 \cdot \mathrm{s}^2 \cdot \mathrm{kg}^{-2}$
Π	Characteristic time ratio (H2TS method)	$-$
ρ	Density	$\mathrm{kg} \cdot \mathrm{m}^{-3}$
τ	Residence time	s
τ_i	Interfacial friction (CATHARE closure term)	$\mathrm{N} \cdot \mathrm{m}^{-3}$
ϕ	Agent of Change (FSA method)	$-$
χ_c	Heating perimeter	m
χ_f	Friction perimeter	m
ω	Fractional Rate of Change (FSA method)	s^{-1}
Ω	Effect metric (FSA method)	$-$

Subscripts

Symbol	Description
0	Initial/reference value
1	Related to the primary system
$acc.$	Related to the accumulator
$break$	Related to the break
$core$	Related to the core
$ext.$	External (source)
f	Related to fluid boundary
i	Related to the interface
in	Inlet
k	Related to the phase k
l	Related to the liquid phase
low	Related to the primary system lower volume
m	Related to liquid-vapour mixture
out	Outlet
ov	Related to other volumes than core and SG
ow	Related to other walls than core and SG
prz	Related to the pressurizer
s	Saturation conditions
SG	Related to steam generators
up	Related to the primary system upper volume
v	Related to the vapour phase
w	Related to walls

Superscripts

Symbol	Description
$'$	Partial derivative
$+$	Dimensionless variable (FSA)
$\bar{}$	Averaged value
$\cdot$	Variation over time

CHAPTER 1

General Introduction

Nuclear safety is defined by the International Atomic Energy Agency (IAEA) as "the achievement of proper operating conditions, prevention of accidents or mitigation of accident consequences, resulting in protection of workers, the public and the environment from undue radiation hazards". This set of technical, human, and organizational measures implemented at all stages of a nuclear power plant life is considered from the design of nuclear installations, integrated during their construction, and reinforced during their operation. They are based on the defence in depth concept which includes successive and independent lines of defence.

The study and prevention of nuclear accidents is an upstream element in the nuclear safety chain. Nuclear reactors can enter an accidental situation in a variety of ways, including instabilities in the nuclear reactions that may cause unexpected behaviour, failure of some systems or structural mechanical degradations that could lead to loss of coolant. This type of event could lead to a melting of the reactor core induced by a lack of fuel cooling. This type of event must be absolutely prevented. This requires the capability to understand the phenomena and mechanisms that would be involved and to predict the behaviour of a nuclear reactor in such accidental situations. Furthermore, it is essential to prevent such situations and limit their consequences by implementing safety systems.

Experimental facilities are required to simulate the thermal-hydraulic aspects of nuclear reactor accidents. However, due to the complexity and cost of implementing full-scale experimental reactors, the nuclear industry has built reduced-scale experimental facilities to simulate the accidents. They are called Integral Test Facilities (ITF) when they can simulate the whole reactor system. The results of these reduced-scale experiments are used to study the behaviour of the reactors in accidental transients and to provide valuable data for the validation of the numerical simulation tools. The numerical tools able to simulate the thermal-hydraulic behaviour of whole system during accidents are called "system codes". The thermal-hydraulic of reactor transients is also simulated using the system codes that were validated on ITF tests: this is the "scale transposition".

A nuclear reactor is a complex system and the accidental transients have a very complex phenomenology. Furthermore, it can be challenging to obtain experimental data sufficiently representative of theses phenomena given the uncertainties related to the scale transposition. These uncertainties are mainly related to the assumptions in the design of the reduced-scale facilities, which may result in discrepancies in transient behaviour with full-scale reactors. These uncertainties could also be induced by scale effects, which cannot achieve a perfect phenomenological similarity. These discrepancies are referred as "distortions" in the behaviour of the reduced-scale experimental facilities compared to the full-scale reactors.

For these reasons, the question of evaluating the transposition of reduced-scale experimental results to the reference full-scale reactors code predictions arises. Therefore, it is crucial to dispose of a tool for assessing both the representativeness (the similarity of transients behaviour) and for quantifying the potential distortions brought on by the reduced-scale facilities.

Methods for scaling analyses have been developed to identify and quantify these distortions. However, they remain theoretical and very general. A state of the art on scaling methods performed in the framework of the OECD-NEA-CSNI-WGAMA (Bestion et al. 2017) has concluded that guidelines

are needed for a sound application of scaling methods to concrete situations. Revisiting and improving the existing methods is required and the support of mature system codes may be envisaged.

The main objective of the present thesis is to clarify the potentialities and understand how these scaling methods can contribute, in relation to the existing means of study. For this purpose, the thesis aims to develop a scaling analysis methodology for the study of nuclear transients thermal-hydraulic behaviour. In order to make this methodology applicable to the nuclear industry, some guidelines must also be established. Figure 1.1 illustrates this purpose of developing a scaling analysis methodology through the use of these means of study, the establishment of these guidelines, and the reinterpretation and improvement of an existing scaling method.

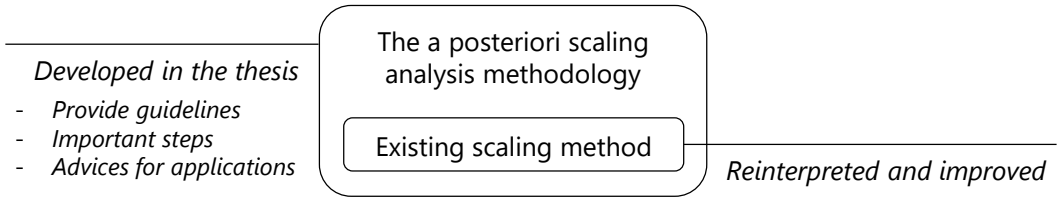

Figure 1.1: Development of the a posteriori scaling analysis methodology

The major issues raised by the state of the art on existing scaling methods, which the current thesis aims to address, are as follows:

- **How scaling analyses can help in the comprehension of transient phenomena?** And how pertinent are the top-down and bottom-up approaches in establishing a structured PIRT?
- **How scaling analyses can identify and quantify distortions?** The relevance of this question stems from the need to assess the impact of design choices for scaled-down experiments and transient results compared to what is predicted by codes for full-scale reactors.
- **Can advanced scaling methods be conducted with the support of system codes to identify multi-scale distortions?** This is an important issue, as scaling methods were not initially designed for this purpose.
- **What are the current limitations of scaling analyses and methods for nuclear transient analysis?**

To answer theses questions and issues, the thesis is divided into three parts. The first part presents the context of the thesis:

- Chapter 2 presents the field of study with a brief overview of the issues related to nuclear energy, a non-exhaustive description of pressurized water reactors and their general operation. Then the Loss Of Coolant Accidents (LOCA) are presented since they are extensively discussed throughout the thesis.
- Chapter 3 presents the state of the art of nuclear thermal-hydraulic and the context in which scaling takes place. The current state of knowledge regarding scaling-related issues, concerns, and techniques are presented through a literature review. The objectives of the thesis are then highlighted from these teachings.
- Chapter 4 presents the CATHARE system code used for the studies in this thesis. A brief history of the code is provided and the main modelling aspects and the equations are described.

The second part of the thesis consists of two chapters with the transient analyses in which the scaling methodology is applied:

- In chapter 5 a first study is conducted as an introduction to the development of the methodology, showing the applicability of a scaling method to a SB-LOCA transient. A scaling analysis is performed on an ITF test. The results are compared with published works and first conclusions are drawn.
- In chapter 6, a scaling analysis of a SB-LOCA transient involving counterpart tests performed in two ITF and a full-scale reactor simulation is performed at system and component scales. It aims to investigate the capability of a scaling method to identify and quantify scale distortions of a SB-LOCA transient by comparing experimental results with reactor calculations and with ITF tests calculations. Conclusions are drawn based on the scaling analysis on the the differences in reactor behaviour with the ITF results. Some methodology improvements are discussed.

In the third part of the thesis, the a posteriori scaling analysis methodology developed during the thesis is described in chapter 7. Conclusions in chapter 8 are drawn from the two studies carried out as well as from an analysis of the reinterpretations and enhancements of the original methodology. Answers to the questions and objectives mentioned in the first part are provided. Finally, perspectives for further methodology improvements and new applications are proposed in chapter 9.

CHAPTER 2

Background: Pressurized Water Reactors (PWR) and Loss Of Coolant Accidents (LOCA)

Over the last decades, the world total electricity final consumption has steadily increased, with the residential and tertiary sectors accounting for a large share of the growth since 1974 (see Figure 2.1a). In 2019, the world total electricity final consumption reached 22 848 TWh (IAEA 2021a).

Figure 2.1b shows the world electricity generation mix by fuel (IAEA 2021b). It is observed that coal remained the dominant fuel for power generation, reaching in 2019 37% of the global electricity production. The share of renewables began to grow strongly in the mid 2000s, overtaking that of natural gas in 2013 and providing almost 27% of global electricity in 2019 (24% for natural gas). Nuclear has remained stable at around 10% for the past eight years, while oil provided less than 3% of global electricity in 2019.

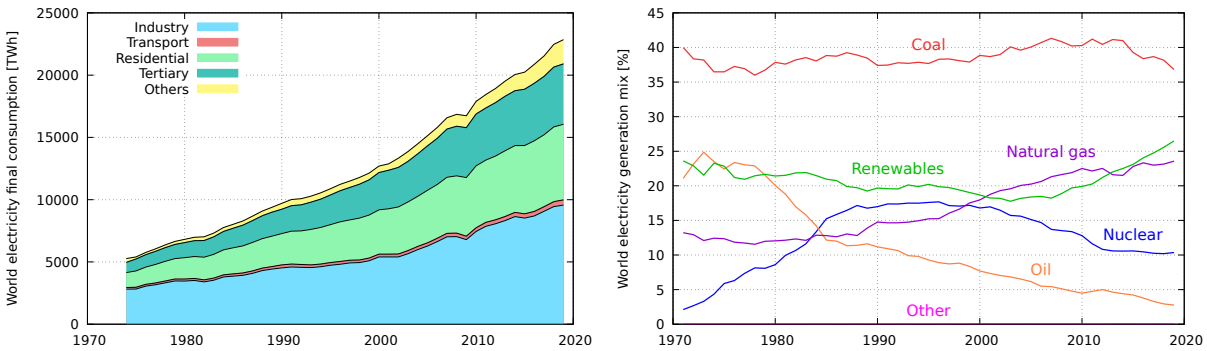

(a) World electricity final consumption by sector **(b)** World electricity generation mix by fuel

Figure 2.1: World electricity consumption and generation

2.1. Pressurized Water Reactors (PWR)

In 2022, there are 441 nuclear reactors in operation in the world for electricity production with a combined energy capacity of nearly 400 GWe. Nuclear energy operate in 32 countries and generate about 10% of the world's electricity and represents the fourth largest source of production. Additionally, 53 reactors are under construction, and 96 are planned. Figure 2.2 depicts a world map of operating nuclear reactors in 2022 (IAEA 2022a). The United States, France and China are the three main countries producing electricity from nuclear source with respectively 92, 56 and 55 nuclear reactors.

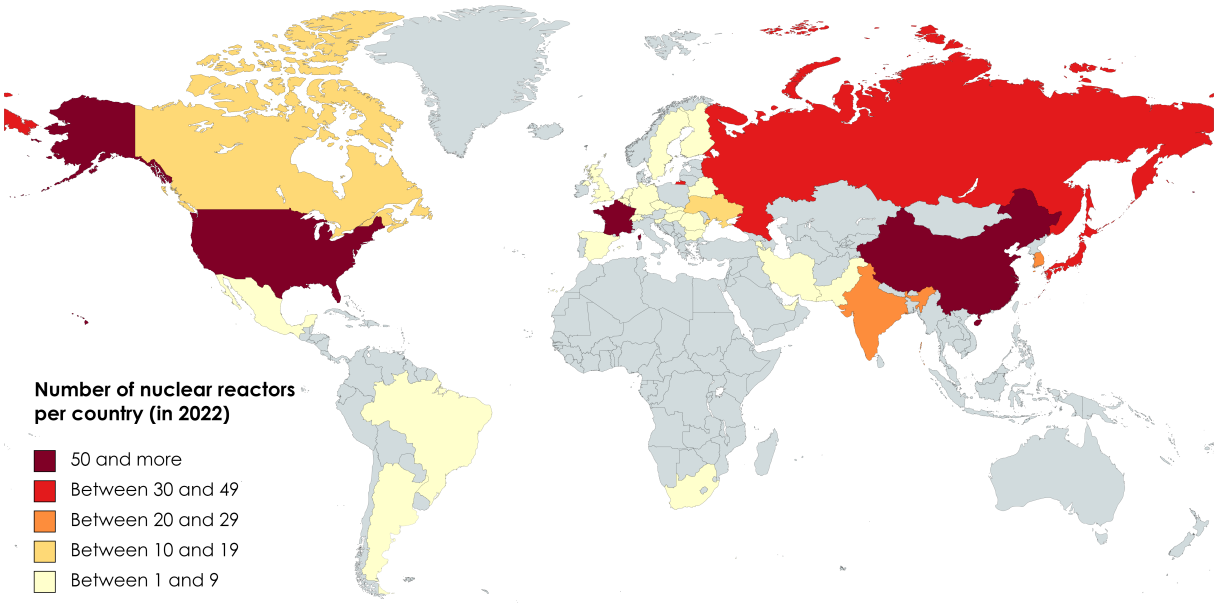

Figure 2.2: Number of nuclear reactors in operation in the world in 2022

Since the beginning of the civil nuclear power industry after the World War II, several reactor types have been developed around the world. These reactor types are distinguished by their choice of technological options, mainly in terms of fuel type, coolant or moderator. The list of in operation nuclear reactors in the world in 2022 is summarized in Table 2.1 (IAEA 2022b).

Table 2.1: In operation nuclear reactors in the world in 2022

Reactor type	Number of reactor	Electrical capacity [MW]
Pressurized Light-Water Moderated and Cooled Reactor (PWR)	307	292 917
Boiling Light-Water Cooled and Moderated Reactor (BWR)	61	61 849
Pressurized Heavy-Water Moderated and Cooled Reactor (PHWR)	48	24 404
Light-Water Cooled, Graphite Moderated Reactor (LWGR)	11	7 433
Gas Cooled, Graphite Moderated Reactor (GCR/RBMK)	10	5 650
Fast Breeder Reactor (FBR)	3	1 400
High Temperature Gas Cooled Reactor (HTGR)	1	200
Total	**441**	**393 853**

With 307 Pressurized Water Reactor (PWR), they are the most common. They represent about 70% of the nuclear reactors in the world. In 2022, French electricity production is provided by 56 PWR. French nuclear industry generate more than 70% of the country's electricity, which represents 61 370 MWe (IAEA 2022b). Three PWR types are operated in France, differentiated by their electrical power (900 MWe, 1 300 MWe and 1 450 MWe). Figure 2.3 details the electricity production share in France in 2021 as well as these three PWR types (EDF 2020). These three types of PWR differ slightly in their characteristics such as the number of loops, specific thermal-hydraulic parameters, thermal powers and therefore their number of fuel assemblies.

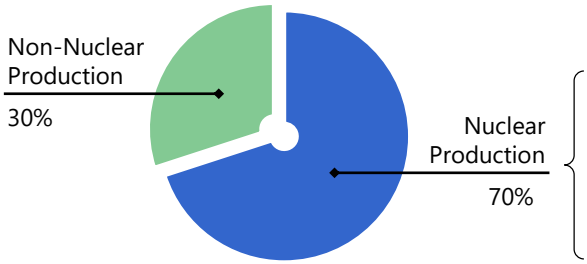

Table 2.2: Number of PWR in France by power

Electrical power	Number of reactors
1 450 MWe	4
1 300 MWe	20
900 MWe	32

Figure 2.3: Electricity production share in France in 2021

PWR use uranium dioxide UO_2 fuel enriched about 3 to 5%, or a mixed fuel composed of depleted or low-enriched uranium dioxide UO_2 and plutonium dioxide PuO_2 (MOX fuel). The fissioned atom is mainly ^{235}U. The thermal power of the reactor is produced mainly by the fission of uranium atoms (90%). The other part is released by radioactive fission products (less than 10%), which emit heat and radiation as they return to a stable state.

The Rankine thermodynamic cycle of a PWR is illustrated in Figure 2.4 (Delhaye 2008). The water circulating in the core acts both as a coolant and as a neutron moderator, slowing them down. The liquid water circulates in a pressurized primary circuit (155 bar) and transfers its energy (from $\approx$ 329 °C to 293 °C) to a secondary circuit through a heat exchanger (called steam generator). The secondary fluid is brought to the boil and drives a turbo-generator which generates electricity.

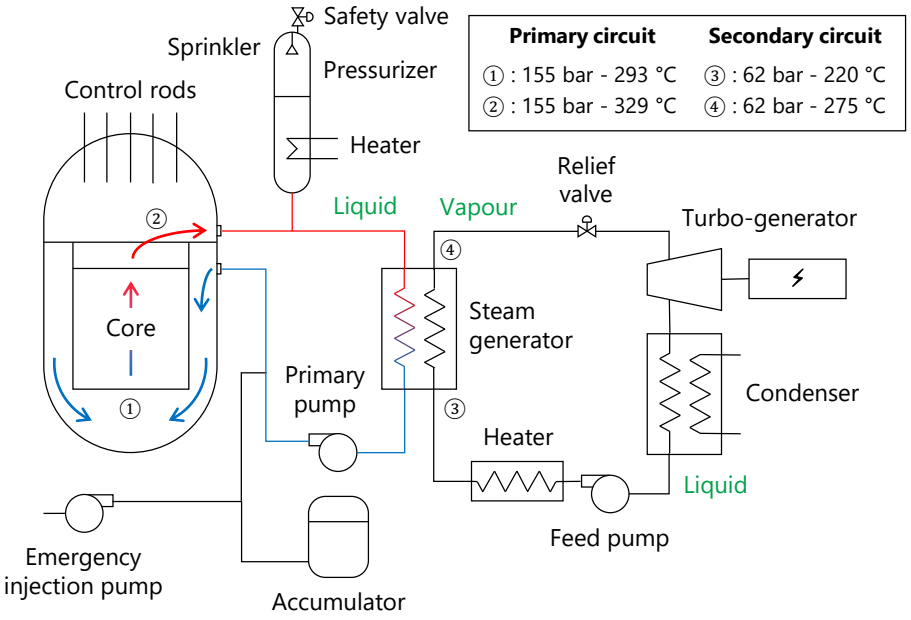

Figure 2.4: General cycle of a Pressurized Water Reactor (PWR)

The stability of the nuclear reactor is ensured by a system of neutron absorbers of two types: rods that control the reaction during operation and the emergency rods that drop into the core and stop the chain reaction. Furthermore, a boric acid solution in the coolant, acting as neutron absorber, ensures reactor control. The intrinsic stability of a PWR then depends on the type of fuel chosen and its moderator. PWR fuel consists of bundles of cylindrical rods made of a zirconium alloy. Ceramic fuel pellets are stacked in the zirconium tubes. The rods are held in place by grids. A fuel assembly usually consists of 17 $\times$ 17 rods made up of 264 fuel rods, 24 guide tubes and 1 central

instrumentation rod. There are 157 to 241 assemblies in the core, depending on the type of PWR.

The Reactor Pressure Vessel (RPV) of a PWR is composed of an annular space (called downcomer) where water circulates from the cold leg to the bottom of the vessel, in the lower plenum. The water flows into the core, through the lower internals, the fuel assemblies and the upper internals. Finally, the water flows through the upper plenum and the dome to the hot legs. The RPV of a PWR and the details of the nuclear fuel are illustrated in Figure 2.5 (Delhaye 2008).

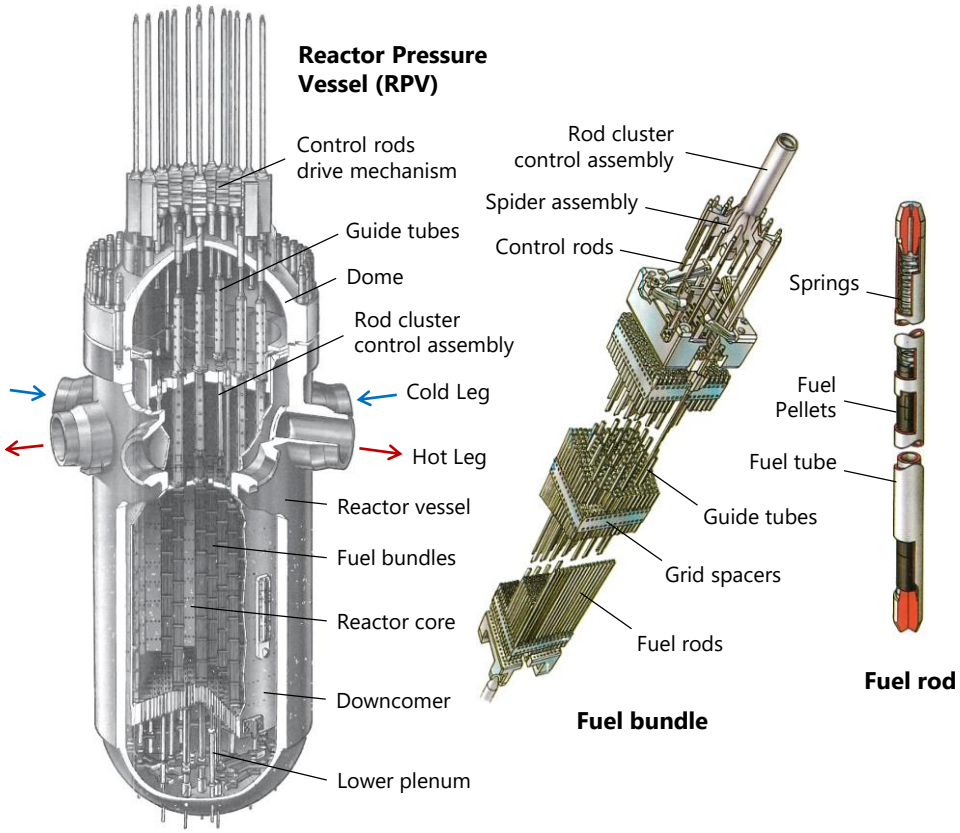

Figure 2.5: Pressurized Water Reactor (PWR) pressure vessel and nuclear fuel

A PWR primary loop consists of a steam generator (SG) and a primary pump located on the cold leg (see Figure 2.4). A 900 MWe reactor's primary circuit has three loops, whereas a 1 300 or 1 450 MWe reactor's primary circuit has four loops. One pressurizer located on a hot leg is connected to the primary circuit. The pressurizer controls the pressure (155 bar) thanks to a balance between a liquid phase that can be vaporized by heaters and a saturated vapour phase that can be condensed by a sprinkler system.

The primary circuit's heat is transferred to the secondary circuit by the SG. The water of the primary circuit, heated by the reactor core, circulates inside inverted U-shaped tubes forming the tube bundle. Preheated water is injected into the SG secondary volume and brought to a boil through contact with the tubes. The primary pumps ensure the circulation of the primary fluid. The pumps compensate for pressure losses in each loop, which are mainly located in the core and in the SG.

Several auxiliary circuits are connected to the primary circuit piping. Their function is to control the behaviour of the reactor in nominal operation or in normal reactor shutdown conditions. For example:

- The Chemical Volume Control System (CVCS) which purpose are - to adjust the boron concentration of the primary circuit by adding demineralized water or boron water in response to core power variations, - to adjust the mass of water in the primary circuit in response to temperature variations and - to maintain the quality of the primary circuit's water by reducing its content in corrosion products.
- The Reactor Heat Removal system (RHR) which function is to evacuate the residual heat produced by the fuel when the reactor is shut down in order to prevent the water from overheating.

Additionally, several backup circuits control and limit the consequences of the reactor in an incident or accident situation. The backup circuits are essentially safety injection circuits. For example:

- The Safety Injection System (SIS) which injects boron water into the core to stop the nuclear reaction and maintain the volume of water in the primary circuit in the case of primary coolant loss. They are made up of - pressurized accumulators operatively passively and - pumps with different flow rates and discharge pressures to react to the different types of accidents. These pumps draw boron water from tanks and inject it into the primary circuit (shown in Figure 2.4).
- The Auxiliary Feedwater supply (AFW) which maintains the water level in the secondary part of the steam generators and cools the water in the primary circuit if the normal water supply to the steam generators is compromised.

2.2. Loss Of Coolant Accidents (LOCA)

Nuclear incidents and accidents are described according to the International Nuclear and Radiological Event Scale (INES) ranging from 1 to 7 depending on the severity with three incident-levels and four accident-levels (IAEA et al. 2009). Events with no safety significance are ranked at the below the scale, at level 0. Figure 2.6 illustrates the different levels of severity classified according to the INES scale, used by nearly 70 countries. The INES scale is logarithmic, i.e. each increasing level represents an accident approximately ten times as severe as the previous level.

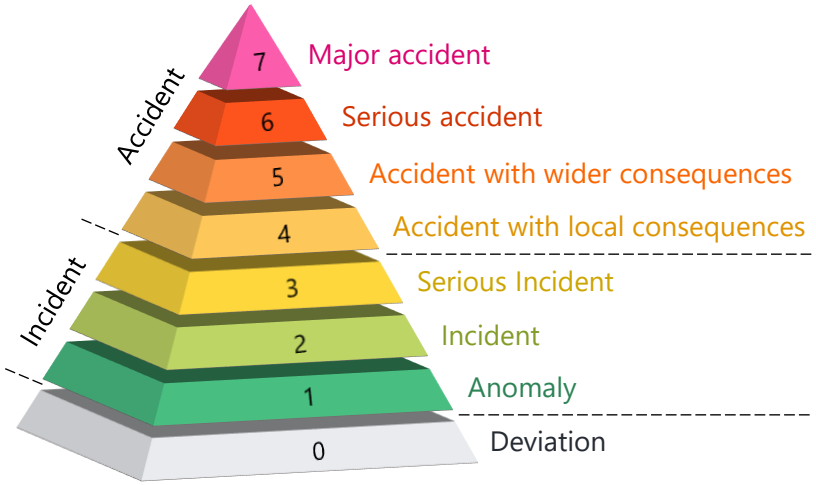

Figure 2.6: The International Nuclear Event Scale (INES) levels

The International Atomic Energy Agency (IAEA) defines that a nuclear reactor is in accidental situation if "an event that has led to significant consequences to people, the environment or the facility. Examples include lethal effects to individuals, large radioactivity release to the environment, reactor core melt" (IAEA et al. 2009). For instance, the Chernobyl disaster (1986) and the Fukushima disaster (2011) are the most serious nuclear power plant accidents (level 7) and have caused impacts on people and the environment. Moreover, accidents with severe consequences (level 5), such as the Three Mile Island accident (1979), are considered to have severe damage to safety barriers and limited radioactive material release.

The Three Mile Island event was a Loss Of Coolant Accidents (LOCA). It led to an interest in studying this type of nuclear transients. The work in this thesis is exclusively concerned with LOCA scenarios. LOCA transients are usually pipe breaks or isolation valve failures in the primary system. Since the 1950s, this type of accident has been postulated as the most credible accident. As a result, the PWR design principle and its safety guidelines require that they withstand the consequences of a LOCA transient (Couturier 2020).

A break in a primary system's pipe results in an sudden drop in pressure and water loss from the circuit. This pressure drop causes mechanical stresses on the PWR structures. In addition, the lost water may cause partial or total uncovering of the core. It can lead to damage of the fuel rods, and even to mechanical failure of some of them. To prevent compromising the core's cooling capability and to lessen the radiological consequences, the damage must remain limited. The location and the size of the break directly affect the evolution and consequences of a LOCA transient. Therefore, the breaks located on the cold legs are the most penalizing to core cooling. The breaks located on the hot legs are the most penalizing for the PWR containment, taking into account the high temperature of the fluid discharged at the break (Couturier 2020).

LOCA are classified into three size categories depending on the size of the break on the broken pipe: - Small-Break (SB), - Intermediate Break (IB) and - Large Break (LB). A significant characteristic in the analysis of LOCA transients is the pressure in the primary system. Figure 2.7 depicts the logarithmic evolution of primary pressures for a SB-, IB- and LB-LOCA. It is observed that the pressure of a LB-LOCA drops instantaneously, making it an extremely violent transient. Although the behaviour of SB- and IB-LOCA is similar, the transients overall duration differs by an order of magnitude.

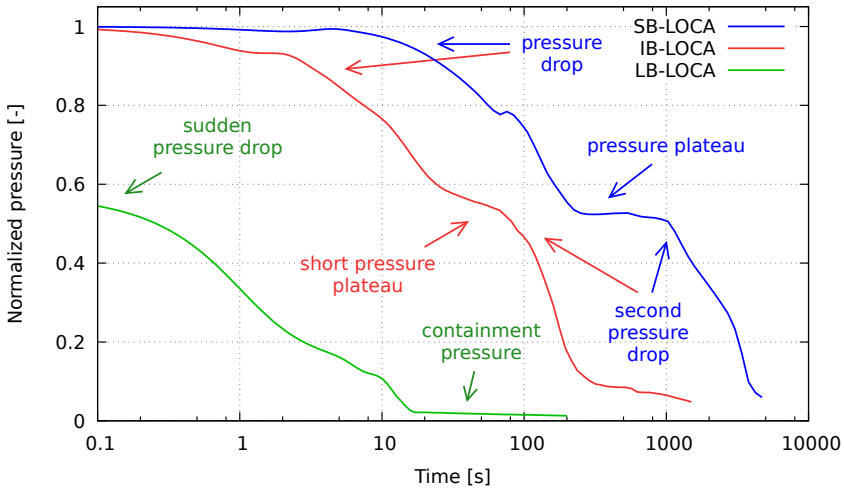

Figure 2.7: Primary pressures of an SB-, IB- and LB-LOCA

2.2.1. Small-Break LOCA (SB-LOCA)

The pipe has a break area roughly ranging from 1% to 6% of its cross-sectional area. The transient is relatively long for these break size ranges. Depending on the size of the break and the operating assumptions of the primary pumps and safety systems, it can last from ten minutes to about one hour.

The primary pressure drops rapidly in the early moments of the transient, while only liquid is discharged at the break. Due to the depressurization, the liquid begins to vaporize. The power generated by the core and transferred by the SG starts to decline, limiting the depressurization.

A quasi-equilibrium pressure condition is reached, that can last for several hundred seconds. The pressure in the primary circuit stabilizes at a pressure plateau close to that of the secondary circuit (see Figure 2.7). The secondary circuit acts as heat sink and natural convection is established in the primary circuit. The void fraction slowly increases in the upper parts of the primary circuit.

The decay heat in the SG begins to be removed by condensation. Liquid from this condensation then falls in the U-shaped section of the cold legs (intermediate legs), creating plugs and two thermodynamically independent volumes. When a sufficient pressure difference between the two volumes separated by the plugs is reached, the plugs are expelled towards the core.

The primary pressure equilibrium is interrupted and starts to decrease again. The secondary pressure becomes higher, and the secondary circuit starts to transfer its heat to the primary circuit. The break flow being almost vapour, the primary mass inventory continues to decrease until the SIS (accumulators and Low Pressure Injection System (LPIS)) are triggered. The primary circuit and the core are refilled and the transient ends when a sufficiently low pressure is reached (Shockling et al. 2012).

The study of SB-LOCA transients is covered in chapters 5, and 6, where the phenomenology is further discussed.

2.2.2. Intermediate-Break LOCA (IB-LOCA)

The pipe has a break area beyond 6% its cross-sectional area. It should be noted that there is no clear agreement on the limits between SB-LOCA and IB-LOCA, and these are still questionable (D'Auria et al. 2017). For these break sizes, the transient lasts less than ten minutes.

Like the SB-LOCA, the primary circuit rapidly depressurizes as soon as the break is opened. However, the residual power of the core is mostly evacuated through the break, resulting in a faster decrease in primary pressure compared to a SB-LOCA (see Figure 2.7).

The primary circuit, especially the cold parts, reaches saturation conditions resulting in a two-phase flow at the break. The mass inventory of the core is lost, resulting in a prolonged and nearly complete uncovery and very high peak temperature in the fuel assemblies (Shockling et al. 2012).

As the primary pressure decreases faster than in SB-LOCA, the SIS (High Pressure Injection System (HPIS) and accumulators) are triggered earlier. The core is then refilled and the fuel rods are cooled. Due to the liquid vaporizing in the primary circuit as a result of the pressure drop, the pressure plateau and the natural circulation phase are therefore much shorter or even absent (see Figure 2.7).

Once the accumulators are emptied, the primary pressure continues to decrease until the LPIS are activated. Only the HPIS and LPIS can then support the refilling of the primary circuit and the core. A second temperature peak may occur if the pumped flow from the safety injections is not high

enough. The transient ends when the safety injections flow exceeds the break flow and the core is quenched (Lorduy-Alós et al. 2020).

2.2.3. Large-Break LOCA (LB-LOCA)

Also called "Double-Ended Guillotine Break (DEGB)", the pipe is assumed to be completely broken (D'Auria et al. 2017). This transient only lasts a few hundred seconds and is extremely fast. The less favourable case of LB-LOCA is a double ended break on a cold leg.

Because of the high break flow rate (limited by the critical flow rate phenomena), the primary pressure drop is extremely sudden compared to the SB- and IB-LOCA (see Figure 2.7). The pressure drop leads to a total uncovery of the core and to very high fuel assemblies temperatures. The emergency safety injections are triggered instantly and inject water into the reactor to maintain core cooling.

Boiling and flashing occur in the core and the flow reverses, passing through the downcomer to be discharged at the break (Bajorek et al. 2001; Shockling et al. 2012). The fuel rods exceed the critical heat flux, resulting in a significant decrease in heat transfer to the coolant. Within seconds, flashing occur in the entire primary circuit. The break flow becomes saturated and significantly reduced.

The water injected into the cold legs by the accumulators flows into the downcomer, reversing the flow again and rewetting the core. Because of the depressurization caused by the vapour flow at the break, the primary circuit reaches a quasi-constant pressure close to that of the containment (see Figure 2.7).

The reflooding of the core begins. The flow in the core is oscillatory due to the cold water rewetting the hot fuel rods, generating vapour. Because the vapour flows in the primary circuit is relatively low, the cladding temperature slowly rises. The temperature of the fuel assemblies begins to decrease after about a hundred seconds. Finally, the entire core is therefore reflooded, starting a long-term cooling phase ending the transient (Shockling et al. 2012).

The LB-LOCA was initially used as reference accident for the design of PWR. It was after the Three Mile Island accident that the interest turned to the study of SB-LOCA and IB-LOCA.

CHAPTER 3

State of the Art : Scaling in Nuclear Thermal-Hydraulic

This chapter aims to provide an overview of the thesis subject study. The evolution of the framework of nuclear thermal-hydraulic in accidental situations and the applications related to scaling are presented. The current state of knowledge, methods, and limitations linked to scaling analyses are detailed in order to establish the perspectives resulting to the thesis questions.

3.1. An Overview of Nuclear Thermal-Hydraulic

Thermal-hydraulic is a fundamental component of nuclear research and engineering. In particular through the study of the behaviour of nuclear reactors in normal and accidental conditions. The functioning and integrity of nuclear installation structures under extreme conditions is a subject of great interest in the scientific literature. Among the many topics related to nuclear thermal-hydraulic, issues concerning accidental investigation emerge.

The first interest in the study of accidental situations appeared in the 1950s, when scenarios were identified to demonstrate the safety of Nuclear Power Plants (NPP). These experimental studies focused on the basis of reactor safety analyses (D'Auria et al. 2017). Small-scale systematic thermal-hydraulic research programs were then initiated in the 1960s. They were intended for the study of individual physical phenomena and provided key points of interest for the study of nuclear transients (Zuber et al. 1965; Forslund et al. 1968; Wallis 1969). Primitive numerical tools were used

to analyse experimental measurements as computer science developed in the 1970s. The first nuclear reactor safety calculation codes were also made available (Moore et al. 1968). Until the end of the 1970s, there were few accidents on civil reactors involving two-phase conditions. Consecutively to the Three Miles Island accident in 1979, the number of accidental transient studies increased (NEA 1991; NEA 2005).

Because of the size, complexity, and safety implications of a nuclear reactor, the costs of simulating a full-scale accidental transient were not affordable. To circumvent this problem, the global nuclear industry has developed small-scale experiments. The aim was to conduct tests on these reduced model reactors under safe and cost-optimized conditions (Bestion et al. 2017). Reduced-scale experimental facilities can be classified into three types:

- Basic tests, aimed at understanding specific phenomena that are not dependent on the geometry or size of the reactor. These experiments are intended to understand the fundamental processes of thermal-hydraulic and are typically carried out under simple steady boundary conditions. They are useful for gathering essential information for the development of models and correlations. Their interest, however have a weak connection with scaling issues.

- Separate Effect Test Facilities (SETF) intended to perform Separate Effect Tests (SET). They are designed to investigate local phenomena that occur during transients in reactors. In general, SETF represent a specific component of the reactor, whose scale and geometry are preserved. They are intended for the understanding, development and validation of physical models and/or empirical correlations. The purpose was then to use the SET experimental results to improve the models used by the calculation codes (see 3.2) (NEA Databank 2015).

- Integral Test Facilities (ITF), which are dedicated to the scaled-down representation of a full-scale reference reactor on which Integral Effect Tests (IET) are performed. They are intended to provide a thermal-hydraulic response to a specific transient over a specified time period. Despite the fact that all of the reactor components (primary and secondary circuits) are represented, the experimental data are allegedly not directly transposable to the reference reactor due to scale effects. The IET are mainly used to understand transients and validate calculation codes. They are established under the recommendations of the Organization for Economic Cooperation and Development (OECD) (NEA Databank 2010).

The transient scenarios are selected in accordance with the Design Basis Accidents (DBA). These are the accidents that are used to determine the design and safety criteria for nuclear power plants. In other words, they are the "reference accidents" as defined by the Design Basis (DB) requirements, which are closely related to the safety regulations that constitute the "licensing basis". The DBA criteria are generally defined as events that could lead in nuclear fuel damage and the release of radioactive material (USNRC 1997; USNRC 2000). The most relevant DBA (or transients) are Loss Of Coolant Accident (LOCA), Loss Of Feed Water (LOFW), Loss Of Offsite Power (LOOP), Main Steam Line Break (MSLB), Station Black Out (SBO) and Steam Generator Tube Rupture (SGTR).

The field of "scaling" research and study takes place in this context of nuclear thermal-hydraulic transients, through the connection between the nuclear reactors parameters with their experimental equivalents on a reduced scale. Scaling is then initially defined as the process of converting the reactor parameters to those of the experimental facility. The terminology "scaling issue" refers to the difficulty and complexity of the procedures and the variety of aspects related to this conversion. Finally, "addressing the scaling issue" refers to the process of demonstrating the applicability of the actions required to perform the scaling (Bestion et al. 2017).

3.2. Contributions of the Calculation Codes

In the early 1980s, advances in computer science contributed to the emergence of calculation codes. With experimental results allowing for version refinement, transient simulation improved, and questions of applicability of addressing the scaling issue with the codes arose. This implies that the codes should be able to reproduce the dominant phenomena of facilities transients, and thus to the reference reactors (scaling-up) with the "scale-transposition".

Over the years, the growing experimental data base contributed to improve activities in the framework of thermal-hydraulic system codes. Their role extends through Verification and Validation (V&V) process (D'Auria et al. 1998) and becomes mandatory computational tools for safety and licensing. They are becoming available to better understand transients by connecting experimental results to the still poorly understood phenomenology, providing key information and allowing to address the scaling issue. As a result of the advancement of codes, certain phenomena were designated as being of interest during the 1980s (NEA/CSNI 1989).

Due to the requirements of Uncertainty Methods (UM), new approaches to the study of transients were proposed in the early 1990s. In particular, the well-known Code Scaling and Applicability and Uncertainty (CSAU) and the Process Identification and Ranking Table (PIRT) were proposed (USNRC 1989; Wilson et al. 1990). The CSAU is an uncertainty methodology procedure that aims to quantify - the accuracy of the experiments and code, - the effects of scaling, and - the characteristics of the reference reactor. Uncertainties and biases can be evaluated using the PIRT by analysing scaling distortions of phenomena occurring in experimental test facilities and evaluating the code scale-up capabilities. The Appendices A and B describes respectively the full CSAU and PIRT methodologies flowcharts.

The code-evaluation process is used to assess safety by comparing the results of code predictions with the experimental data of SET and IET. The aim is for the code to predict the same results, in order to ensure that the phenomena of these tests could be confidently scaled to those expected in the reference reactor. Because it is not possible to design tests for all geometrical configurations and operating conditions of full-scale reactors, this approach remains ideal and theoretical. This is why scaling evaluations studies for each application are required (Wulff et al. 1999). Figure 3.1 illustrates the codes involvement in the framework of nuclear thermal-hydraulic transients.

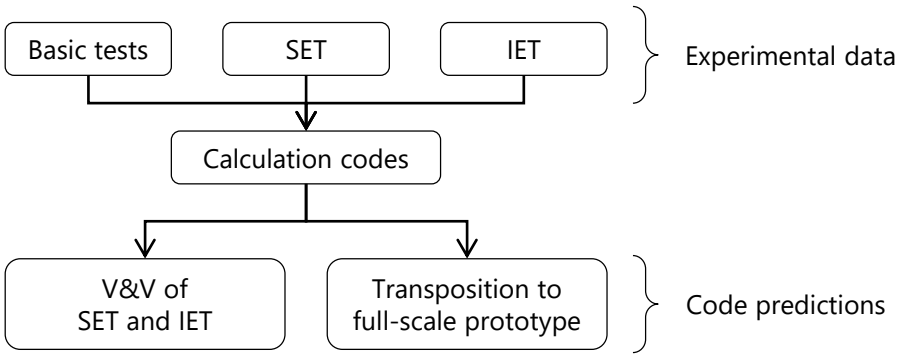

Figure 3.1: Code involvement in nuclear thermal-hydraulic transients

In France, joint guides between the Autorité de Sûreté Nucléaire (ASN) and the Institut de Radioprotection et de Sûreté Nucléaire (IRNS) publish the regulatory objectives, recommendations, and practices related to the use of scientific calculation tools in the context of legal decrees (ASN et al. 2022). In particular, the guide n°28 describes the process contributing to the elaboration of the qualification document of the calculation codes with respect to their field of use (ASN et al. 2017). Qualification of the code is done first by identifying - the quantities of interest of nuclear transients, - the dominant physical phenomena that influence these quantities of interest, - and the ranking of these phenomena to guide the scope of use of the codes, as well as the most important physical models. A parallel can be drawn between the code requirements and the scaling methods discussed in the following sections of this thesis.

This guide also establishes the scale-transposition objectives through the code validation processus by identifying differences in physics caused by the design of SETF and ITF or by "scale effects". It defines the evaluation of the models capability to remain predictive in their domain of use, as well as the modelling choices for safety studies (physical models, spatial meshing, temporal discretization, numerical schemes, convergence criteria, calculation options, etc.). The quantification of code uncertainties which can be based on sensitivity analyses is also discussed.

Finally, guide n°28 addresses the evaluation of the calculation codes pre- and post-processing parameters, their coupling, the user effects, and the links with the study methods. Scaling and its applications then appear to be directly correlated to the guide expectations and objectives, as demonstrated by its application supported by the calculation codes, as it will be discussed in the thesis.

The continuous progress of computer performance allows to use more refined nodalization and the use of several modelling scales in a multi-scale approach to reactor thermal-hydraulic issues. These multi-scales can be used in coupling (i.e. where a finer scale tool is required to predict a local domain simulated by a more macroscopic tool) or independently to study reactor transients (Bestion et al. 2012). Calculation codes in nuclear thermal-hydraulic can be divided into four categories: system, component, local and micro scales. These categories are mainly related to the characteristic size of the simulation domain for which the studies are intended.

The nuclear thermal-hydraulic multi-scales categories are illustrated in Figure 3.2 (Höhne et al. 2010; Bestion et al. 2012) and presented in the following sections.

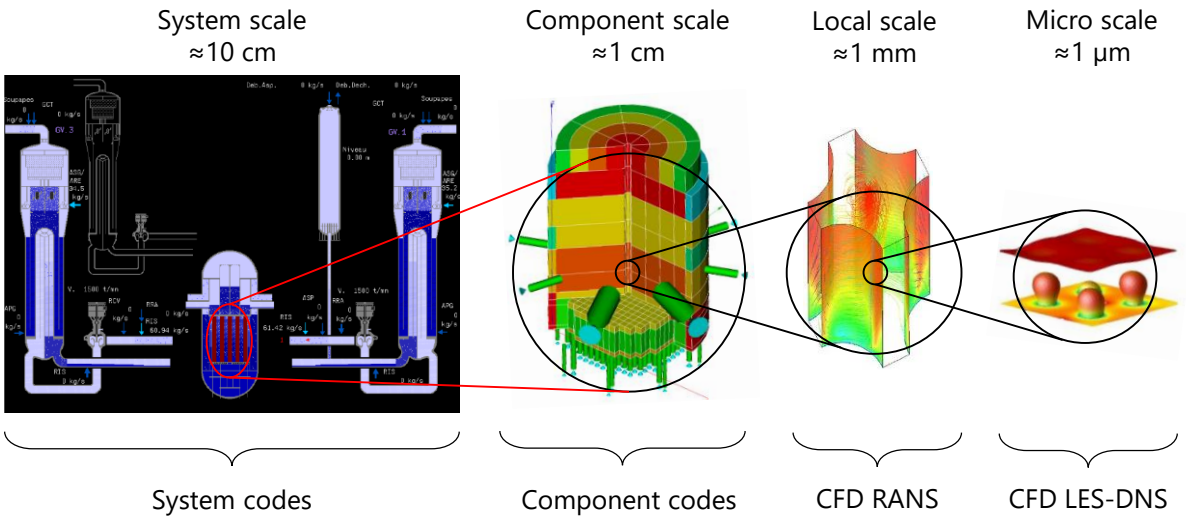

Figure 3.2: Codes scales categories in nuclear thermal-hydraulic

3.2.1. System Scale Codes

The system scale is dedicated to the study and description of reactor circuits as a whole. Due to the size of a reactor and the large number of components and phenomena that occur within it, simulation of transients at the system scale is typically achieved using system codes. Because of their wide range of applicability, they can cover the DBA.

In order to correctly simulate a nuclear transient, the system codes must actually be multi-scale and multi-physics computational tool. They are based on the resolution of a model of six mass, momentum, and energy equations (for liquid and vapour) in order to predict the overall thermal-hydraulic behaviour of the plant. This type of resolution requires a suitable set of closure laws and can be coupled with heat transfer and neutron kinetics models.

The primary and secondary systems of a reactor are modelled by coupling several dozen of 0-D, 1-D, and 3-D modules and sub-modules to represent the different components. These modules are made up of few hundred 0-D and 1-D meshes, and about a thousand 3-D meshes. These meshes range in size from several metres for 0-D modules, to ten centimetres for 1-D modules, and to millimetres for 3-D modules. Having coarse meshes allows system codes to perform simulations of accidental scenarios in reasonable CPU time.

The simulations performed by system codes are mainly for industrial purpose and intended for safety studies. System codes are expected to be highly robust, with strictly measured uncertainties and justified versions. Certain safety demonstration procedures, such as the establishment of specific documentation, are then required. The code must be validated and verified, and its scalability must be demonstrated. System codes can also be implemented in plant simulators for operator training. Real-time calculations must then be doable, allowing for operator actions.

A Best-Estimate (BE) system code aims to model all dominant processes that occur in the simulation domain with sufficient reliability. In comparison to a "conservative code," which predicts the lower and upper limits of a process, BE codes aim to predict the process with the best accuracy throughout the transient (D'Auria et al. 2017). BE codes come after the first codes that were used for licensing the first reactors. The first four BE codes developed in the late 1970s and 1980s are TRAC (USNRC, United-States), RELAP5 (INL, United-States), ATHLET (GRS, Germany) and CATHARE (CEA - EDF - Framatome - IRSN, France).

More details are provided in Chapter 4, which specifically presents the French CATHARE system code that will be used for the work of the present thesis.

3.2.2. Component Scale Codes

The component codes or component scale are dedicated to the simulation of some components of the primary and secondary circuits for design, safety, and operation studies. Reactor cores and tubular heat exchangers such as steam generators, condensers, and auxiliary heat exchangers are examples of these (D'Auria et al. 2017).

Component scale codes use Computational Fluid Dynamics (CFD) of 3-D modules in porous medium approach (such as the 3-D modules of the system codes). The porosity concept is used to model the presence of walls of rods or bundle tubes within each. The local instantaneous equations are multiplied by a fluid characteristic function, then by a phase or field characteristic function, before being averaged over time and over a spatial domain (D'Auria et al. 2017). The minimum spatial resolution corresponds to the size of the sub-channels (of the order of centimetres) ; this gives the "sub-channel models".

The component codes simulations are intended for applications such as - instability studies in reactor cores with 3-D neutron kinetics coupling, - the study of specific Anticipated Transient Without Scram (ATWS) or Main Steam Line Break (MSLB) type transients, - studies of boron dilution transients, - rod ejection reactivity transients, or - core reflooding processes. Usually, the entire core is modelled. Typically, a row of mesh is used for each fuel assembly. Component codes are frequently coupled to system codes or neutron kinetics modules in many applications.

Other applications for SG and heat exchangers include heat transfer efficiency studies of exchangers for design, - mass inventory and recirculation ratio in SG tubes, - fouling in SG and heat exchangers, or - SG tubes vibration issues.

In component codes, two-phase models can be three equations with drift flux (GENEPI, France), four equations with drift flux allowing one phase to be out of thermodynamic equilibrium (FLICA, France), six equations, or even a three-field model with eight or nine equations to describe the liquid films and droplets separately (COBRA-TF, United-States).

3.2.3. Local and Micro Scales Codes

Local and micro scales codes refer to a description of fluid movement or heat transfer at scales much smaller than duct characteristic size (e.g. below a millimetre for the local scale and as small as a micrometer for the micro scale). In the field of nuclear thermal-hydraulic, they are generally intended for modelling 3-D mixing processes either in large size components (cold legs, annular downcomer, lower plenum) or within sub channels in rod bundles.

CFD codes that can predict phenomena in steady state and transient flows. Mixing problems controlled by turbulence and possibly influenced by buoyancy, heat transfer in boiling flows and stratified flows are some examples of application. They are also used for a better understanding of local areas or critical components in specific scenarios (D'Auria et al. 2017). Local and micro scales studies can be used for design verification as well as for optimization of fuel assembly design (Höhne et al. 2010).

The main difference between CFD applications and system or component codes is the importance of the modelling of turbulence. In porous medium approaches of system codes and component codes, wall transfers play a major role compared to turbulent transfers. Another difference lies in the capability to predict the small scale geometrical effects (e.g of spacer grids) instead of using empirical models, which is necessary with component and system codes due to the space resolution. Furthermore, due to the drastic reduction in mesh size at CFD scales and the need of satisfying the mesh convergence, these applications may have a considerably higher computation cost.

There are several CFD approaches based on different space and time averaging or filtering of local instantaneous equations. These models can be classified with respect to their computational expense, corresponding to the ranges of scales that are modelled versus resolved.

The Reynolds-averaged Navier-Stokes (RANS) approach solves a set of time-averaged (or time-filtered) governing equations whose expectation values of a quantity are separated from their fluctuations (Reynolds decomposition). The RANS approach is the most resource-efficient and is widely used in industrial applications, such as in local scale thermal-hydraulic studies.

The Large Eddy Simulation (LES) approach applies a space filtering of local instantaneous equations. The LES approach resolves the largest turbulent eddies and models the effects of the smallest scales. The Detached Eddy Simulation (DES) approach is a hybrid RANS-LES model. This approach is based on RANS and uses a sub-mesh formulation, which allows LES to be applied at smaller scales. This non-zonal approach provides a smooth resolution by regions, although more

expensive in computation time. Finally, the Direct Numerical Simulation (DNS) approach aims to simulate all flow phenomena, including the smallest turbulent eddies and the smallest bubbles and drops. The DNS solves the entire length scale range, inducing extremely expensive computation times, limiting its use to very small simulation domains. In nuclear thermal-hydraulic, LES, DES and DNS approaches are used for micro-scale investigations.

3.3. Addressing the Scaling Issue

The study of scaling distortions is at the center of scaling activities. Distortions can refer to discrepancies between:

- The experimental results and the codes predictions. For a perfectly validated calculation code, these distortions are assumed to be non-existent. In reality, the validation condition is only relative and must be approved for each experimental condition (SET or IET) individually. As the validations progresses, the representativeness of the codes results improves, and confidence in them increases. And it is an open question: how can be certain that the codes accurately represent reality?
- The facilities results (experimental and/or code predictions) and the full-scale reactor code predictions. These distortions, however, can be referred as "scale-effect" when they are caused exclusively by deviations due to the size difference between the ITF and its reference model reactor. These distortions may also be the result of facility design methods, initial parameter choices, and a variety of other factors. The present thesis focuses on these two types of distortions.

Addressing the scaling issue is the set of procedures conducted in order to complete the "scaling achievement". This is accomplished through the strategy of identifying, quantifying, and resolving the distortions caused by the scaling issues. It is also fulfilled by implementing technologies that allow for a detailed knowledge of the tools available for resolving the scaling issues. Scaling analyses, in particular, can be used to investigate and establish the requirements for the thermal-hydraulic of nuclear power plant transients. This is one of the aims of the thesis, which intends to provide guidance on scaling methodology.

3.3.1. Design Scaling Methods

To identify the sources of the distortions, it is worth understanding the multiple steps that may lead to them. This requires going back to the facilities design. SETF are typically designed using non-dimensional analyses such as the Buckingham Pi theorem and the derivation of governing equations for scaling parameters for local phenomena (Bestion et al. 2017). However, for ITF in which a system-scale interest appears, other important parameters to be preserved are taken into account to ensure the preservation of system behaviour through important phenomena and processes. Guidelines describing the major characteristics to be considered focus on ensuring a certain degree of similarity. Because the thesis focuses on the analysis of distortions using in the framework of ITF, only the methods and techniques for the ITF design will be presented here.

Given the complexity of the processes that occur during a nuclear transient, it is to be expected that the physical behaviours of the facility will differ from the prototype depending on design characteristics and geometry choices. This is referred to the "scaling limitations" in the design scaling methods used for ITF (Bestion et al. 2017). The inappropriate designs that can be made

are commonly recognized to be due to the age of the methods that allowed the design of ITF at the time. These methods show incomplete similarity to the reference reactor, and they most likely did not go far enough in prioritizing important processes. Despite the designers intentions to select the best method based on the experimental objectives or the acceptance criteria (or design criteria) defined in the Design Basis, the assumptions and compromises made by design scaling methods are likely to distort certain phenomena (D'Auria et al. 2017).

3.3.1.1. General Criteria

Some questions arise before the application of design scaling methods in the framework of ITF design. Despite the objective of attaining appropriate transient scenarios through PIRT work, there appear to be constraints related to the cost of building ITF. Some general design parameters related to engineering, regulatory requirements, manufacturing issues, and facility operability are selected outside the scope of these design scaling methods (Bestion et al. 2017). Therefore, one must not forget about the optimization of "cost/representativeness" and the minimization of scale effects through the selection of the operating parameters. Here are some examples of characteristics, general parameters, and boundary conditions that have to be considered when designing ITF and their IET:

Number of loops

The number of loops in an ITF compared to its reference reactor. It is obvious that the design of a prototype reactor requires significant reductions for its proper operation at a reasonable cost. It is widely accepted that taking advantage of reactor symmetry considerations allows for substantial savings by dividing the number of loops. However, there is a tangible benefit to keeping a full-number of loops for an ITF. It allows the investigation of a broader spectrum of transients while maintaining more homogeneous boundary and initial conditions. Furthermore, in some types of transients (particularly LOCA), reducing the number of loops may unbalance some phenomena (mass distributions, flow stagnation, natural circulation) (NEA/CSNI 1989). Thus, ITF based on Pressurized Water Reactor (PWR) are typically designed either - with a full number of loops (if 3 or 4) - or with half-loops when necessary (if the reference reactor has 4, i.e. 2 loops on the ITF). Figure 3.1 shows some examples of comparison of the number of loops between ITF and their reference reactor.

Table 3.1: Number of ITF loops compared to their reference PWR

	Preserved loops number				Lumped loops number			
	ATLAS	BETHSY	SPES	PKL	LOBI	LOFT	LSTF	SEMISCALE
ITF loops	2	3	3	4	2	2	2	2
PWR loops	2	3	3	4	4	4	4	4

Technical choices

Some components of the ITF primary and secondary circuits can be intrinsically modified in comparison to the reference reactor. This could be due to technical constraints, in which certain geometries or configurations must be changed. Thus, in some prototypes, the dimensions of some loops have been lengthened or shortened, and some pipe elevations have been changed independently of the scaling design method guidelines. Because of the assumptions of the transients, some ITF components behaviours are also modified, directly through the IET. This is especially true for some safety systems, such as safety injections or pumps, that can be considered compromised during a specific transient. On some ITF, for example, pump simulation can be inertial, programmed, or controlled, which is likely to change the physics of the transient (NEA/CSNI 1989).

Core power and distribution

The reactor nuclear core power is obviously not suitable for a reduced ITF. The only exception is the 50.6 MW American LOFT facility, where some tests were performed with a nuclear power ascension. These tests were carried out to provide information on fission product release and transport from failed fuel due to severe core damage (Reeder 1978). For safety reasons, ITF are designed with electrical-heating methods with significant scaling factors to simulate the thermal response of a nuclear core during a transient. As a result, the internal structure of the core (sub-channels), the materials used to simulate the fuel rods, and the radial and axial heat flux distributions are part of the technical choices and may lead to distortions. Moreover, electrically heated simulators generally have lower thermal capacities than real nuclear fuels (NEA/CSNI 1989). Note that most ITF also use a scaled nominal power (determined by design scaling methods) and that the decay power is simulated.

Initial and boundary conditions

Some initial and boundary conditions are important parameters considered when designing ITF. This is especially true for fluid properties, and more specifically for pressure and temperature conditions. The most common method is to maintain initial full-pressure and full-temperature conditions (in the primary and secondary circuits). Scaling pressure is essential in ITF because some phenomena occur only in specific pressure ranges. Above all, because many safety systems rely on instantaneous operating pressures, a parameter of similarity or proportionality with the full-scale reactor must be maintained (Bestion et al. 2017). There are, however, cases of ITF operating at high reduced pressures due to specific constraints, but where the relevant phenomena can be qualitatively reproduced (e.g. the PKL ITF (Umminger et al. 2012)). It should be noted that water is the working fluid in all cases of ITF simulating PWR due to the good linearity in the pressure response for transient depressurizations (Reyes et al. 1998). Note that only a few simulated Boiling Water Reactor (BWR) ITF use a simulant working fluid (e.g. like Freon-12 (de Kruijf et al. 2003)).

Dimensional parameters

The dimensional parameters of the ITF compared to the reactor references is a fundamental and still debated issue in the literature concerning the design framework. The lengths of the loops, and inevitably the heights of the components, are important parameters in the transients behaviour and physics. They contribute to the ITF ability to accurately simulate gravitational effects, natural circulation flows, frictional pressure drops and time preservation (Kocamustafaogullari et al. 1983). Full-height conservation is thus required to accurately represent the natural circulation driving force. Reducing the height as well as the hydraulic diameters can alter the preservation of pressure drops and non-prototypic phenomena such as surface tension effects and transitions in the flow regimes in the scaled-down facility. This can lead to lower hydraulic resistances, which are especially important in SB-LOCA whose cooling is dominated by natural circulation. ITF reduced-height scales usually range from half- to quarter-height. There are still no criteria on the minimum height scales that do not lead to significant scaling distortions (Bestion et al. 2017).

As a result, the diameters and lengths of horizontal legs are usually designed using Froude number. Some loop configurations can be changed to preserve the typical pressure drops. This is achieved by maintaining a scaled fluid volume in an oversized diameter and shortened length pipe. This was done for the SEMISCALE (volume scale of 1/1705 with full height (Larson et al. 1980)) and MIST (volume scale of 1/817 with full height (Habib et al. 1991)) ITF primary piping. Some studies, particularly for LOCA, show distortions as a result of the reduced height (NEA/CSNI 1989). Some authors also mention the difficulties in preserving certain local phenomena, such as Critical Heat Flux (CHF) and reflooding phenomena, in reduced-height ITF (Bestion et al. 2017).

Time representativity

As mentioned in the previous paragraph, some scaling choices can cause time distortions. The time scale, for example, is not preserved in the reduced-height ITF. It may be more interesting to keep the same timing of events and the same characteristic time response of the processes and thermal-hydraulic phenomena as the reference reactor. During fast transients, time-acceleration may complicate operations and control (Bestion et al. 2017). Different time scales, according to some authors, would also cause distortions in the phase transition processes, especially in the heat-transfer processes (NEA/CSNI 1989). However, in ITF with reduced height (and thus distorted time scale), time is controlled and can be extrapolated to the full-scale reactor (e.g. the ATLAS ITF (Choi et al. 2014)). Simulating transients with long-term behaviour is a major interest of time acceleration (Peterson et al. 1998).

Volume scaling

The conservation of a volumetric ratio is most likely the key parameter in the design differences between a reference reactor and an ITF. Most scaling methods, as explained in the following sections, agree on a procedure to reduce the size, and thus the volume, of an ITF design. However, not all ratios chosen for all ITF are the same. The volumetric ratios range from 1:21.4 (for the CCTF ITF) to 1:1705 (for the SEMISCALE ITF) (NEA/CSNI 1989; NEA Databank 2010). However, the choice of this ratio is subject to distortions in the literature. Reducing the volume involves reducing the cross-sections and, as a result, the ratio of wall surface to hydraulic volume. When compared to its reference reactor, an ITF will have this distorted ratio, which may affect surface heat transfer, energy contained in structures, or heat losses (NEA/CSNI 1989; NEA/CSNI 1996). To ensure that the phenomena in the ITF components are comparable to those in the reference full-scale reactor, the distribution of volume between the different components should be preserved. Resulting energy and mass distributions, in particular, may be sensitive parameters for certain processes during transients (Bestion et al. 2017).

Beyond these general aspects and parameters in the choice of ITF designs, the following subsections describe the most commonly used design scaling methods. Over the years, groups of experts have developed these methods for the transposition of thermal-hydraulic transients processes between the full-scale reference reactors and reduced-scale facilities. They are based on the preservation of an important parameter, such as geometric properties, power, volume, mass, flow rate, or time scale.

3.3.1.2. Linear Scaling

One of the first methods for designing facilities was the linear scaling method (Carbiener et al. 1969). It aims at keeping dimensional similarity criteria such as lengths and heights of components. In this way, the velocity will be preserved between the ITF and the full-scale reactor. The drawback of this method is that it distorts the gravity effects compared to the reference reactor. This is especially the case for ITF which may be much smaller than the full-scale reactor. Therefore, this scaling method has been used only rarely, and mainly on SETF. This simple method is however the basis of the other methods.

It should be noted that a modified version of the linear scaling method has recently been proposed to investigate some local phenomena (Yun et al. 2004). This method is based on twelve dimensionless groups derived from the continuity and momentum equations. It requires the same similarity criteria as the ITF geometry, but it allows for the preservation of gravity effects.

3.3.1.3. Power-to-volume Scaling

The power-to-volume scaling method is established in accordance with works that have adapted the criterion of similarities of the linear scaling method (Nahavandi et al. 1979). An additional layer of criteria is added, focusing on heat exchange phenomena. The aim is to keep the lengths and heights constant while reducing the volumes proportionally to the exchanged powers (in particular the power of the reactor core). Thereby, the phenomena associated with thermo-gravitational effects (such as vaporization, condensation, and natural circulation) are much more representative in transients situations than with the standard linear scaling method. The power-to-volume method was thus widely used in the design of most ITF, including - LOFT (Ybarrondo et al. 1974), - SEMISCALE (Larson et al. 1980), - LOBI (Addabbo et al. 2012), - PKL (Umminger et al. 2012), - LSTF (The ROSA-V Group 1985), and - BETHSY (Deruaz et al. 1982).

The drawbacks of this power-to-volume approach are that the cost of the facilities remains high due to the Full-Height, Full-Pressure (FHFP) criterion and the need to maintain high power. However, some authors assume that when this method is used to design an ITF with a too small area scale compared to its total volume, some phenomena (e.g. pressure drops, heat losses, accumulated heat transfers) may be distorted (Bestion et al. 2017). Some of the studies in this thesis can help to quantify the distortions that could have been caused by the use of this method for the design of ITF.

3.3.1.4. Three-Level Scaling

Three types of principles have been identified in the development of design scaling methods. These principles enabled existing design scaling methods to be assigned to their primary purpose (Nahavandi et al. 1979):

- Time reducing through linear scaling involving a linear reduction in size compared to the prototype.
- Time preserving with power-to-volume scaling involving the conservation of space dimensions.
- Idealized time preserving similar to the previous one, but with greater flexibility supplied by a time proportionality ratio.

A group of authors then suggested the three scaling laws, based on the conservation of the three-dimensional form of the continuity momentum and energy equations (Ishii et al. 1983). The resulting laws attempted to satisfy the requirements of the third principle by preserving natural circulation phenomena (and thus time) under reduced-height ITF. These were then established as the three-level scaling method through the design of the PUMA (Ishii et al. 1996; Ishii et al. 1998) and the ATLAS (Kim et al. 2008) ITF.

The three-level scaling method is based on the similarity of dimensionless groups between the ITF and its reference reactor. This method is characterized by a reduction in the length scale as a result of the conservation of some thermal-hydraulic processes. As a consequence, and as mentioned in the section 3.3.1.1, the time scale of the transient is reduced. The three-level scaling method consists of three steps:

- A global scaling analysis with the aim of maintaining natural single-phase and two-phase circulation. The objective of this step is to keep the macroscopic behaviour of the entire system similar to the facility.
- A mass and energy balance equation-based inter-component scaling analysis.

- An analysis of the local phenomena that allows for the conservation of the important thermal-hydraulic phenomena occurring in each component.

Table 3.2 summarizes the main scaling parameters (scaling ratios) between the facilities and their full-scale prototype, suggested by the above-mentioned linear scaling, modified linear scaling, power-to-volume, and three-level scaling methods (Bestion et al. 2017). A value of 1 indicates that the parameter will be fully conserved between a facility and its reference reactor. A value based on l_0, d_0, or A_0 indicates that the parameter depends on the ratio of length, diameter, or area respectively.

Table 3.2: Comparison of the main scaling ratios of design scaling methods

Parameter ratios	Linear scaling	Modified linear scaling	Power-to-volume	Three-level scaling
Length l_0	l_0	l_0	1	l_0
Diameter d_0	l_0	$-$	d_0	d_0
Area A_0	l_0^2	l_0^2	d_0^2	d_0^2
Volume V_0	l_0^3	l_0^3	d_0^2	$l_0 \cdot A_0$
Core ΔT_0	$-$	$-$	1	1
Velocity u_0	1	$l_0^{1/2}$	1	$l_0^{1/2}$
Time t_0	l_0	$l_0^{1/2}$	1	$l_0^{1/2}$
Gravity g_0	$1/l_0$	1	1	1
Power / volume q_0'''	$1/l_0$	$-$	1	$l_0^{-1/2}$
Heat flux q_0''	$1/l_0$	$-$	1	$l_0^{-1/2}$
Core power q_0	$1/l_0^2$	$-$	d_0^2	$A_0 \cdot l_0^{1/2}$
Rod diameter D_0	1	$-$	1	1
Rods number n_0	l_0^2	$-$	d_0^2	A_0
Flow rate $\dot{m}_0$	l_0^2	$l_0^{5/2}$	d_0^2	$A_0 \cdot l_0^{1/2}$

3.3.1.5. Power-to-mass Scaling

The power-to-mass scaling method is intended for the design of ITF with Reduced-Height, Reduced-Pressure (RHRP) test conditions. The power-to-mass method was especially used in the design of the IIST ITF (Liu et al. 1997; Liu et al. 1998). Because the fluid properties could not be maintained due to the low pressure, and the natural circulation phenomenon being distorted due to the reduced-height, similarity criteria had to be established. The criteria of the previous methods do not allow for suitable scaling of the core power under RHRP conditions. As a result, the power-to-mass method uses a relationship between the thermal core power q_{core} and initial reactor mass inventory M_0. This method has the advantage of accounting for the impact of heat losses in the system q_{loss}:

$$\left[\frac{q_{core} - q_{loss}}{M_0}\right]_{ITF} = \left[\frac{q_{core}}{M_0}\right]_{PWR} \tag{3.1}$$

However, many parameters, such as fluid temperatures and flow rates at various locations in the reactor, must be scaled. Therefore, the degree of subcooling relative to the saturation temperature in the primary system $T_{sat}(P_1)$ defines the temperature of the hot leg T_{HL}:

$$[T_{sat}(P_1) - T_{HL}]_{ITF} = [T_{sat}(P_1) - T_{HL}]_{PWR} \tag{3.2}$$

The temperature difference in the core then determines the temperature of the cold leg T_{CL}:

$$[T_{HL} - T_{CL}]_{ITF} = [T_{HL} - T_{CL}]_{PWR} \tag{3.3}$$

The initial flow rate in the core $\dot{M}_{core}$ is scaled by the initial core power $q_{core,0}$, corrected by the heat capacity C_p change due to reduced-pressure, in order to preserve the temperature differential in the core:

$$\frac{\dot{M}_{core,ITF}}{\dot{M}_{core,PWR}} = \frac{[(q_{core,0} - q_{loss}/C_p)]_{ITF}}{[q_{core,0}/C_p]_{PWR}} \tag{3.4}$$

Counterpart tests were performed to validate the power-to-mass method used for IIST design, by comparing it to the ROSA-IV LSTF and BETHSY, both being FHFP test facilities (Liu et al. 2004). Several significant discrepancies have been identified, which are related to geometric and dynamic distortions. Compensations for heat losses, transfers between primary and secondary circuits, and potential deficiencies in local phenomena could be at the origin of these discrepancies. Despite these design discrepancies, the majority of the thermal-hydraulic parameters and events timing remain consistent.

Figure 3.3 outlines key design parameters for the ITF mentioned previously (OECD/NEA 2022).

Table 3.3: Main design parameters of some ITF

ITF	Scaling method	Loops	Core type	Power scale	Max. primary pressure [MPa]	Height scale	Time scale	Volume scale
APEX	H2TS	2	Elect.	2%	2.76 (RP)	1/4	1/2	1/192
ATLAS	3-level-s[1]	2	Elect.	10%	20.0 (FP)	1/2	$1/\sqrt{2}$	1/288
BETHSY	P-to-v[2]	3	Elect.	10%	17.2 (FP)	1/1	1/1	1/100
CCTF	P-to-v	4	Elect.	100%	0.6 (RP)	1/1	1/1	1/21
IIST	P-to-m[3]	3	Elect.	6.5%	2.1 (RP)	1/4	1/2	1/400
LOBI	P-to-v	2	Elect.	100%	15.5 (FP)	1/1	1/1	1/712
LOFT	P-to-v	2	Nuclear	100%	15.5 (FP)	1/2	1/1	1/60
LSTF	P-to-v	2	Elect.	14%	16.0 (FP)	1/1	1/1	1/48
MIST	P-to-v	2	Elect.	10%	15.5 (FP)	1/1	1/1	1/819
PKL	P-to-v	4	Elect.	10%	5.0 (RP)	1/1	1/1	1/145
PUMA	3-level-s	3	Elect.	100%	1.03 (RP)	1/4	1/2	1/400
SEMISCALE	P-to-v	2	Elect.	100%	15.0 (FP)	1/1	1/1	1/1705
SPES	P-to-v	3	Elect.	140%	20.0 (FP)	1/1	1/1	1/427

[1]Three-Level Scaling
[2]Power-to-volume
[3]Power-to-mass

3.3.2. Advanced Scaling Methods

3.3.2.1. Structure of Advanced Scaling Methods

As mentioned in section 3.3.1, there are deficiencies in the design methods that lead to suspected discrepancies between the reduced-scale and full-scale reactors. Because the similarity cannot be perfect, scaling distortions are unavoidable as a result of the compromises made in the reduced-scale facilities. Nonetheless, as suggested by PIRT, it is essential to prioritise the processes of greatest importance in a transient. It appears that there is a growing need to identify and quantify distortions. Furthermore, there are limitations when analysing these distortions observed using design scaling methods. It may be then considered contradictory to use design scaling methods to evaluate the results obtained from their application.

Different types of scaling methods have then emerged to address the need for analysis of experimental results, identification and quantification of distortions, and process prioritisation. These advanced methods or analyses are gradually becoming relevant in the nuclear power plant safety-review process. The multiplication of safety methods for the safety-review process appears to be of interest, with scaling analyses added to uncertainty analyses, CFD codes, component-scale codes, or system-scale codes for exemple. Thus, scaling now plays a role in the CSAU (USNRC 1989) and the Evaluation Model Development and Assessment Procedure (EMDAP) (USNRC 2005). This integration into the Evaluation Model (EM) procedure aims to demonstrate that the experimental database and models developed are suitable for the transposition to full-scale analysis. In other words, the scaling must demonstrate that the database and codes adequately represent the expected response of accidental transients (USNRC 2005; Bestion et al. 2017). The Appendice C describes the full EMDAP process.

In the context of advanced methods, one of the questions the thesis aims to answer is: **how scaling can identify and quantify distortions?** This question is also related to the clear intention of these methods to provide a deeper understanding of the complex phenomena that occur during a transient. This raises the second question to be addressed in the thesis: **how scaling can help in the comprehension of transient phenomena?**

In the 1990s and 2000s, there was also a growing interest in the intention to identify important phenomena in a reactor during an accident, particularly using a reinforced PIRT approach (Zuber 1991; Wilson et al. 1998; Song 2006). Thanks of the previous studies efforts, practicality, and simplicity in the previous success of the PIRT, the experts decided to adopt a four-level scale for ranking the importance of phenomena during transients (Wilson et al. 1998). This four-level scale is described in the Table 3.4 (USNRC 2008). This PIRT interest can be found in the advanced scaling methods described below. This phenomenon ranking methodology will be used in a number of studies relating to the investigation of hazards and accidents related to nuclear power plants (OECD/NEA 2018).

The PIRT criteria are established by a panel of international experts, including members of the NEA CSNI Working Groups on Fuel Safety (WGFS) and Analysis and Management of Accidents (WGAMA), as well as invited experts from industry, research organisations, and nuclear regulatory bodies. Each organisation has one vote in the ranking process (OECD/NEA 2018). The panel of international experts is listed in the Appendice D.

Table 3.4: The four-level scale used for phenomena importance ranking

Rank	Definition	Implication
High (H)	The phenomenon has a dominant impact on any of the evaluation criteria.	The phenomenon should be explicitly considered in experimental programmes and modelled with high accuracy in computational tools.
Medium (M)	The phenomenon has only a moderate impact on the evaluation criteria.	Experimental studies and analytical modelling are required, but the scope and accuracy may be compromised.
Low (L)	The phenomenon has small or no impact on the evaluation criteria.	The phenomenon should be exhibited experimentally and considered in computational tools. However, almost any model will be sufficient.
Uncertain (U)	No existing database or low-resolution database in existence. The panel is unaware of the existing modeling tools with respect to this phenomenon.	Importance should be explored through sensitivity study and/or discovery experiments and the PIRT revised accordingly.

Although the three-level scaling method was beginning to introduce them (see section 3.3.1.4), Zuber's work improved and clarified the concepts of top-down and bottom-up approaches for the framework of transients analyses (Zuber 1991).

Top-down and bottom-up approaches are concepts in the field of information processing that can be applied in a variety of situations (computer science, management, environment, philosophy, ...). The top-down approach (also known as stepwise design) divides a system into smaller sub-systems that are easier to manage. A process is characterised by bringing in raw material in order to transform it in stages, often by removing unwanted parts. The bottom-up approach, on the other hand, is the reverse process which brings together individual information from basic building blocks to a complex system. This philosophy allows for the delimitation of hard concepts or projects. The challenge lies in obtaining a solution which is simple enough to be manipulated while not sacrificing too much information. Figure 3.3 illustrates the concept of top-down and bottom-up approaches.

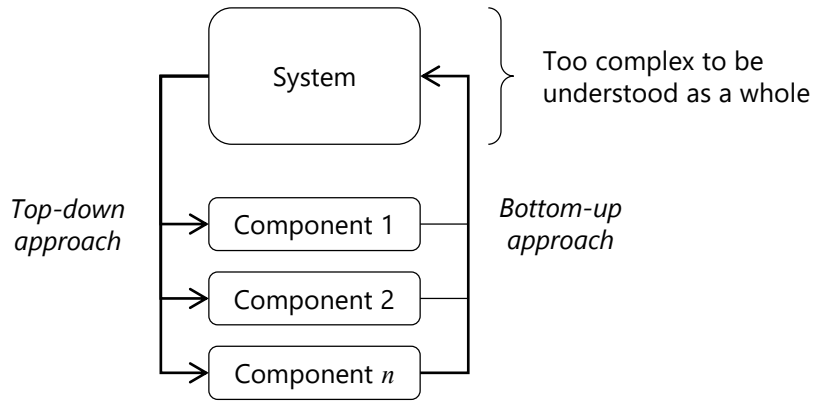

Figure 3.3: The top-down and bottom-up approaches

Scaling a global system response, as mentioned in Zuber's work, is the first top-down step. Top-down scaling approach begins with a comprehensive analysis of the system as a whole

(Zuber 1991; Zuber et al. 1998). The top-down method allows for a greater emphasis on the comprehensiveness and simplicity of the scaling methodology used. Zuber also mentions that this approach provides efficiency by resolving issues in a cost-effective and timely resolution. The advanced scaling methods, which incorporate both top-down and bottom-up approaches in their scaling analyses, are divided into two parts which go hand in hand and which operate one after the other:

- The top-down integral response analysis which implies taking the complex study system (the reactor, the ITF or the transient) as a whole and dividing it into non-dimensional parts (components). This top-down approach is a simplified way of characterizing the studied system in order to apply a scaling method. This allows the study of "scaling criteria" that will qualify the system and its complex phenomena.
- The local bottom-up approach which considers these scaling criteria to conduct the scaling analysis which allows the study of the system as a whole or the comparison to other systems.

Zuber describes the top-down approach in the context of nuclear transient thermohydraulics as an analysis - of the system as a whole, - through subsystems, - their modules - their constituents, - the different phases, - the geometrical configurations, - the fields, - and finally, the processes (Zuber 1991; Zuber 2001). A different interpretation of the scaling structure from the top-down approach is nevertheless proposed in this work, motivated on the one hand by the use of a system code for scaling method application. This is reflected in the modesty of numerical tools capabilities and the uncertainties they can introduce at too fine a scale. On the other hand, these analytical methods are claimed to be able to substitute complex computer codes and establishing overly complex scenario analyses (D'Auria et al. 2017). Authors consider that this exceeds the methods capabilities and that they are not predictive tools (Wulff et al. 2005). However, the initial description can be interpreted as an objective to be achieved in the scaling analyses framework. Figure 3.4 illustrates these top-down approaches in the context of nuclear transients.

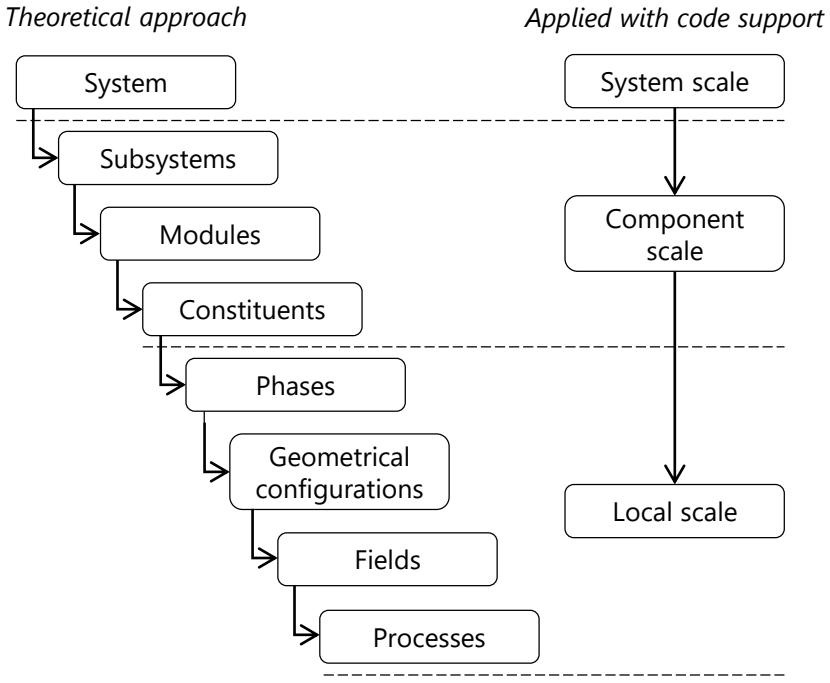

Figure 3.4: Theoretical and code support applied top-down approaches in nuclear transients

This system hierarchy allows for an orderly organisation of the scaling analysis and demonstrates an aspect that is both global and specific to the study. With this method of dividing the system, a new question arises, which the thesis must address: **can advanced scaling methods be conducted with the support of system codes to identify multi-scale distortions?**

Whereas design scaling methods were based on the respect of ratios between certain parameters or were derived from simple non-dimensional parameters, advanced scaling methods are based on the analysis and transformation of balance equations. Two facilities of different sizes can be scaled if a solution to a system of scaling equations describes the transient responses of both facilities. This is done using the same scaled and normalized time and state variables. They are in the order of unity and describe the relative magnitude of each term of the governing equations. These equations, which can be derived from mass, energy, or momentum equations, characterize the state of the global system or the selected components. For the analysis of local phenomena, constitutive relations may be added. Scaled state variables include initial and boundary conditions, scaled time, and constant coefficients in the governing equations. Depending on the method, there are several ways to obtain these non-dimensional scaling criteria from the transformation of the equations. To ensure effective scaling, these criteria must be similar for both facilities (or between the ITF and its reference reactor). Figure 3.5 illustrates these differences between design and advanced scaling methods.

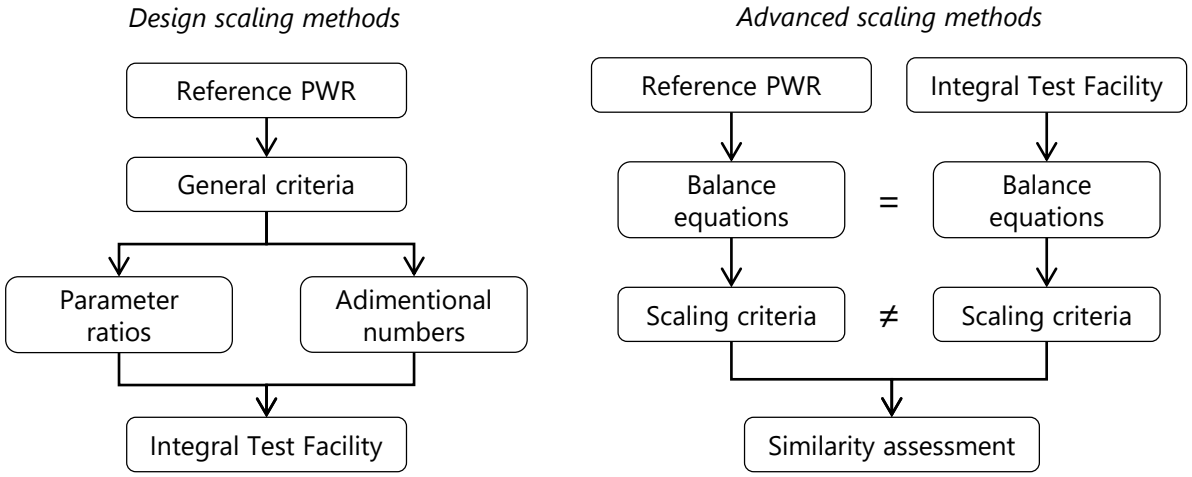

Figure 3.5: Comparison of design and advanced scaling methods

Scaling criteria represent the causality of a phenomenon and quantify the relative magnitude of their respective terms. They consider the importance of the associated transfer processes in relation to the causative process (Wulff et al. 1999). The balance equations are written to obtain the effect on the variable as well as the multiple causes of the effect. The bottom-up approach is therefore achieved through the analysis of the obtained scaling criteria.

In general, one can identify a dominant process that will be scaled with priority. The dominant process is the one that corresponds to the equation term with the largest scaling criteria. It will cause the greatest change for a state variable of the control volume. This process is the most important, unless it is known to last only a very short time in comparison to the time characteristic of the phase. For example, causing a brief and insignificant spike and being overpowered by a lesser but longer-lasting transfer process (Wulff et al. 1999). Scaling, in general, cannot catch abrupt and/or more complex system changes. The conservation equation can be scaled with the normalizing factor of its dominant term or with a common causative term for the transient phase under study. The hierarchy of phenomena and the analysis of scale distortions would be the same, only if the different systems used the same choices of normalizing factors (Wulff et al. 1999).

3.3.2.2. Concept of Scaling Analyses

Scaling analyses should be flexible and adaptable, allowing for the study of an ITF design scalability. This is accomplished by identifying and evaluating distortions between several systems and facilities in order to study, for example, the same transient. However, it should also assess the scalability of an ITF and its full-scale reference reactor. Through the state of the art of the different advanced scaling methods that will be presented in the following sections, a first interpretation is suggested, based on the basic steps of scaling analyses, that are common to the different approaches, such as those presented in Zuber's work (Zuber 1991; Zuber et al. 1998; Zuber 2005; Zuber et al. 2007):

1. Identify the phenomena of maximum importance of the transient under consideration and define a criterion to quantify it. This criterion is the Figure of Merit (FoM), as assured by the top-down approach. It could be a criterion for reactor safety. In the context of nuclear safety (e.g. for LOCA studies), the FoM is defined as the Peak Clad Temperature (PCT) or the mixture level in the core (USNRC 1989; NEA/CSNI 1989), as inspired by the CSAU and EMDAP applications (see CSAU and EMDAP flowcharts in Appendices A and C). These are crucial criteria because they prevent the core from overheating and even the release of radioactive material. As a result, the FoM enables scaling analyses and various linked studies to be focused on the ability of the nuclear reactor first containment barrier to remain intact. Following the definition of the FoM, the Parameters of Interest (PoI) that should be respected must be defined. The PoI are the criteria or phenomena that have the greatest influence and importance on the FoM within the reactor. They are identified through expert judgments, such as mentioned in section 3.3.2.1, sensitivity studies, or scaling analyses, and thus contribute to the establishment of the PIRT (ASN et al. 2017). PoI for LOCA transients can be, for example, the primary mass inventory or the primary pressure.

2. Identify the relevant phases (time periods) to properly describe the temporal evolution of the different phenomena contributing to the transient physics. It is worth noting that this stage is not explicitly defined in the first definitions of advanced scaling methods, but it appears in the first applications by the authors (Zuber et al. 1998; Wulff et al. 1999; Wulff et al. 2005; Catton et al. 2005; Zuber et al. 2007). While SET focus on a single phenomenon, IET present evolutions in transient behaviour. Phases (also known as chronological windows) are thus established based on "bifurcating events", which are temporal events where the status of the system or scenario of the transient changes more or less significantly. It is essential to delimit the phases correctly because the applications of scaling methods and calculations will be carried out through them. For example, in LOCA transients, phases can be defined based on changes in mass inventories, pressures, and specific events such as the occurrence of certain phenomena or the actuation of safety systems. These changes in the transient scenario are usually followed by changes in the physics and, as a result, important criteria and distortion possibilities. LOCA transients are typically defined in the literature by three, four, or five phase splits, characterised by physical processes and phenomena. This thesis work will take a particular interest in the phase selection (see Appendice E for considerations on transients phases establishment).

3. Identify the key (most important) phenomena that are likely to influence the Parameters of Interest (PoI). This work is established when identifying the balance equations to describe the object of study, i.e. the transient. The choice of equations is important because it provides the starting point for scaling analyses using the advanced scaling methods. The nature of the equations indirectly defines which processes and phenomena that will be focused within the

transient (Wulff et al. 1999). The equations can be applied at the chosen scales (see Figure 3.4), such as the entire system, individual or coupled components, or local areas (Bestion 2020). The "control volumes" are the regions to which the equations are applied. They are also applied to the different phases defined in the previous step. The assumptions of the equations are also an important part of the scaling analysis and the uncertainties of the results that will be obtained (Bestion et al. 2017), as it will be demonstrated in the thesis work.

4. Rank the dominant, influent, and negligible processes based on the scaling analysis. The scaling criteria for each equation, phase, and control volume defined are obtained through the application of the methods to the transient scenario. Their ranking allows to complete the PIRT process, as indicated in Table 3.4 (Wilson et al. 1998; Zuber et al. 2007; Bestion et al. 2017; Bestion 2020).

5. Identify and quantify potential distortions by comparing the scaling criteria obtained in the previous step. This evaluation can be done using expert judgement, a counterpart test between the same transient from different ITF, or a transposition to full-scale reactor. This step also allows for the identification of possible scale effects. Due to a lack of experimental data to solve the equations, these steps are mostly completed using calculation codes.

Scaling analyses take place at each of these stages. Figure 3.6 illustrates the suggested summary of these top-down and bottom-up approaches to studying nuclear transient with scaling studies. This road map depicts the thread of the different steps of scaling analyses that will be used to characterise the transients studied in this thesis.

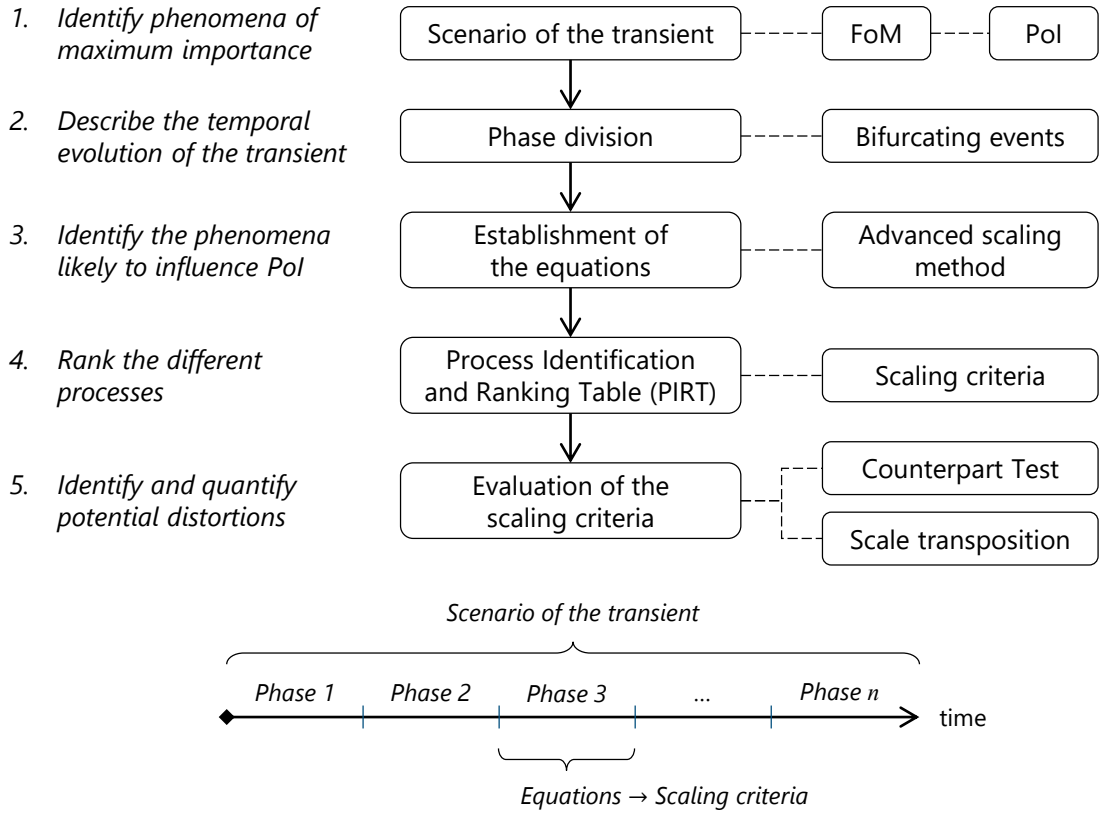

Figure 3.6: Advanced scaling analysis method road map

The intent of advanced scaling methods is clarified through these steps, which allow to assess a PIRT and an analysis of distortions and scale effects. Thereby, scaling analysis is a concrete

application aimed at addressing the scaling issue through quantitative study of various phenomena and processes in order to obtain an efficient and compact scaled data synthesis (Zuber 1991). By following this structured methodology, the thesis work will aim to provide an application guideline for scaling analyses. The following sections present advanced scaling methods for scaling analyses.

3.3.2.3. Hierarchical Two-Tiered Scaling (H2TS)

The Hierarchical Two-Tiered Scaling (H2TS) method was developed with two main objectives, as indicated by its authors (Zuber 1991; Zuber et al. 1998):

- To provide a comprehensible, systematic, practical, auditable, traceable, and technically justifiable scaling analysis.
- To provide a hierarchy through its scaling factors, providing design requirements, and thus eliminating arbitrariness in scaling through a quantitative estimation of the importance of scaling criteria.

This method is based on top-down and bottom-up approaches and is influenced by hierarchy theory (Simon 1962). H2TS introduces the concept of decomposing a complex system into several subdivided parts at different scales (see Figure 3.4). This method is also based on the normalisation of balance equations and introduces the concepts of identifying the processes important to be addressed for the PIRT through the analysis of similarity criteria. It expresses time ratios as the product of "specific frequency" and "residence time", which can be compared and ranked based on numerical values, resulting in the scaling hierarchy.

For each process, the π-monomial Π of a given magnitude ψ (mass, momentum or energy) to the control volume V_i is given by the product of the transfer characteristic frequency ω of the process n and the characteristic time τ, for the evolution of the amount of the property contained in the control volume. This product is expressed as (Zuber 1991):

$$\Pi_{\psi,n\to i} = \omega_{\psi,n\to i} \cdot \tau_{\psi,i} \tag{3.5}$$

Where the characteristic frequency $\omega_{\psi,n\to i}$ for the transfer process of a given property ψ between constituents n and i through the transfer area A_{in} is given by (Zuber 1991):

$$\omega_{\psi,n\to i} = \frac{j_{\psi,n\to i} \cdot A_{in}}{V_i \cdot \psi_i} \tag{3.6}$$

With $j_{\psi,n\to i} \cdot A_{in}$ is the transference of the property per second through the area A_{in} where $j_{\psi,n\to i}$ is the flux between constituent volumes n and i. Finally $V_i \cdot \psi_i$ is the total amount of the property contained in the volume V_i. The step 1 discussed in section 3.3.2.2 is complete. And since this can be done for each phase of the scenario, the step 2 is also complete.

The characteristic time $\tau_{\psi,i}$ can be expressed as the ratio between the property evolution on the volume and the property being transported via the volumetric flow rate Q_i:

$$\tau_{\psi,i} = \frac{V_i \cdot \psi_i}{Q_i \cdot \psi_i} \tag{3.7}$$

So the control volume balance equation can be written as:

$$\frac{V_i \cdot \psi_i}{dt} = \Delta \left[Q_i \cdot \psi_i \right] \pm \sum \left[j_{\psi,n \to i} \cdot A_{in} \right] + S_i \tag{3.8}$$

Where:

$$\Delta \left[Q_i \cdot \psi_i \right] = \Delta \left[Q_i \cdot \psi_i \right]_{in} - \Delta \left[Q_i \cdot \psi_i \right]_{out} \tag{3.9}$$

In the Eq. 3.8, ψ_i can represent a conserved property (mass, momentum, energy, ...) and S_i represents the distributed sources, such as power or forces acting internal to the control volume. The step 3 is validated.

The contributing terms of the Eq. 3.8 are normalized. Dividing by the boundary conditions $Q_{i,0} \cdot \psi_{i,0}$ yields:

$$\tau_{\psi,i} \cdot \frac{V_i^+ \cdot \psi_i^+}{dt} = \Delta \left[Q_i^+ \cdot \psi_i^+ \right] \pm \sum \Pi_{\psi,n \to i} \cdot \left[j_{\psi,n \to i}^+ \cdot A_{in}^+ \right] + \Pi_{\psi,s \to i} \cdot S_i^+ \tag{3.10}$$

The characteristic residence time of constituent i of Eq. 3.7, also called residence time is written:

$$\tau_{\psi,i} = \frac{V_{i,0}}{Q_{i,0}} \tag{3.11}$$

And the characteristic time ratio for a transfer process between constituents volumes n and i:

$$\Pi_{\psi,n \to i} = \frac{j_{\psi,n \to i,0} \cdot A_{in,0}}{Q_{i,0} \cdot \psi_{i,0}} \tag{3.12}$$

Each characteristic time ratio $\Pi_{\psi,s \to i}$ indicates the number of transfer units (of mass, momentum or energy) transferred to or from constituent i by a specific process during its residence time $\tau_{\psi,i}$ (Zuber et al. 1998). The characteristic time ratio for the distributed source term within the control volume is given by (Zuber 1991):

$$\Pi_{\psi,s \to i} = \frac{S_{i,0}}{Q_{i,0} \cdot \psi_{i,0}} \tag{3.13}$$

Transfer processes can be ranked by order of magnitude since they are defined as characteristic time ratios. These ratios will be preserved if a specific process transfer has the same effect between a model and its prototype (Zuber 1991). Once the π-monomial has been defined, the system is divided into subsystems, and each subsystem is divided into transient phases. According to Wulff et al. 1999, two criteria are necessary to complete the methodology:

- Each π-monomial group should consider the order of magnitude relative to the one whose value is equal to unity by establishing a hierarchy. The step 4 is here complete.
- Evaluating the differences between several systems, i.e. the distortions, is accomplished by dividing the π-monomial groups of one system Π_{ψ,S_1} by the π-monomial groups of another Π_{ψ,S_2}. This is done for each of the dominant processes in each phase of the transient, completing the step 5. The system with the highest π-monomial groups correspond to the system with the highest transfer processes:

$$\frac{\Pi_{\psi,S_1}}{\Pi_{\psi,S_2}} \tag{3.14}$$

Therefore, if a specific transfer process has the same effect in two systems S_1 and S_2, then the characteristic time ratios must be preserved:

$$\Pi_{\psi,S_1} = \Pi_{\psi,S_2} \tag{3.15}$$

Theses characteristic time ratio can be utilized to determine the scaling distortion D between S_1 and S_2 (Zuber 1991):

$$D = \frac{\Pi_{\psi,S_1} - \Pi_{\psi,S_2}}{\Pi_{\psi,S_1}} \tag{3.16}$$

Although the H2TS was initially developed to perform scaling analysis, it was used in the design of the APEX ITF (Reyes et al. 1998). The method has also been used in EMDAP and CSAU to perform uncertainty and safety analyses (USNRC 2005). The H2TS method is therefore at the crossroads of scaling design and scaling analysis objectives.

3.3.2.4. Fractional Scaling Analysis (FSA)

The Fractional Scaling Analysis (FSA) method, based on the general theory of fractional analysis (Novozhilov 1997), was established in three papers (Wulff et al. 2005; Catton et al. 2005; Zuber et al. 2007). The method was developed as an improvement to the previous H2TS, which required a more permissive code implementation with more "degrees of freedom" (Zuber 2001). This method presentation is also based on discussions of the main author (Zuber 2005), as well as an application carried out by its authors (Wulff et al. 2009). Like the H2TS, the FSA is a top-down and bottom-up systematic method aimed at ranking components, phenomena and processes, as well as behaviours and their importance on the FoM. It intends to simplify complex systems, such as nuclear transients, by improving flexibility, i.e. by identifying the phenomena and components of greatest interest to be studied.

The first step in the FSA is to define the studied system (see Figure 3.4) and the duration of the transient through the definition of the phases. The analysis is carried out using balance equations of mass, pressure, energy, or any other state variable which characterizes the system in an evolutionary manner. If a control volume is characterized by a single state variable denoted by ψ with change over time, one can write:

$$\frac{d\psi}{dt} \tag{3.17}$$

The previously discussed step 1 in section 3.3.2.2 is therefore completed by defining which PoI must be studied. The j terms contributing to the evolution of the variable ψ are defined for each phase of the scenario, validating the step 2. These contributors are denoted by χ. It is obtained for a specific phase:

$$\frac{d\psi}{dt} = \sum_{j}^{n} \chi_j(\psi, t) \tag{3.18}$$

Step 3 is validated by defining the contributing terms and writing the corresponding balance equations. The definition of contributing terms determines the efficiency of the scaling analysis. They can differ depending on the type of transient being studied, as well as the chosen balance equation and the assumptions that are made.

The ranking process is the next step, which aims to achieve the hierarchy of the different processes and phenomena (Wilson et al. 1998). To conduct the PIRT and beyond the scaling work, scaling criteria must be normalized. Each term χ_j, composed of one or more time-dependent $Y(t)$ variables, is normalized such as non-dimensional variables. In general, all possible combinations of thermo-physical properties and time-dependent flows or heating rates are normalized with their estimated maximum value Y_{max} (Wulff 1996; Zuber et al. 2007; Wulff et al. 2009). In many cases, the value Y_{max} corresponds to the initial value Y_0 when there is a monotonically decreasing trend of $Y(t)$ as shown in Figure 3.7. The dimensionless $Y^+(t)$ can then be defined using only the initial values, relevant operating conditions, and design parameters (Wulff et al. 2009).

$$\chi_j(\psi, t) = f(Y(t)) \tag{3.19}$$

$$Y^+(t) = \frac{Y(t)}{Y_{max}} = \frac{Y(t)}{Y_0} \tag{3.20}$$

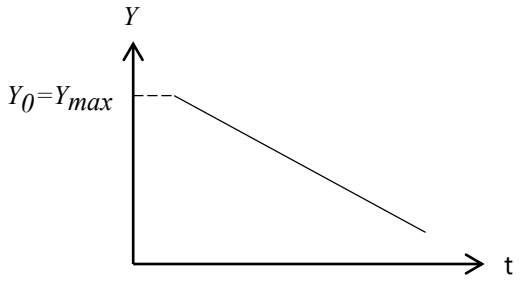

Figure 3.7: Normalization of the variables

This choice seems to be consistent with the FSA's effort to get rid of complex computational tools. There was indeed a will from the authors of the method not to make the FSA a predictive tool. Furthermore, the original aim of these methods was to drastically reduce the need for calculation codes in the design of reduced scale experiments. Given the number of studies that use these methods to support calculation codes, the author highlights this paradoxical aspect. One of the thesis questions is moreover to provide guidance in the use of scaling methodologies for code support applications.

The normalized contributing terms are obtained. They correspond to the non-dimensional Agents of Change (AoC) $\phi^+_{\dot{\psi},\chi_j}$ and define the processes acting on the studied variable ψ. AoC are calculated by multiplying Fractional Rate of Change (FRC) $\omega_{\dot{\psi},\chi_j}$ expressed in s^{-1}. They are measures of the relative magnitude of a phenomenon on the variable (Zuber et al. 2007; Wulff et al. 2009). Considering the expression of $\phi^+_{\dot{\psi},\chi_j}$:

$$\frac{d\psi^+}{dt} = \sum_j \omega_{\dot{\psi},\chi_j} \cdot \phi^+_{\dot{\psi},\chi_j} \tag{3.21}$$

According to the application of Wulff et al. 2009, the AoC are represented by the product of fixed FRC, i.e the initial $\omega_{\dot{\psi},\chi_j}$ and a time-dependent non-dimensional rate of change (e.g.

the depressurization rate of change for LOCA application). An adaptation of this term within the framework of the thesis is to take an average of the variables during the phase into account. This allows the variables to be more representative of the transient behaviour by taking into account their evolution over time. For example, in the case where an initial value would not be representative of the changes that occur during the phase. The term $\bar{Y}$ replaces the term corresponding to the maximum value Y_{max} or the initial value Y_0.

The FRC are shown being the cause ϕ over the effect ψ (Zuber 2001; Zuber 2005; Zuber et al. 2007). The facility characteristics and operating conditions are then incorporated into the fixed FRC (Wulff et al. 2009):

$$\omega_{\psi,\chi_j} = \frac{1}{\psi} \cdot \frac{d\psi}{dt} = \frac{\phi_{\psi,\chi_j}}{\psi} \tag{3.22}$$

The dominant phenomena in the different phases of the transient are identified by ranking them according to the relative magnitude of the FRC $|\omega_{\psi,\chi_j}|$ or the effect metrics $|\Omega_{\psi,\chi_j}|$ (Wulff et al. 2009). They represent the rate of change of the variable ψ over a reference period $\tau_{ref} = \tau$, consequence of the contribution of the AoC. The work of phenomena ranking (step 4) contributing to the PIRT process is reached.

$$\Omega_{\psi,\chi_j} = \omega_{\psi,\chi_j} \cdot \tau_{ref} \tag{3.23}$$

As a first approximation, the residence time or clock time τ can be defined as the ratio of the volume of the system studied to the volume flow rate, as in open flow systems or convective processes (Zuber 2001; Zuber 2005; Zuber et al. 2007):

$$\tau = \frac{V}{Q} \tag{3.24}$$

As shown in Figure 3.8, the effect metrics can be synthesised in a system matrix that combines components and processes. The system matrix can represent the scaling criteria derived from a system balance equations and can be used to depict the interactions between its various components (Zuber et al. 2007). For example, by defining the temporal phases, the evolution of the system as a result of the processes can be obtained. The impact of the hierarchy of scaling criteria is then directly observed.

Components	**Process Effect Metric**			
	Ω_1	Ω_2	…	Ω_n
Phase 1				
Phase 2				
Phase 3				
Phase *n*				

System Matrix

Hierarchy of processes
$\Omega_1 > \Omega_2 > \ldots > \Omega_n$

Figure 3.8: Hierarchy of scaling criteria

Step 4 contributing to the PIRT, and scaling work can be finished at this point if we only want to consider the hierarchical analysis of an individual system through its processes. However, the application of time scaling can be taken a step further by considering the entire study through a temporal analysis. This work is required in order to compare the scaling criteria on different systems and allows to identify potential distortions or scale effects (validating step 5). There are two approaches to time scaling, both with the aim of normalizing the time t. This condition can be satisfied depending on the objectives of the intended scaling work (Wulff et al. 2005; Catton et al. 2005; Zuber et al. 2007):

- Either by dividing the FRC by a dominant reference FRC, in which case they will reflect their relative importance in comparison to the reference, but time may be incorrectly interpreted.
- Either by normalizing the FRC by an aggregated global FRC that reflects the system temporal representation.

In the case of the *Time Scaling for Relative Importance of Agents* (Zuber et al. 2007), all the FRC of Eq. 3.21 are divided by the dominant one of the phase, noted $\omega_{\dot{\psi},\chi_D}$, to allow evaluation of the contribution of each term:

$$\frac{d\psi^+}{dt^+} = \frac{\sum\limits_j \omega_{\dot{\psi},\chi_j} \cdot \phi^+_{\dot{\psi},\chi_j}}{\left|\omega_{\dot{\psi},\chi_D}\right|} \tag{3.25}$$

Simplifying and denoted by the relative FRC $\widehat{\omega}_{\dot{\psi},\chi_j}$:

$$\widehat{\omega}_{\dot{\psi},\chi_j} = \frac{\omega_{\dot{\psi},\chi_j}}{\left|\omega_{\dot{\psi},\chi_D}\right|} \tag{3.26}$$

It is obtained:

$$\frac{d\psi^+}{dt^+} = \widehat{\omega}_{\dot{\psi},\chi_D} \cdot \phi^+_{\dot{\psi},\chi_D} + \sum_j \widehat{\omega}_{\dot{\psi},\chi_j} \cdot \phi^+_{\dot{\psi},\chi_j} \tag{3.27}$$

With:

$$\left|\widehat{\omega}_{\dot{\psi},\chi_j}\right| < 1 \tag{3.28}$$

$$\widehat{\omega}_{\dot{\psi},\chi_D} = 1 \tag{3.29}$$

Taking into account the dominant phenomenon, the transient new characteristic reference time can be approximated as:

$$\tau_{ref} = \tau_D \approx \frac{1}{\left|\omega_{\dot{\psi},\chi_D}\right|} \tag{3.30}$$

The dimensionless time t^+ of Eq. 3.27 is finally defined as:

$$t^+ = \frac{t}{t_D} = \tau_D^+ \tag{3.31}$$

The effect metrics $\Omega_{\dot{\psi},\chi_j}$ that allow scale distortions to be quantified are expressed as (Zuber et al. 2007):

$$\Omega_{\dot{\psi},\chi_j} = \omega_{\dot{\psi},\chi_j} \cdot \tau_D = \widehat{\omega}_{\dot{\psi},\chi_j} \tag{3.32}$$

The *Time Scaling for an Aggregate Response Time* (Zuber 2005; Zuber et al. 2007) defines a global FRC denoted $\bar{\omega}_{\dot{\psi}}$, which is the sum of all the FRC of Eq. 3.21 in consideration of their sign:

$$\bar{\omega}_{\dot{\psi}} = \sum_j \omega_{\dot{\psi},\chi_j} \tag{3.33}$$

And the characteristic reference time:

$$\tau_{ref} = \frac{1}{\left|\bar{\omega}_{\dot{\psi}}\right|} \tag{3.34}$$

This overall FRC considers a correct time-dependent response rate for all AoC combined. With the normalized time t^+, the effect metrics $\Omega_{\dot{\psi},\chi_j}$ are defined as follows:

$$\left|\Omega_{\dot{\psi}}\right| = \left|\bar{\omega}_{\dot{\psi}}\right| \cdot t = t^+ \tag{3.35}$$

Step 5 has been validated. The use of this method and its interpretation enables scaling analyses to be performed by comparing the scaling criteria, which are the effect metrics $\Omega_{\dot{\psi},\chi_j}$, between several systems (e.g. differents ITF or between an ITF and its reference reactor). Because FRC and effect metrics are defined as additives (Zuber 2001), the distortions D can directly be determined as the difference between the effect metrics of two systems S_1 and S_2:

$$D = \Delta\Omega_{\dot{\psi},\chi_j} = \left(\Omega_{\dot{\psi},\chi_j}\right)_{S_1} - \left(\Omega_{\dot{\psi},\chi_j}\right)_{S_2} \tag{3.36}$$

The H2TS and the FSA, both established by Zuber, have strong similarities. Reasons for the "scaling controversy" include the choice of the of equations to define the scaling criteria, as well as the perspective of code applicability and the impact that the user may have on the results of the methods. More details about the similarities and differences between the H2TS and FSA methods will be discussed in this thesis through a comparative study of theses methods in chapter 5.

3.3.2.5. Dynamical System Scaling (DSS)

The Dynamical System Scaling (DSS) method was developed with the aim of providing a method for incorporating the dynamic response of thermal-hydraulic processes into the scaling framework (Reyes 2015). The limitations of the H2TS and FSA approaches in correctly evaluating time-dependent effects can explain this approach (Reyes et al. 2015). Attempts were made to assess the development of methods that considers the dynamics of the phenomena in order to extend the time-dependent effects to H2TS and FSA (Dzodzo 2009; Achilli et al. 2012). The DSS is a method derived from H2TS and FSA that incorporates the dynamic response of the system into the scaling analysis.

Through the development of the DSS, a demonstrative analysis of the method applicability to the optimization of facility design for simple transients was carried out (Yurko et al. 2015). Another study presented preliminary results on the use of DSS for predicting dynamic responses to LB-LOCA transient data tests on LOFT and SEMISCALE ITF (Frepoli et al. 2015).

The DSS concept is based on converting the physical processes of the transient into space-time coordinates. The physical similarity of two trajectories in an inertial space-time can be interpreted as the similarity of two physical processes in two clock-time systems using the inertial coordinate invariance transformation (Reyes 2015). The evaluative analysis of distortions is based on the quantification of the deviation of curves (corresponding to time-dependent processes) in this space.

Consider a control volume V containing a conserved quantity Ψ (specific mass, momentum or energy, validating the step 1 and 3) that varies in relation to an external reference time measurement t, depending on the position $\vec{x}$ in the control volume. A local instantaneous surface velocity $\vec{u}_S$ within the control volume defined by a deformable control surface and an outward vector $\vec{n}$ is assumed. This amount may change as a result of material transport $\Psi(\vec{u}-\vec{u}_S)\cdot\vec{n}$ into or out of the control volume, or as a result of a flux transport $(\vec{j}\cdot\vec{n})$ applied to a surface. It may also change due to volumetric sources or sinks ϕ_v. External fields actions ϕ_f can also change the amount of retained quantity. The integral balance equation for the system is finally written with all of these agents of change φ_i (Reyes 2015):

$$\frac{d}{dt}\iiint_V \Psi(\vec{x},t)\,dV = \iiint_V (\phi_v+\phi_f)\,dV + \iint_A (\vec{j}\cdot\vec{n})\,dA - \iint_A \Psi\,(\vec{u}-\vec{u}_S)\cdot\vec{n}\,dA = \sum_{i=1}^{n}\varphi_i \quad (3.37)$$

The normalized integral amount of a conserved quantity β at a given instant is defined by dividing the conserved quantity by a reference quantity Ψ_0:

$$\beta(t) = \frac{1}{\Psi_0}\iiint_V \Psi(\vec{x},t)\,dV \quad (3.38)$$

The reference quantity is a temporal variable ideally defined as the maximum value of the integrated conserved quantity for the considered process or the maximum value in the studied interval (phases of the step 2). This reference quantity is analogous to the normalization performed in Eq. 3.20 of the FSA. The parameter $\omega(t)$ corresponding to the sum of agents of change is then defined:

$$\omega(t) = \frac{1}{\Psi_0}\left[\iiint_V (\phi_v+\phi_f)\,dV + \iint_A (\vec{j}\cdot\vec{n})\,dA - \iint_A \Psi(\vec{u}-\vec{u}_S)\cdot\vec{n}\,dA\right] = \frac{1}{\Psi_0}\sum_{i=1}^{n}\varphi_i \quad (3.39)$$

By substituting the equations 3.38 and 3.39 in 3.37, the process time τ is obtained:

$$\frac{\beta}{t} = \omega \Rightarrow \tau = \frac{\beta}{\omega} \quad (3.40)$$

Taking the process derivative of Eq. 3.40 with respect to clock time, the differential change of β and ω are obtained:

$$\frac{d\tau}{dt} = \frac{1}{\omega}\frac{d\beta}{dt} - \frac{\beta}{\omega^2}\frac{d\omega}{dt} = 1 - \frac{\beta}{\omega^2}\frac{d\omega}{dt} \quad (3.41)$$

Finally, the time process transformation is obtained by defining the temporal displacement rate D (Reyes 2015):

$$D = \frac{d\tau - dt}{dt} = -\frac{\beta}{\omega^2}\frac{d\omega}{dt} \tag{3.42}$$

The "1-metric" is defined by the following equation, which accounts for the infinitesimal time reference interval, allowing measurement of the time dilation or contraction (and thus distortions) of the studied processes:

$$d\tau = (1 + D)\ dt \tag{3.43}$$

Each point on the $\beta - \omega$ plane represents a system state. A curve is drawn by calculating τ, and its trajectory represents the evolution of a transient process in the $\beta - \omega - \tau$ space-time. The arc length (also known as the action) describes the process trajectory and can be compared to others processes, which contributes to the PIRT (validating step 4):

$$\tau_S = \int_{t_1}^{t_2} (1 + D)\ dt \tag{3.44}$$

The thermodynamic response of two processes will be similar if the curves of the two processes remain merged. This concept illustrated in the Figure 3.9 (Reyes 2015). The covariance principle, on the other hand, can be used to measure the potential distortions between two systems S_1 and S_2 (e.g. differents ITF or an ITF and its reference reactor):

$$\frac{1}{\omega_{S_1}}\frac{d\beta_{S_1}}{dt_{S_1}} = \frac{1}{\omega_{S_2}}\frac{d\beta_{S_2}}{dt_{S_2}} \tag{3.45}$$

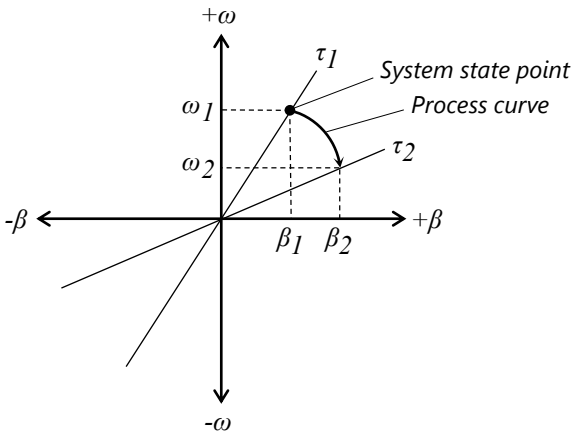

Figure 3.9: Concept of process curve in $\beta - \omega - \tau$ space-time of the DSS method

The following Eq. 3.46 introduces an effect parameter $\tilde{\Omega}$ inspired by Zuber's effect metrics Ω in Eq. 3.23. This effect parameter represents the combination of all the transient transfer processes and their varying characteristic times. It allows the normalization of the coordinates, enabling for the normalized temporal displacement rate and the quantification of distortions between two systems (validating step 5).

$$\tilde{\Omega} = \omega \cdot \tau_S \tag{3.46}$$

More details on this complex method can be found in the method's full description (Reyes 2015), particularly through the generalisation of the possible transformations. Recent studies shows results for scaling distortion assessment using the DSS (Liu et al. 2022). Nonetheless, the DSS is still limited to applications involving simple dynamic processes, and the author of the method emphasises that its application to integral systems is still in development.

3.3.2.6. Analogies Between H2TS, FSA and DSS

Several common aspects can be found between these advanced scaling methods. The first reason for these similarities is the fact that H2TS and FSA are proposed by the same authors and based on the similar concepts. According to D'Auria et al. 2010, "Zuber's numerous contributions deserves special mention for his work and impact in the framework of scaling analyses". The H2TS is a first method that aims to approach scaling as it was conceived in a different way, with the intention of minimizing arbitrariness in determining scaling parameters. This gives to the H2TS a particular place in thermal-hydraulic and transient behaviour analyses. This was particularly successful with its use in projects related to EMDAP and CSAU (USNRC 2005). The FSA was then developed to improve the H2TS in the analysis of complex systems by giving the user more flexibility and opening up the parallel of their applications with the calculation codes, despite the fact that they are not specifically designed for that (Bestion et al. 2017). The DSS then incorporated the H2TS and FSA visions, but on a different formalism (Reyes 2015). The DSS intended to develop an analysis to close gaps in the consideration of the temporal dynamics of transient processes.

The same normalisation concept is used for the contributing terms of the balance equations. These are the Agents of Change in the FSA that represent these individual reference values, whereas phenomena in the H2TS are represented by the transference of the property. In terms of physical meaning, the DSS conservation equation is also similar to those established in H2TS and FSA. For comparison, these equations can be rearranged to match a similar form. This is accurate only if the same equations are selected initially.

The three methods calculate scaling criteria, but in different ways. In the H2TS, the scaling criteria are the time-dependant π-monomials, and in the FSA, they are the non-dimensional effect metrics. H2TS and FSA take into account the ratio of the indicators of the intensities of the processes over the studied variable to calculate them. Individual reference values are used to determine the scaling criteria in the H2TS. In the FSA, an aggregate of individual values is used. This is also the case in DSS, where the effect parameters are defined by a combination of transfer processes.

The three methods differ noticeably in how they account for time. The reference time in H2TS is defined as the ratio of the control volume and the convective volumetric flow rate (Zuber 1991). FSA equivalence corresponds to the time scaling for relative importance of agents, or effective FRC (Zuber et al. 2007). Dimensionless effect metrics are directly linked to the dominant process because FRC take the characteristic time of the processes into account. As stated in Bestion et al. 2017, "The FSA determines scale distortion quantitatively from the ratios of fractional rate changes for each specific agent of change. H2TS computes scale distortion by taking ratios of dimensionless characteristic-time ratios". Although the FSA has better time scaling than the H2TS, the time consideration in both methods remains "static" and has no direct influence on the scaling analysis results. The DSS assess the normalized time constant and accounts for a temporal displacement rate during the transient period of interest.

Finally, in the quantification of distortions, H2TS and FSA evaluate the normalized scaling criteria of the same process between two (or more) systems to evaluate the differences between them. These normalized criteria are constant and evaluated at fixed reference values. The time-dependence of the distortion analyses due to the arc lengths describing the trajectory of the curves corresponding to the processes is an undeniable improvement of the DSS.

In the applications realized so far by the different methods, only the H2TS was used as an advanced design method for an ITF (Reyes et al. 1998). Furthermore, only H2TS and FSA have been used for scaling analyses on IET at the system scale (Wulff et al. 2009; Muñoz-Cobo et al. 2018; Dzodzo et al. 2019; Berna et al. 2022). The DSS still needs to be optimized as it cannot yet be used on a complete transient (Reyes 2015; Yurko et al. 2015).

3.4. Assessment and Objectives

As seen throughout this chapter, scaling is a current challenge that is becoming increasingly relevant in nuclear thermal-hydraulic studies in accidental situations.

A challenge in its application aimed at the design of new reduced-scale facilities. Indeed, scaling must always provide better methods to meet cost-efficiency or cost-representativeness requirements, as in the design of ITF.

A challenge in its post-experimental applications, for the treatment of results, and its intention to provide analyses of identification and ranking of key transient phenomena to participate in the establishment of the PIRT. There is also an ambition to address scaling issues and acquire a methodology for identifying and quantifying transient distortions between systems.

An observation that can be made about transients studies in thermal-hydraulic, and therefore about the intentions of scaling, is their peremptory transition to the use of numerical tools. This is clearly the case in the applications of scaling methods, where a transition characterized by the support of the calculation codes can be distinguished. Given their simplicity of application, design scaling methods are not intended to be used with codes. However, although they were not initially conceived for this purpose, advanced scaling methods appear to be suitable for a posteriori analyses that could be supported by codes. This is illustrated in Figure 3.10.

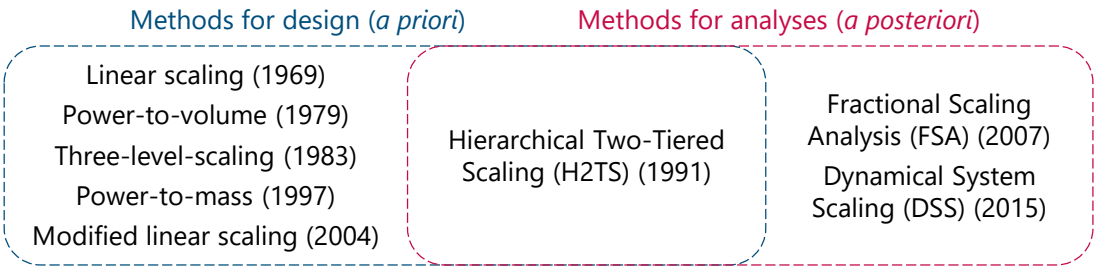

Figure 3.10: Evolution of the applications of the scaling methods

The current manuscript intends to address a number of issues and questions raised by this state of the art. First, the manuscript aims to answer how scaling analyses can help in the complex transient phenomena comprehension. This question is part of the process of improving scaling methods for analyses by considering how far the top-down and bottom-up approaches can be carried.

An important topic addressed in the manuscript is how advanced scaling methods allow the identification and quantification of inter-system distortions. The relevance of this question stems

from the objective of evaluating the impact of ITF design choices and IET results in comparison to what is predicted for their respective full-scale reactor. Particular attention will be paid here to the top-down and bottom-up approaches, with the intention of providing a connection between the different depths that scaling may allow, such as system, component, and local scales.

The use of calculation codes in scaling support is a significant concern, particularly when used with methods that were not initially conceived for this purpose. The use of a system code for scaling analyses (presented in chapter 4) emphasizes the importance of its capability to evaluate multi-scale distortions. Furthermore, one can inquire whether scaling can support and improve system codes.

The thesis also intends to highlight the current limitations of scaling analysis and scaling methods for the study of transients in nuclear thermal-hydraulic. Suggestions for perspectives, improvement and applications of the scaling analyses and methods are made relying on the thesis results.

Finally, since no handbook for scaling methods exists, one objective of this manuscript is to provide guidance in scaling methodology application to nuclear transients with system code support.

The FSA method was chosen to answer these questions through the studies in this thesis. This choice is justified on the one hand, by already existing studies using the H2TS method (see section 3.3.2.3). The FSA has so far few concrete applications to complex transients and remains theoretical. The FSA presents therefore a certain research interest in its assessment. On the other hand, the FSA is an improvement of the H2TS, with a better structure of top-down and bottom-up approaches, as well as a more comprehensive consideration of temporal parameters (see section 3.3.2.4). Finally, as mentioned in section 1, the DSS method is not yet mature enough to conduct complex analyses (see section 3.3.2.5).

Several studies will be conducted to address these questions and issues in the thesis. The objective of chapter 5 is to investigate the applicability of the FSA method on a part of a 1% SB-LOCA transient. On the one hand, to establish the hierarchy of the influence of transient phenomena. And on the other hand, to confirm that FSA method achieves the same results as the H2TS method. For this purpose, mass and simplified pressure equations characterising an experimental transient at the system/component scale have been established. The aim is to identify the phenomena that have the most influence on the transient in order to evaluate its behaviour using the scaling criteria obtained by applying the FSA, which can be analytically compared to those obtained with the H2TS.

The objective of chapter 6 is to apply the FSA method to an 6% SB-LOCA transient in order to evaluate its capability to identify and quantify inter-systems distortions at the system/component scale. For this purpose, the FSA method was applied to mass and general pressure equations to establish the hierarchy of the influence of transient phenomena. The analysis is performed on the full-transient of a counterpart test of two experimental facilities and a full-scale nuclear reactor. Finally, this study identifies some key transient processes that merit further investigation.

CHAPTER 4
The CATHARE System Code

This chapter is intended to provide a brief presentation of the CATHARE calculation code. In this thesis, CATHARE is used to obtain the validated predictive results required for the scaling analyses of the studies in the following chapters. A history of the CATHARE code development is provided. The generic set of equations is described, as well as the components modelling structure. Finally, the code validation work is presented.

4.1. History of the CATHARE Code

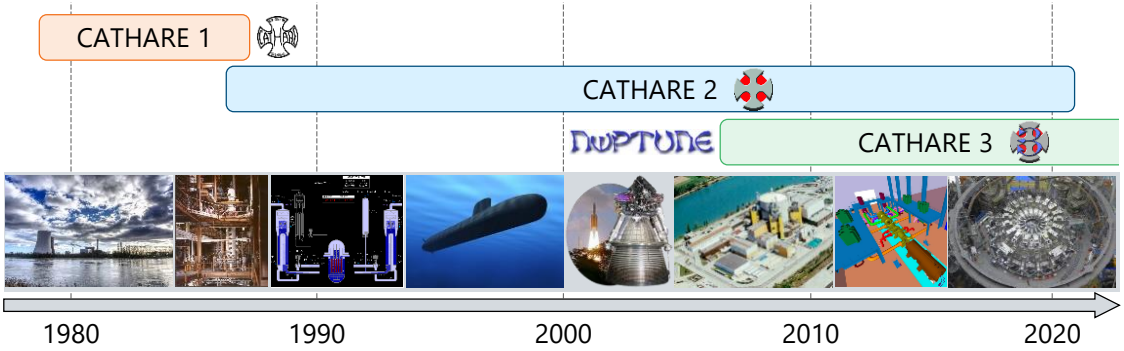

Figure 4.1: History of the CATHARE code

CATHARE (Code Avancé de ThermoHydraulique pour les Accidents de Réacteurs à Eau) (CEA 2021a) is a system code that was developed in 1979 by a collaboration between the CEA (French Atomic Energy Commission) and EDF (Electricity of France) in its first version, CATHARE 1. It was initially developed to perform safety analysis with best estimate computations (i.e the best one with current technology in a moving target) of thermal-hydraulic transients in PWR. It has also been used as a nuclear power plant analyser in simulator applications since 1983, providing real-time results for a full training scope. The first tests on the french BETHSY ITF in 1986 established the basis for the Verification, Validation & Qualification Strategy (VV&Q) process (CEA 2021b), resulting in the release of the first validated version of the CATHARE 1 code in 1987 (Bestion 1990).

The development of the CATHARE 2 version was launched in 1988 and its industrial version was released in 1996, integrating new modules and features into the code. The collaboration between TechnicAtome and the CATHARE team began in 2000 in order to collaborate on improving the safety and efficiency of nuclear propulsion. The CATHARE code has also been used in the framework of projects for space applications since 2004, notably through collaborations with ArianeGroup (Bachelet

2018).

The CATHARE 3 version was launched in 2006 in the frame of the NEPTUNE project (Guelfi et al. 2007; Emonot et al. 2011), which began in 2001 with the support of Framatome (ex-AREVA-NP) and IRSN (Radio-protection and Nuclear Safety Institute). In 2019, the first industrial version of CATHARE 3 for PWR applications was released (Préa et al. 2020). Figure 4.1 shows the history of the CATHARE code.

The CATHARE 3 code is used for the studies presented in this manuscript. The following sections then describe the equations and modelling structure of this version of the code.

4.2. The Two-Fluid-6-Equations Model

CATHARE is established on the solution of a two-phase flow (liquid-vapour) six-equations model of mass, energy and momentum, described in Ishii 1975. These equations are solved for each phase: liquid l and vapour v. The vapour phase may also contain non-condensible gases. The main unknown variables are the enthalpy H_l, H_v (or temperature T_l, T_v), the pressure P, the void fraction α_k (or mass fraction X_i), and the velocity u_l, u_v. These variables represent the averaged values over the cross section (area A). Validated physical closure laws, shown in red in Eq. 4.1, 4.2, and 4.3, solve the transfers of mass, momentum, and energy between phases (Bestion 1990).

Mass balance equation

$$\begin{aligned} \frac{\partial}{\partial t}(A\cdot\alpha_k\cdot\rho_k)+\frac{\partial}{\partial z}(A\cdot\alpha_k\cdot\rho_k\cdot u_k) = &\quad \text{Advection terms} \\ (-1)^{\alpha}\cdot A\cdot\Gamma &\quad \text{Phase change} \\ +S_k &\quad \text{Source term} \end{aligned} \tag{4.1}$$

Γ is the mass exchange between the liquid and vapour phases (Bestion 1990). The S_k term gathers any mass sources (or sinks) for each phase.

Momentum balance equation

$$\begin{aligned} A\cdot\alpha_k\cdot\rho_k\cdot\left[\frac{\partial u_k}{\partial t}+u_k\cdot\frac{\partial u_k}{\partial z}\right] &\quad \text{Advection terms} \\ +A\cdot\alpha_k\cdot\frac{\partial P}{\partial z}+A\cdot P_i\cdot\frac{\partial\alpha_k}{\partial z} &\quad \text{Pressure terms} \\ +(-1)^{\alpha}\cdot A\cdot\beta\cdot\alpha\cdot(1-\alpha)\cdot\rho_m &\quad \text{Added mass terms} \\ \cdot\left[\frac{\partial u_v}{\partial t}-\frac{\partial u_l}{\partial t}+u_v\cdot\frac{\partial u_v}{\partial z}-u_l\cdot\frac{\partial u_l}{\partial z}\right] = & \\ (-1)^{\alpha}\cdot A\cdot\Gamma\cdot(u_i-u_k) &\quad \text{Momentum transfer} \\ -(-1)^{\alpha}\cdot A\cdot\tau_i &\quad \text{Interfacial friction} \\ -\chi_f\cdot C_k\cdot\frac{\rho_k}{2}\cdot u_k\cdot|u_k| &\quad \text{Wall regular friction} \\ -A\cdot\frac{\kappa}{2\cdot\Delta Z}\cdot\alpha_k\cdot\rho_k\cdot u_k\cdot|u_k| &\quad \text{Singular friction} \\ +A\cdot\alpha_k\cdot\rho_k\cdot g_z &\quad \text{Gravity force} \\ +\frac{R\cdot(1-\alpha_k)}{4}\cdot P_i\cdot\frac{\partial A}{\partial z} &\quad \text{Stratification term} \\ +SM_k &\quad \text{Source term} \end{aligned} \tag{4.2}$$

On the first line, the advection terms is described including the eulerian acceleration term. Then comes the pressure terms on the second line, P_i being the interfacial pressure (between liquid and vapour). It reflects the presence of a force at the interface as a result of pressure field heterogeneity in the transverse direction, especially in the case of stratified flows. On the third line, there is a term called added or virtual mass β, which is important for highly dispersed flows (Bestion 1990) (with ρ_m the liquid-vapour mixing density). After the equal sign, there is a term quantifying the contribution of momentum from one phase to the other by phase change, u_i being the velocity at the interface. The following term describes interfacial friction τ_i, quantifying the viscous volume forces at the interface. The next terms represent wall friction (with the wall friction factor C_k, the friction perimeter χ_f), singular (with the friction coefficient κ) and then gravity losses (with the gravitational acceleration g_z). The penultimate term considers the pressure distribution in a variable cross-section flow, where R is the stratification rate. The final term provides the source or sink of momentum contributions SM_k to the control volume.

Energy balance equation

$$
\begin{aligned}
& A \cdot \frac{\partial}{\partial t}\left(\alpha_k \cdot \rho_k \cdot \left[H_k + \frac{u_k^2}{2}\right]\right) && \text{Advection terms} \\
& + \frac{\partial}{\partial z}\left(A \cdot \alpha_k \cdot \rho_k \cdot u_k \cdot \left[H_k + \frac{u_k^2}{2}\right]\right) && \\
& -A \cdot \alpha_k \cdot \frac{\partial P}{\partial t} = && \text{Pressure term} \\
& A \cdot q_{ki} + \chi_c \cdot q_{wk} && \text{Heat transfer} \\
& +(-1)^{\alpha} \cdot A \cdot \Gamma \left[H_k + \frac{{u_i}^2}{2}\right] && \text{Impulsion transfer} \\
& +A \cdot \alpha_k \cdot \rho_k \cdot u_k \cdot g_z && \text{Gravity force} \\
& +SE_k && \text{Source term}
\end{aligned}
\tag{4.3}
$$

The advection terms are written on the first and second lines and are made up of enthalpy and kinetic mass energy variation terms from the k phase. The term on the third line corresponds to the pressure variation $\partial P/\partial t$ induced by the way the energy equation is written: this balance is expressed in enthalpy rather than internal energy of the fluid. Since $H = U + PV$, this term is subtracted from the balance. The first term after the equal sign represents heat exchange at the phase-interface q_{ki}. The second term represents the heat exchange contributions at the walls-phase q_{wk} (with the heating perimeter χ_c). The next line describes the energy input due to phase changes. The penultimate term describes the variation of gravitational potential energy. Finally, the last term SE_k describes the energy sources or sinks.

CATHARE allows for the prediction of two-phase flows encountered in a wide range of parameters in PWR simulation. It provides pressures ranging from 0.1 to 20 MPa and temperatures ranging from 0 to 1500 °C, with high thermal non-equilibrium between phases possible.

4.3. The Modelling Structure

CATHARE uses a modular structure for thermal-hydraulic modelling, allowing the meshing of assemblies ranging from experimental test facilities to complex installations such as nuclear power plants. The following modules are used to represent any SETF, ITF, or reactor primary and secondary

circuits:

- The 1-D (or axial) module used to describe pipe flow. The 1-D module is a succession of truncated cones (or cylinders) in which the local instantaneous mass, momentum and energy equations are averaged for each phase over the continuous cross section and over time. The 1-D module is used to represent circuits formed by a series of axial pipes (at an angle θ). It allows the representation of a reactor core, SG, cold and hot legs for example. The 1-D module neglects the viscous stress tensor, the work of interfacial forces and pressure distribution, and the axial mass diffusion in the energy equation.
- The 0-D (or volume) module, composed of two nodes describing large size plena. The 0-D module is divided into four phases: - a continuous liquid phase, - a dispersed gas phase (or bubble phase), - a continuous gas phase - and a dispersed liquid phase (or drop phase). The 0-D module is used to represent large-capacity components with several connections such as pressurizer, plenum or SG channel head. The thermal-hydraulic quantities are assumed to be horizontally uniform, with a vertical stratification of temperatures and void fraction. The velocities in the volume are assumed to be small in comparison to the velocities at the junctions. The inertial forces are also assumed to be negligible in comparison to the gravity forces.
- The 3-D module to describe multidimensional effects in the RPV. The 3-D model contains a large number of solid structures allowing a better definition of the volumes occupied by the fluid and by the structures (volumic and surface porosity). The 3-D module is mainly used to model the Reactor Pressure Vessel (RPV) of a reactor. It supports the representation of a larger number of solid structures (rod-bundles, spacer grids, ...). And the purpose is to get a three-dimensional representation flow circulation, thermal diffusion and void fraction.
- The BC (boundary condition) module, set at the extremity of the previous modules, and giving model directives and properties for incoming or outgoing flows. The hydraulic conditions and the nature of the fluid are defined in the BC module, including pressures, enthalpies, velocities, mass flow rates for liquid or vapour, and void fraction (or mass fraction).

Various sub-modules can be connected to the main modules to complete the modelling and to better describe the mechanical and thermal non-equilibrium which may be found in various components of reactor circuits. The discretisation of the terms in the set of equations is fully implicit in the 1-D and 0-D modules, and semi-implicit in the 3-D elements. The resulting non-linear equations are solved using an iterative Newton solver. Figure 4.2 depicts the 1-D, 0-D, and 3-D modules of the CATHARE code.

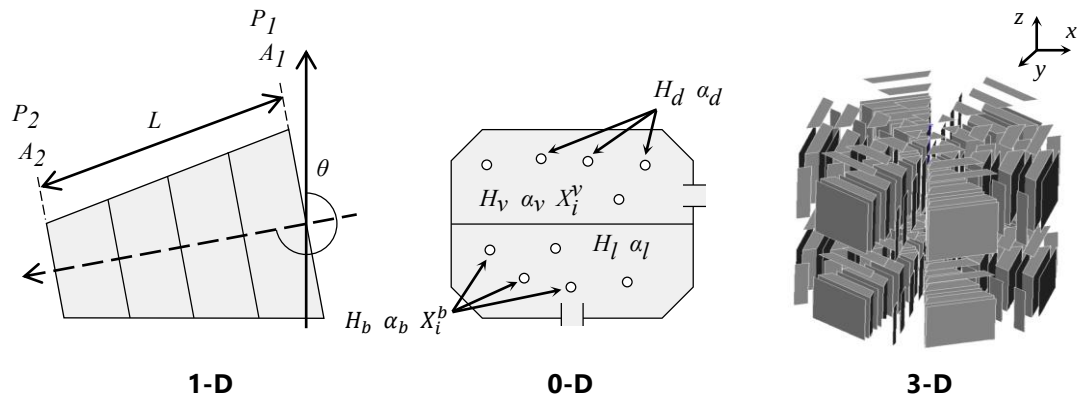

Figure 4.2: The CATHARE modules

4.4. The CATHARE Verification and Validation

To achieve a confidence in the results of the CATHARE code predictions, it is necessary to ensure that the physical laws and models are accurate (ASN et al. 2017). These closure laws represent 15 terms in the three balance equations solved for each phase, and they involve about 200 correlations deduced from the literature and validated on SET. The CATHARE 3 closure terms are summarized in the Table 4.1.

Table 4.1: The CATHARE 3 closure terms

Momentum transfers terms			**Energy transfers terms**		
E	Entrainment fraction	-	q_{li}	Liquid-interface heat flux	W/m^3
P_i	Interfacial pressure	Pa	q_{vi}	Vapour-interface heat flux	W/m^3
R	Stratification rate	-	q_{wl}	Wall-liquid heat flux	W/m^2
τ_i	Interfacial friction	N/m^3	q_{wv}	Wall-vapour heat flux	W/m^2
β	Added/virtual mass coefficient	-	q_{wi}	Wall-interface heat flux	W/m^2
u_i	Interface velocity	m/s	**Other terms**		
C_l	Liquid-wall friction coefficient	-	G_{cr}	Critical flow rate	kg/s
C_v	Vapour-wall friction coefficient	-	δ	Droplet diameter	m

Research and Development (R&D) work is thus undertaken to identify good relationships describing all the phenomena and mechanisms at work in a nuclear reactor in an accidental situation. This code Verification and Validation (V&V) work is carried out in particular by comparing the SET experimental results and the results of the predictions of the CATHARE code. Figure 4.3 illustrates the various SET used for CATHARE V&V within the many components of a reactor.

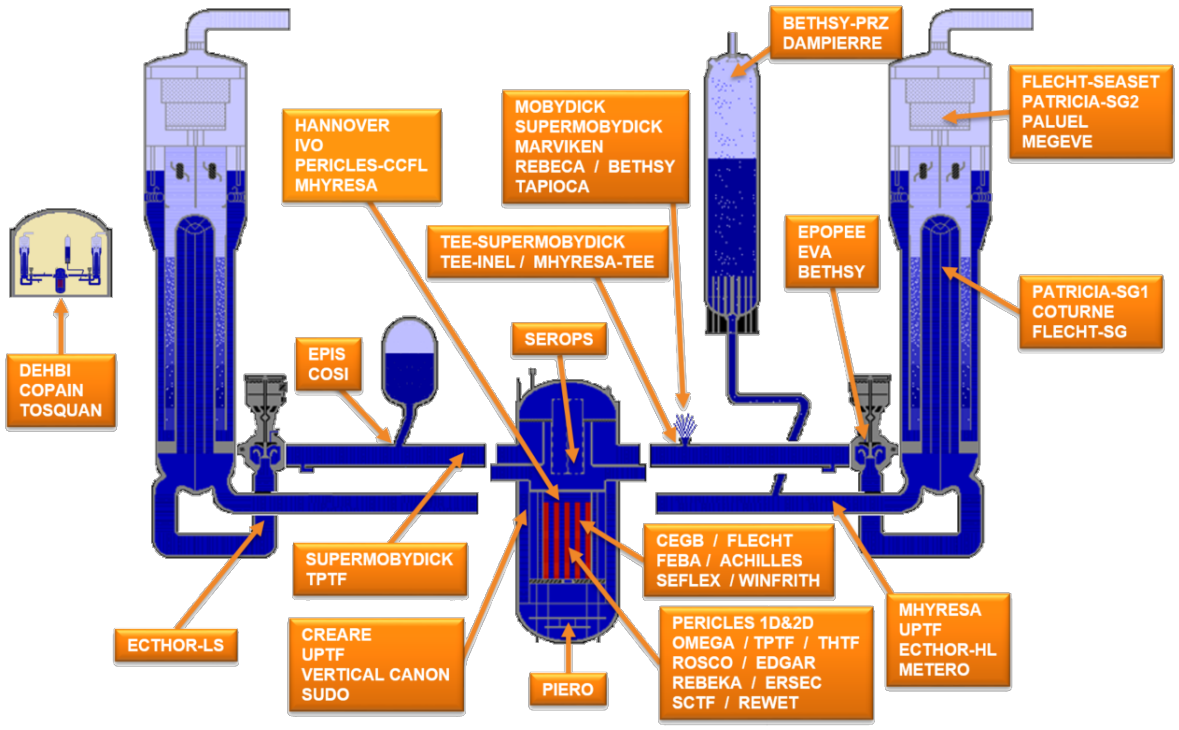

Figure 4.3: SET used in the CATHARE code Verification and Validation (V&V)

CATHARE is also a Best-Estimate (BE) code using boundary conditions to describe the behaviour of complex thermal-hydraulic phenomena in reactors in accident situations in a more realistic view than previous models based on conservative approaches (see section 3.2.1). The best estimate approach requires the application of techniques such as "change rather than tradition", while maintaining an adequate level of qualification. As defined in D'Auria et al. 2017, "best estimate computer code or analysis method may be deemed validated if the applicability and sufficient accuracy of the code applied has been demonstrated for the respective application within the framework of the validation scope performed and documented." Several qualitative judgements of agreement justify code validation. They are evaluated based on the similarity of the codes predictions to the trends of the corresponding data during the transients time phases (D'Auria et al. 2012). CATHARE is thus deemed as a best estimate code due to its agreement with highly ranked phenomena for transients of interest.

The CATHARE code strategy for development VV&Q is described in Appendice F.

CHAPTER 5

Study of the Applicability of the FSA Method to a 1% SB-LOCA Transient for Comparison with the H2TS Method

The Fractional Scaling Analysis (FSA) method presented in section 3.3.2.4 was chosen to carry out the work of this thesis and answer some of the scaling issues raised in section 3.4. The objective of this chapter is to verify the applicability of the FSA to a nuclear transient. For this purpose, a scaling analysis is performed using the FSA and compared to an application of the Hierarchical Two-Tiered Scaling (H2TS) method done by the Polytechnic University of Valencia (UPV) (Muñoz-Cobo et al. 2018). This analysis will be achieved if the two methods obtain similar results when applied to a 1% Hot-Leg SB-LOCA transient studied over two temporal phases of particular interest. The selected transient is performed by the ROSA 1.2 test on the Japanese LSTF-ROSA-IV facility (The ROSA-V Group 2003). Some differences and similarities of these two methods are identified to highlight the cause and importance of the choices that can be made during a scaling analysis.

This chapter also intends to demonstrate the applicability of the FSA supported by system codes. For this purpose, the scaling analysis of this study is performed with the validated CATHARE 3 code, presented in chapter 4. For their scaling analysis, the UPV uses the TRACE code.

The present study was published at the NURETH-19 conference, in "Application of the FSA Scaling Method to the LSTF ROSA 1.2 Test and Comparison to an Application of the H2TS Method", (Ciechocki et al. 2022a).

5.1. Description of the LSTF ROSA 1.2 Test

5.1.1. The LSTF Facility

The LSTF ROSA 1.2 test was performed on the Large Scale Test Facility (LSTF) of the Japan Atomic Energy Research Institute (JAERI) (The ROSA-V Group 2003; OECD/NEA 2013). LSTF is an ITF designed to simulate a Westinghouse four-loops PWR with a full power of 3423 MWt – 1100 MWe. The reference PWR is the Tsuruga Unit-2 of the Japan Atomic Power Company (JAPC). As shown in Figure 5.1a, LSTF has two loops, two steam generators consisting of 141 inverted U-tubes and one pressurizer. The facility is designed using the power-to-volume method (described

in section 3.3.1.3), which involves using the same scaling factor for power and volume. The volume is thus scaled by a factor of $1/48$. The core, composed of 1008 full-length electrically heater rods, has a maximum power equal to 14% of the $1/48$ nominal power of the reference reactor, i.e. 10 MWt. The height and pressures reference conditions were kept the same as in the reference reactor (FHFP ITF). This scaling respects the timing of events. Since each loop represents two reactor loops, the flow area in the pressure vessel is $1/48$ scaled and $1/24$ scaled in the cold and hot legs and steam generators. The flow areas of the hot and cold legs are scaled to preserve the ratio of the length to the square root of pipe diameter $L/\sqrt{D}$ of the reference reactor, in order to better simulate the flow regime transitions in the primary loops (The ROSA-V Group 2003). The scaling ratio of the hot and cold legs of LSTF compared to its reference PWR is detailed in Table 5.1.

Table 5.1: Characteristics of the hot and cold legs of LSTF compared to its reference PWR

	LSTF		PWR		LSTF/PWR	
	Hot leg	Cold leg	Hot leg	Cold leg	Hot leg	Cold leg
Diameter D	0.207 m	0.207 m	0.7366 m	0.6985 m		
Length L	3.686 m	3.4381 m	6.9927 m	7.2465 m		
Volume V	0.124 m^3	0.1157 m^3	2.98 m^3	2.777 m^3	1/24.03	1/24.00
$L/\sqrt{D}$	8.102 $m^{1/2}$	7.557 $m^{1/2}$	8.148 $m^{1/2}$	8.671 $m^{1/2}$	1/1.006	1/1.147

The CATHARE system code is used in this study to simulate the LSTF ROSA 1.2 test. Both primary and secondary systems are modelled in the CATHARE dataset. The primary side contains the Reactor Pressure Vessel (RPV), two hot and cold legs with main coolant pumps, the pressurizer, and the U-tubes of the two steam generators. The system also includes High Pressure Injection System (HPIS) and Accumulator Injection System (AIS). Figure 5.1b depicts the nodalization of the LSTF primary system using the CATHARE code. LSTF primary system is modelled with 1-D modules, except for the pressurizer, lower and upper plenums and upper head where 0-D modules are used (see CATHARE modelling structure in section 4.3).

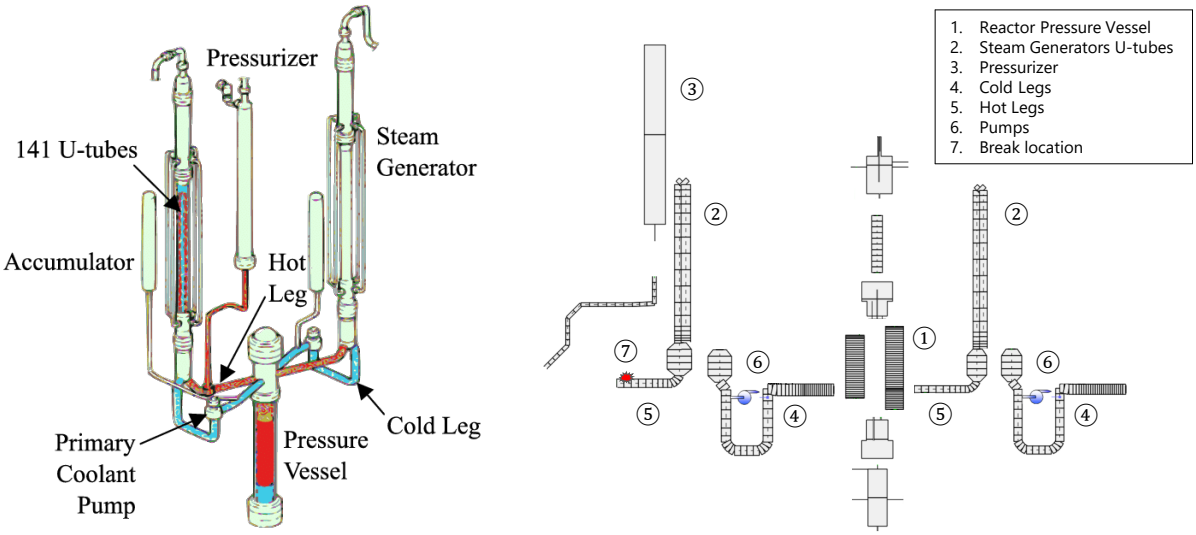

(a) Schematic view of the LSTF primary system (Clifford et al. 2016)

(b) CATHARE nodalization of the LSTF ROSA 1.2 primary sytem

Figure 5.1: The Large Scale Test Facility (LSTF) primary system

5.1.2. The 1% SB-LOCA Transient

The LSTF ROSA 1.2 test scenario consists of a SB-LOCA experiment. The break corresponds to 1% of the volumetrically scaled cross-sectional area of the reference reactor cold leg. Eq. 5.1 details the break size calculation, corresponding to a break diameter of 10.1 mm for LSTF and 67.7 mm for the reference PWR. The horizontally oriented break is located on the hot leg of the loop without pressurizer.

$$\frac{A_{HL,LSTF}}{V_{HL,LSTF}} = \frac{A_{HL,PWR}}{V_{HL,PWR}} \tag{5.1}$$

The test starts at operating full-pressure of 15.5 MPa and at a nominal power of 10 MWt. The reactor SCRAM signal occurs at 12.97 MPa resulting in the core power decay. The main coolant pumps gradually shut down as well as the pressurizer heaters and the secondary feed water. At a pressure of 12.27 MPa, the safety injection signal triggers the HPIS pumps with a 12 seconds delay. The Accumulator Injection System (AIS) is activated at 4.51 MPa.

At the break opening, the primary fluid is discharged first in subcooled liquid state. With decreasing pressure and decreasing mass inventory, the steam quality of discharged fluid at the break gradually increases. Throughout the transient, the main concern is the core cooling which may be challenged when a partially uncovered core induces a dry-out and a clad temperature excursion. This event mainly depends on the primary mass inventory, which itself depends a lot on the primary pressure evolution that influences the break flow rate and the safety injections. These two parameters are thus essential to describe the SB-LOCA transient. They are the PoI that will be used to establish the balance equations for the scaling analysis (see step 1 in section 3.3.2.2).

In the framework of the phenomenological analysis, but also for the purposes of the scaling analysis, the transient is divided into five chronological phases (see step 2 in the section 3.3.2.2). These phases depend on the phenomena and on system parameters evolution. Bifurcating events that correspond to abrupt changes of phenomena, delimit the phases. In the current study, the 1% SB-LOCA of the ROSA 1.2 test is divided into five phases following the UPV analysis (Muñoz-Cobo et al. 2018). This choice allows for the separation of the dominant processes throughout the transient. The phases are illustrated in Figure 5.2, which describes the evolution of the primary and secondary pressures as well as the primary mass inventory. Letters on the top (A to E) and numbers (1 to 5) on the bottom indicates the bifurcating events and phases according to Table 5.2.

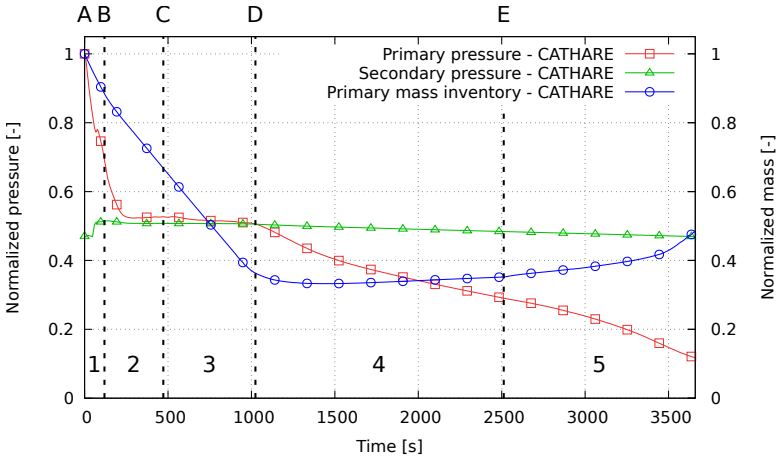

Figure 5.2: Primary and secondary evolutions during the phases of the 1% SB-LOCA of the ROSA 1.2 test - CATHARE predictions

Table 5.2: Phases and initial bifurcating events of the 1% SB-LOCA of the ROSA 1.2 test

Phases	Initial bifurcating events
1. Subcooled Blowdown (SBD)	A. Break opening
2. Natural Circulation (NC)	B. Pressurizer emptied, pumps stop
3. Two-Phase Discharge (TPD)	C. Top of SG tubes emptied (no liquid flow)
4. High-Quality Mixture Discharge (HQMD)	D. Primary-secondary pressure reversal
5. Reactor Refilling (RR)	E. Accumulator discharge

1. The Subcooled Blowdown (SBD) phase:

After the opening of the break, the primary system depressurizes quickly from 15.5 MPa to about 10.7 MPa in 119 seconds. The primary system remains liquid in the loops and in the pressure vessel up to 60 seconds. Flashing (vaporization of liquid due to pressure drop) occurs first in the pressurizer due to its higher temperature. The SCRAM signal triggers at around 50 seconds and the core power will join a decay power curve, which is truncated at 14%. The primary pumps are stopped and the rotation speed gradually decreases. Depending on the flywheel, the transition to natural circulation begins. The end of the subcooled blowdown is defined as the emptying of the pressurizer (less than 1% of its initial liquid mass). Figure 5.3 illustrates the Subcooled Blowdown phase.

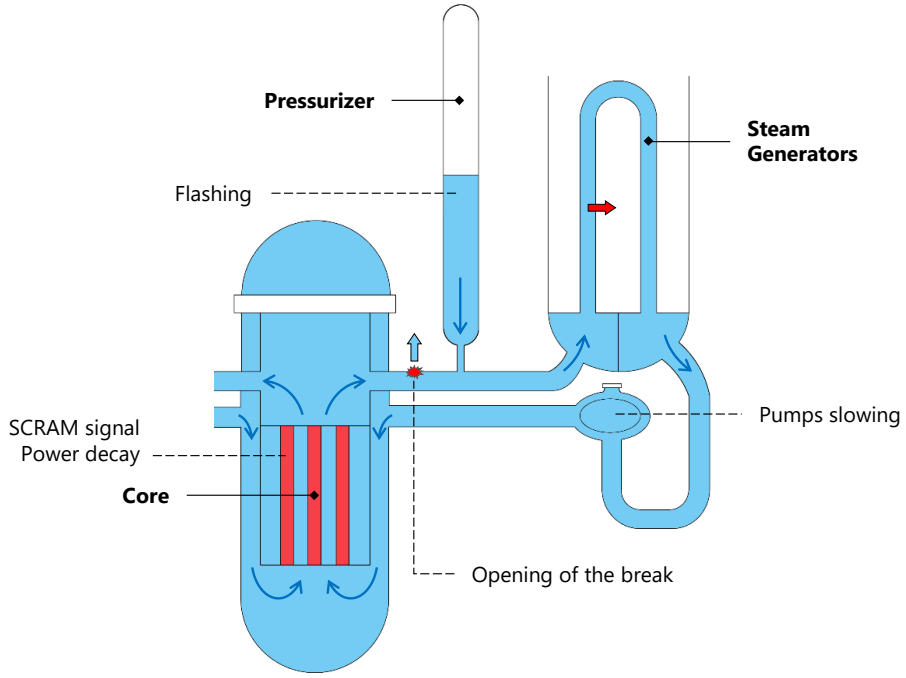

Figure 5.3: The Subcooled Blowdown (SBD) phase

2. The Natural Circulation (NC) phase:

The pumps being stopped, the fluid circulation is due to the differences in density between the ascending and descending parts of the cooling loops. The ascending part is the core, the upper plenum, the hot legs and the ascending part of the steam generators U-tubes. The descending part is the descending part of the steam generators U-tubes, the cold legs, and the vessel downcomer. Friction and singular pressure losses compensate for the difference in gravity in the ascending and descending parts of the circuit. During this phase, the primary pressure decreases slowly (from

10.7 MPa to 8.2 MPa) and stays above the secondary pressure to be able to transfer energy to the steam generators. During this phase, the core provides more energy to the fluid than is lost at the break and the primary fluid needs to give the rest of power to the steam generators. This requires a higher temperature and higher pressure than in the secondary side of the steam generators. Figure 5.4 illustrates the Natural Circulation phase.

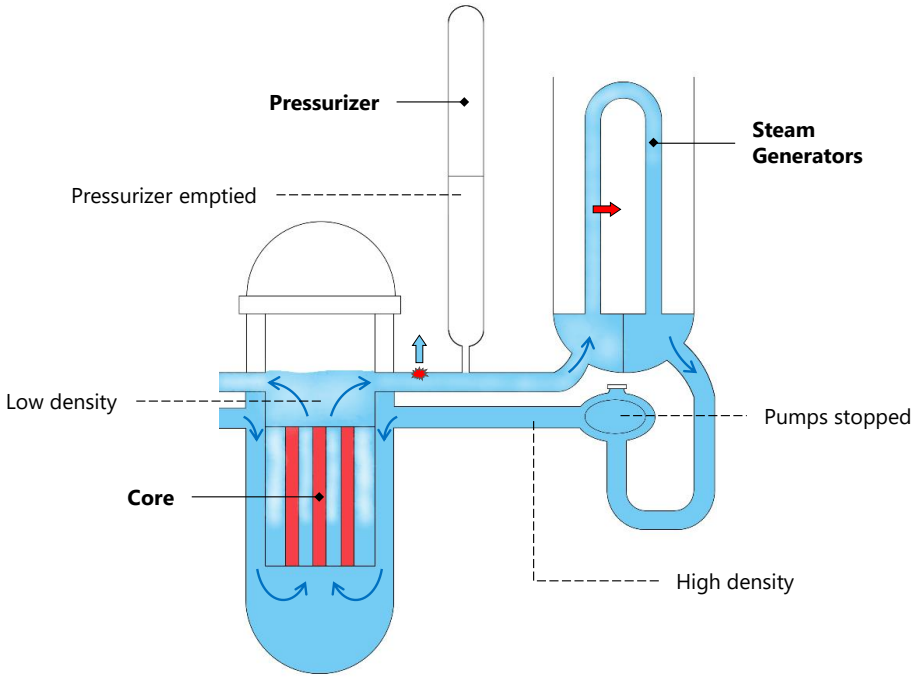

Figure 5.4: The Natural Circulation (NC) phase

3. The Two-Phase Discharge (TPD) phase:

Some vapour created in the core condenses in the steam generators U-tubes. The condensate water is first entrained in co-current flow to the intermediate leg (IL) and the cold leg. Then the mass of water decreasing, the void fraction increases in steam generators tubes and the vapour is no more capable to entrain the condensate water to the top of the steam generators tubes. This is the end of the natural circulation and the beginning of the Reflux Condenser Mode (RCM). Some decay power is still removed by condensation in steam generators. The condensate water flows back to the hot legs in the ascending part of steam generators tubes whereas the condensate in the descending part of steam generators tubes fills the intermediate legs: this is the Loop Seal Plugging (LSP) phenomena.

With the end of the natural circulation, water tends to settle in the lower part of the circuit, the steam quality at the break increases and more power is evacuated at the break. The plugs created in the intermediate legs isolate the cold and hot legs resulting in a faster pressure decrease in the cold legs due to the HPIS. The remaining liquid mass in the IL is not available to cool the core and creates an unfavourable pressure difference, which induces a core uncovery. This core uncovery creates a dry-out and a temperature excursion with a first Peak Clad Temperature (PCT). The Loop Seal Clearing (LSC) phenomenon occurs when there is a sufficient pressure difference between the hot and cold legs to evacuate the plugs towards the pressure vessel. This ends the core uncovery and temperature excursion. Note that for the 1% SB-LOCA, the Loop Seal Plugging occurs without Loop Seal Clearing during the five phases considered. During this Two-Phase Discharge, the primary pressure drops from 8.2 MPa to 7.7 MPa in 581 seconds. Figure 5.5 illustrates the Two-Phase Discharge phase.

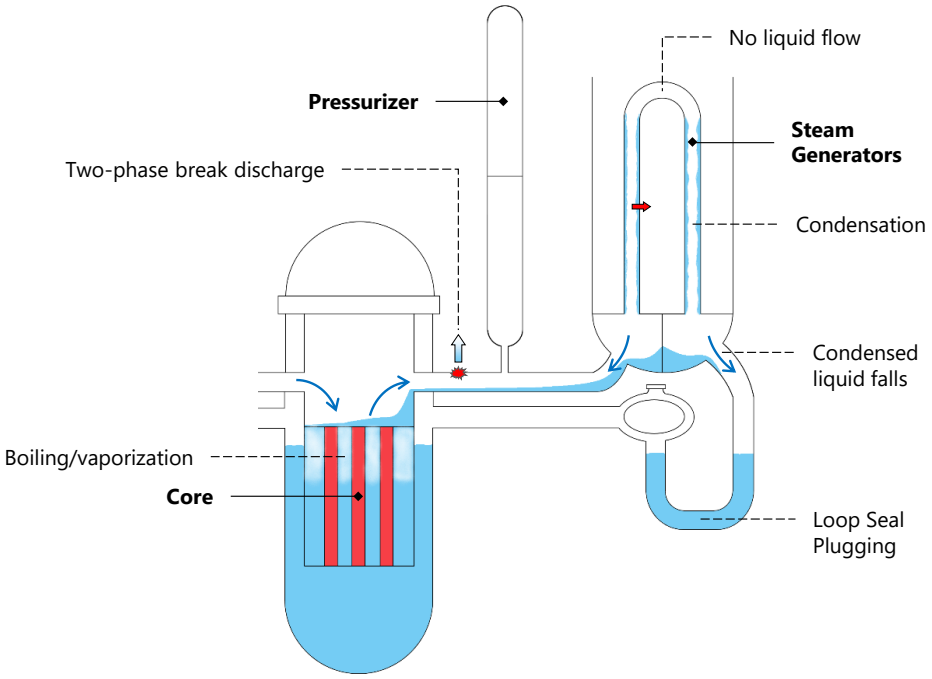

Figure 5.5: The Two-Phase Discharge (TPD) phase

4. The High-Quality Mixture Discharge (HQMD) phase:

The beginning of this phase is marked by the passage of the primary pressure below the secondary pressure. From this moment, the heat flux at the steam generators U-tubes is reversed. The gradual decrease of primary pressure increases the HPIS flow rate. The vapour condensation on the cold injected water increases the depressurization rate. During this phase, the pressure decreases significantly, from 7.7 MPa to 4.5 MPa in 1484 seconds. The liquid level in hot legs falls until it reaches the height of the break. The discharge at the break is then almost vapour. Figure 5.6 illustrates the High-Quality Mixture Discharge phase.

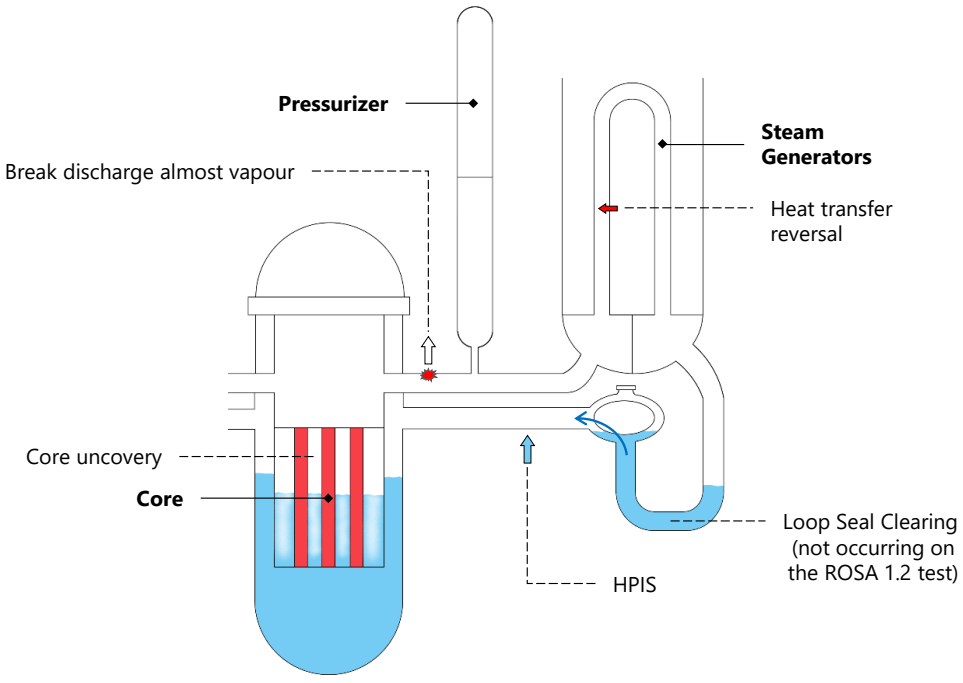

Figure 5.6: The High-Quality Mixture Discharge (HQMD) phase

5. The Reactor Refilling (RR) phase:

This phase starts when the accumulator injection is triggered. A large flow rate of sub-cooled liquid is discharged into the primary system thanks to AIS and HPIS. From the beginning to the end of the accumulator discharge, the pressure decreases from 4.5 MPa to 1.8 MPa in 1148 seconds and the mass inventory starts increasing. Figure 5.7 illustrates the Reactor Refilling phase.

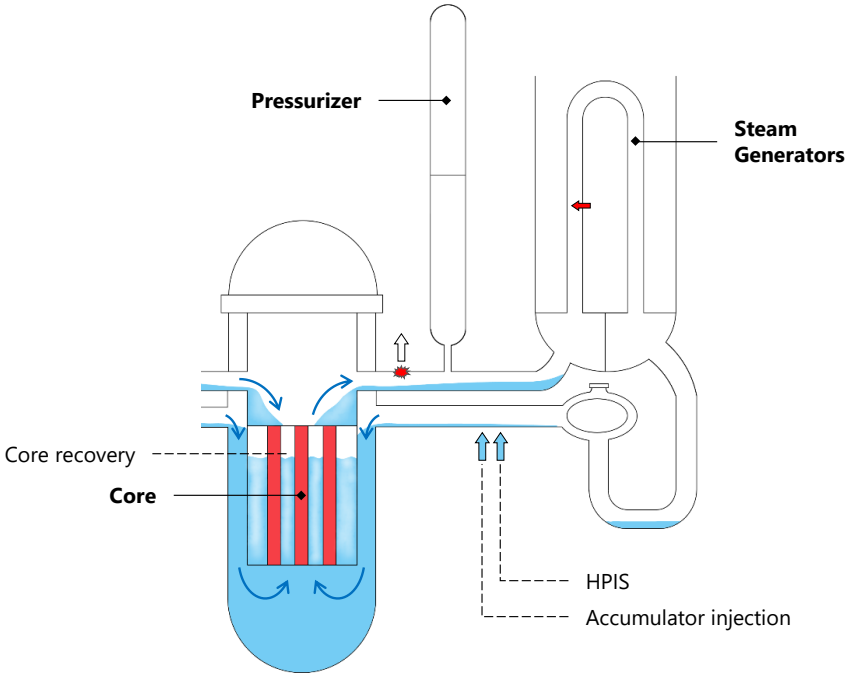

Figure 5.7: The Reactor Refilling (RR) phase

5.2. Top-Down Scaling Analysis of the 1% SB-LOCA Transient with the FSA Method

In order to evaluate its applicability, the FSA method (see section 3.3.2.4) is applied to two of the five SB-LOCA phases. The scaling analyses is performed on the subcooled blowdown and the high-quality mixture discharge phases since they are important from the transient phenomenological perspective. The subcooled blowdown is a brief but intense phase caused by a rapid pressure drop in the primary system. The High-Quality Mixture Discharge is also an important phase since it delimits the system second depressurization (see Figure 5.2).

For the SB-LOCA transient, the Figure of Merit (FoM) is defined as the Peak Clad Temperature (PCT). As mentioned in section 3.3.2.2, the PCT is a major safety criterion for LOCA. It is a key parameter in the design of nuclear reactors and their safety systems to prevent that a specific temperature within the core could never be reached in an accidental situation, thereby avoiding core meltdown. The primary mass inventory M_1 and the primary pressure P_1 are the two most important Parameters of Interest (PoI) that influence the FoM. On the one hand, the PCT is directly dependent on the core liquid level and thus the primary system mass inventory. On the other hand, the state of the water in the primary system (liquid or vapour) and the triggering of safety systems such as safety injections, which are dependent on the primary pressure, govern the mass inventory.

Equations are then written for the primary mass and pressure evolution. The primary pressure is first driven by the pressurizer until it is empty, and then it is driven by the mass and energy

exchanges in the whole primary circuit. Therefore, the mass and pressure equations is also written for the pressurizer volume.

5.2.1. Mass Balance Equations in a Volume V

The rate of mass change in a constant volume V is equal to the mass flow rate of incoming fluid by its constant boundary surface A and can be expressed as:

$$\frac{d}{dt}\int_V \rho\, dV = \int_{A_f} \rho \cdot \vec{u} \cdot \vec{n}\, dA \tag{5.2}$$

With $\vec{u}$ the fluid velocity normal vector to the constant surface A. The mass balance equation then simplifies to:

$$\frac{dM}{dt} \triangleq \dot{M} = \dot{M}_{in} - \dot{M}_{out} \tag{5.3}$$

$\dot{M}$ is the time rate change of fluid mass in V. $\dot{M}_{in}$ and $\dot{M}_{out}$ are respectively the mass flow rates entering (indicated by the subscript in) and leaving (indicated by the subscript out) V through fluid boundaries A_f. For a two-phase flow, this equation can be split into liquid and vapour contributions. Mass balance equation becomes:

$$\dot{M} = \dot{M}_l + \dot{M}_v = \dot{M}_{l,in} - \dot{M}_{l,out} + \dot{M}_{v,in} - \dot{M}_{v,out} \tag{5.4}$$

The Eq. 5.3 applied to the primary system volume V_1 and the pressurizer volume V_{prz} of the LSTF ROSA 1.2 test gives respectively Eq. 5.4 and 5.5:

$$\dot{M}_1 = \dot{M}_{l,HPIS} + \dot{M}_{l,acc.} - \dot{M}_{l,break} - \dot{M}_{v,break} \tag{5.5}$$

$\dot{M}_{l,HPIS}$ and $\dot{M}_{l,acc.}$ denotes the liquid mass flow rate injected into the primary system respectively by the HPIS and the accumulators. HPIS and accumulators injections are assumed to be only liquid. Since HPIS are only triggered below 12.27 MPa, the HPIS term is only considered during the HQMD phase. Since the accumulators are only triggered below 4.51 MPa, the accumulator term is not considered in this study. $\dot{M}_{l,break}$ and $\dot{M}_{v,break}$ are the mass flow rates discharged at the break.

$$\dot{M}_{prz} = -\dot{M}_{l,prz} - \dot{M}_{v,prz} \tag{5.6}$$

The mass changes in the pressurizer are those caused by the liquid and vapour mass flowing out.

Each contributor to the mass rate of change $\dot{M}$ is normalized with time-averaged of variables $\bar{Y}$ during the phases. Although the FSA method recommends normalization with an initial value Y_0 (see Eq. 3.20 (Zuber et al. 2007)), it is chosen here to use this average calculated values thanks to the support of the calculation code. This is motivated by the intention to provide better accuracy in the estimation of equations terms in order to quantify each process through the studied phases rather than at given instants.

$$Y^+(t) = \frac{Y(t)}{\bar{Y}} \tag{5.7}$$

Introducing the Fractional Rate of Change (FRC) $\omega_{\dot{M},j}$ quantifying the relative magnitude of the processes on the primary system and pressurizer mass, the Eq. 5.5 and 5.6 then write respectively:

$$\left.\frac{dM^+}{dt}\right|_1 = \omega_{\dot{M}_{l,HPIS}} \cdot \dot{M}^+_{l,HPIS} + \omega_{\dot{M}_{l,acc.}} \cdot \dot{M}^+_{l,acc.} - \omega_{\dot{M}_{l,break}} \cdot \dot{M}^+_{l,break} - \omega_{\dot{M}_{v,break}} \cdot \dot{M}^+_{v,break} \quad (5.8)$$

$$\left.\frac{dM^+}{dt}\right|_{prz} = -\omega_{\dot{M}_{l,prz}} \cdot \dot{M}^+_{l,prz} - \omega_{\dot{M}_{v,prz}} \cdot \dot{M}^+_{v,prz} \quad (5.9)$$

The normalized mass balance equations are obtained, function of the j Agents of Change $\phi^+_{\dot{M},j}$ which define the processes acting on the mass rate of change $\dot{M}$ (see Eq. 3.21):

$$\left.\frac{dM^+}{dt}\right|_1 = \omega_{\dot{M}_{l,HPIS}} \cdot \phi^+_{\dot{M}_{l,HPIS}} + \omega_{\dot{M}_{l,acc.}} \cdot \phi^+_{\dot{M}_{l,acc.}} - \omega_{\dot{M}_{l,break}} \cdot \phi^+_{\dot{M}_{l,break}} - \omega_{\dot{M}_{v,break}} \cdot \phi^+_{\dot{M}_{v,break}} \quad (5.10)$$

$$\left.\frac{dM^+}{dt}\right|_{prz} = -\omega_{\dot{M}_{l,prz}} \cdot \phi^+_{\dot{M}_{l,prz}} - \omega_{\dot{M}_{v,prz}} \cdot \phi^+_{\dot{M}_{v,prz}} \quad (5.11)$$

5.2.2. Pressure Equations in a Volume V

The first principle of thermodynamics in a constant volume V with constant boundaries A to derive a total energy equation is written as the sum of the internal energy and the kinetic energy:

$$\begin{aligned}
&\frac{d}{dt}\int_V \rho\left(e + \frac{u^2}{2}\right) dV = && \text{Rate of change of total energy} \quad (5.12)\\
&\int_V \rho\left(\vec{F}\cdot\vec{u} + q_{ext}\right) dV && \text{Power of external forces}\\
&-\int_{A_f} \rho\left(e + \frac{u^2}{2}\right)\vec{u}\cdot\vec{n}\, dA && \text{Convective total energy flux}\\
&-\int_A \vec{q}\cdot\vec{n}\, dA && \text{Heat flux}\\
&-\int_{A_f} \left(\bar{\bar{T}}\cdot\vec{u}\right)\cdot\vec{n}\, dA && \text{Power of surface forces}
\end{aligned}$$

With e the internal mass energy and q the surface heat flux. Some simplifications are considered by neglecting:

- The kinetic energy $u^2/2$, which is much lower than the internal energy at low Mach numbers.
- The conductive heat flux along fluid boundaries, which is negligible compared to conductive heat flux along solid boundaries.
- External energy sources (radiative heat flux) q_{ext} and work of external force (gravity) $\vec{F}\cdot\vec{u}$, which is negligible compared to convective and diffusive energy fluxes when pumps are off.

Finally, the energy balance is expressed using enthalpy h instead of internal energy ($h = e + p/\rho$). The two-phase energy balance equation for a volume V writes:

$$\frac{dM_l \cdot H_l}{dt} + \frac{dM_v \cdot H_v}{dt} - V\frac{dP}{dt} = W_w + \dot{M}_{l,in} \cdot h_{l,in} - \dot{M}_{l,out} \cdot H_l + \dot{M}_{v,in} \cdot h_{v,in} - \dot{M}_{v,out} \cdot H_v \quad (5.13)$$

With P, H_l and H_v representing the volume averaged pressure, specific liquid and vapour enthalpies, $h_{l,in}$ and $h_{v,in}$ representing the liquid and vapour entering specific enthalpies, and W_w representing the thermal power received from the walls. It is here assumed that the phases leave the volume with the mass weighted averaged specific enthalpy H_l and H_v of the volume.

Using the energy balance at the interfaces, the mass balance equation and a constant volume equation, a pressure equation expressed in terms of fluid Volume Rate of Change (VRC, measured in m^3/s) is obtained (Bestion 2020):

$$\begin{aligned}
&(\mu_l \cdot M_l + \mu_v \cdot M_v) \cdot \dot{P} = && (1)\\
&\dot{M}_{l,in} \cdot \left[\nu_l + \nu'_{l,h} \cdot (h_{l,in} - H_l)\right] + \dot{M}_{v,in} \cdot \left[\nu_v + \nu'_{v,h} \cdot (h_{v,in} - H_v)\right] && (2)\\
&-\dot{M}_{l,out} \cdot \nu_l - \dot{M}_{v,out} \cdot \nu_v && (3)\\
&+\nu'_{l,h} \cdot W_{wl} + \nu'_{v,h} \cdot W_{wv} + \nu'_{l,h} \cdot W_{il} + \nu'_{v,h} \cdot W_{iv} && (4)\\
&-\frac{W_{il} + W_{iv}}{\varpi} && (5)\\
&+\frac{W_{wi}}{\varpi} && (6)
\end{aligned} \quad (5.14)$$

With:

$$\mu_k = -\nu'_{k,p} - \nu_k \cdot \nu'_{k,h} \;\; ; \;\; \nu'_{k,p} \triangleq \left.\frac{\partial \nu_k}{\partial p}\right|_{h_k} \;\; ; \;\; \nu'_{k,h} \triangleq \left.\frac{\partial \nu_k}{\partial h_k}\right|_{p} \;\; ; \;\; \varpi \triangleq \frac{H_v - H_l}{\nu_v - \nu_l}$$

The term on the l.h.s (1) is the VRC corresponding to fluid expansion/contraction in pressure increase/decrease. On the r.h.s, the terms are:

(2) The VRC due to entering liquid and vapour volume flow rates and the associated thermal expansion when mixing with internal fluid.

(3) The VRC by exiting liquid and vapour flow rates.

(4) The VRC by liquid and vapour thermal expansion by wall heating and by interfacial exchanges.

(5) The VRC by vaporization or condensation.

(6) The VRC by wall boiling or wall condensation.

This formulation provides an easy interpretation of the impact of fluid volume changes on pressure. Fluid volume may change by mass source or sink at boundaries, by heat exchange expansion/contraction, by vaporization or condensation and by isentropic expansion/contraction. The total control volume being constant, when the r.h.s terms create volume, the pressure increases to lose the same volume by contraction (l.h.s term). When the r.h.s terms lose some volume, the

depressurization compensates by fluid expansion (l.h.s term). Figure 5.8 illustrates the physics of the Eq. 5.14.

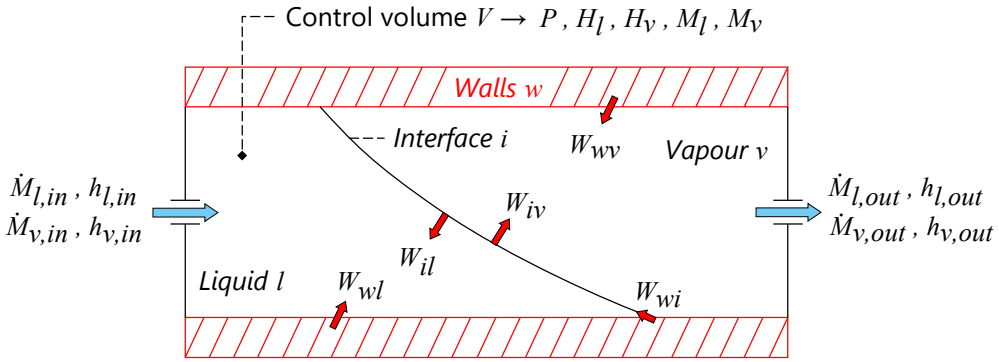

Figure 5.8: Illustration of the physics in the general pressure by Volume Rate of Change (VRC) equation

To match the conditions of the UPV analysis (Muñoz-Cobo et al. 2018), a simpler equation with a saturation assumption assuming thermal equilibrium is written (Bestion 2020):

$$\begin{gathered}(\lambda_l \cdot M_l + \lambda_v \cdot M_v) \cdot \dot{P} = \\ \dot{M}_{l,in} \cdot \left(\nu_{ls} + \frac{h_{l,in} - h_{ls}}{\varpi_s}\right) + \dot{M}_{v,in} \cdot \left(\nu_{vs} + \frac{h_{v,in} - h_{vs}}{\varpi_s}\right) \\ -\dot{M}_{l,out} \cdot \nu_{ls} - \dot{M}_{v,out} \cdot \nu_{vs} \\ + \frac{W_w}{\varpi_s}\end{gathered} \tag{5.15}$$

With:

$$\lambda_k = \frac{h'_{ks,p}}{\varpi_s} - \frac{\nu_{ks}}{\varpi_s} - \nu'_{ks,p} \;\; ; \;\; h'_{ks,p} \triangleq \frac{dh_{ks}}{dp} \;\; ; \;\; \nu'_{ks,p} \triangleq \frac{d\nu_{ks}}{dp} \;\; ; \;\; \varpi_s \triangleq \frac{h_{vs} - h_{ls}}{\nu_{vs} - \nu_{ls}}$$

For this equation, the l.h.s term represents all VRC due to expansion (or contraction) by pressure change; it includes isentropic expansion plus vaporization by flashing and thermal expansion following saturation curve.

The Eq. 5.15 applied to the primary system volume V_1 of the LSTF ROSA 1.2 test gives:

$$\begin{gathered}(\lambda_{l,1} \cdot M_{l,1} + \lambda_{v,1} \cdot M_{v,1}) \cdot \dot{P}_1 = \quad (1) \\ \dot{M}_{l,HPIS} \cdot \nu_{ls,1} + \dot{M}_{l,HPIS} \cdot \frac{(h_{l,HPIS} - h_{ls,1})}{\varpi_{s,1}} \quad (2) \\ + \dot{M}_{l,acc.} \cdot \nu_{ls,1} + \dot{M}_{l,acc.} \cdot \frac{(h_{l,acc.} - h_{ls,1})}{\varpi_{s,1}} \quad (3) \\ -\dot{M}_{l,break} \cdot \nu_{ls,1} - \dot{M}_{v,break} \cdot \nu_{vs,1} \quad (4) \\ + \frac{W_{core}}{\varpi_{s,1}} - \frac{W_{SG}}{\varpi_{s,1}} + \frac{W_{ow}}{\varpi_{s,1}} \quad (5)\end{gathered} \tag{5.16}$$

With the rate of pressure change in the primary system volume (1) due to the contributions by:

(2) The liquid flow rate entering the primary system and the resulting thermal expansion by condensation thanks to HPIS.

(3) The liquid flow rate entering the primary system and the resulting thermal expansion by condensation thanks to accumulator discharge.

(4) Liquid and vapour flow rates leaving the primary system through the break.

(5) Thermal expansion by condensation or vaporization due to - the core heat generation, - SG tubes heat exchanges, - and other wall heat exchanges in the primary system.

The Eq. 5.15 applied to the pressurizer volume V_{prz} of the LSTF ROSA 1.2 test gives:

$$\begin{aligned}(\lambda_{l,prz} \cdot M_{l,prz} + \lambda_{v,prz} \cdot M_{v,prz}) \cdot \dot{P}_{prz} = \quad & (1) \\ -\dot{M}_{l,prz} \cdot \nu_{ls,prz} - \dot{M}_{v,prz} \cdot \nu_{vs,prz} \quad & (2) \\ +\frac{W_{prz,heaters}}{\varpi_{s,prz}} + \frac{W_{prz,ow}}{\varpi_{s,prz}} \quad & (3)\end{aligned} \tag{5.17}$$

With the rate of pressure change in the pressurizer volume (1) due to the contributions by:

(2) The liquid and vapour flow rates leaving the pressurizer to the surge line.

(3) Thermal expansion by condensation or vaporization due to - the pressurizer heaters, - and other wall heat exchanges in the pressurizer.

To simplify the notation of the pressure change due to VRC, global expansion coefficients with saturation assumption $K_{s,1}$ and $K_{s,prz}$ are defined:

$$K_{s,1} = (\lambda_{l,1} \cdot M_{l,1} + \lambda_{v,1} \cdot M_{v,1}) \tag{5.18}$$

$$K_{s,prz} = (\lambda_{l,prz} \cdot M_{l,prz} + \lambda_{v,prz} \cdot M_{v,prz}) \tag{5.19}$$

Each contributor to the pressure rate of change $\dot{P}$ is normalized in the same way as in Eq. 5.7. The Eq. 5.16 and 5.17 then write respectively, introducing the Fractional Rate of Change (FRC) $\omega_{\dot{P},j}$:

$$\begin{aligned}\left.\frac{dP^+}{dt}\right|_1 = {} & \omega_{\dot{P},Q_{l,HPIS}} \cdot \frac{\dot{M}^+_{l,HPIS} \cdot \nu^+_{ls,1}}{K^+_{s,1}} + \omega_{\dot{P},Q_{cond,HPIS}} \cdot \frac{\dot{M}^+_{l,HPIS} \cdot \left(h^+_{l,HPIS} - h^+_{ls,1}\right)}{K^+_{s,1} \cdot \varpi^+_{s,1}} \\ & + \omega_{\dot{P},Q_{l,acc.}} \cdot \frac{\dot{M}^+_{l,acc.} \cdot \nu^+_{ls,1}}{K^+_{s,1}} + \omega_{\dot{P},Q_{cond,acc.}} \cdot \frac{\dot{M}^+_{l,acc.} \cdot \left(h^+_{l,acc.} - h^+_{ls,1}\right)}{K^+_{s,1} \cdot \varpi^+_{s,1}} \\ & - \omega_{\dot{P},Q_{l,break}} \cdot \frac{\dot{M}^+_{l,break} \cdot \nu^+_{ls,1}}{K^+_{s,1}} - \omega_{\dot{P},Q_{v,break}} \cdot \frac{\dot{M}^+_{v,break} \cdot \nu^+_{vs,1}}{K^+_{s,1}} \\ & + \omega_{\dot{P},Q_{core}} \cdot \frac{W^+_{core}}{K^+_{s,1} \cdot \varpi^+_{s,1}} - \omega_{\dot{P},Q_{SG}} \cdot \frac{W^+_{SG}}{K^+_{s,1} \cdot \varpi^+_{s,1}} + \omega_{\dot{P},Q_{ow}} \cdot \frac{W^+_{ow}}{K^+_{s,1} \cdot \varpi^+_{s,1}}\end{aligned} \tag{5.20}$$

$$\left.\frac{dP^+}{dt}\right|_{prz} = -\omega_{\dot{P},Q_{l,prz}} \cdot \frac{\dot{M}^+_{l,prz} \cdot \nu^+_{ls,prz}}{K^+_{s,prz}} - \omega_{\dot{P},Q_{v,prz}} \cdot \frac{\dot{M}^+_{v,prz} \cdot \nu^+_{vs,prz}}{K^+_{s,prz}} \tag{5.21}$$
$$+\omega_{\dot{P},Q_{prz,heaters}} \cdot \frac{W^+_{prz,heaters}}{K^+_{s,prz} \cdot \varpi^+_{s,prz}} + \omega_{\dot{P},Q_{prz,ow}} \cdot \frac{W^+_{prz,ow}}{K^+_{s,prz} \cdot \varpi^+_{s,prz}}$$

Normalized pressure equations are obtained, function of the j Agents of Change $\phi^+_{\dot{P},j}$ which define the processes acting on the pressure rate of change $\dot{P}$:

$$\left.\frac{dP^+}{dt}\right|_1 = \omega_{\dot{P},Q_{l,HPIS}} \cdot \phi^+_{\dot{P},Q_{l,HPIS}} + \omega_{\dot{P},Q_{cond,HPIS}} \cdot \phi^+_{\dot{P},Q_{cond,HPIS}} \tag{5.22}$$
$$+\omega_{\dot{P},Q_{l,acc.}} \cdot \phi^+_{\dot{P},Q_{l,acc.}} + \omega_{\dot{P},Q_{cond,acc.}} \cdot \phi^+_{\dot{P},Q_{cond,acc.}}$$
$$-\omega_{\dot{P},Q_{l,break}} \cdot \phi^+_{\dot{P},Q_{l,break}} - \omega_{\dot{P},Q_{v,break}} \cdot \phi^+_{\dot{P},Q_{v,break}}$$
$$+\omega_{\dot{P},Q_{core}} \cdot \phi^+_{\dot{P},Q_{core}} - \omega_{\dot{P},Q_{SG}} \cdot \phi^+_{\dot{P},Q_{SG}} + \omega_{\dot{P},Q_{ow}} \cdot \phi^+_{\dot{P},Q_{ow}}$$

$$\left.\frac{dP^+}{dt}\right|_{prz} = -\omega_{\dot{P},Q_{l,prz}} \cdot \phi^+_{\dot{P},Q_{l,prz}} - \omega_{\dot{P},Q_{v,prz}} \cdot \phi^+_{\dot{P},Q_{v,prz}} \tag{5.23}$$
$$+\omega_{\dot{P},Q_{prz,heaters}} \cdot \phi^+_{\dot{P},Q_{prz,heaters}} + \omega_{\dot{P},Q_{prz,ow}} \cdot \phi^+_{\dot{P},Q_{prz,ow}}$$

The time scaling for relative importance of agents (see from Eq. 3.25) is performed using Eq. 5.10, 5.11, 5.22 and 5.23. The FRC are divided by the dominant one. The effect metrics are obtained thanks to this process, denoting the rate of change due to the contribution of Agents of Change. Figure 5.9 illustrates the established mass and pressure effects metrics for the ROSA 1.2 test.

$$\Omega_{\dot{M},\chi_j} = \frac{\omega_{\dot{M},\chi_j}}{\left|\omega_{\dot{M},\chi_D}\right|} \;\; ; \;\; \Omega_{\dot{P},\chi_j} = \frac{\omega_{\dot{P},\chi_j}}{\left|\omega_{\dot{P},\chi_D}\right|} \tag{5.24}$$

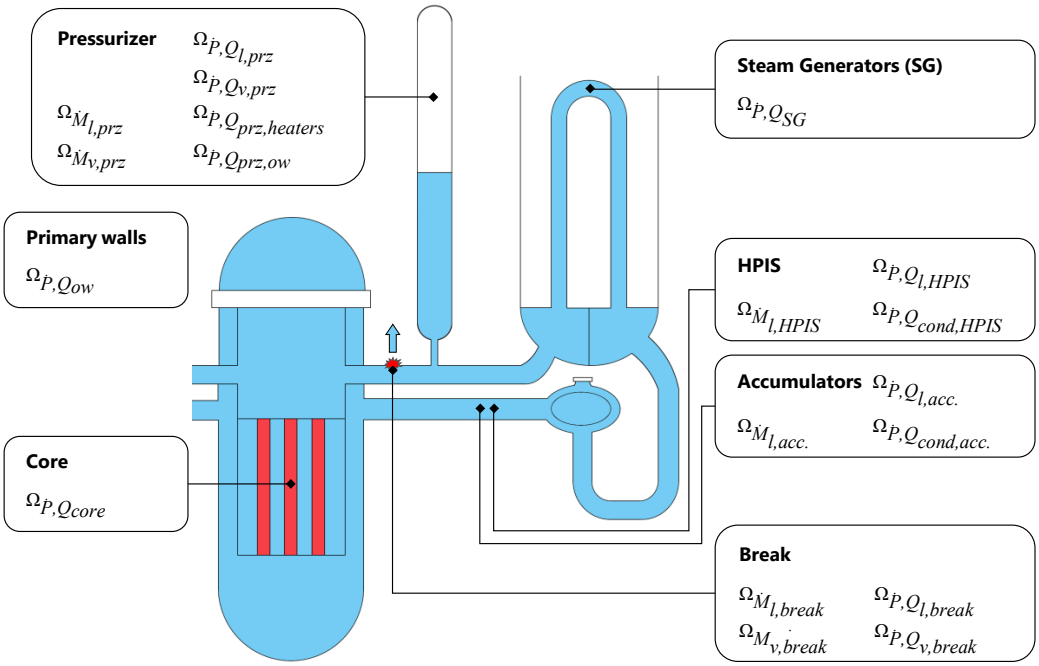

Figure 5.9: Established mass and pressure effect metrics for the ROSA 1.2 test

The established effect metrics range from -1.000 to 1.000 depending on their relative importance to the dominant process. The results of the scaling analyses presented in this manuscript are classified according to four effect metrics ranks, as shown in Table 5.3:

Table 5.3: Effect metrics hierarchy

Rank	Effect Metrics
Dominant	$\mathbf{0.800} \leq \lvert\Omega_{\dot{\psi},\chi_j}\rvert \leq \mathbf{1.000}$
Very influent	$\mathbf{0.500} \leq \lvert\Omega_{\dot{\psi},\chi_j}\rvert < \mathbf{0.800}$
Little influent	$\mathbf{0.050} \leq \lvert\Omega_{\dot{\psi},\chi_j}\rvert < \mathbf{0.500}$
Negligible	$0.000 \leq \lvert\Omega_{\dot{\psi},\chi_j}\rvert < 0.050$

5.2.3. Results of the A Posteriori Scaling Analysis using the Code Predictions

Before performing the scaling analysis, it is necessary to validate the results of the calculation code against the experimental results on the PoI. Figure 5.10 compares the CATHARE code predictions of primary and secondary pressures to experimental results through the SBD and HQMD phases. CATHARE is observed to predict the pressures evolution rather well.

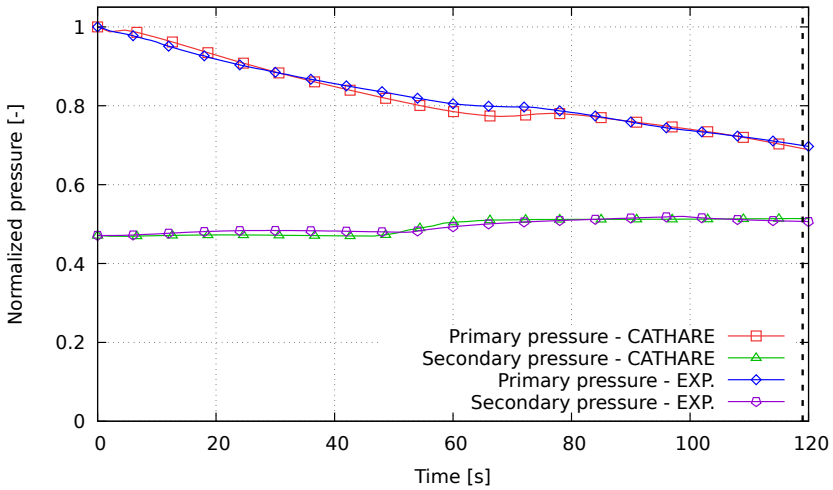

(a) Pressures during the SBD phase

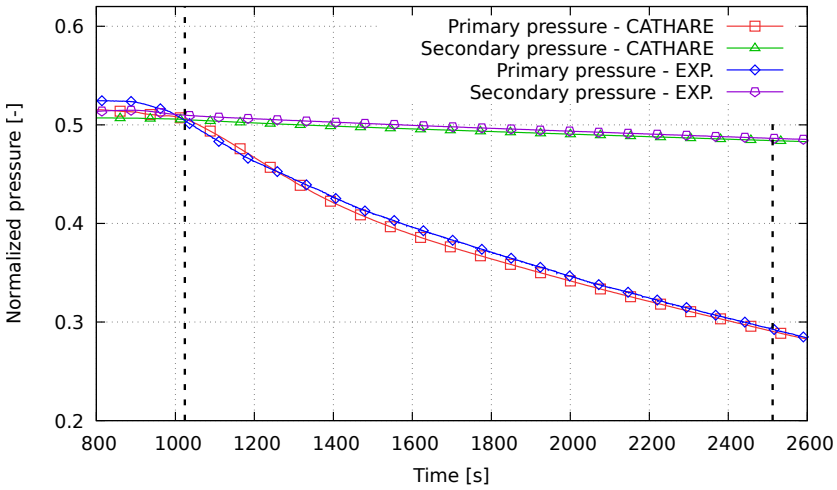

(b) Pressures during the HQMD phase

Figure 5.10: Primary and secondary pressures of the ROSA 1.2 test

Figure 5.11 shows the comparaison between the CATHARE predictions and experimental results of the break mass flow rate which is directly related to the primary mass inventory. It is found to be rather well predicted with a delay in the transition to HQMD and a higher flow at the end of accumulator discharge.

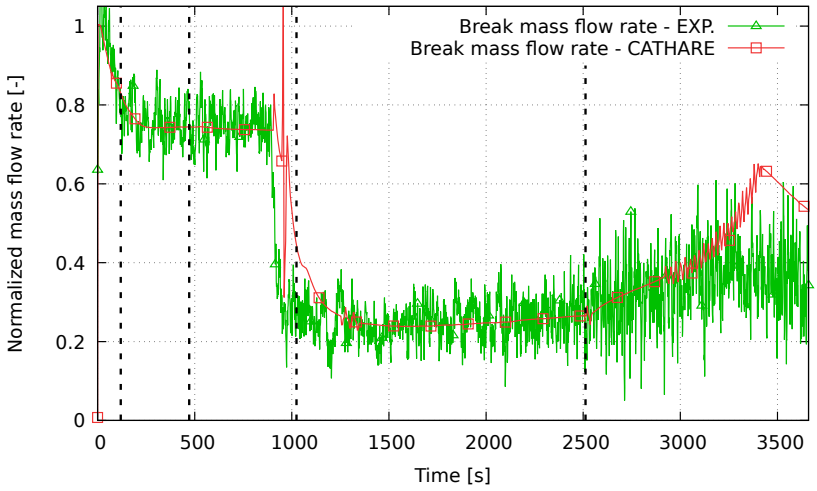

Figure 5.11: Break mass flow rate of the ROSA 1.2 test

The good predictions of pressures and break mass flow rate demonstrate the quality of the CATHARE code (less than 1% error for pressures and less than 4% for the mass flow rate in SBD and HQMD phases). It can then be used as a support to the scaling analysis. Main parameters of the study are shown in Table 5.4.

Table 5.4: Main parameters of the SBD and HQMD phases of the LSTF ROSA 1.2 test - CATHARE predictions

	1. SBD	4. HQMD
Initial primary mass $M_{1,0}$	5642 kg	2044 kg
Initial pressurizer mass $M_{prz,0}$	508 kg	-
Phase duration Δt	119 s	1484 s
Primary mass variation ΔM_1	652 kg	58.6 kg
Pressurizer mass variation ΔM_{prz}	434 kg	-
Pressure variation during the phases ΔP	$4.80 \cdot 10^6$ Pa	$3.34 \cdot 10^6$ Pa
Averaged mass flow rate at the break $\bar{\dot{M}}_{break}$	5.38 kg/s	1.56 kg/s
Averaged mass flow rate leaving the pressurizer $\bar{\dot{M}}_{prz}$	3.59 kg/s	-
Averaged mass flow rate of the HPIS $\bar{\dot{M}}_{HPIS}$	-	1.52 kg/s
Averaged core power $\bar{\dot{W}}_{core}$	$8.34 \cdot 10^6$ W	$1.37 \cdot 10^6$ W
Averaged pressurizer heaters power $\bar{\dot{W}}_{prz,heaters}$	$8.50 \cdot 10^4$ W	-
Averaged SG tubes heat exchanges $\bar{\dot{W}}_{SG}$	$-8.30 \cdot 10^6$ W	$1.05 \cdot 10^4$ W
Averaged primary wall heat exchanges $\bar{\dot{W}}_{ow}$	$3.86 \cdot 10^4$ W	$1.84 \cdot 10^5$ W
Averaged pressurizer wall heat exchanges $\bar{\dot{W}}_{prz,ow}$	$1.42 \cdot 10^5$ W	-

The values of the effect metrics for the mass equation $\Omega_{\dot{M},\chi_j}$ and the pressure equation $\Omega_{\dot{P},\chi_j}$ are displayed for the primary system and pressurizer volumes for the SBD phase respectively in Tables 5.5 and 5.6.

Table 5.5: Effect metrics for the primary system volume of the LSTF ROSA 1.2 test during the SBD phase

Rate of mass change in V_1 due to the contribution by:		
Liquid flow rate leaving the primary system through the break	$\Omega_{\dot{M}_{l,break}}$	**-1.000**
Vapour flow rate leaving the primary system through the break	$\Omega_{\dot{M}_{v,break}}$	-0.002

Rate of pressure change in V_1 due to the contribution by:		
Liquid flow rate leaving the primary system through the break	$\Omega_{\dot{P},Q_{l,break}}$	**-0.100**
Vapour flow rate leaving the primary system through the break	$\Omega_{\dot{P},Q_{v,break}}$	-0.002
Thermal expansion by condensation or vaporization due to the core heat generation	$\Omega_{\dot{P},Q_{core}}$	**1.000**
Thermal expansion by condensation or vaporization due to SG tubes heat exchanges	$\Omega_{\dot{P},Q_{SG}}$	**-0.995**
Thermal expansion by condensation or vaporization due to wall heat exchanges in the primary system*	$\Omega_{\dot{P},Q_{ow}}$	0.005

**except SG tubes and fuel rods*

Analysis of the effect metrics of the primary system volume during the SBD phase:

- Regarding the primary system control volume, the dominant effect metric on the rate of mass change is the one related to the liquid flow rate at the break with a very small contribution of the vapour break flow (500 times smaller). Although this repartition cannot be confirmed by measured data, this evaluation is easily accepted since almost only liquid water flows in the loops and pressure vessel.
- It can be observed on the rate of pressure change that the two processes related to heat exchange in the core and the SG tubes are dominant and almost compensate each other.
- The liquid volume flow rate at the break can be considered as influent.
- The vapour volume flow rate and wall heat exchanges are negligible during the SBD phase.

Table 5.6: Effect metrics for the pressurizer volume of the LSTF ROSA 1.2 test during the SBD phase

Rate of mass change in V_{prz} due to the contribution by:		
Liquid flow rate leaving the pressurizer	$\Omega_{\dot{M}_{l,prz}}$	**-1.000**
Vapour flow rate leaving the pressurizer	$\Omega_{\dot{M}_{v,prz}}$	-0.039

Rate of pressure change in V_{prz} due to the contribution by:		
Liquid volume flow rate leaving the pressurizer	$\Omega_{\dot{P},Q_{l,prz}}$	**-1.000**
Vapour volume flow rate leaving the pressurizer	$\Omega_{\dot{P},Q_{v,prz}}$	**-0.329**
Thermal expansion by condensation or vaporization due to the pressurizer heaters	$\Omega_{\dot{P},Q_{prz,heaters}}$	**0.159**
Thermal expansion by condensation or vaporization due to wall heat exchanges in the pressurizer	$\Omega_{\dot{P},Q_{prz,ow}}$	**0.265**

Analysis of the effect metrics of the pressurizer volume during the SBD phase:

- For the pressurizer control volume, the effect metrics that govern the mass and pressure change are those related to the flow rate leaving the pressurizer, which is close to the flow rate to the break. This was also observed by the UPV with the H2TS method. The scaling of the break flow rate should then respect the volume scale ratio. Since the choke flow mass flux is almost independent on the break diameter, this means that a good break scaling should apply the volume scaling factor to the break area.

- The effect metrics related to the pressurizer heaters and wall heat exchanges can be considered as influents. The UPV has instead taken into account a net heat term obtained from the subtraction of the pressurizer heat losses to the heat provided by the heaters (Muñoz-Cobo et al. 2018). Their corresponding scaling criteria (from π-monomial) has a value of 0.160. An effect metric of 0.158 is obtained with the same net heat calculation and with their assumptions.

  As shown by the UPV when comparing LSTF data to reactor scale calculation, the distortion of this contribution of the external pressurizer wall is large. It could be then considered that a pressurizer scaling which would not respect the height (e.g. by adopting a linear scaling) would be better for this LOCA subcooled blowdown phase. Note that the design of the LSTF pressurizer has been revised to simulate an AP1000 pressurizer and is relatively larger than a conventional Westinghouse PWR pressurizer.

- It can also be noted that in the CATHARE code predictions, the vapour mass flow rate leaving the pressurizer is negligible but its volume flow rate is a significant contribution to pressure decrease. It may then be considered that a 0-D modelling of the pressurizer is not sufficiently precise to predict the entrainment of bubbles from pressurizer to the surge line and to the hot leg. This vapour is due to flashing of the water and it may be expected a gradient of void fraction from bottom to the level with a minimum value at the connection to the surge line.

  A too simple 0-D modelling of the pressurizer may overestimate this void fraction and the vapour flow rate entrained in surge line. This is an example showing how an a posteriori scaling analysis with a system code may help improving the modelling.

The values of the effect metrics for the mass equation $\Omega_{\dot{M},\chi_j}$ and the pressure equation $\Omega_{\dot{P},\chi_j}$ are displayed for the primary system volume for the HQMD phase in Table 5.7.

Table 5.7: Effect metrics for the primary system volume of the LSTF ROSA 1.2 test during the HQMD phase

Rate of mass change in V_1 due to the contribution by:		
Liquid flow rate entering the primary system thanks to HPIS	$\Omega_{\dot{M}_{l,HPIS}}$	**1.000**
Liquid flow rate leaving the primary system through the break	$\Omega_{\dot{M}_{l,break}}$	**-0.802**
Vapour flow rate leaving the primary system through the break	$\Omega_{\dot{M}_{v,break}}$	**-0.225**

Rate of pressure change in V_1 due to the contribution by:		
Liquid flow rate entering the primary system thanks to HPIS system	$\Omega_{\dot{P},Q_{l,HPIS}}$	**0.062**
Thermal expansion by condensation due to the liquid flow rate entering the primary system thanks to HPIS system	$\Omega_{\dot{P},Q_{cond,HPIS}}$	**-1.000**
Liquid flow rate leaving the primary system through the break	$\Omega_{\dot{P},Q_{l,break}}$	**-0.050**
Vapour flow rate leaving the primary system through the break	$\Omega_{\dot{P},Q_{v,break}}$	**-0.356**
Thermal expansion by condensation or vaporization due to the core heat generation	$\Omega_{\dot{P},Q_{core}}$	**0.862**
Thermal expansion by condensation or vaporization due to SG tubes heat exchanges	$\Omega_{\dot{P},Q_{SG}}$	0.007
Thermal expansion by condensation or vaporization due to wall heat exchanges in the primary system*	$\Omega_{\dot{P},Q_{ow}}$	**0.116**

**except SG tubes and fuel rods*

Analysis of the effect metrics of the primary system volume during the HQMD phase:

- During the HQMD phase, the total contribution of the break mass flow rates to the primary mass is almost compensated by the HPIS.
- The three most important effect metrics for the rate of pressure change are the one related to the HPIS, to the core heat generation and to the break (mainly the vapour flow rate).
- The UPV gives a contribution from HPIS of 0.498. Having assumed here a saturation state overestimate the condensation of HPIS water.
- The UPV analysis found the net heat term (heat balance between the core, the SG tubes and the losses (Muñoz-Cobo et al. 2018)) as the dominant term. It is actually observed that the SG tubes exchanges term is negligible.
- Contributions of the wall heat exchanges can be considered as influent.
- On the contrary, the UPV found an almost zero break vapour flow rate while the analysis here gives a value of -0.356. These differences could be explained by the nature of the corresponding terms in the pressure equations, which do not refer exactly to the same quantities.
- An order of magnitude analysis of the terms of the pressure equation assuming saturation conditions (see Eq. 5.16) can estimates the global expansion coefficient K_s at the moment of the primary-secondary pressure reversal. It is found that the equation is not exactly balanced probably because the saturation assumption is not respected.

5.3. Discussions

An a posteriori scaling analysis is here applied to the 1% hot leg SB-LOCA of the ROSA 1.2 test performed on the Japanese LSTF-ROSA-IV facility. As defined at the beginning of this chapter, the objectives of this work were threefold.

The first objective was to verify the applicability of the FSA method on a complex nuclear transient. For this purpose, mass and pressure PoI were identified, and the FSA method was applied to established balance equations for the primary system and pressurizer volumes. The a posteriori scaling analysis was performed on two phases considered important (as these are the major depressurization phases) of this 1% SB-LOCA transient: the subcooled blowdown and high-quality mixture discharge phases. The formulation of pressure equation for the primary system and for the pressurizer as a volume rate of change equation helps giving a clear physical meaning to each contributor. Any fluid volume source or sink contributes to pressurization or depressurization. Any heating or cooling contributes to pressurization or depressurization. Since the control volume is constant, any imbalance between heating, cooling, fluid volume sources and sinks is compensated by a fluid volume expansion or contraction by pressure decrease or increase.

The second objective of this work was intended to provide a comparison between the results of the FSA with the one obtained by the UPV with the H2TS. The comparative analysis of these methods carried out shows that they are based on the same methodological approaches. The FSA may be seen as an improvement of the older H2TS method. However, several common aspects may be found in H2TS and FSA:

- To identify the scaling criteria and therefore distortions, H2TS performs time scaling through a characteristic time for the variable evolution. This characteristic time is the ratio between the control volume and the convective volumetric flow rate (Zuber 1991; Muñoz-Cobo et al. 2018). The equivalence in FSA corresponds to the time scaling for relative importance of agents. Since FRC takes into account the characteristic time of the processes, dimensionless effect metrics are directly linked to the dominant process (Zuber et al. 2007). As mentioned in Bestion et al. 2017 where a theoretical comparison of H2TS and FSA is carried out: "The FSA determines scale distortion quantitatively from the ratios of fractional rate changes for each specific agent of change. H2TS computes scale distortion by taking ratios of dimensionless characteristic-time ratios." To summarize, both methods establish scaling criteria but in different ways. The π-monomial in the H2TS and the effect metrics in the FSA. To calculate them, scaling methods take into account the ratio of the indicators of the intensities of the processes over the studied variable.

- The same normalization concept of the contributing terms of the balance equations are used. The H2TS and FSA methods suggest the use of boundary conditions for this normalization.

- As shown by the application made here, the results obtained by the two methods are similar when the nature of the equations is equivalent. The most important is not the method itself but the choice of equations, the possible simplifications that are used, and the way to evaluate each term. Their choice is therefore essential for the qualitative study of a transient. In addition, the FSA improvements are likely to provide better temporal analysis.

- According to the results of this scaling analysis, the hierarchy of the processes acting on mass and pressure change during the subcooled blowdown and the high-quality mixture discharge phases is established. All methods identify the same scaling criteria to apply to power and to break area. Both methods identify distortions due to heat exchanges with walls (other than

fuel rods and SG tubes). Surprisingly no ITF which used the power-to-volume scaling and full height scaling (e.g. BETHSY, LSTF, LOBI, SPES) adopted another scaling criterion for the pressurizer which would minimize the distortion by using a reduced height of this component only.

The third objective of this work was to demonstrate the applicability of an advanced scaling method supported by a system code, particularly the CATHARE code. For this purpose, averaged quantities of the equations intended to provide the scaling criteria were normalized using the CATHARE calculation. It is demonstrated through its use that a mature and sufficiently validated system code allows the method user to limit the assumptions about the values chosen for the study. The code actually provides more precision by averaging these values rather than relying on estimates at the phase boundaries. Scaling analyses can now be performed with the support of system codes. Moreover, scaling methods can also support the improvement of the code modelling as shown in the pressurizer pressure equation analysis for the subcooled blowdown phase.

The applicability of the FSA method on complex transient has been validated, and its choice for scaling studies in this thesis has been confirmed: - by the comparison with the H2TS method, - and by its ability to be supported by the CATHARE system code. It is now proposed to deepen the potentials of a posteriori scaling analyses. Although the work in this chapter has yielded satisfying results, it is worthwhile to assess the capabilities of scaling on a full-transient without using a saturation assumption in the pressure equation.

CHAPTER 6

Investigation of the Capability of the FSA Method to Identify and Quantify System/Component Scale Distortions Between Facilities and a PWR for a 6% SB-LOCA Transient

The applicability of the Fractional Scaling Analysis (FSA) method was demonstrated in chapter 5, through its application to a complex nuclear transient and achieving consistent results. Furthermore, it was shown that the FSA could be supported by the CATHARE 3 system code for a posteriori scaling analyses.

The objective of this chapter is to investigate the capability of the FSA method to identify and quantify distortions at system/component scale between several systems. For this purpose, a scaling analysis is performed using the FSA method on a counterpart test of three systems, on which the same 6% Cold Leg SB-LOCA transient is conducted. This counterpart test is carried out on two IET and a reference reactor transient simulations (Kumamaru et al. 1992; D'Auria et al. 1992):

- The 6.2-TC test performed on the French BETHSY facility.
- The SB-CL-21 test performed on the Japanese LSTF-ROSA-IV facility.

- A full-scale model of a Framatome commercial Pressurized Water Reactor (PWR), which is the reference reactor of the BETHSY facility.

This work is done by revisiting a posteriori the phenomenology and the scaling of rather old integral tests using current knowledge and tools. To ensure a numerically justified analysis, the transients CATHARE 3 code predictions will be validated through a comparison to experimental results. Furthermore, the scaling analysis for this study will be performed on the whole transient, through all of its phases, and using mass and general pressure equations, without saturation assumption.

The present study was published in the Journal of Nuclear Engineering and Design as "Scaling analysis of a SB-LOCA counterpart test between BETHSY and LSTF facilities and a three loops PWR", (Ciechocki et al. 2022b).

6.1. Description of the Counterpart Test

The 6.2-TC test was performed on the BETHSY (Boucle d'Etude ThermoHydraulique SYstème) facility defined by the French partners Framatome, EDF and CEA (Equipe BETHSY 1990). It was designed to simulate a Framatome three loops PWR with a full power of 2775 MWt – 900 MWe. As shown in Figure 6.1a, BETHSY has three loops, three steam generators and one pressurizer. The facility was designed using the same power-to-volume method (described in section 3.3.1.3), a full height scaling and a 1/100 scaled volume at full-pressure reference condition (FHFP ITF). The scaling of BETHSY respects the timing of events. The core is composed of 428 full-length electrically heated rods. The maximal core power is equal to 10% of the 1/100 nominal power of the reference reactor. i.e. 2.86 MWt. Each steam generator is composed of a tube bundle consisting of 34 full-size U-tubes. For the 6.2-TC test, the break unit is located on the side of the horizontal cold leg of the pressurizer loop.

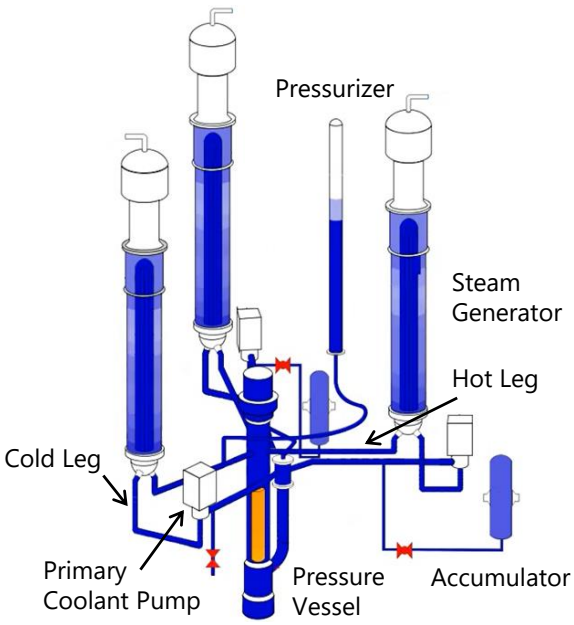

(a) Schematic view of the BETHSY primary system (Prošek et al. 2012)

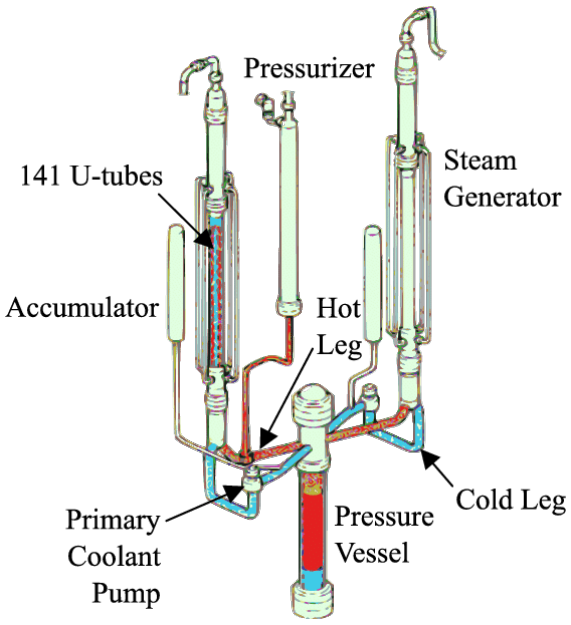

(b) Schematic view of the LSTF primary system (Clifford et al. 2016)

Figure 6.1: Schematic view of the BETHSY and LSTF primary systems

The SB-CL-21 test was performed on the the Large Scale Test Facility (LSTF) facility, described in section 5.1.1. For this test, the LSTF initial core power is set to 11% of nominal power of its reference reactor, corresponding to 7.93 MWt. The break unit is located on the side of the horizontal cold leg of the loop without the pressurizer (The ROSA-V Group 1985).

The Framatome three loops reference PWR of BETHSY is also studied in this counterpart test in order to identify the potential distortions between the two ITF and a full-scale reactor. The core for this typical 900 MWe PWR consists of 157 fuel assemblies, each composed of 264 fuel rods, supplying the 2775 MWt. The 6% SB-LOCA transient for this PWR is referred as "PWR 900-SBL" in this study.

The CATHARE system code is used in this study to simulate the BETHSY 6.2-TC, LSTF SB-CL-21 and PWR 900-SBL tests. The three input decks represent the primary and secondary systems. The primary side contains the Reactor Pressure Vessel (RPV), hot and cold legs with main coolant pumps, the pressurizer and the U-tubes of the steam generators. The tests also include Accumulator Injection Systems (AIS). The 6% SB-LOCA transient represented by these tests assumes the absence of HPIS and LPIS. The nodalization of the primary systems of BETHSY, LSTF and the PWR are shown in Figure 6.2. Their primary system is modelled with 1-D modules, except for the pressurizer, lower and upper plenums and upper head where 0-D modules are used (see CATHARE modelling structure in section 4.3). Note that the channel heads of the LSTF steam generators are also modelled with 0-D modules.

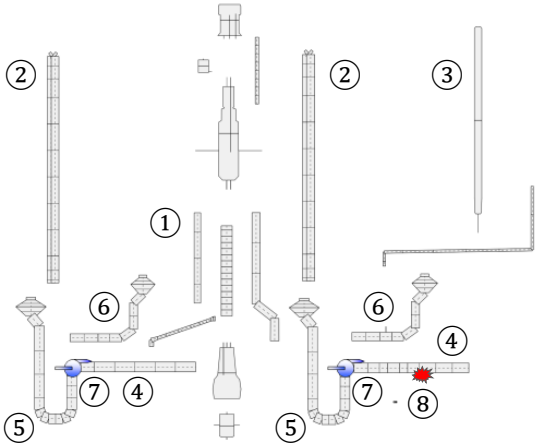

(a) CATHARE nodalization of the BETHSY 6.2-TC test

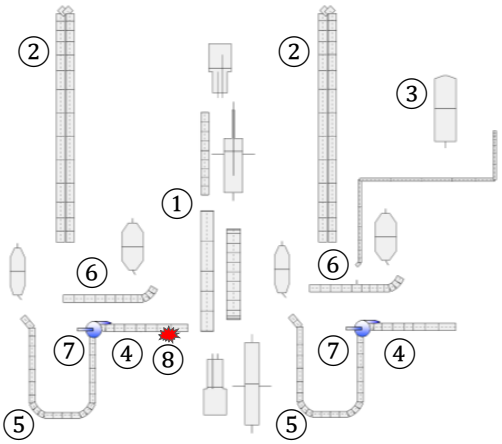

(b) CATHARE nodalization of the LSTF SB-CL-21 test

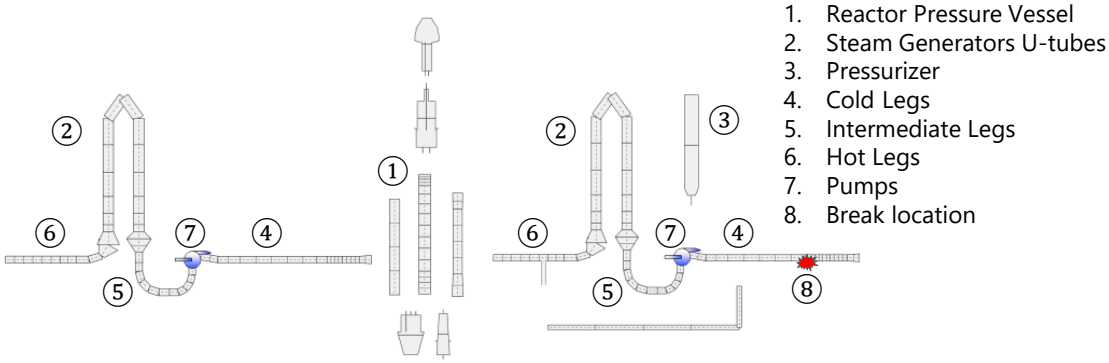

(c) CATHARE nodalization of the PWR 900-SBL test

Figure 6.2: BETHSY, LSTF and PWR CATHARE primary systems nodalization

The current work aims to revisit the counterpart test between the 6.2-TC and the SB-CL-21 transients of the respective BETHSY and LSTF facilities (Kumamaru et al. 1992; D'Auria et al. 1992). The main conditions of both tests were jointly defined by CEA and JAERI, with the main objectives being:

- To investigate design and scale effects between the two facilities for a SB-LOCA transient.
- To provide a data base for code assessment to better validate the extrapolation of this type of transient to nuclear plant.

This is why the 6% SB-LOCA code simulation of reference PWR of BETHSY is included in the initial counterpart test. However, it should then be highlighted that the LSTF reference reactor is different than the BETHSY reference reactor. As a result, LSTF may have inherent scaling differences with the simulated PWR due to the initial and boundary conditions. Therefore, some results related to the design differences of LSTF from BETHSY and the PWR are discussed in the analyses. The main characteristics of BETHSY, LSTF and the PWR are summarized in Table 6.1.

Table 6.1: Main characteristics of BETHSY, LSTF and the PWR

	BETHSY	LSTF	PWR
Reference reactor	F-PWR-3L	W-PWR-4L	-
Number of loops	3	2	3
Reference reactor loops number	3	4	-
Scaling method	Power-to-volume	Power-to-volume	-
Volume scale	1/100	1/48	1/1
Height scale	1/1	1/1	1/1
Time scale	1/1	1/1	1/1
Power scale	10%	14%	100%
Maximum power	2.86 MWt	10.0 MWt	2 775 MWt
Reference reactor maximum power	2 775 MWt	3 423 MWt	-
Total heated rods	428	1 008	41 448
Break area	$1.882 \cdot 10^{-4}$ m^2	$5.187 \cdot 10^{-4}$ m^2	$1.824 \cdot 10^{-2}$ m^2

6.2. The 6% SB-LOCA Transient

6.2.1. Description of the 6% SB-LOCA Transient

The BETHSY 6.2-TC and LSTF SB-CL-21 tests scenarios consist of a SB-LOCA experiment with the break located on one of the horizontal cold legs, without High Pressure Injection System (HPIS) and Auxiliary Feedwater (AFW) System. The ratios of break area, initial mass inventory and core power of LSTF to BETHSY are set to 2.76. This scaling factor is equal to the ratio of the SG U-tubes flow area, that is important to the liquid holdup phenomena in the SG U-tubes. The ratios of break area, initial mass inventory and core power of LSTF to BETHSY are set to 2.76. In both facilities, the break is equivalent to a 6 inches cold leg break, oriented horizontally, in their reference reactors. This break size corresponds to about respectively 5% and 6.5% of the corresponding cold leg flow area in BETHSY and LSTF references reactors (Kumamaru et al. 1992).

The transient starts at operating full-pressure of 15.5 MPa and at 10% of the nominal scaled power. The reactor SCRAM signal occurs at 13 MPa resulting in the core power decay and pumps trip. The steam generators vapour lines are isolated and the set point of atmospheric relief valves is fixed to 7.2 MPa. The normal feedwater is stopped. Finally, the AIS is activated at 4.2 MPa.

The overall phenomenology of the 6% SB-LOCA is essentially the same as the 1% SB-LOCA transient described in section 5.1.2. However, some discrepancies must be noted due to processes directly related to the size of the break or to some safety systems that are not operated in the context of the present 6% SB-LOCA:

- The 6% SB-LOCA transient is faster than the 1% SB-LOCA. This is due to the larger break, which discharges more fluid and depressurizes the system more quickly. The LOCA events follow each other faster and sometimes overlap, which can cause differences in the phases and phenomenology of the transient.
- This transient assumes that HPIS and LPIS are not operational. These tests also do not include pressurizer heaters, which allow for temporary pressure maintenance.
- The Subcooled Blowdown (SBD) phase is more violent: the primary system rapidly depressurizes from 15.5 MPa to 8.0 MPa about 20 seconds. The SCRAM signal is then activated after about 6 seconds. Because of the sudden drop in pressure, flashing occurs almost instantly after the break opening in the hottest parts of the primary system.
- The reduced initial core power is maintained for the facilities for 53 seconds after the SCRAM signal. The core power will then follow the JAERI conservative decay power curve. For the PWR, the core power decreases because of the control rod insertion, following the decay power.
- The primary pump trip occurs at the SCRAM signal and pump speed decreases and stops in both facilities. For the PWR, the pumps rotation speed decreases more slowly due to a higher initial velocity, initiating the transition to the natural circulation.
- The Two-Phase Discharge (TPD) phase of the 1% SB-LOCA was characterised by an intermediate void fraction in the primary circuit and at the break. Because the transition from liquid to vapour state is faster in the 6% SB-LOCA and the Counter-Current Flow Limitation (CCFL) phenomenon is more important, the TPD phase is renamed according to the Reflux Condenser Mode (RCM) for this 6% SB-LOCA transient.
- Because the pressure difference between the cold and hot parts of the system increases more rapidly as the break discharges, the LSP/LSC phenomena become more significant and likely to occur.
- In comparison to the 1% SB-LOCA HQMD phase, the discharge at the break is almost pure vapour, accelerating the depressurization.

The 6% SB-LOCA transient is divided into the five chronological phases according to the bifurcating events, defined in Table 5.2 of the 1% SB-LOCA transient study. Theses phases are illustrated in Figure 6.3 for the BETHSY 6.2-TC, the LSTF SB-CL-21 and the PWR 900-SBL tests, along with transient parameters of interest.

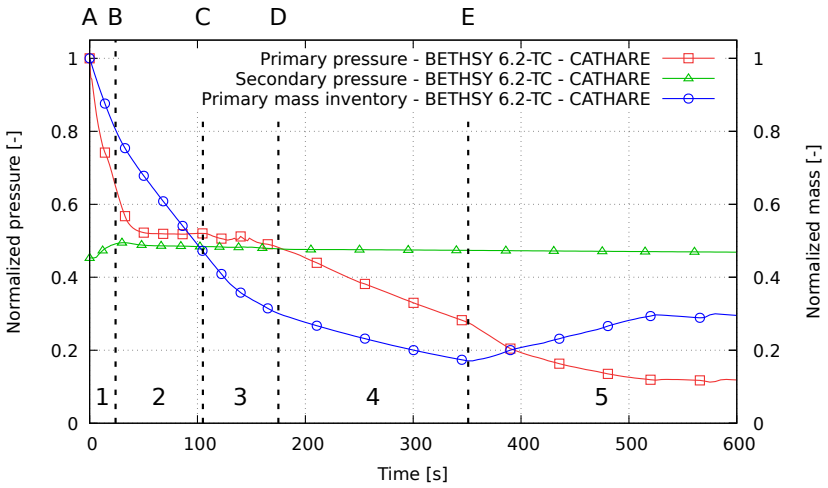

(a) The BETHSY 6.2-TC test

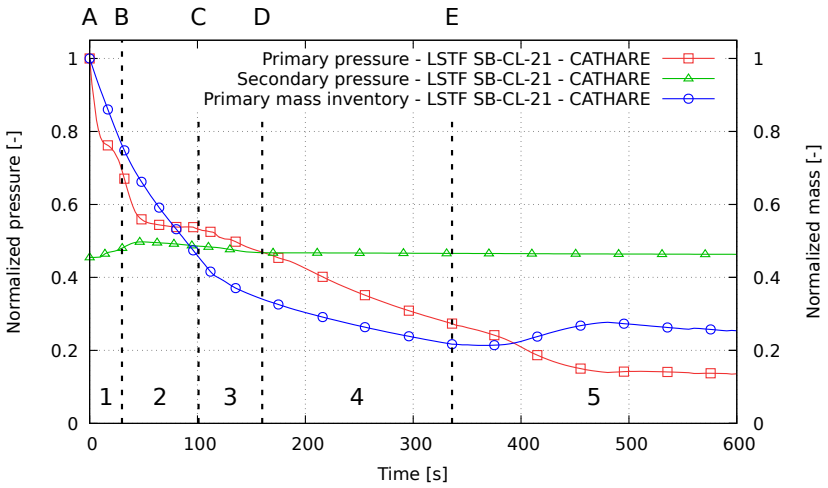

(b) The LSTF SB-CL-21 test

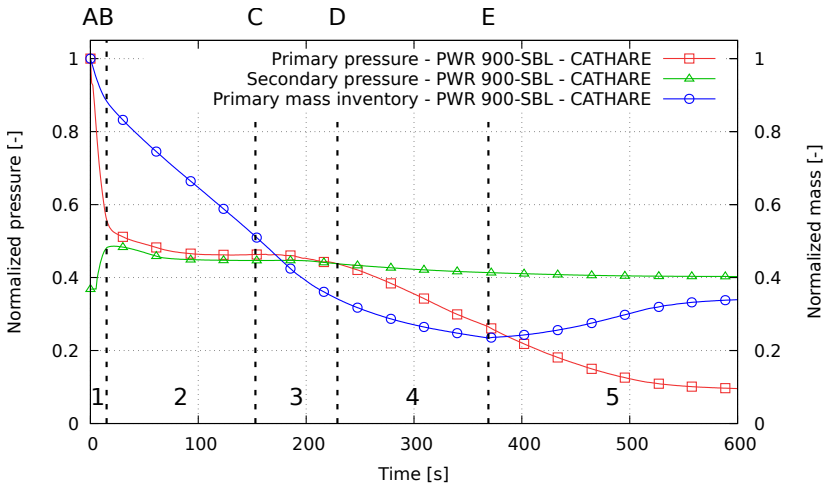

(c) The PWR 900-SBL test

Figure 6.3: Primary and secondary evolutions during the phases of the 6% SB-LOCA transient - CATHARE predictions

6.2.2. Experimental and Simulated Results: Comparison Between Facilities and PWR

To conduct a coherent scaling analysis, the main parameters and evolutions predicted by the calculation code must be validated. In addition, the author proposes a systematic phenomenological analysis of the transients studied in a counterpart test to strengthen the methodology and identify the distortions inherent to the code.

The phenomenological analysis of the BETHSY 6.2-TC, LSTF SB-CL-21 and PWR 900-SBL tests is presented in this section. When available, CATHARE predictions and experimental results are displayed together. The parameter evolutions are shown as normalized values, which are the values at any given time divided by a representative value (e.g. initial or maximum value). Table 6.2 provides a comparison of initial and boundary conditions at steady state, between experimental measured data and code predictions.

Table 6.2: Steady state comparison of initial and boundary conditions of the 6% SB-LOCA counterpart test between experimental data and code predictions

	BETHSY 6.2-TC		LSTF SB-CL-21		PWR 900-SBL
	EXP.	CATHARE	EXP.	CATHARE	CATHARE
Core power	2.86 MWt	2.84 MWt	7.93 MWt	7.93 MWt	2830 MWt
Primary system pressure	15.35 MPa	15.13 MPa	15.37 MPa	15.40 MPa	15.68 MPa
Secondary system pressure	6.85 MPa*	6.86 MPa*	7.00 MPa*	7.00 MPa*	5.78 MPa*
Pressurizer liquid level	7.45 m	7.35 m	1.70 m	1.70 m	7.32 m
Cold leg fluid temperature	285 °C*	285.2 °C*	287 °C*	287.2 °C*	280.0 °C*
Hot leg fluid temperature	316 °C*	316.1 °C*	317 °C*	316.6 °C*	315.7 °C*
Primary liquid mass	1 984 kg	1 947 kg	5 404 kg	5 543 kg	190 351 kg

**loops averaged*

The initial test conditions predicted by CATHARE are found to be consistent with the experimental data. Minor differences that can be attributed to measurement errors. For example, BETHSY experimental data are given with a core power error of 0.03 MWt, a pressure error of 0.15 MPa, a pressurizer liquid level error of 0.2 m and a primary liquid mass error of 50 kg.

In comparison to the PWR, the scaling of the two facilities respects the timing of events. Nonetheless, there are some minor differences between the experimental results and the CATHARE predictions, as well as between the facilities and the extrapolated PWR. Table 6.3 summarizes the main events that occurred during the transient. Examples of notable temporal differences or occurrences are:

- For this counterpart test, the pump coastdown of the facilities was not simulated to minimize the effect of different pump characteristics for the BETHSY and LSTF reference PWR (Kumamaru et al. 1992). Then, the time at which the pumps are stopped differs. Although the LSTF pumps take longer to stop than the BETHSY pumps, the main difference is the inertia of the PWR pumps, which prevents them from completely stopping. The impact of theses difference in pumps behaviour will be discussed in the following sections.
- CATHARE predicts a too late pressurizer emptying. The duration of the PWR pressurizer emptying is also longer than for facilities. The investigation of the Subcooled Blowdown (SBD)

phase in section 6.3.3 will discuss this distortion.

- Reflux Condenser Mode (RCM) phase events occur in the PWR later than in the facilities, resulting in a later primary-secondary pressure reversal.
- The Loop Seal Plugging (LSP) and Loop Seal Clearing (LSC) phenomena appear distorted. There is few experimental data on these phenomena, and they are only mentioned as LSC. This will be discussed in section 6.3.5.
- Experimental and predicted results show a second core uncovery leading to a second PCT on BETHSY, but not on LSTF nor on the PWR.
- Although the accumulator discharge occurs at roughly the same time, both experimentally and predicted by the code, the discharge durations are vastly different. These discrepancies will be discussed in sections 6.3.7 and 6.3.8.

Table 6.3: Chronology of the main events of the 6% SB-LOCA transient

Event	BETHSY 6.2-TC		LSTF SB-CL-21		PWR 900-SBL
	EXP.	CATHARE	EXP.	CATHARE	CATHARE
1. SBD					
Break opening	0 s	0 s	0 s	0 s	0 s
SCRAM signal	8 s	6 s	6 s	6 s	5 s
Pump stopped	8 s	8 s	n/a	17 s	n/a
2. NC					
Pressurizer empty	18 s	24 s	16 s	30 s	15 s
3. RCM					
No flow rate at the top of SG tubes	110 s	105 s	110 s	101 s	153 s
First core uncovery	134 s	126 s	94 s	118 s	188 s
First Peak Clad Temperature	134 s	134 s	94 s	118 s	188 s
Loop Seal Plugging	n/a	134 s	n/a	125 s	128 s
Loop Seal Clearing	140 s	151 s	110 s	154 s	161 s
4. HQMD					
Primary-secondary pressure reversal	176 s	175 s	165 s	160 s	229 s
Second core uncovery	342 s	355 s	n/a	n/a	n/a
Second Peak Clad Temperature	375 s	360 s	n/a	n/a	n/a
5. RR					
Activation of accumulator discharge	345 s	351 s	346 s	336 s	369 s
Minimum primary side mass	350 s	355 s	346 s	336 s	369 s
End of accumulator discharge	976 s	890 s	688 s	720 s	1467 s

n/a: not available

With the purpose to show some of the major evolutions, Figure 6.4 depicts the mass flow rate at the break. A rather good agreement between the code predictions and the experimental results is observed although the strange oscillatory results of LSTF (a possible measurement artefact) is

not predicted by CATHARE. During the RCM phase, differences between BETHSY and LSTF are observed. In LSTF, the transition to high void fraction flow and then to vapour flow rate at the break occurs earlier than in BETHSY. This may be related to the geometry of two facilities: the volume above the break elevation is about 65% of the total primary volume in LSTF whereas it is 70% in BETHSY. This reflects differences in the geometry of the reference reactors of the two facilities. The break flow rate predicted in the PWR simulation is lower than in the experiments up to the decrease due to high quality. It may be due to a longer pumps rotation, which brings a little higher quality at the break. As a result, the transition to high quality break flow is later than in the experiments as shown by the primary mass inventory in Figure 6.5.

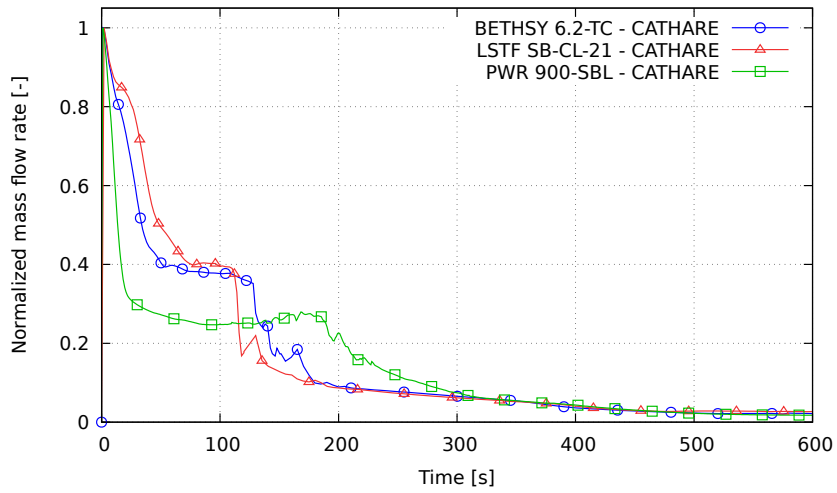

(a) CATHARE predictions

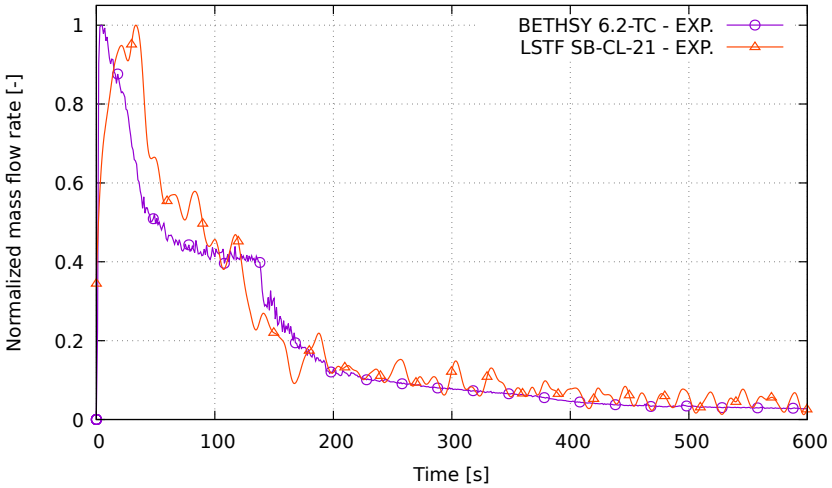

(b) Experimental results

Figure 6.4: Break mass flow rate of the 6% SB-LOCA counterpart test

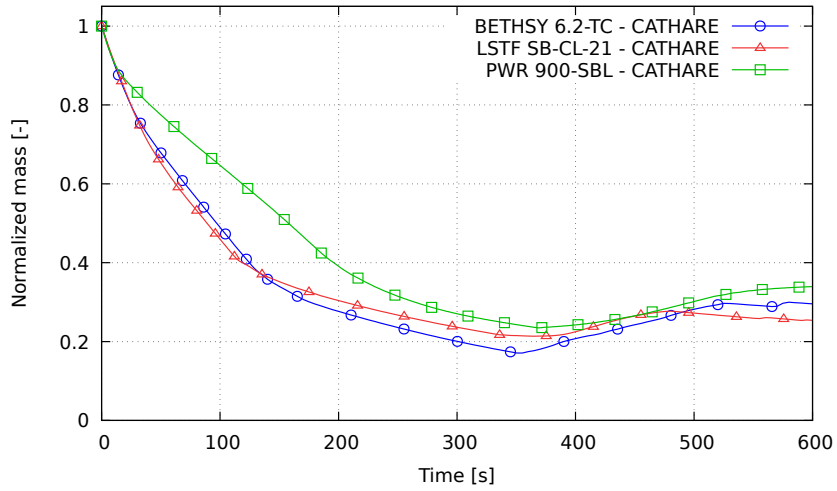

(a) CATHARE predictions

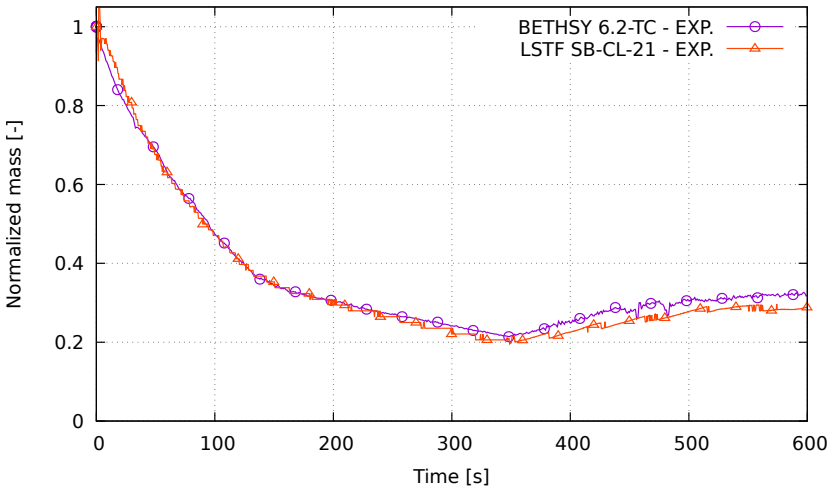

(b) Experimental results

Figure 6.5: Primary mass inventory of the 6% SB-LOCA counterpart test

Figure 6.6 depicts the primary system pressure. The pressure drops rapidly during the first seconds of the transient due to the liquid lost at the break and the pressurizer emptying. Then the pressure has a plateau above the secondary pressure as long as the core gives a higher power than the power lost at the break. This requires that the power difference is transferred to the secondary circuit. Finally, when the liquid to vapour transition occurs at the break, the power lost at the break is higher than the core power and the system depressurizes below secondary pressure. As shown in Figure 6.6a and Figure 6.6b, simulations provide pressure evolutions that are very close to the experimental values.

There are some discrepancies between the facility results and the PWR predictions. During the SBD phase, the PWR primary system depressurizes faster and during the pressure plateau the PWR primary pressure is lower than in the experiment.

It is worth mentioning that the BETHSY secondary pressure had to be increased to 6.85 MPa for the comparative test with LSTF, which differs from its PWR reference nominal pressure (5.78 MPa). This explains the pressure plateau difference between BETHSY and the PWR, as demonstrated in Appendix H.

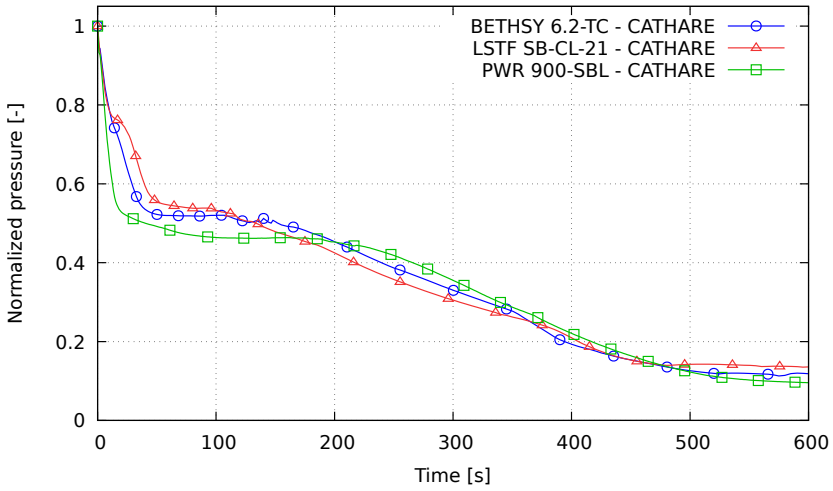

(a) CATHARE predictions

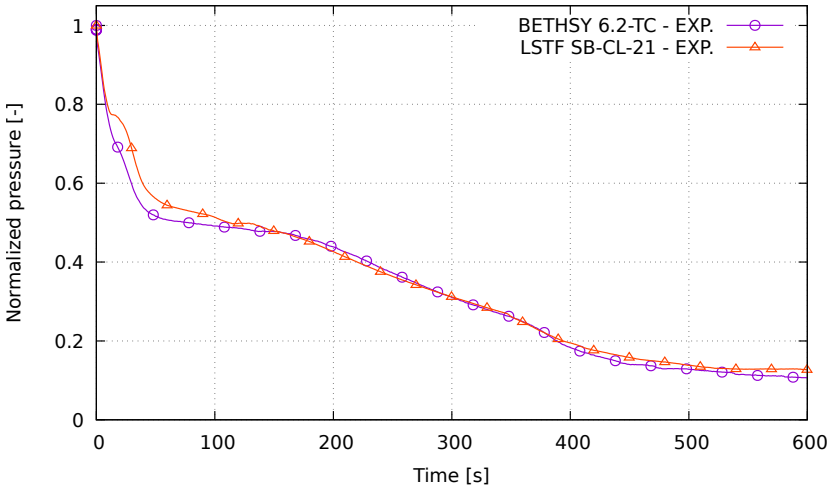

(b) Experimental results

Figure 6.6: Primary pressure of the 6% SB-LOCA counterpart test

As mentioned in section 6.1, the initial core power is 10% of their reference reactor in BETHSY and 11% in LSTF although it is 100% in the reactor. After the SCRAM signal, the JAERI conservative power decay curve was used experimentally for BETHSY as well as for LSTF. However, the time at which the core power in the experiment leaves the scaled power was delayed to compensate the total core power delivered between 100% and the scaled power. Figure 6.7 shows the normalized power decay (power/initial power of the reference reactor). It is clear that the PWR power drop is faster than in the facilities. The three power curves evolve in a similar way only after about 300 seconds of transient.

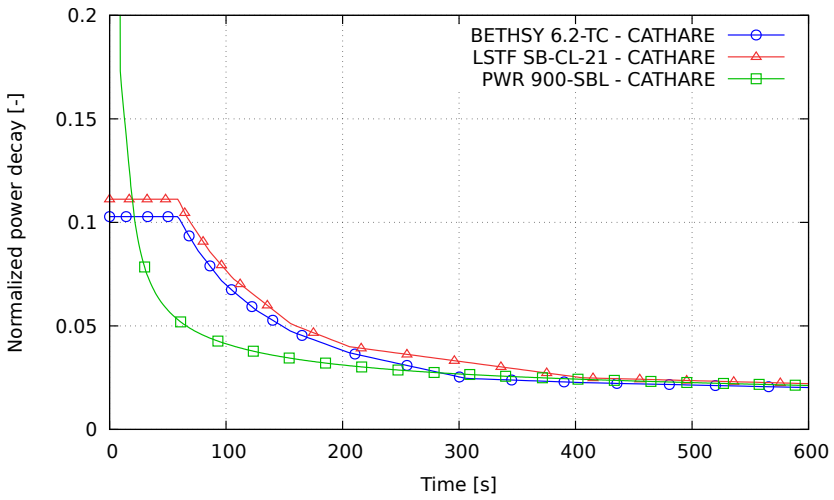

Figure 6.7: Core power decay of the 6% SB-LOCA counterpart test - CATHARE predictions

The core-collapsed level (i.e. the liquid level assumed in the core if there were no bubbles) is an important parameter to consider, as it is directly related to the Peak Clad Temperature (PCT) safety criterion. Figures 6.9 and 6.10 shows differences in the core collapsed level and the PCT. On LSTF, the first core uncovery is almost total and occurs slightly earlier than on BETHSY. On BETHSY, there is a slight difference in the minimum collapsed level intensity between the code predictions and the experimental results. The PCT appears to be very sensitive to the duration of the core uncovery. As has been observed as well as in other tests, the maximum temperature reached in the core is more dependent on the time the core is uncovered than on the uncovery depth. Figure 6.8 illustrate the core uncovery and the resulting PCT phenomena.

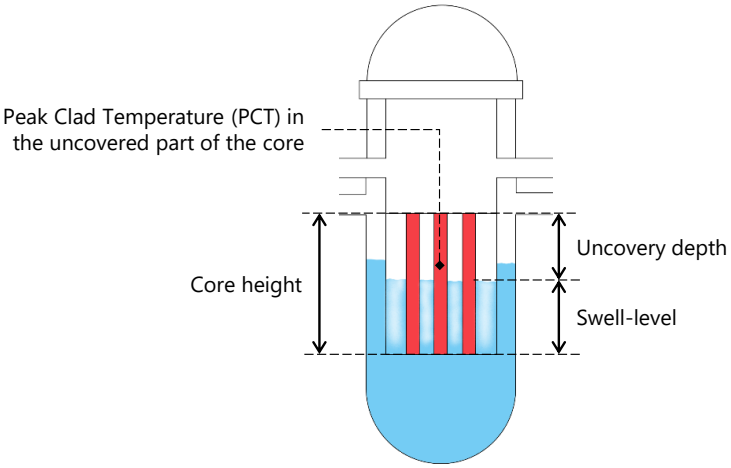

Figure 6.8: The core uncovery and Peak Clad Temperature (PCT) phenomena

Some differences between the code predictions and the experimental results are observed. The PWR core uncovery is predicted later than in BETHSY and LSTF (see Table 6.3). It should be noted that the PCT occurs at different elevations depending on the depth of the core uncovering and on some reverse flow from upper plenum. The code predicts the PCT at 51% of the core height in BETHSY, 16% in LSTF and 75% in the PWR.

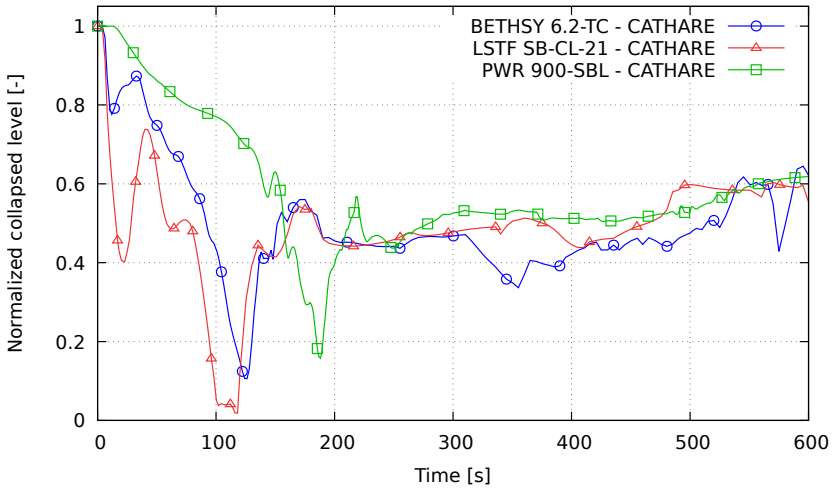

(a) CATHARE predictions

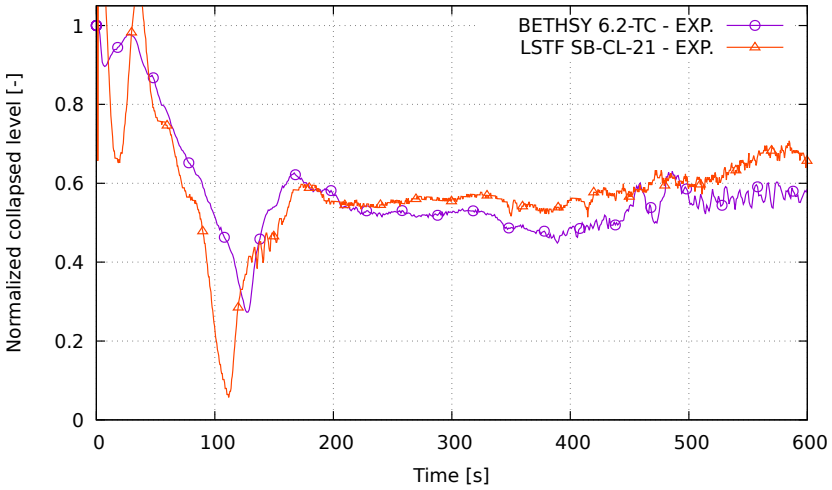

(b) Experimental results

Figure 6.9: Core-collapsed level of the 6% SB-LOCA counterpart test

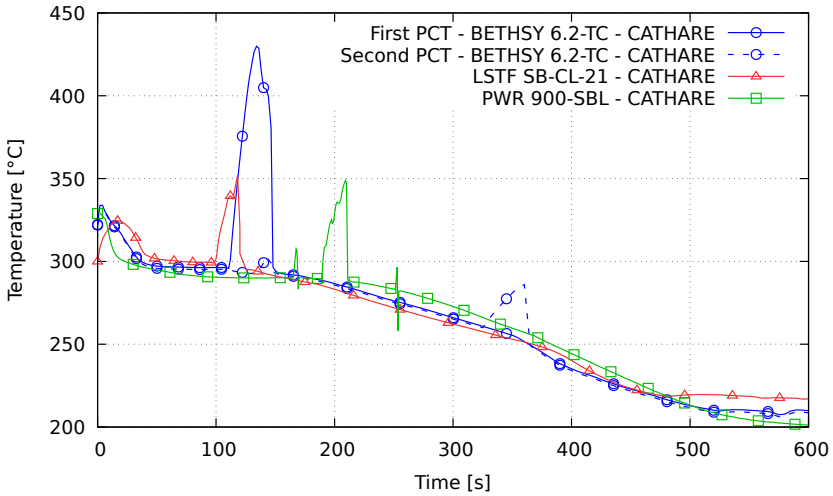

(a) CATHARE predictions

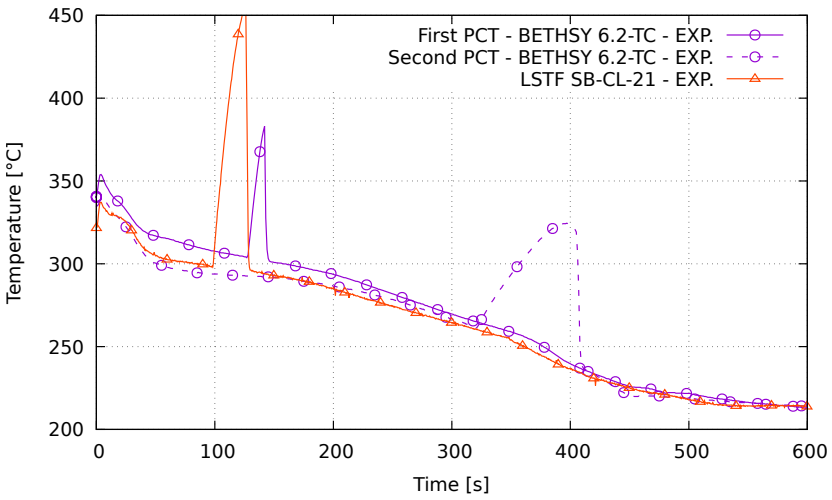

(b) Experimental results

Figure 6.10: Peak Clad Temperature of the 6% SB-LOCA counterpart test

6.3. Top-Down Scaling Analysis of the 6% SB-LOCA Transient with the FSA Method

In order to evaluate its capability to identify and quantify inter-system distortions at the system/component scale, the FSA method (see section 3.3.2.4) is applied independently to each of five transient phases. As for the 1% SB-LOCA, the PCT is the Figure of Merit (FoM) of the 6% SB-LOCA, resulting in the definition of the most important Parameters of Interest (PoI): the primary mass inventory M_1 and the primary pressure P_1 (see section 5.2). The pressurizer controls the primary pressure evolution until it is emptied, hence the mass and pressure equations for the primary system and pressurizer volumes are written.

6.3.1. Mass Balance Equations in a Volume V

The mass balance equations are derived in the same approach as they were in section 5.2.1 for the present counterpart test analysis. Applied to the primary system volume V_1, this results in Eq. 5.5 and 5.8 from which the HPIS terms are absent, as they are assumed not to be triggered for the 6% SB-LOCA transient. Eq. 5.6 and 5.9 related to the mass balance applied to the pressurizer volume V_{prz} remain unchanged.

6.3.2. Pressure Equations in a Volume V

As discussed in section 3.4, an aim of the current study is to apply the general pressure by Volume Rate of Change (VRC) equation. This equation is more detailed in its consideration of the phenomena than the one used in the chapter 5 study with the saturation assumption. The Eq. 5.14 applied to the primary systems volumes V_1 of the 6% SB-LOCA of the BETHSY 6.2-TC, the LSTF SB-CL-21 and the PWR 900-SBL transients gives:

$$
\begin{aligned}
(\mu_{l,1} \cdot M_{l,1} + \mu_{v,1} \cdot M_{v,1}) \cdot \dot{P}_1 = & \quad (1) \\
\dot{M}_{l,acc.} \cdot \nu_{l,1} + \dot{M}_{l,acc.} \cdot \nu'_{l,h,1} \cdot (h_{l,acc.} - H_l) & \quad (2) \\
-\dot{M}_{l,break} \cdot \nu_{l,1} - \dot{M}_{v,break} \cdot \nu_{v,1} & \quad (3) \\
+\nu'_{l,h,1} \cdot W_{wl,core} + \nu'_{l,h,1} \cdot W_{wl,SG} + \nu'_{l,h,1} \cdot W_{owl} & \quad (4) \\
+\nu'_{v,h,1} \cdot W_{wv,core} + \nu'_{v,h,1} \cdot W_{wv,SG} + \nu'_{v,h,1} \cdot W_{owv} & \quad (5) \\
+\frac{W_{wi,core}}{\varpi_1} + \frac{W_{wi,SG}}{\varpi_1} + \frac{W_{owi}}{\varpi_1} & \quad (6) \\
+\nu'_{l,h,1} \cdot W_{il,core} + \nu'_{l,h,1} \cdot W_{il,SG} + \nu'_{l,h,1} \cdot W_{il,ov} & \quad (7) \\
+\nu'_{v,h,1} \cdot W_{iv,core} + \nu'_{v,h,1} \cdot W_{iv,SG} + \nu'_{v,h,1} \cdot W_{iv,ov} & \quad (8) \\
-\frac{W_{il,core} + W_{iv,core}}{\varpi_1} - \frac{W_{il,SG} + W_{iv,SG}}{\varpi_1} - \frac{W_{il,ov} + W_{iv,ov}}{\varpi_1} & \quad (9)
\end{aligned}
\tag{6.1}
$$

With the rate of pressure change in the primary system volume (1) due to the contributions by:

(2) The thermal expansion and the resulting condensation due to the liquid flow rate entering the primary system thanks to the accumulator discharge.

(3) Liquid and vapour volume flow rate leaving the primary system through the break.

(4) Thermal expansion or contraction by wall-liquid heat transfers in the core, the SG tubes, and the primary system.

(5) Thermal expansion or contraction by wall-vapour heat transfers in the core, the SG tubes, and the primary system.

(6) Volume change by wall boiling or condensation in the core, the SG tubes, and the primary system.

(7) Thermal expansion or contraction by interface-liquid heat transfers in the core, the SG tubes, and the primary system.

(8) Thermal expansion or contraction by interface-vapour heat transfers in the core, the SG tubes, and the primary system.

(9) Volume change by vaporization or condensation by interfacial transfers in the core, the SG tubes, and the primary system.

The Eq. 5.14 applied to the pressurizers volumes V_{prz} of the 6% SB-LOCA of the BETHSY 6.2-TC, the LSTF SB-CL-21 and the PWR 900-SBL transients gives:

$$
\begin{aligned}
(\mu_{l,prz} \cdot M_{l,prz} + \mu_{v,prz} \cdot M_{v,prz}) \cdot \dot{P}_{prz} = \quad & (1) \\
-\dot{M}_{l,prz} \cdot \nu_{l,prz} - \dot{M}_{v,prz} \cdot \nu_{v,prz} \quad & (2) \\
+\nu'_{l,h,prz} \cdot W_{wl,prz} \quad & (3) \\
+\nu'_{v,h,prz} \cdot W_{wv,prz} \quad & (4) \\
+\frac{W_{wi,prz}}{\varpi_{prz}} \quad & (5) \\
+\nu'_{l,h,prz} \cdot W_{il,prz} \quad & (6) \\
+\nu'_{v,h,prz} \cdot W_{iv,prz} \quad & (7) \\
-\frac{W_{il,prz} + W_{iv,prz}}{\varpi_{prz}} \quad & (8)
\end{aligned}
\tag{6.2}
$$

With the rate of pressure change in the pressurizer volume (1) due to the contributions by:

(2) Liquid and vapour volume flow rate leaving the pressurizer to the surge line.

(3) Thermal expansion or contraction by wall-liquid heat transfers in the pressurizer.

(4) Thermal expansion or contraction by wall-vapour heat transfers in the pressurizer.

(5) Volume change by wall boiling or condensation in the pressurizer.

(6) Thermal expansion or contraction by interface-liquid heat transfers in the pressurizer.

(7) Thermal expansion or contraction by interface-vapour heat transfers in the pressurizer.

(8) Volume change by vaporization or condensation by interfacial transfers in the pressurizer.

To simplify the notation of the pressure change due to VRC, the global expansion coefficients K_1 and K_{prz} are defined:

$$K_1 = (\mu_{l,1} \cdot M_{l,1} + \mu_{v,1} \cdot M_{v,1}) \tag{6.3}$$

$$K_{prz} = (\mu_{l,prz} \cdot M_{l,prz} + \mu_{v,prz} \cdot M_{v,prz}) \tag{6.4}$$

Each contributor to the pressure rate of change $\dot{P}$ is normalized in the same way as in Eq. 5.7. The Eq. 6.1 and 6.2 then write respectively, introducing the Fractional Rate of Change (FRC) $\omega_{\dot{P},j}$, expressed in s^{-1} and quantifying the relative magnitude of the processes on the primary system mass (Zuber et al. 2007; Wulff et al. 2009):

$$\left.\frac{dP^+}{dt}\right|_1 = \omega_{\dot{P},Q_{l,acc.}} \cdot \frac{\dot{M}^+_{l,acc.} \cdot \nu^+_{l,1}}{K^+_1} + \omega_{\dot{P},Q_{cond.l,acc.}} \cdot \frac{\dot{M}^+_{l,acc.} \cdot \nu'^+_{l,h,1} \cdot \left(h^+_{l,acc.} - H^+_{l,1}\right)}{K^+_1} \tag{6.5}$$
$$-\omega_{\dot{P},Q_{l,break}} \cdot \frac{\dot{M}^+_{l,break} \cdot \nu^+_{l,1}}{K^+_1} - \omega_{\dot{P},Q_{v,break}} \cdot \frac{\dot{M}^+_{v,break} \cdot \nu^+_{v,1}}{K^+_1}$$
$$+\omega_{\dot{P},Q_{wl,core}} \cdot \frac{\nu'^+_{l,h,1} \cdot W^+_{wl,core}}{K^+_1} + \omega_{\dot{P},Q_{wl,SG}} \cdot \frac{\nu'^+_{l,h,1} \cdot W^+_{wl,SG}}{K^+_1} + \omega_{\dot{P},Q_{owl}} \cdot \frac{\nu'^+_{l,h,1} \cdot W^+_{owl}}{K^+_1}$$
$$+\omega_{\dot{P},Q_{wv,core}} \cdot \frac{\nu'^+_{v,h,1} \cdot W^+_{wv,core}}{K^+_1} + \omega_{\dot{P},Q_{wv,SG}} \cdot \frac{\nu'^+_{v,h,1} \cdot W^+_{wv,SG}}{K^+_1} + \omega_{\dot{P},Q_{owv}} \cdot \frac{\nu'^+_{v,h,1} \cdot W^+_{owv}}{K^+_1}$$
$$+\omega_{\dot{P},Q_{wi,core}} \cdot \frac{W^+_{wi,core}}{K^+_1 \cdot \varpi^+_1} + \omega_{\dot{P},Q_{wi,SG}} \cdot \frac{W^+_{wi,SG}}{K^+_1 \cdot \varpi^+_1} + \omega_{\dot{P},Q_{owi}} \cdot \frac{W^+_{owi}}{K^+_1 \cdot \varpi^+_1}$$
$$+\omega_{\dot{P},Q_{il,core}} \cdot \frac{\nu'^+_{l,h,1} \cdot W^+_{il,core}}{K^+_1} + \omega_{\dot{P},Q_{il,SG}} \cdot \frac{\nu'^+_{l,h,1} \cdot W^+_{il,SG}}{K^+_1} + \omega_{\dot{P},Q_{il,ov}} \cdot \frac{\nu'^+_{l,h,1} \cdot W^+_{il,ov}}{K^+_1}$$
$$+\omega_{\dot{P},Q_{iv,core}} \cdot \frac{\nu'^+_{v,h,1} \cdot W^+_{iv,core}}{K^+_1} + \omega_{\dot{P},Q_{iv,SG}} \cdot \frac{\nu'^+_{v,h,1} \cdot W^+_{iv,SG}}{K^+_1} + \omega_{\dot{P},Q_{iv,ov}} \cdot \frac{\nu'^+_{v,h,1} \cdot W^+_{iv,ov}}{K^+_1}$$
$$-\omega_{\dot{P},Q_{i,core}} \cdot \frac{W^+_{il,core} + W^+_{iv,core}}{K^+_1 \cdot \varpi^+_1} - \omega_{\dot{P},Q_{i,SG}} \cdot \frac{W^+_{il,SG} + W^+_{iv,SG}}{K^+_1 \cdot \varpi^+_1} - \omega_{\dot{P},Q_{i,ov}} \cdot \frac{W^+_{il,ov} + W^+_{iv,ov}}{K^+_1 \cdot \varpi^+_1}$$

$$\left.\frac{dP^+}{dt}\right|_{prz} = \omega_{\dot{P},Q_{l,break}} \cdot \frac{\dot{M}^+_{l,prz} \cdot \nu^+_{l,prz}}{K^+_{prz}} - \omega_{\dot{P},Q_{v,break}} \cdot \frac{\dot{M}^+_{v,prz} \cdot \nu^+_{v,prz}}{K^+_{prz}} \tag{6.6}$$
$$+\omega_{\dot{P},Q_{wl,prz}} \cdot \frac{\nu'^+_{l,h,1} \cdot W^+_{wl,prz}}{K^+_{prz}} + \omega_{\dot{P},Q_{wv,prz}} \cdot \frac{\nu'^+_{v,h,1} \cdot W^+_{wv,prz}}{K^+_{prz}} + \omega_{\dot{P},Q_{wi,prz}} \cdot \frac{W^+_{wi,prz}}{K^+_{prz} \cdot \varpi^+_{prz}}$$
$$+\omega_{\dot{P},Q_{il,prz}} \cdot \frac{\nu'^+_{l,h,1} \cdot W^+_{il,prz}}{K^+_{prz}} + \omega_{\dot{P},Q_{iv,prz}} \cdot \frac{\nu'^+_{v,h,1} \cdot W^+_{iv,prz}}{K^+_{prz}} - \omega_{\dot{P},Q_{i,prz}} \cdot \frac{W^+_{il,prz} + W^+_{iv,prz}}{K^+_{prz} \cdot \varpi^+_{prz}}$$

Normalized pressure equations are obtained, function of the j non-dimensional Agents of Change $\phi^+_{\dot{P},j}$ which define the processes acting on the pressure rate of change $\dot{P}$:

$$\left.\frac{dP^+}{dt}\right|_1 = \omega_{\dot{P},Q_{l,acc.}} \cdot \phi^+_{\dot{P},Q_{l,acc.}} + \omega_{\dot{P},Q_{cond.l,acc.}} \cdot \phi^+_{\dot{P},Q_{cond.l,acc.}} \tag{6.7}$$
$$-\omega_{\dot{P},Q_{l,break}} \cdot \phi^+_{\dot{P},Q_{l,break}} - \omega_{\dot{P},Q_{v,break}} \cdot \phi^+_{\dot{P},Q_{v,break}}$$
$$+\omega_{\dot{P},Q_{wl,core}} \cdot \phi^+_{\dot{P},Q_{wl,core}} + \omega_{\dot{P},Q_{wl,SG}} \cdot \phi^+_{\dot{P},Q_{wl,SG}} + \omega_{\dot{P},Q_{owl}} \cdot \phi^+_{\dot{P},Q_{owl}}$$
$$+\omega_{\dot{P},Q_{wv,core}} \cdot \phi^+_{\dot{P},Q_{wv,core}} + \omega_{\dot{P},Q_{wv,SG}} \cdot \phi^+_{\dot{P},Q_{wv,SG}} + \omega_{\dot{P},Q_{owv}} \cdot \phi^+_{\dot{P},Q_{owv}}$$
$$+\omega_{\dot{P},Q_{wi,core}} \cdot \phi^+_{\dot{P},Q_{wi,core}} + \omega_{\dot{P},Q_{wi,SG}} \cdot \phi^+_{\dot{P},Q_{wi,SG}} + \omega_{\dot{P},Q_{owi}} \cdot \phi^+_{\dot{P},Q_{owi}}$$
$$+\omega_{\dot{P},Q_{il,core}} \cdot \phi^+_{\dot{P},Q_{il,core}} + \omega_{\dot{P},Q_{il,SG}} \cdot \phi^+_{\dot{P},Q_{il,SG}} + \omega_{\dot{P},Q_{il,ov}} \cdot \phi^+_{\dot{P},Q_{il,ov}}$$
$$+\omega_{\dot{P},Q_{iv,core}} \cdot \phi^+_{\dot{P},Q_{iv,core}} + \omega_{\dot{P},Q_{iv,SG}} \cdot \phi^+_{\dot{P},Q_{iv,SG}} + \omega_{\dot{P},Q_{iv,ov}} \cdot \phi^+_{\dot{P},Q_{iv,ov}}$$
$$-\omega_{\dot{P},Q_{i,core}} \cdot \phi^+_{\dot{P},Q_{i,core}} - \omega_{\dot{P},Q_{i,SG}} \cdot \phi^+_{\dot{P},Q_{i,SG}} - \omega_{\dot{P},Q_{i,ov}} \cdot \phi^+_{\dot{P},Q_{i,ov}}$$

$$\left.\frac{dP^{+}}{dt}\right|_{prz} = \omega_{\dot{P},Q_{l,break}} \cdot \phi^{+}_{\dot{P},Q_{l,break}} - \omega_{\dot{P},Q_{v,break}} \cdot \phi^{+}_{\dot{P},Q_{v,break}} \tag{6.8}$$
$$+\omega_{\dot{P},Q_{wl,prz}} \cdot \phi^{+}_{\dot{P},Q_{wl,prz}} + \omega_{\dot{P},Q_{wv,prz}} \cdot \phi^{+}_{\dot{P},Q_{wv,prz}} + \omega_{\dot{P},Q_{wi,prz}} \cdot \phi^{+}_{\dot{P},Q_{wi,prz}}$$
$$+\omega_{\dot{P},Q_{il,prz}} \cdot \phi^{+}_{\dot{P},Q_{il,prz}} + \omega_{\dot{P},Q_{iv,prz}} \cdot \phi^{+}_{\dot{P},Q_{iv,prz}} - \omega_{\dot{P},Q_{i,prz}} \cdot \phi^{+}_{\dot{P},Q_{i,prz}}$$

The time scaling for relative importance of agents (see from Eq. 3.25) is performed using Eq. 5.10, 5.11, 6.7 and 6.8. This approach gives the effect metrics in the same way as described in Eq. 5.24. Figure 6.11 illustrates the established mass and pressure effects metrics for the 6% SB-LOCA counterpart test.

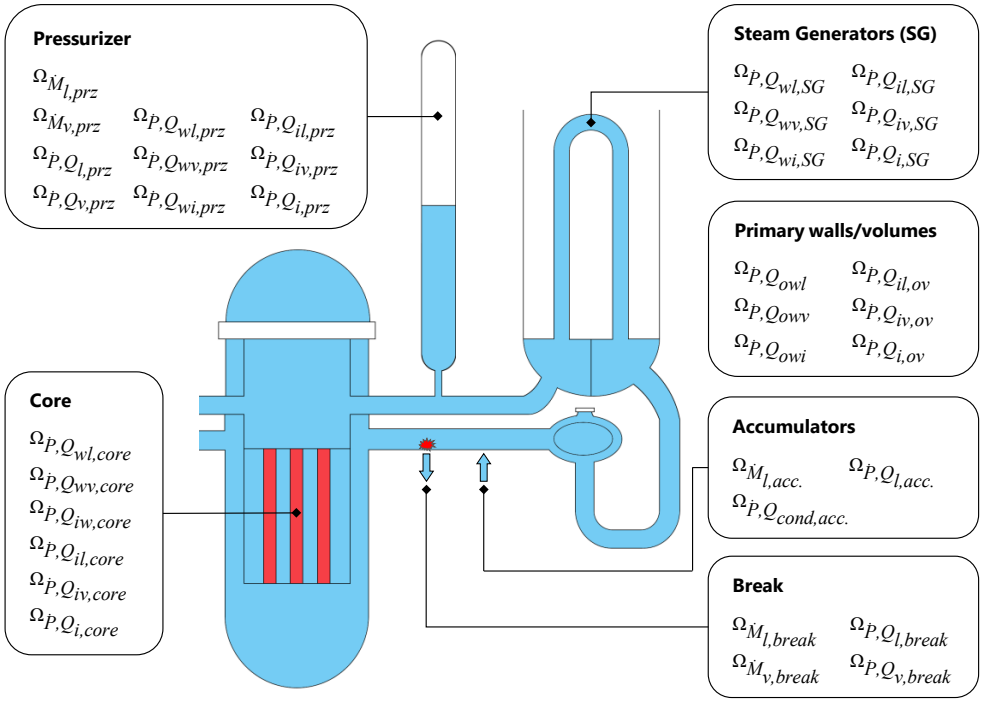

Figure 6.11: Established mass and pressure effect metrics for the 6% SB-LOCA counterpart test

6.3.3. Results of the A Posteriori Scaling Analysis of the Subcooled Blowdown (SBD) Phase

The volume of fluid lost at the break is replaced mainly by vaporization (flashing) and by fluid expansion. The water in the pressurizer is initially saturated and becomes superheated due to pressure decrease. In the rest of the primary circuit the water remains sub-cooled until it reaches saturation and starts flashing. The pressurizer is the key component at the start of the SBD phase since it controls the primary pressure. The emptying of the pressurizer is the bifurcating event that determines the end of this phase. Figure 6.12 shows the pressurizer emptying behaviour. Since the LSTF pressurizer is scaled with volume and has a reduced-height compared to the BETHSY and the PWR pressurizers, the emptying is normalized with the liquid volume instead of the liquid level.

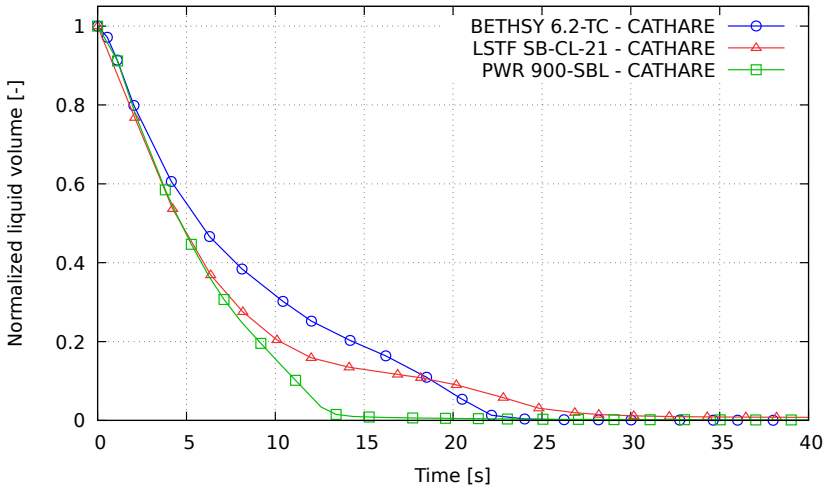

Figure 6.12: Pressurizer liquid volume during the SBD phase of the 6% SB-LOCA counterpart test - CATHARE predictions

The pressurizer emptying appears slightly different between the facilities and the PWR. The difference in the BETHSY pressurizer emptying compared to the PWR is due to the increase in the initial secondary pressure for the comparative test with LSTF in the counterpart test. The difference in the LSTF pressurizer emptying compared to BETHSY and the PWR would appears to be caused by its different geometry and its lower initial liquid level. This difference causes a distorted ratio between the pressurizer initial mass and the total mass of the primary system (see Table 6.4). It should be noted that the LSTF pressurizer design has been revised to simulate the pressurizer of the AP1000. It is relatively larger than the pressurizer of the conventional Westinghouse PWR (Cummins et al. 2003).

Table 6.4: Pressurizers design data

	BETHSY	LSTF	PWR
PRZ inner diameter	0.210 m	0.600 m	3.650 m
PRZ height	11.931 m	4.187 m	11.520 m
PRZ initial liquid level ratio	0.62	0.41	0.64
PRZ/primary initial liquid mass ratio	$8.43 \cdot 10^{-2}$	$6.38 \cdot 10^{-2}$	$8.68 \cdot 10^{-2}$

The depressurization of the SBD phase is also subject to distortions, as shown in Figure 6.13. As discussed in the section 6.2.1, the core power decay could explain the PWR higher depressurization as well as the initial secondary pressure (see Figure H.1b in the Appendice H). The different connections to the pressurizer might explain the minor discrepancies amongst the BETSHY and LSTF facilities (the pressurizer is connected to the intact loop in LSTF and to the broken loop in BETHSY).

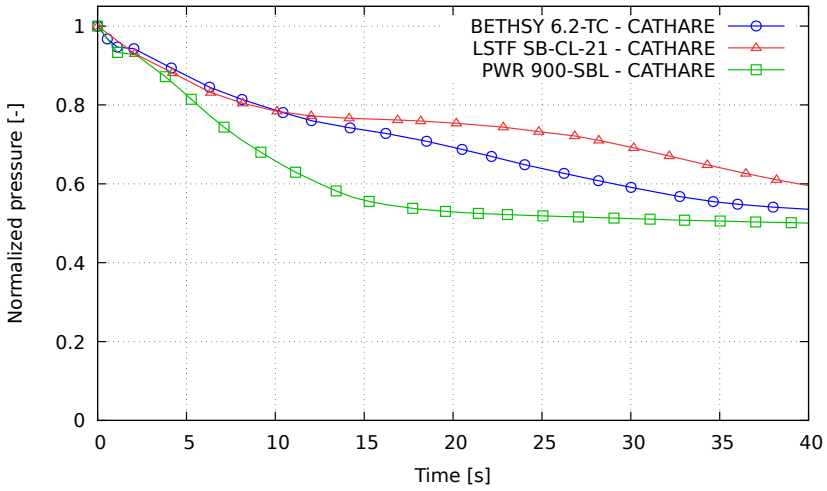

(a) CATHARE predictions

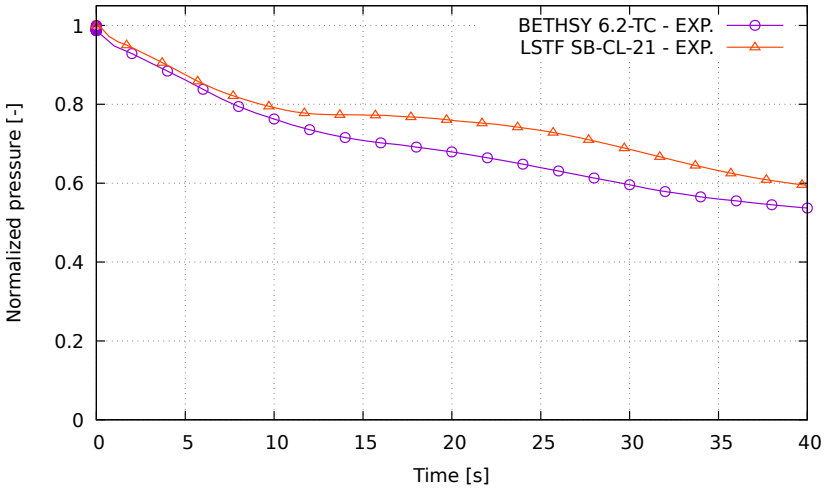

(b) Experimental results

Figure 6.13: Primary pressure during the SBD phase of the 6% SB-LOCA counterpart test

The depressurization of the SBD phase is investigated using the FSA method applied to mass and pressure by VRC equations, for the primary system and the pressurizer control volumes. Table 6.5 shows the main parameters of the SBD phase. In order to validate the pressure by VRC equation, a verification of the equation resolution is performed on the pressurizer results. This validation work is presented in Appendice G.

Table 6.5: Main parameters of the SBD phase of the 6% SB-LOCA counterpart test - CATHARE predictions

	BETHSY 6.2-TC	LSTF SB-CL-21	PWR 900-SBL
Initial primary mass $M_{1,0}$	1 963 kg	5 612 kg	191 935 kg
Initial pressurizer mass $M_{prz,l,0}$	150 kg	290 kg	15 077 kg
Phase duration Δt_{SBD}	24 s	30 s	15 s
Primary mass difference ΔM_1	384 kg	1 339 kg	22 607 kg
Pressurizer mass difference ΔM_{prz}	143 kg	285 kg	14 594 kg
Pressure difference ΔP_{SBD}	5.32 MPa	4.76 MPa	6.98 MPa
Averaged mass flow rate at the break $\bar{\dot{M}}_{break}$	15.20 kg/s	41.42 kg/s	1 321.5 kg/s
Averaged mass flow rate leaving the PRZ $\bar{\dot{M}}_{prz}$	6.24 kg/s	8.16 kg/s	819.89 kg/s
Averaged core power $\bar{\dot{W}}_{core}$	$2.79 \cdot 10^6$ W	$8.13 \cdot 10^6$ W	$1.97 \cdot 10^9$ W
Averaged core power ratio (facilities/PWR)	1/706	1/242	-
Averaged SG tubes heat exchanges $\bar{\dot{W}}_{SG}$	$3.93 \cdot 10^6$ W	$9.90 \cdot 10^6$ W	$2.11 \cdot 10^9$ W
Averaged primary wall heat exchanges $\bar{\dot{W}}_{ow}$	$1.39 \cdot 10^5$ W	$1.51 \cdot 10^5$ W	$2.19 \cdot 10^7$ W
Averaged PRZ wall heat exchanges $\bar{\dot{W}}_{prz,w}$	$2.20 \cdot 10^5$ W	$6.55 \cdot 10^4$ W	$1.24 \cdot 10^7$ W
Averaged liquid temperature $\bar{T}_{1,l}$	279.1 °C	298.2 °C	292.3 °C
Averaged vapour temperature $\bar{T}_{1,v}$	325.3 °C	325.4 °C	322.5 °C

The values of the effect metrics for the mass equation $\Omega_{\dot{M},\chi_j}$ and the pressure equation $\Omega_{\dot{P},\chi_j}$ are displayed for the primary system and pressurizer volumes for the SBD phase respectively in Tables 6.6 and 6.7. They are classified according to the four effect metrics ranks described in Table 5.3.

Table 6.6: Effect metrics of the pressurizer volume during the SBD phase of the 6% SB-LOCA counterpart test

		BETHSY 6.2-TC	LSTF SB-CL-21	PWR 900-SBL
Rate of mass change in V_{prz} due to the contribution by:				
Liquid flow rate leaving the pressurizer	$\Omega_{\dot{M}_{l,prz}}$	**-1.000**	**-1.000**	**-1.000**
Vapour flow rate leaving the pressurizer	$\Omega_{\dot{M}_{v,prz}}$	-0.002	-0.001	-0.004
Rate of pressure change in V_{prz} due to the contribution by:				
Liquid volume flow rate leaving the pressurizer	$\Omega_{\dot{P},Q_{l,prz}}$	**-1.000**	**-1.000**	**-1.000**
Vapour volume flow rate leaving the pressurizer	$\Omega_{\dot{P},Q_{v,prz}}$	**-0.298**	**-0.269**	**-0.649**
Thermal expansion/contraction by wall-liquid heat transfers in the pressurizer	$\Omega_{\dot{P},Q_{wl,prz}}$	0.003	0.000	0.000
Thermal expansion/contraction by wall-vapour heat transfers in the pressurizer	$\Omega_{\dot{P},Q_{wv,prz}}$	0.013	0.000	0.000
Volume change by wall boiling or condensation in the pressurizer	$\Omega_{\dot{P},Q_{wi,prz}}$	**0.163**	0.029	**0.080**

Continued on next page

Table 6.6 continued from previous page

		BETHSY 6.2-TC	LSTF SB-CL-21	PWR 900-SBL
Thermal expansion/contraction by interface-liquid heat transfers in the pressurizer	$\Omega_{\dot{P},Q_{il,prz}}$	-0.062	-0.067	-0.102
Thermal expansion/contraction by interface-vapour heat transfers in the pressurizer	$\Omega_{\dot{P},Q_{iv,prz}}$	0.290	0.466	0.437
Volume change by vaporization or condensation by interfacial transfers in the pressurizer	$\Omega_{\dot{P},Q_{i,prz}}$	0.448	0.230	0.584

Analysis of the effect metrics of the pressurizer volume during the SBD phase:

- The mass and pressure rate of change in the pressurizer are mainly due to the liquid flow rate leaving the pressurizer.
- The vapour mass flow rate leaving the pressurizer is negligible in the CATHARE code calculation. Nevertheless, the vapour volume flow rate contributes significantly to pressure decrease, as demonstrated by the effect metrics contributing to the pressure change. It should be noted that the predicted impact of the vapour volume flow rate is lower in the facilities (BETHSY: -0.298; LSTF: -0.269) than in the PWR (-0.649).
- Because the same ratio between the initial liquid mass of the pressurizer and the initial mass of the primary system is found (see Table 6.4), it can be deduced that higher contribution of the predicted vapour exiting flow rate for the PWR is related to the faster depressurization which creates more flashing of the water (see Figure 6.13a).
- Because of the sudden pressure decrease, the vaporization is an influent process in all three systems but it is found to be smaller in LSTF (0.230) than in BETHSY (0.448) and the PWR (0.584).
- One may add that a simple two-node modelling of the pressurizer with CATHARE cannot predict the void fraction gradient from the bottom to the water level and then cannot predict very precisely the void fraction entrained in the expansion line (see also section 5.2.3). This suggests that a 1-D modelling of the pressurizer with smaller meshes could be more precise.
- Because the pressurizer height was preserved in BETHSY, the ratio of the walls exchange surface to volume is higher than in LSTF, where the height was reduced (see Table 6.4).
- Because the pressurizer heaters are turned off prior to the start of the transient, only the wall and interfacial heat exchange terms remain.

Table 6.7: Effect metrics of the primary system volume during the SBD phase of the 6% SB-LOCA counterpart test

		BETHSY 6.2-TC	LSTF SB-CL-21	PWR 900-SBL
Rate of mass change in V_1 due to the contribution by:				
Liquid flow rate leaving the primary system through the break	$\Omega_{\dot{M}_{l,break}}$	**-1.000**	**-1.000**	**-1.000**
Vapour flow rate leaving the primary system through the break	$\Omega_{\dot{M}_{v,break}}$	-0.013	-0.015	-0.019
Rate of pressure change in V_1 due to the contribution by:				
Liquid volume flow rate leaving the primary system through the break	$\Omega_{\dot{P},Q_{l,break}}$	**-1.000**	**-1.000**	**-0.718**
Vapour volume flow rate leaving the primary system through the break	$\Omega_{\dot{P},Q_{v,break}}$	**-0.129**	**-0.153**	**-0.155**
Thermal expansion/contraction by wall-liquid heat transfers in the core	$\Omega_{\dot{P},Q_{wl,core}}$	**0.053**	0.022	**0.604**
Thermal expansion/contraction by wall-vapour heat transfers in the core	$\Omega_{\dot{P},Q_{wv,core}}$	0.000	0.004	0.000
Volume change by wall boiling or condensation in the core	$\Omega_{\dot{P},Q_{wi,core}}$	**0.593**	**0.668**	**0.075**
Thermal expansion/contraction by interface-liquid heat transfers in the core	$\Omega_{\dot{P},Q_{il,core}}$	0.010	0.008	0.002
Thermal expansion/contraction by interface-vapour heat transfers in the core	$\Omega_{\dot{P},Q_{iv,core}}$	0.005	0.007	0.000
Volume change by vaporization or condensation by interfacial transfers in the core	$\Omega_{\dot{P},Q_{i,core}}$	**-0.130**	**-0.101**	-0.030
Thermal expansion/contraction by wall-liquid heat transfers in SG tubes	$\Omega_{\dot{P},Q_{wl,SG}}$	**-0.138**	**-0.126**	**-1.000**
Thermal expansion/contraction by wall-vapour heat transfers in SG tubes	$\Omega_{\dot{P},Q_{wv,SG}}$	0.000	0.000	0.000
Volume change by wall boiling or condensation in SG tubes	$\Omega_{\dot{P},Q_{wi,SG}}$	0.000	0.000	0.000
Thermal expansion/contraction by interface-liquid heat transfers in the SG tubes	$\Omega_{\dot{P},Q_{il,SG}}$	0.036	0.033	0.031
Thermal expansion/contraction by interface-vapour heat transfers in the SG tubes	$\Omega_{\dot{P},Q_{iv,SG}}$	0.004	0.003	0.004
Volume change by vaporization or condensation by interfacial transfers in the SG tubes	$\Omega_{\dot{P},Q_{i,SG}}$	**-0.473**	**-0.425**	**-0.455**
Thermal expansion/contraction by wall-liquid heat transfers in the primary system*	$\Omega_{\dot{P},Q_{owl}}$	-0.006	0.000	-0.003

Continued on next page

Table 6.7 continued from previous page

		BETHSY 6.2-TC	LSTF SB-CL-21	PWR 900-SBL
Thermal expansion/contraction by wall-vapour heat transfers in the primary system*	$\Omega_{\dot{P},Q_{owv}}$	0.005	0.000	0.000
Volume change by wall boiling or condensation in the primary system*	$\Omega_{\dot{P},Q_{owi}}$	0.031	0.018	**0.087**
Thermal expansion/contraction by interface-liquid heat transfers in the primary system*	$\Omega_{\dot{P},Q_{il,ov}}$	-0.042	-0.014	-0.038
Thermal expansion/contraction by interface-vapour heat transfers in the primary system*	$\Omega_{\dot{P},Q_{iv,ov}}$	**0.183**	**0.133**	**0.253**
Volume change by vaporization or condensation by interfacial transfers in the primary system*	$\Omega_{\dot{P},Q_{i,ov}}$	**0.448**	**0.116**	**0.417**

**except SG tubes and fuel rods*

Analysis of the effect metrics of the primary system volume during the SBD phase:

- The effect metric related to the liquid mass flow rate at the break has the greatest influence on the rate of mass change in the primary system control volume.
- The vapour break flow is contributing only for a very small amount. Although measured data cannot confirm this repartition, this evaluation is easily accepted because almost only liquid water flows in the loops and in the pressure vessel during SBD phase.
- The term related to the liquid volume flow rate at the break is seen to be dominant on the rate of primary pressure change in the facilities. This term contributes to system depressurization.
- Likewise, the thermal contraction caused by condensation by interfacial transfers in the SG tubes is regarded as influent for both facilities (BETHSY: -0.473; LSTF: -0.425) and the PWR (-0.455).
- The dominant process contributing to the PWR depressurization is the contraction by wall-liquid heat transfers in SG tubes. This process has limited impact in the facilities (BETHSY: -0.138; LSTF: -0.126). This is also corresponding to a situation with more vapour in loops during SBD in the PWR compared to the facilities.
- The volume change by vaporization in the primary system is one of the terms contributing to the pressurization. There is a difference in the impact of this phenomenon in LSTF (0.116) compared to BETHSY (0.448) and the PWR (0.417).
- Similarly, the term related to thermal expansion by interface-vapour heat transfers in the primary system volume is influent, but it is higher in the PWR (BETHSY: 0.183; LSTF: 0.133; PWR: 0.253).
- The relative effect of the volume change caused by wall boiling in the core is significant in the facilities (BETHSY: 0.593; LSTF: 0.668) but negligible in the PWR (0.075).

- On the contrary, thermal expansion caused by wall-liquid heat transfers in the core is more important in the PWR (0.604) than in facilities (BETHSY: 0.053; LSTF: 0.022). This difference is explained by the lower averaged liquid temperature predicted in the PWR core (297.2 °C) compared to BETHSY (307.4 °C) and LSTF (321.1 °C). The power provided by the PWR core is mostly transferred to the liquid. While in the facilities, with a liquid temperature closer to the saturation temperature, the core power leads to boiling.

- The discrepancies in the process hierarchy between the simulated experiments and the PWR, observed in Table 6.7, can be explained by the core initial power. During the SBD phase, the PWR core injects more power into the primary system compared to the BETHSY and LSTF cores, as shown in Figure 6.7. The PWR SG tubes transfer then more power from the core to the secondary system.

6.3.4. Results of the A Posteriori Scaling Analysis of the Natural Circulation (NC) Phase

The NC phase entry conditions were initially chosen as the emptying of the pressurizer and the primary pumps trip. However, as shown in Figure 6.14, the inertia of the PWR pumps prevents them from completely stopping. Since the pump coastdown was not simulated on the facilities, their speed rapidly decreases to zero, while the PWR pumps rotation gradually decreases because of the inertia. The distortion caused by the initial core power between the PWR and the facilities is still present in this phase (see Figure 6.7).

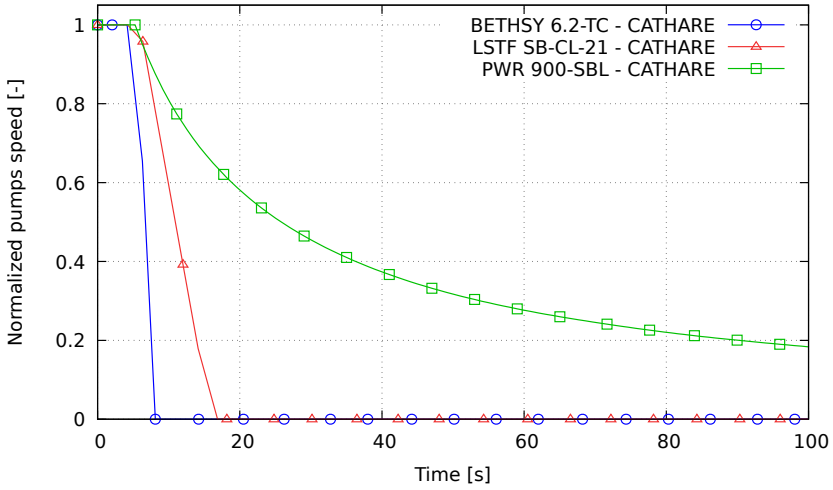

Figure 6.14: Primary pumps rotational speed of the 6% SB-LOCA counterpart test - CATHARE predictions

The NC phase continues until there is no more liquid mass flow rate at the top of the SG tubes (see Figure 5.5). There is no longer any natural circulation in the primary circuit. Figure 6.15 demonstrates that the liquid mass flow rate at the top of the SG tubes does not evolve in the same way in all three systems. Although the flow rate decreases faster (after 38 seconds) on LSTF than on BETHSY, the occurrence of the zero flow rate occurs almost simultaneously. Because the pumps are still running at a reduced speed, the NC phase in the PWR lasts longer.

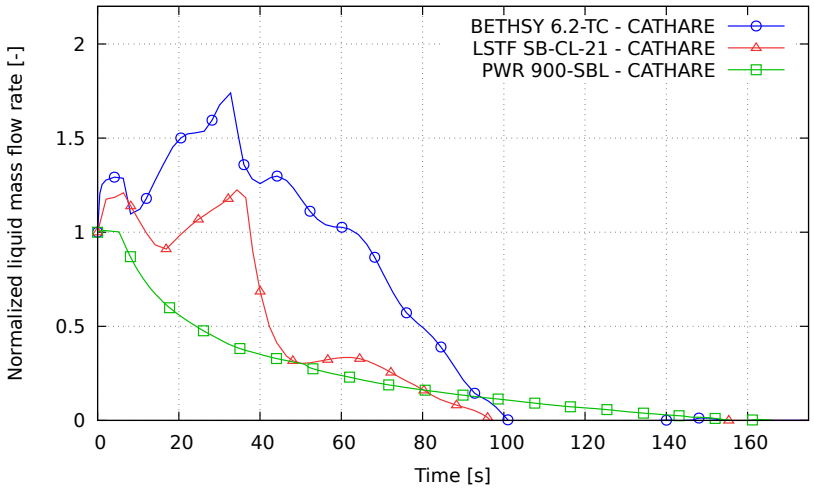

(a) Intact loop(s)

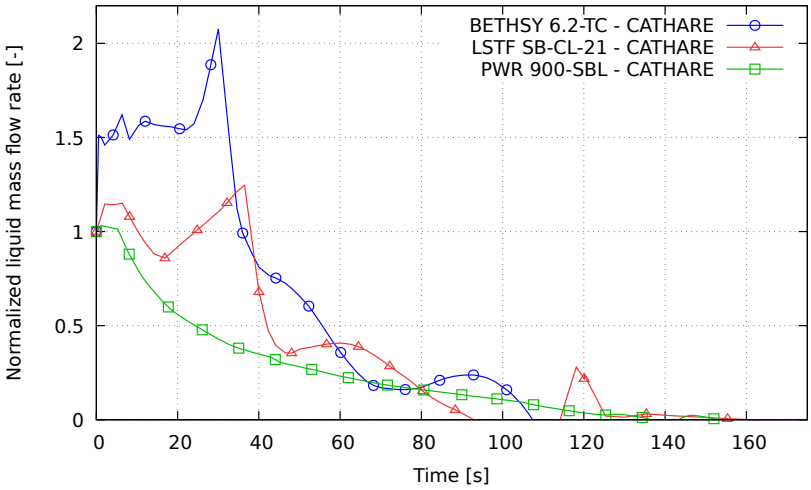

(b) Broken loop

Figure 6.15: Liquid mass flow rate at the top of the SG tubes of the 6% SB-LOCA counterpart test - CATHARE predictions

The depressurization of the NC phase is investigated using the FSA method applied to mass and pressure by VRC equations, for the primary system control volume. Table 6.8 shows the main parameters of the NC phase.

Table 6.8: Main parameters of the NC phase of the 6% SB-LOCA counterpart test - CATHARE predictions

	BETHSY 6.2-TC	LSTF SB-CL-21	PWR 900-SBL
Initial primary mass $M_{1,0}$	1 551 kg	4 198 kg	168 527 kg
Phase duration Δt_{NC}	81 s	70 s	138 s
Primary mass difference ΔM_1	623 kg	1 625 kg	69 637 kg
Pressure difference ΔP_{NC}	1.60 MPa	2.13 MPa	1.32 MPa
Averaged mass flow rate at the break $\bar{\dot{M}}_{break}$	8.03 kg/s	24.06 kg/s	526.59 kg/s
Averaged core power $\bar{\dot{W}}_{core}$	$2.57 \cdot 10^6$ W	$7.37 \cdot 10^6$ W	$1.65 \cdot 10^8$ W
Averaged core power ratio (facilities/PWR)	1/64	1/22	-
Averaged SG tubes heat exchanges $\bar{\dot{W}}_{SG}$	$2.23 \cdot 10^6$ W	$6.82 \cdot 10^6$ W	$1.39 \cdot 10^8$ W
Averaged primary wall heat exchanges $\bar{\dot{W}}_{ow}$	$1.01 \cdot 10^5$ W	$1.47 \cdot 10^5$ W	$1.11 \cdot 10^7$ W
Averaged liquid temperature $\bar{T}_{1,l}$	292.0 °C	293.7 °C	289.1 °C
Averaged vapour temperature $\bar{T}_{1,v}$	298.3 °C	299.8 °C	290.7 °C

The values of the effect metrics for the mass equation $\Omega_{\dot{M},\chi_j}$ and the pressure equation $\Omega_{\dot{P},\chi_j}$ are displayed for the primary system NC phase in Table 6.9. They are classified according to the four effect metrics ranks described in Table 5.3.

Table 6.9: Effect metrics of the primary system volume during the NC phase of the 6% SB-LOCA counterpart test

		BETHSY 6.2-TC	LSTF SB-CL-21	PWR 900-SBL
Rate of mass change in V_1 due to the contribution by:				
Liquid flow rate leaving the primary system through the break	$\Omega_{\dot{M}_{l,break}}$	**-1.000**	**-1.000**	**-1.000**
Vapour flow rate leaving the primary system through the break	$\Omega_{\dot{M}_{v,break}}$	**-0.087**	**-0.078**	**-0.171**
Rate of pressure change in V_1 due to the contribution by:				
Liquid volume flow rate leaving the primary system through the break	$\Omega_{\dot{P},Q_{l,break}}$	**-0.304**	**-0.358**	**-0.267**
Vapour volume flow rate leaving the primary system through the break	$\Omega_{\dot{P},Q_{v,break}}$	**-0.463**	**-0.438**	**-0.846**
Thermal expansion/contraction by wall-liquid heat transfers in the core	$\Omega_{\dot{P},Q_{wl,core}}$	0.009	0.007	0.012
Thermal expansion/contraction by wall-vapour heat transfers in the core	$\Omega_{\dot{P},Q_{wv,core}}$	0.000	0.004	0.000
Volume change by wall boiling or condensation in the core	$\Omega_{\dot{P},Q_{wi,core}}$	**1.000**	**0.736**	**1.000**
Thermal expansion/contraction by interface-liquid heat transfers in the core	$\Omega_{\dot{P},Q_{il,core}}$	0.004	0.003	0.000

Continued on next page

Table 6.9 continued from previous page

		BETHSY 6.2-TC	LSTF SB-CL-21	PWR 900-SBL
Thermal expansion/contraction by interface-vapour heat transfers in the core	$\Omega_{\dot{P},Q_{iv,core}}$	0.001	0.003	0.000
Volume change by vaporization or condensation by interfacial transfers in the core	$\Omega_{\dot{P},Q_{i,core}}$	**-0.087**	**-0.056**	-0.001
Thermal expansion/contraction by wall-liquid heat transfers in SG tubes	$\Omega_{\dot{P},Q_{wl,SG}}$	-0.048	**-0.058**	**-0.051**
Thermal expansion/contraction by wall-vapour heat transfers in SG tubes	$\Omega_{\dot{P},Q_{wv,SG}}$	0.000	0.000	0.000
Volume change by wall boiling or condensation in SG tubes	$\Omega_{\dot{P},Q_{wi,SG}}$	0.000	0.000	0.001
Thermal expansion/contraction by interface-liquid heat transfers in the SG tubes	$\Omega_{\dot{P},Q_{il,SG}}$	0.041	**0.051**	0.032
Thermal expansion/contraction by interface-vapour heat transfers in the SG tubes	$\Omega_{\dot{P},Q_{iv,SG}}$	0.005	0.013	0.003
Volume change by vaporization or condensation by interfacial transfers in the SG tubes	$\Omega_{\dot{P},Q_{i,SG}}$	**-0.882**	**-1.000**	**-0.739**
Thermal expansion/contraction by wall-liquid heat transfers in the primary system*	$\Omega_{\dot{P},Q_{owl}}$	-0.003	0.001	-0.001
Thermal expansion/contraction by wall-vapour heat transfers in the primary system*	$\Omega_{\dot{P},Q_{owv}}$	0.044	0.006	0.005
Volume change by wall boiling or condensation in the primary system*	$\Omega_{\dot{P},Q_{owi}}$	**0.101**	0.043	**0.087**
Thermal expansion/contraction by interface-liquid heat transfers in the primary system*	$\Omega_{\dot{P},Q_{il,ov}}$	-0.004	-0.007	-0.002
Thermal expansion/contraction by interface-vapour heat transfers in the primary system*	$\Omega_{\dot{P},Q_{iv,ov}}$	0.006	0.046	0.011
Volume change by vaporization or condensation by interfacial transfers in the primary system*	$\Omega_{\dot{P},Q_{i,ov}}$	**0.090**	**0.119**	0.044

**except SG tubes and fuel rods*

Analysis of the effect metrics of the primary system volume during the NC phase:

- The dominant effect metric on the rate of mass change remains the liquid mass flow rate at the break.
- Because of the boiling in the core, the vapour flow rate is slightly higher (BETHSY: -0.087; LSTF: -0.078; PWR: -0.171) than in the SBD phase (BETHSY: -0.013; LSTF: -0.015; PWR: -0.019). Because of the higher relative power in the core, the PWR vapour mass flow rate is higher (-0.171) than in the facilities (BETHSY: -0.087; LSTF: -0.078). This difference could also possibly be due to the PWR pumps, which, unlike the facilities, are still operating and shift the natural convection.

- The dominant effect metric on the pressurization is the volume change by wall-boiling in the core (BETHSY: 1.000; LSTF: 0.736; PWR: 1.000). This term is primarily balanced by volume change due to condensation by interfacial transfers in SG tubes (BETHSY: -0.882; LSTF: -1.000; PWR: -0.739). Note that the preponderant term is inverted on LSTF compared to BETHSY and PWR.
- The volume leaving the system at the break is also influent in the contribution to the depressurization. But the higher vapour generated in the PWR than in the facilities during the SBD phase is still visible during this NC phase (BETHSY: -0.463; LSTF: -0.438; PWR: -0.846). As shown in Figure 6.16, the ratio of vapour flow rate to liquid flow rate is distorted in the facilities compared to the PWR.
- Finally, the volume change due to wall-boiling in the primary system has little effect (BETHSY: 0.101; LSTF: 0.043; PWR: 0.087). However, because of its higher wall heat exchange surface to primary volume ratio, it is higher on BETHSY.

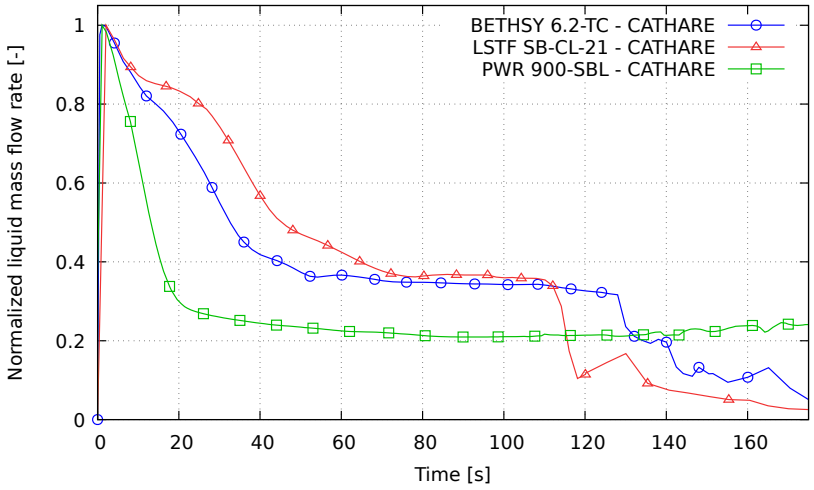

(a) Liquid flow rate

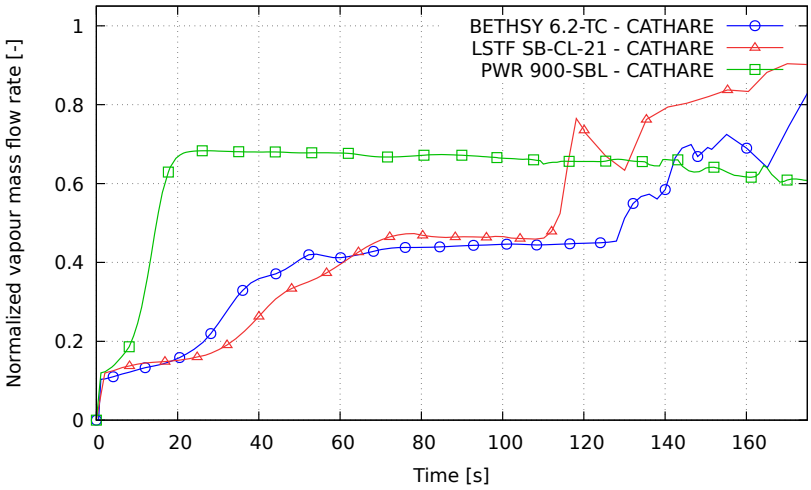

(b) Vapour flow rate

Figure 6.16: Break liquid and vapour mass flow rates of the 6% SB-LOCA counterpart test - CATHARE predictions

6.3.5. Results of the A Posteriori Scaling Analysis of the Reflux Condenser Mode (RCM) Phase

The primary system depressurization rate is nearly as low during the Reflux Condenser Mode (RCM) phase as it is during the NC phase. Figure 6.17 depicts a transition of the void fraction in the CL upstream of the break. The break mass flow continues to transition from liquid to vapour, eventually reaching the HQMD phase. It can be seen that the facilities behaviour is temporally distorted because of the premature stop of the pumps compared to the PWR. The void fraction of the facilities reaches 1 shortly after 200 seconds, while the PWR reaches it after 300 seconds.

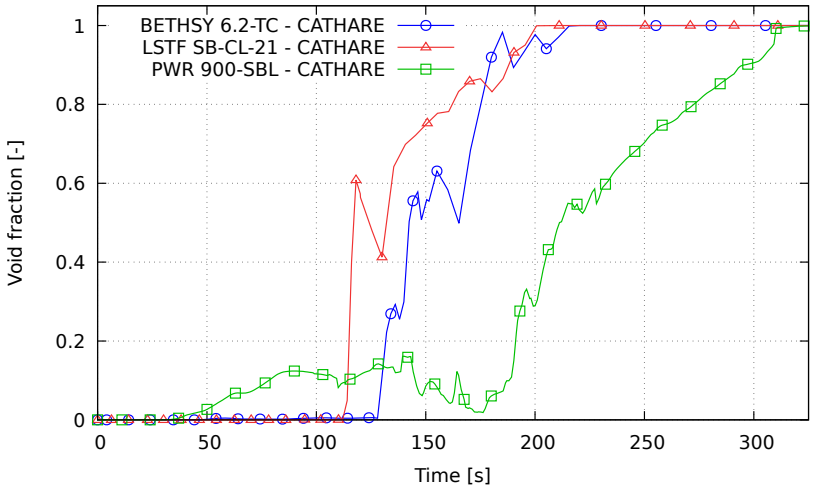

Figure 6.17: Void fraction at the break of the 6% SB-LOCA counterpart test - CATHARE predictions

At end of NC, some liquid from SG tubes is accumulated in the intermediate legs and creates a plug which isolates two almost independent thermodynamic systems with different pressure evolution. This is the Loop Seal Plugging (LSP) phenomenon.

- V_{up}: Lower plenum, core, upper plenum, upper head, hot legs, steam generators, descending part of the intermediate leg.
- V_{low}: Ascending part of the intermediate legs, cold legs, downcomer.

The pressure in the upper volume P_{up} stabilizes above the secondary pressure while the pressure in the lower volume P_{low} decreases due to break flow. The plug is evacuated towards the pressure vessel when the pressure difference between the two volumes is high enough. This is the Loop Seal Clearing (LSC) phenomenon. The LSP and LSC phenomena, also presented in section 5.1.2 are illustrated in Figure 6.18.

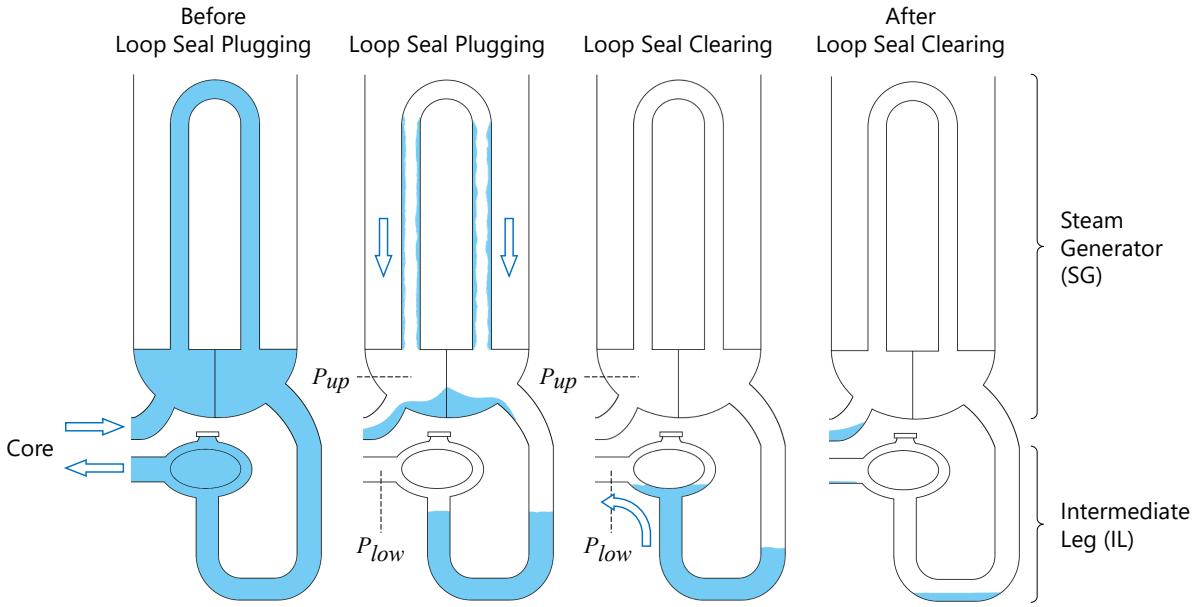

Figure 6.18: The Loop Seal Plugging (LSP) and Loop Seal Clearing (LSC) phenomena

Figure 6.19 depicts the predicted LSP and LSC phenomena, which are responsible for core uncovery and core reflooding, respectively (see Figure 6.9). It is observed that CATHARE only predicts the LSP phenomenon on one Intermediate Leg (IL) of the facilities. This is predicted to occur only in the broken IL in BETHSY. On LSTF, however, it is predicted only in the intact IL.

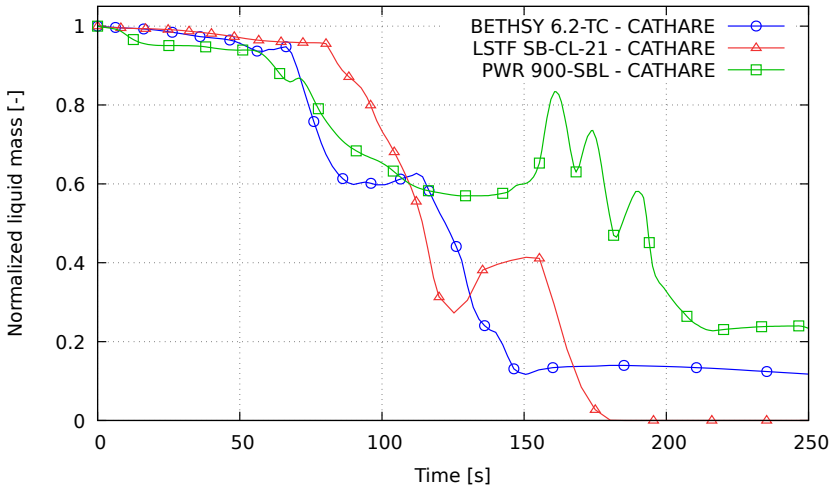

(a) Intact loop(s)

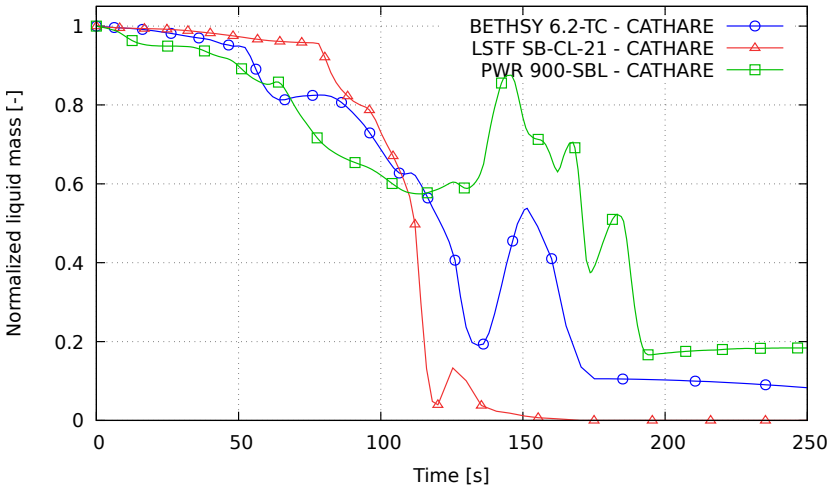

(b) Broken loop

Figure 6.19: Liquid mass plugged in IL of the 6% SB-LOCA counterpart test - CATHARE predictions

The LSP/LSC phenomenon has been observed experimentally on all the IL of the facilities. However, the code results predict the LSP on a single IL. A certain randomness of the LSC process has been observed, which makes it is difficult to predict by the codes (Hwang et al. 2019). The literature on studies of the LSC phenomenon provides analyses that highlight different behaviours based on:

- The size and location of the break. It has been demonstrated that the IL of the broken loop was generally cleared first, and the number of cleared loops is increasing with the break size (Kim et al. 2014; Hwang et al. 2019).
- The nodalization structure and initial conditions. For example, the presence of a pressurizer on a loop, which adds an additional amount of liquid to the loop, can affect the order in which loop LSP/LSC can occur (Kauppinen et al. 2015).
- The number of loops could have a significant impact on the LSC behaviour (Kukita et al. 1989), especially given the difference between the facilities, which generally have fewer loops than the reference PWR (i.e. between LSTF and its reference PWR).
- The facilities design, which may be be distorted in comparison to the full-scale PWR, particularly due to the initial conditions (like the pumps coastdown) and the geometry of the leg cross-sectional area, which are not correctly scaled on the facilities with respect to the LSC phenomenon (Kukita et al. 1989).
- The design in the IL can affect the pressure difference between the upper-head and the downcomer (Park et al. 2020). This pressure difference plays a key role in the occurrence of the LSP/LSC phenomenon. Since the facilities have their own reference reactor, this is related to the design characteristics of each test facility.
- Some experimental tests also revealed asymmetry (Lee 1987; Kukita et al. 1989), while repeatable tests revealed different LSC behaviour. These investigations revealed that the IL were not fully cleared for some tests, as predicted on BETHSY and PWR but not on LSTF (see Figure 6.19).

Figure 6.20 summarizes the main phenomena involved in the LSP/LSC, as well as known main sources of behaviour change. Theses phenomena are still incompletely understood due to their difficult to predict nature and numerous influencing parameters. There are few studies on different facilities and configurations. As a result, drawing general conclusions is challenging.

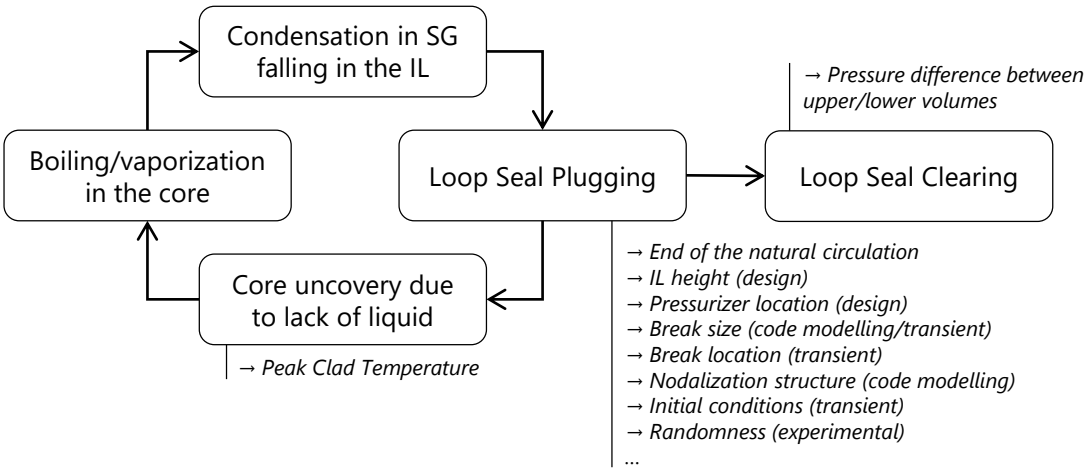

Figure 6.20: Summary of the Loop Seal Plugging (LSP) and Loop Seal Clearing (LSC) phenomena

To better analyse the LSC phenomenon, one should look at the pressure difference between the two thermodynamically independent systems on either side of the plug. Figure 6.21 shows that the pressure difference is greater on LSTF than on BETHSY and in the PWR. It should be noted that the remaining mass in non-cleared loops reduces the collapsed level in the core and thus has an effect on the PCT.

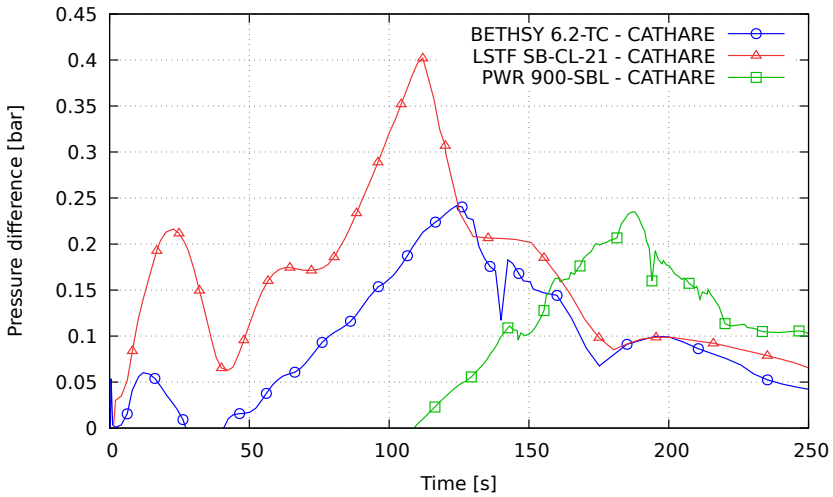

(a) Intact loop(s)

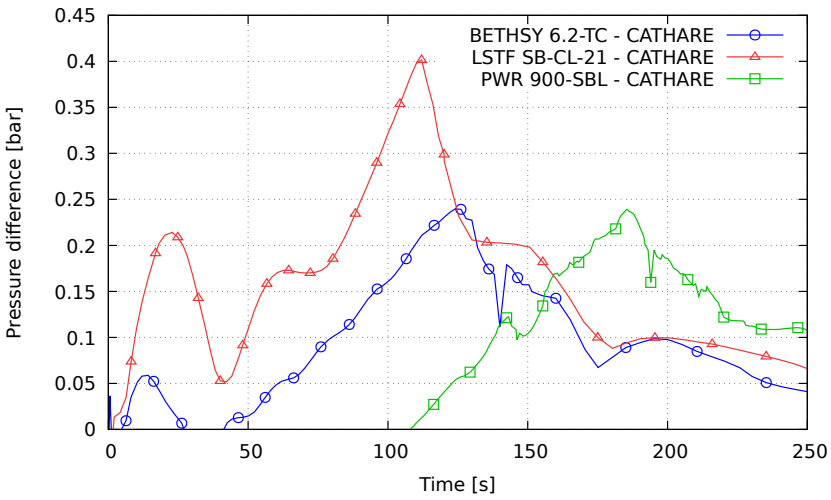

(b) Broken loop

Figure 6.21: Pressure difference between HL and CL outlet of the 6% SB-LOCA counterpart test - CATHARE predictions

Several effects can explain the asymmetric behaviour:

- There is no significant differences between intact and broken loop pressure difference (see Figure 6.21) since it is the pressure difference between the upper plenum and top of downcomer.
- Differences in IL height between BETHSY and LSTF are observed. The difference between the elevation of the horizontal CL and the bottom of the IL is 2.2 m on BETHSY and 3.7 m on LSTF.
- The heat transfer coefficient in the SG tubes may slightly differ between SG, resulting in more or less condensate liquid falling in the IL.
- The first loop to be cleared may equalize pressures before the other(s) can be cleared. The predicted differences between loops is visible in the liquid mass in IL (see Figure 6.19). They show that at the time a first loop is cleared, the other still did not fully clear and some water flows back to it. Small differences in initial fluid mass in the IL can result in different behaviour.

An additional analysis based on the identification of characteristic time ratios could provide preliminary information about the distortions associated with the LSP/LSC and core uncovery phenomena during the RCM phase. Characteristic time ratios are similarity criteria that allow the definition of dimensionless Π-groups based of the H2TS methodology (Zuber 1991). They can be used at each level of system subdivision of the top-down approach. To obtain characteristic time ratio, a specific frequency ω_k of a constituent k is associated with the residence time constant τ_k of the control volume V. Following a set of scaling criteria based on characteristic time ratios is a rational choice for the design of test facilities and their operating conditions (Reyes et al. 1998).

Even if CATHARE predicts these phenomena asymmetrically, it may be interesting to conduct this analysis on the loops where the phenomena occur. The LSP and LSC processes can be expressed as filling and recirculation residence time using this method. The residence time for LSP τ_{LSP} is defined as the ratio between the difference of liquid mass plugged in the IL before and after the phenomenon ΔM_{LSP} and the sum of the mean mass flow rates entering the IL $\bar{\dot{M}}_{IL,in}$. The residence time for

the LSC τ_{LSC} is defined as the ratio between the total mass plugged in the IL M_{IL} and the mean mass flow rate leaving the IL $\bar{\dot{M}}_{IL,out}$. The characteristic time ratio of the loop seal phenomenon Π_{LS} is defined as the ratio of the sum of the mean mass flow rates entering and leaving the IL.

$$\tau_{LSP} = \frac{\Delta M_{IL}}{\bar{\dot{M}}_{IL,in}} \tag{6.9}$$

$$\tau_{LSC} = \frac{M_{IL}}{\bar{\dot{M}}_{IL,out}} \tag{6.10}$$

$$\Pi_{LS} = \frac{\bar{\dot{M}}_{IL,in}}{\bar{\dot{M}}_{IL,out}} \tag{6.11}$$

The residence time for the core uncovery is defined as the ratio core lost mass $\Delta M_{core,unc.}$ and the difference in mass flow rate leaving $\bar{\dot{M}}_{core,out}$ and entering $\bar{\dot{M}}_{core,in}$ the core. The core uncovery characteristic time ratio is the ratio of the mass flow rate leaving and entering the core.

$$\tau_{core,unc.} = \frac{\Delta M_{core,unc.}}{\bar{\dot{M}}_{core,out} - \bar{\dot{M}}_{core,in}} \tag{6.12}$$

$$\Pi_{core,unc.} = \frac{\bar{\dot{M}}_{core,in}}{\bar{\dot{M}}_{core,out}} \tag{6.13}$$

Table 6.10 shows the results of this analysis using the RCM phase characteristic time ratios. The LSP residence times of LSTF and the PWR are similar, but BETHSY is 46% shorter. Conversely, the residence time of the PWR LSC is almost twice slower than in the facilities. As a result, the overall loop seal phenomenon differs significantly between the three systems. This confirms the complex and sensible nature of the phenomenon. Because of the delayed occurrence, the PWR core uncovery has a longer residence time than facilities. The core empties more slowly due to distortions of the previous phenomena induced by the inertia of the primary pumps. Nevertheless, the PWR characteristic time ratio is closer to the BETHSY one than to the LSTF one. Figure 6.9 depicts their similar uncovery behaviour.

Table 6.10: Characteristic time ratio of the LSP/LSC and core uncovery processes of the 6% SB-LOCA counterpart test - CATHARE predictions

	BETHSY 6.2-TC	LSTF SB-CL-21	PWR 900-SBL
LSP residence time τ_{LSP}	19.5 s	37.2 s	35.7 s
LSC residence time τ_{LSC}	30.0 s	27.4 s	56.1 s
Loop seal characteristic time ratio Π_{LS}	0.99	0.25	0.54
Core uncovery residence time $\tau_{core,unc.}$	135.8 s	125.1 s	199.2 s
Core uncovery characteristic time ratio $\Pi_{core,unc.}$	0.91	0.78	0.98

The depressurization of the RCM phase is investigated using the FSA method applied to mass and pressure by VRC equations, for the primary system control volume. Table 6.11 shows the main parameters of the RCM phase.

Table 6.11: Main parameters of the RCM phase of the 6% SB-LOCA counterpart test - CATHARE predictions

	BETHSY 6.2-TC	LSTF SB-CL-21	PWR 900-SBL
Initial primary mass $M_{1,0}$	914 kg	2 536 kg	98 237 kg
Phase duration Δt_{RCM}	71 s	60 s	76 s
Primary mass difference ΔM_1	324 kg	627 kg	32 410 kg
Pressure difference ΔP_{RCM}	0.58 MPa	0.96 MPa	0.38 MPa
Averaged mass flow rate at the break $\bar{\dot{M}}_{break}$	5.12 kg/s	12.61 kg/s	447.71 kg/s
Averaged core power $\bar{\dot{W}}_{core}$	$1.62 \cdot 10^6$ W	$5.49 \cdot 10^6$ W	$9.09 \cdot 10^7$ W
Averaged core power ratio (facilities/PWR)	1/56	1/17	-
Averaged SG tubes heat exchanges $\bar{\dot{W}}_{SG}$	$9.16 \cdot 10^6$ W	$2.77 \cdot 10^6$ W	$3.54 \cdot 10^7$ W
Averaged primary wall heat exchanges $\bar{\dot{W}}_{ow}$	$1.21 \cdot 10^5$ W	$8.37 \cdot 10^4$ W	$1.03 \cdot 10^7$ W
Averaged liquid temperature $\bar{T}_{1,l}$	290.8 °C	291.3 °C	285.9 °C
Averaged vapour temperature $\bar{T}_{1,v}$	297.8 °C	293.6 °C	287.9 °C

The values of the effect metrics for the mass equation $\Omega_{\dot{M},\chi_j}$ and the pressure equation $\Omega_{\dot{P},\chi_j}$ are displayed for the primary system RCM phase in Table 6.12. They are classified according to the four effect metrics ranks described in Table 5.3.

Table 6.12: Effect metrics of the primary system volume during the RCM phase of the 6% SB-LOCA counterpart test

		BETHSY 6.2-TC	LSTF SB-CL-21	PWR 900-SBL
Rate of mass change in V_1 due to the contribution by:				
Liquid flow rate leaving the primary system through the break	$\Omega_{\dot{M}_{l,break}}$	**-1.000**	**-1.000**	**-1.000**
Vapour flow rate leaving the primary system through the break	$\Omega_{\dot{M}_{v,break}}$	**-0.218**	**-0.293**	**-0.219**
Rate of pressure change in V_1 due to the contribution by:				
Liquid volume flow rate leaving the primary system through the break	$\Omega_{\dot{P},Q_{l,break}}$	**-0.245**	**-0.193**	**-0.229**
Vapour volume flow rate leaving the primary system through the break	$\Omega_{\dot{P},Q_{v,break}}$	**-1.000**	**-1.000**	**-1.000**
Thermal expansion/contraction by wall-liquid heat transfers in the core	$\Omega_{\dot{P},Q_{wl,core}}$	0.002	0.002	0.002
Thermal expansion/contraction by wall-vapour heat transfers in the core	$\Omega_{\dot{P},Q_{wv,core}}$	**0.138**	0.020	0.023
Volume change by wall boiling or condensation in the core	$\Omega_{\dot{P},Q_{wi,core}}$	**0.997**	**0.796**	**0.727**
Thermal expansion/contraction by interface-liquid heat transfers in the core	$\Omega_{\dot{P},Q_{il,core}}$	-0.001	-0.002	-0.002

Continued on next page

Table 6.12 continued from previous page

		BETHSY 6.2-TC	LSTF SB-CL-21	PWR 900-SBL
Thermal expansion/contraction by interface-vapour heat transfers in the core	$\Omega_{\dot{P},Q_{iv,core}}$	-0.094	-0.041	-0.010
Volume change by vaporization or condensation by interfacial transfers in the core	$\Omega_{\dot{P},Q_{i,core}}$	0.084	0.073	0.055
Thermal expansion/contraction by wall-liquid heat transfers in SG tubes	$\Omega_{\dot{P},Q_{wl,SG}}$	-0.027	-0.030	-0.008
Thermal expansion/contraction by wall-vapour heat transfers in SG tubes	$\Omega_{\dot{P},Q_{wv,SG}}$	0.000	0.000	0.002
Volume change by wall boiling or condensation in SG tubes	$\Omega_{\dot{P},Q_{wi,SG}}$	-0.006	0.001	0.006
Thermal expansion/contraction by interface-liquid heat transfers in the SG tubes	$\Omega_{\dot{P},Q_{il,SG}}$	0.027	0.029	0.011
Thermal expansion/contraction by interface-vapour heat transfers in the SG tubes	$\Omega_{\dot{P},Q_{iv,SG}}$	0.007	0.015	0.005
Volume change by vaporization or condensation by interfacial transfers in the SG tubes	$\Omega_{\dot{P},Q_{i,SG}}$	-0.624	-0.634	-0.285
Thermal expansion/contraction by wall-liquid heat transfers in the primary system*	$\Omega_{\dot{P},Q_{owl}}$	-0.001	-0.001	0.001
Thermal expansion/contraction by wall-vapour heat transfers in the primary system*	$\Omega_{\dot{P},Q_{owv}}$	0.014	0.002	0.008
Volume change by wall boiling or condensation in the primary system*	$\Omega_{\dot{P},Q_{owi}}$	0.069	0.044	0.044
Thermal expansion/contraction by interface-liquid heat transfers in the primary system*	$\Omega_{\dot{P},Q_{il,ov}}$	-0.002	-0.006	-0.002
Thermal expansion/contraction by interface-vapour heat transfers in the primary system*	$\Omega_{\dot{P},Q_{iv,ov}}$	-0.045	0.018	-0.010
Volume change by vaporization or condensation by interfacial transfers in the primary system*	$\Omega_{\dot{P},Q_{i,ov}}$	0.081	0.115	0.065

**except SG tubes and fuel rods*

Analysis of the effect metrics of the primary system volume during the RCM phase:

- The liquid mass flow rate at the break remains the dominant effect metric on the rate of mass change.
- The RCM phase is a transition phase in which the primary system gradually loses liquid. As a result, the break vapour mass flow rate effect metric is higher than in the NC phase (BETHSY: -0.218; LSTF: -0.293; PWR: -0.219).
- The vapour volume flow rate at the break is now the dominant process in terms of effect metric related to rate of pressure change.

- Volume change by condensation from interfacial transfers in SG tubes also contributes to depressurization. It appears to be lower in the PWR (-0.285) than in the facilities (BETHSY: -0.624; LSTF: -0.634).

- The predicted liquid volume flow rate at the break is still significant, but its importance diminishes as the transient progresses. It is also higher on BETHSY (-0.245) than in LSTF (-0.193) and the PWR (-0.229).

- The volume change caused by wall-boiling in the core compensates partially for the depressurization. This term also appears to be relatively higher in BETHSY (0.997) than in LSTF (0.796) and the PWR (0.727).

- It should be noted that the effect metric related to thermal expansion by wall-vapour in the core is influent on BETHSY (0.138), whereas it is negligible on LSTF (0.020) and PWR (0.023). This is due to the prediction of a rather long core dry-out period with wall and vapour superheating in BETHSY compared to the predicted core uncovery in LSTF and in PWR. However, the core dry-out duration is over-predicted in BETHSY calculation and under-predicted in the LSTF calculation (see Figure 6.9 and Figure 6.10).

6.3.6. Results of the A Posteriori Scaling Analysis of the High-Quality Mixture Discharge (HQMD) Phase

The HQMD phase is characterized by a void fraction at the break very close to 1 (> 0.99), as shown in Figure 6.17. The crossing of the primary and secondary pressures is the HQMD phase's bifurcating event. This is a significant event for the remainder of the transient because it is at this point that the SG cease to function as heat sinks. Figure 6.22 depicts the predicted and measured pressure reversal, which occurs earlier and at higher pressure in the facilities than in the PWR since the mass inventory in the PWR remains higher due to a lower break flow rate resulting from a lower pressure plateau (see Figures 6.4a, 6.5a and 6.6a). Because of the discharge of vapour through the break, the primary pressure begins to fall again after the plateau of the NC and RCM phases. Given the absence of HPIS, the primary mass inventory continues to decline.

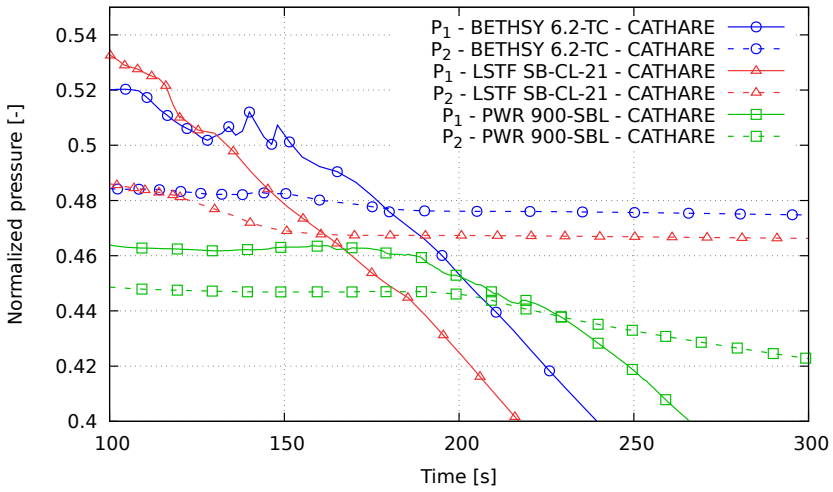

(a) CATHARE predictions

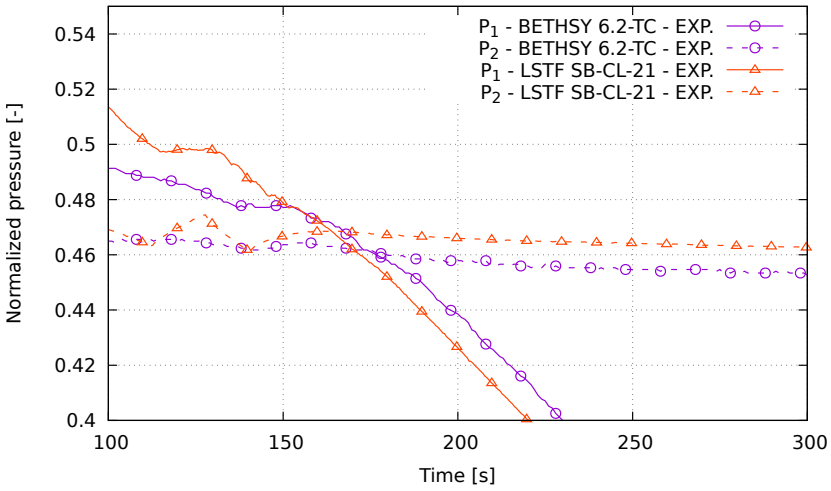

(b) Experimental results

Figure 6.22: Primary and secondary pressures at HQMD bifurcating event of the 6% SB-LOCA counterpart test

The depressurization of the HQMD phase is investigated using the FSA method applied to mass and pressure by VRC equations, for the primary system control volume. Table 6.13 shows the main parameters of the HQMD phase.

Table 6.13: Main parameters of the HQMD phase of the 6% SB-LOCA counterpart test - CATHARE predictions

	BETHSY 6.2-TC	LSTF SB-CL-21	PWR 900-SBL
Initial primary mass $M_{1,0}$	9 580 kg	1 882 kg	65 483 kg
Phase duration Δt_{HQMD}	175 s	175 s	140 s
Primary mass difference ΔM_1	224 kg	664 kg	20 428 kg
Pressure difference ΔP_{HQMD}	3.01 MPa	2.94 MPa	2.69 MPa
Averaged mass flow rate at the break $\bar{\dot{M}}_{break}$	1.43 kg/s	3.90 kg/s	163.12 kg/s
Averaged core power $\bar{\dot{W}}_{core}$	$9.02 \cdot 10^5$ W	$2.89 \cdot 10^6$ W	$8.15 \cdot 10^7$ W
Averaged core power ratio (facilities/PWR)	1/90	1/28	-
Averaged SG tubes heat exchanges $\bar{\dot{W}}_{SG}$	$8.45 \cdot 10^4$ W	$2.50 \cdot 10^5$ W	$4.27 \cdot 10^6$ W
Averaged primary wall heat exchanges $\bar{\dot{W}}_{ow}$	$5.51 \cdot 10^5$ W	$8.78 \cdot 10^5$ W	$2.94 \cdot 10^7$ W
Averaged liquid temperature $\bar{T}_{1,l}$	271.2 °C	270.7 °C	269.3 °C
Averaged vapour temperature $\bar{T}_{1,v}$	283.5 °C	276.9 °C	272.2 °C

The values of the effect metrics for the mass equation $\Omega_{\dot{M},\chi_j}$ and the pressure equation $\Omega_{\dot{P},\chi_j}$ are displayed for the primary system HQMD phase in Table 6.14. They are classified according to the four effect metrics ranks described in Table 5.3.

Table 6.14: Effect metrics of the primary system volume during the HQMD phase of the 6% SB-LOCA counterpart test

		BETHSY 6.2-TC	LSTF SB-CL-21	PWR 900-SBL
Rate of mass change in V_1 due to the contribution by:				
Liquid flow rate leaving the primary system through the break	$\Omega_{\dot{M}_{l,break}}$	-0.043	**-0.065**	**-0.533**
Vapour flow rate leaving the primary system through the break	$\Omega_{\dot{M}_{v,break}}$	**-1.000**	**-1.000**	**-1.000**
Rate of pressure change in V_1 due to the contribution by:				
Liquid volume flow rate leaving the primary system through the break	$\Omega_{\dot{P},Q_{l,break}}$	-0.001	-0.002	-0.019
Vapour volume flow rate leaving the primary system through the break	$\Omega_{\dot{P},Q_{v,break}}$	**-1.000**	**-1.000**	**-1.000**
Thermal expansion/contraction by wall-liquid heat transfers in the core	$\Omega_{\dot{P},Q_{wl,core}}$	0.001	0.000	0.001
Thermal expansion/contraction by wall-vapour heat transfers in the core	$\Omega_{\dot{P},Q_{wv,core}}$	0.001	0.000	0.001
Volume change by wall boiling or condensation in the core	$\Omega_{\dot{P},Q_{wi,core}}$	**0.362**	**0.322**	**0.474**
Thermal expansion/contraction by interface-liquid heat transfers in the core	$\Omega_{\dot{P},Q_{il,core}}$	-0.001	-0.001	-0.002
Thermal expansion/contraction by interface-vapour heat transfers in the core	$\Omega_{\dot{P},Q_{iv,core}}$	-0.001	-0.002	-0.001
Volume change by vaporization or condensation by interfacial transfers in the core	$\Omega_{\dot{P},Q_{i,core}}$	0.042	0.048	**0.061**
Thermal expansion/contraction by wall-liquid heat transfers in SG tubes	$\Omega_{\dot{P},Q_{wl,SG}}$	0.000	0.000	0.000
Thermal expansion/contraction by wall-vapour heat transfers in SG tubes	$\Omega_{\dot{P},Q_{wv,SG}}$	**0.059**	**0.066**	**0.099**
Volume change by wall boiling or condensation in SG tubes	$\Omega_{\dot{P},Q_{wi,SG}}$	0.014	0.004	**0.059**
Thermal expansion/contraction by interface-liquid heat transfers in the SG tubes	$\Omega_{\dot{P},Q_{il,SG}}$	0.000	0.000	0.001
Thermal expansion/contraction by interface-vapour heat transfers in the SG tubes	$\Omega_{\dot{P},Q_{iv,SG}}$	0.001	0.000	-0.021
Volume change by vaporization or condensation by interfacial transfers in the SG tubes	$\Omega_{\dot{P},Q_{i,SG}}$	0.000	0.000	0.031
Thermal expansion/contraction by wall-liquid heat transfers in the primary system*	$\Omega_{\dot{P},Q_{owl}}$	0.002	0.001	0.001

Continued on next page

Table 6.14 continued from previous page

		BETHSY 6.2-TC	LSTF SB-CL-21	PWR 900-SBL
Thermal expansion/contraction by wall-vapour heat transfers in the primary system*	$\Omega_{\dot{P},Q_{owv}}$	0.042	0.009	0.009
Volume change by wall boiling or condensation in the primary system*	$\Omega_{\dot{P},Q_{owi}}$	**0.140**	**0.104**	**0.082**
Thermal expansion/contraction by interface-liquid heat transfers in the primary system*	$\Omega_{\dot{P},Q_{il,ov}}$	-0.005	-0.006	-0.006
Thermal expansion/contraction by interface-vapour heat transfers in the primary system*	$\Omega_{\dot{P},Q_{iv,ov}}$	-0.034	0.017	0.006
Volume change by vaporization or condensation by interfacial transfers in the primary system*	$\Omega_{\dot{P},Q_{i,ov}}$	**0.205**	**0.206**	**0.225**

**except SG tubes and fuel rods*

Analysis of the effect metrics of the primary system volume during the HQMD phase:

- The pressure reversal results from a quasi-vapour flow at the break, as demonstrated by the dominant effect metric related to the break volume flow rate for the BETHSY and LSTF facilities. Figure 6.17 shows that the void fraction at the break is lower on the PWR than on the facilities at the start of the HQMD phase.
- Because of the different pump behaviours, the effect metric related to the liquid mass flow rate is distorted (lower) on the facilities (BETHSY: -0.043; LSTF: -0.065) compared to PWR (-0.533).
- The vapour volume flow rate at the break is the dominant effect metric related to the rate of pressure change. It dominates the other phenomena, which explains the second depressurization after the pressure plateau (see Figure 6.6).
- When compared to the RCM phase, the effect metric related to volume change caused by wall-boiling in the core has decreased. The core boiling is then no longer sufficient to compensate for the fluid volume lost at the break. However, the core boiling is still slightly influent and its impact on the PWR (0.474) is greater than on the facilities (BETHSY: 0.362; LSTF: 0.322).
- Because of the decreased pressure, wall-boiling and vaporization by flashing in the primary system are slightly higher than in the NC and RCM phases.
- Given the void fraction close to 1, the effect metric related to the liquid volume flow rate at the break is now negligible (BETHSY: -0.001; LSTF: -0.002; PWR: -0.019).
- Thermal contraction by wall-liquid in SG tubes heat transfers is now zero given the absence of liquid.
- Thermal expansion caused by wall-vapour in SG tubes heat transfers begins to have a minor impact on pressure (BETHSY: 0.059; LSTF: 0.066; PWR: 0.099).

- Likewise, volume change by wall-boiling (BETHSY: 0.140; LSTF: 0.104; PWR: 0.082) and by vaporization (BETHSY: 0.205; LSTF: 0.206; PWR: 0.225) in the primary system become influent during HQMD phase.

6.3.7. Results of the A Posteriori Scaling Analysis of the Reactor Refilling (RR) Phase

The Reactor Refilling (RR) phase starts with the accumulator injection, triggered when the primary pressure drops below 4.2 MPa. The primary circuit mass inventory is at its minimum at the start of this phase (see Figure 6.5). The code predicts a second Peak Clad Temperature (PCT), which is observed experimentally on BETHSY and not on LSTF (see Figure 6.10). It is smaller than the first PCT. The BETHSY second PCT occurs at 92% of the core height and reaches a temperature of 286 °C (324 °C experimentally). The primary system refills and the mass inventory grows after a few seconds.

Figure 6.23 depicts the accumulator liquid mass. The injection behaviour of the three systems is observed to be different. After 520 seconds of transient, several stages of injections are predicted in BETHSY calculation. These stages are not detected experimentally and are thus code-induced errors. A single stage is observed at 480 seconds in LSTF predictions, but it lasts much longer in the code predictions than experimentally. The PWR predictions show more stages, but they are much less intense. Figure 6.24 depicts the core-collapsed level during the RR phase. Predicted liquid level oscillations in the BETHSY core are found to correspond to the injections stages. It should be noted that both BETHSY and the PWR have two accumulators on the two intact cold legs. On the other hand, LSTF has only one accumulator on the broken cold leg.

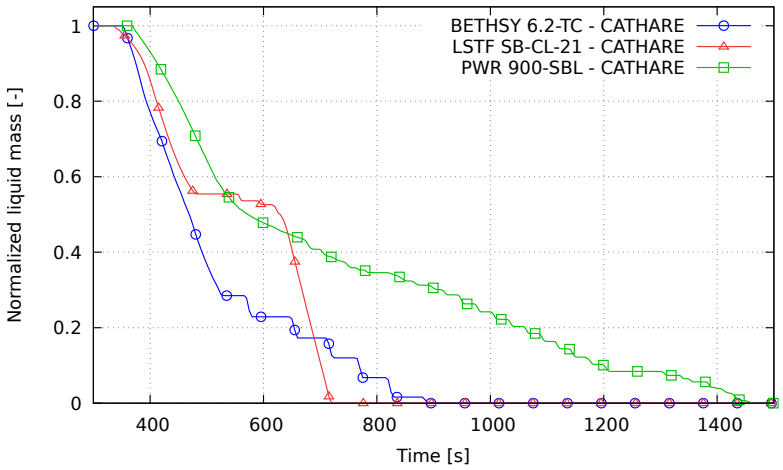

(a) CATHARE predictions

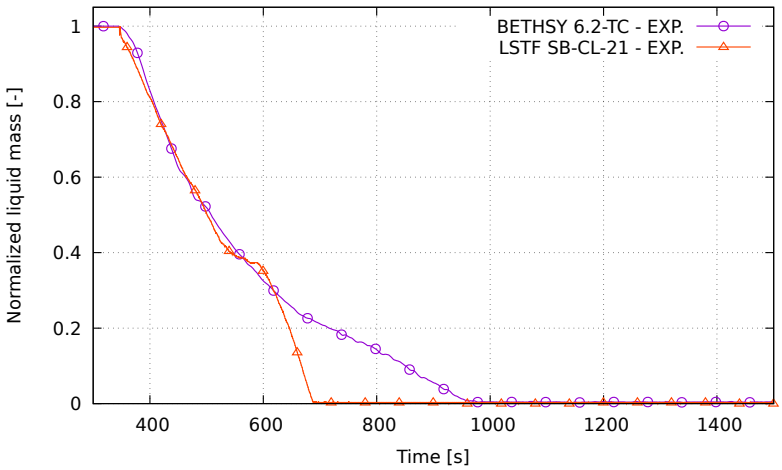

(b) Experimental results

Figure 6.23: Accumulator liquid mass of the 6% SB-LOCA counterpart test

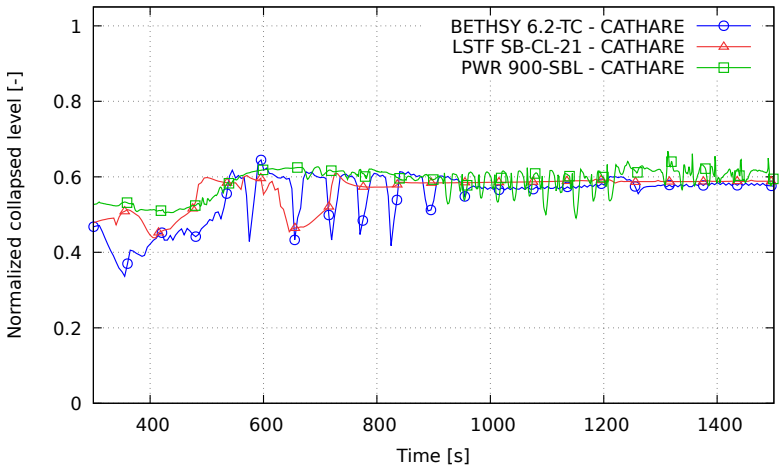

(a) CATHARE predictions

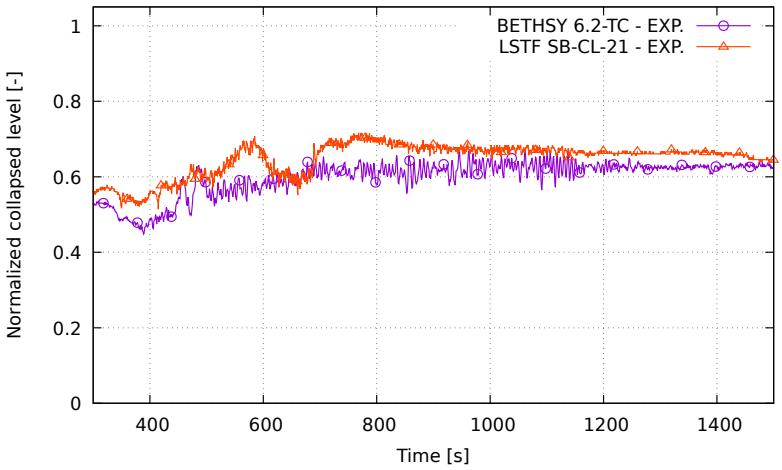

(b) Experimental results

Figure 6.24: Core-collapsed level during the RR phase of the 6% SB-LOCA counterpart test

An analysis through characteristic time ratio is performed on the accumulator discharge, similar to the one performed in section 6.3.5. The residence time $\tau_{acc.}$ is defined as the ratio between the total mass of liquid in the accumulators $M_{l,acc.}$ and the mean mass flow rate injected during the RR phase $\bar{\dot{M}}_{l,acc.}$. The accumulator discharge characteristic time ratio $\Pi_{acc.}$ is defined as the ratio of the mean mass flow rate injected by the accumulators and leaving the primary system through the break.

$$\tau_{acc.} = \frac{M_{l,acc.}}{\bar{\dot{M}}_{l,acc.}} \tag{6.14}$$

$$\Pi_{acc.} = \frac{\bar{\dot{M}}_{l,acc.}}{\bar{\dot{M}}_{break}} \tag{6.15}$$

Table 6.15 shows the results of this analysis using characteristic time ratio. Because the residence times are calculated based on the full injection duration of the accumulators, values close to the RR phase duration are observed. The characteristic time ratios of BETHSY and LSTF are similar. During this phase, the PWR mean mass flow rates compensate for each other.

Table 6.15: Characteristic time ratio of the accumulator discharge of the 6% SB-LOCA counterpart test - CATHARE predictions

	BETHSY 6.2-TC	LSTF SB-CL-21	PWR 900-SBL
Accumulator discharge residence $\tau_{acc.}$	523.8 s	380.5 s	1098.6 s
Accumulator characteristic time ratio $\Pi_{acc.}$	2.1	2.4	1.0

The depressurization of the RR phase is investigated using the FSA method applied to mass and pressure by VRC equations, for the primary system control volume. Table 6.16 shows main parameters of the RR phase.

Table 6.16: Main parameters of the RR phase of the 6% SB-LOCA counterpart test - CATHARE predictions

	BETHSY 6.2-TC	LSTF SB-CL-21	PWR 900-SBL
Initial primary mass $M_{1,0}$	335 kg	1 215 kg	45 045 kg
Phase duration Δt_{RR}	539 s	384 s	1 098 s
Primary mass difference ΔM_1	247 kg	818 kg	24 331 kg
Pressure difference ΔP_{RR}	2.67 MPa	2.85 MPa	3.28 MPa
Averaged mass flow rate at the break $\bar{\dot{M}}_{break}$	0.46 kg/s	1.54 kg/s	47.91 kg/s
Averaged accumulator mass flow rate $\bar{\dot{M}}_{acc.}$	0.95 kg/s	3.71 kg/s	50.00 kg/s
Averaged core power $\bar{\dot{W}}_{core}$	$6.06 \cdot 10^5$ W	$1.85 \cdot 10^6$ W	$5.21 \cdot 10^7$ W
Averaged core power ratio (facilities/PWR)	1/86	1/28	-
Averaged SG tubes heat exchanges $\bar{\dot{W}}_{SG}$	$1.11 \cdot 10^5$ W	$2.31 \cdot 10^5$ W	$1.41 \cdot 10^7$ W
Averaged primary wall heat exchanges $\bar{\dot{W}}_{ow}$	$5.59 \cdot 10^5$ W	$2.25 \cdot 10^6$ W	$2.88 \cdot 10^7$ W
Averaged liquid temperature $\bar{T}_{1,l}$	207.1 °C	216.7 °C	186.2 °C
Averaged vapour temperature $\bar{T}_{1,v}$	265.6 °C	247.9 °C	227.9 °C

The values of the effect metrics for the mass equation $\Omega_{\dot{M},\chi_j}$ and the pressure equation $\Omega_{\dot{P},\chi_j}$ are displayed for the primary system RR phase in Table 6.17. They are classified according to the four effect metrics ranks described in Table 5.3.

Table 6.17: Effect metrics of the primary system volume during the RR phase of the 6% SB-LOCA counterpart test

		BETHSY 6.2-TC	LSTF SB-CL-21	PWR 900-SBL
Rate of mass change in V_1 due to the contribution by:				
Liquid flow rate leaving the primary system through the break	$\Omega_{\dot{M}_{l,break}}$	-0.022	-0.002	**-0.438**
Vapour flow rate leaving the primary system through the break	$\Omega_{\dot{M}_{v,break}}$	**-0.464**	**-0.414**	**-0.521**
Liquid flow rate entering the primary system thanks to the accumulator	$\Omega_{\dot{M}_{l,acc.}}$	**1.000**	**1.000**	**1.000**
Rate of pressure change in V_1 due to the contribution by:				
Liquid volume flow rate leaving the primary system through the break	$\Omega_{\dot{P},Q_{l,break}}$	0.000	0.000	-0.005
Vapour volume flow rate leaving the primary system through the break	$\Omega_{\dot{P},Q_{v,break}}$	**-1.000**	**-1.000**	**-0.997**
Thermal expansion/contraction by wall-liquid heat transfers in the core	$\Omega_{\dot{P},Q_{wl,core}}$	0.000	0.000	0.000
Thermal expansion/contraction by wall-vapour heat transfers in the core	$\Omega_{\dot{P},Q_{wv,core}}$	0.001	0.000	0.000
Volume change by wall boiling or condensation in the core	$\Omega_{\dot{P},Q_{wi,core}}$	**0.627**	**0.421**	**0.990**
Thermal expansion/contraction by interface-liquid heat transfers in the core	$\Omega_{\dot{P},Q_{il,core}}$	0.000	-0.001	0.000
Thermal expansion/contraction by interface-vapour heat transfers in the core	$\Omega_{\dot{P},Q_{iv,core}}$	0.001	0.001	0.001
Volume change by vaporization or condensation by interfacial transfers in the core	$\Omega_{\dot{P},Q_{i,core}}$	**0.072**	**0.083**	**0.106**
Thermal expansion/contraction by wall-liquid heat transfers in SG tubes	$\Omega_{\dot{P},Q_{wl,SG}}$	0.000	0.000	0.000
Thermal expansion/contraction by wall-vapour heat transfers in SG tubes	$\Omega_{\dot{P},Q_{wv,SG}}$	**0.199**	**0.161**	**0.581**
Volume change by wall boiling or condensation in SG tubes	$\Omega_{\dot{P},Q_{wi,SG}}$	**0.051**	0.000	**1.000**
Thermal expansion/contraction by interface-liquid heat transfers in the SG tubes	$\Omega_{\dot{P},Q_{il,SG}}$	0.000	0.000	0.001
Thermal expansion/contraction by interface-vapour heat transfers in the SG tubes	$\Omega_{\dot{P},Q_{iv,SG}}$	-0.001	0.000	**-0.084**

Continued on next page

Table 6.17 continued from previous page

		BETHSY 6.2-TC	LSTF SB-CL-21	PWR 900-SBL
Volume change by vaporization or condensation by interfacial transfers in the SG tubes	$\Omega_{\dot{P},Q_{i,SG}}$	0.001	0.000	**-0.269**
Thermal expansion/contraction by wall-liquid heat transfers in the primary system*	$\Omega_{\dot{P},Q_{owl}}$	0.002	0.004	0.001
Thermal expansion/contraction by wall-vapour heat transfers in the primary system*	$\Omega_{\dot{P},Q_{owv}}$	**0.088**	**0.029**	**0.065**
Volume change by wall boiling or condensation in the primary system*	$\Omega_{\dot{P},Q_{owi}}$	**0.373**	**0.286**	**0.255**
Thermal expansion/contraction by interface-liquid heat transfers in the primary system*	$\Omega_{\dot{P},Q_{il,ov}}$	0.001	0.000	0.000
Thermal expansion/contraction by interface-vapour heat transfers in the primary system*	$\Omega_{\dot{P},Q_{iv,ov}}$	**-0.073**	-0.001	-0.020
Volume change by vaporization or condensation by interfacial transfers in the primary system*	$\Omega_{\dot{P},Q_{i,ov}}$	-0.049	-0.017	-0.014
Thermal expansion by liquid flow entering the primary system thanks to accumulator discharge	$\Omega_{\dot{P},Q_{l,acc.}}$	0.020	0.029	0.012
Thermal expansion by condensation due to the liquid flow rate entering the primary system thanks to accumulator discharge	$\Omega_{\dot{P},Q_{cond,l,acc.}}$	-0.005	-0.008	-0.002

**except SG tubes and fuel rods*

Analysis of the effect metrics of the primary system volume during the RR phase:

- The liquid mass flow rate provided by the accumulator discharge is the dominant process in terms of effect metrics on the rate of mass change during the RR phase.
- The distribution of liquid (BETHSY: -0.022; LSTF: -0.002; PWR: -0.438) and vapour (BETHSY: -0.464; LSTF: -0.414; PWR: -0.521) mass flow rates at the break, on the other hand, is not evenly distributed between the facilities and the PWR. According to the results of the characteristic time ratio analysis in Table 6.15, the mass flow rate at the break, particularly the liquid flow rate, is proportionally higher in the PWR than in the facilities.
- The behaviour in the facilities seems to be distorted compared to the PWR, as shown in Figure 6.23. The longer duration of the PWR accumulator injection alters the process behaviour of this phase.
- The vapour volume flow rate at the break is the dominant effect metric contributing to the depressurization.
- Volume change by wall-boiling in the core plays a dominant role in compensating for the depressurization, but its impact is significantly higher in the PWR (0.990) than in the facilities (BETHSY: 0.627; LSTF: 0.421).

- Similarly, thermal expansion by interface-vapour heat transfers (BETHSY: 0.199; LSTF: 0.083; PWR: 0.581) and volume change by wall-boiling (BETHSY: 0.051; LSTF: 0.000; PWR: 1.000) in the SG tubes occur with higher intensity in the PWR than in the facilities. The liquid discharged from the PWR accumulators condenses some vapour. There is some vaporization in the system hot spots, the core and the SG tubes, slowing the system depressurization.

- It should also be noted that volume change by wall-boiling in the primary system now plays a significant role (BETHSY: 0.373; LSTF: 0.286; PWR: 0.255). It is slightly higher in the facilities, particularly in BETHSY, due to the ratio between the primary circuit exchange surface and the primary volume.

The significant distortions observed during the RR phase on the PWR compared to the facilities are investigated. Sensitivity studies have been carried out regarding several parameters of the accumulator injection process. The simplest accumulator model of CATHARE is modelled as a fluid injection sub-module using a constant expansion coefficient for the nitrogen without modelling the thermal exchanges with accumulator walls. Thermal exchanges between accumulator walls and the nitrogen are higher on scaled facilities than in the PWR. An isentropic expansion coefficient γ equal to 1.4 has been used in PWR calculation (corresponding to zero thermal exchanges with walls) whereas values of 1.0 and 1.15 have been used respectively for BETHSY and LSTF. These expansion coefficients values were initially calculated to better fit the experimental results, as used with the fluid injection sub-module. A more accurate modelling of the BETHSY accumulators is used to investigate the differences in the discharge behaviour between the facilities and the PWR. This modelling is based on a 0-D module for the accumulator tank and a 1-D module for the discharge line. Thus, wall exchanges are modelled and calculated instead of relying on an estimated mean expansion coefficient.

Figure 6.25 depicts the accumulator discharge behaviours of BETHSY and the PWR with expansion coefficients:

- Predicted by CATHARE, with an expansion coefficient calculated to better fit with BETHSY experimental results (i.e. with the fluid injection sub-module, $\gamma = 1.0$).

- Predicted by CATHARE, using a more accurate accumulator modelling (i.e. with 0-D and 1-D modules), which calculates heat exchanges between nitrogen and walls.

- From the BETHSY experimental results.

- Predicted by CATHARE, assuming isentropic expansion for the PWR ($\gamma = 1.4$).

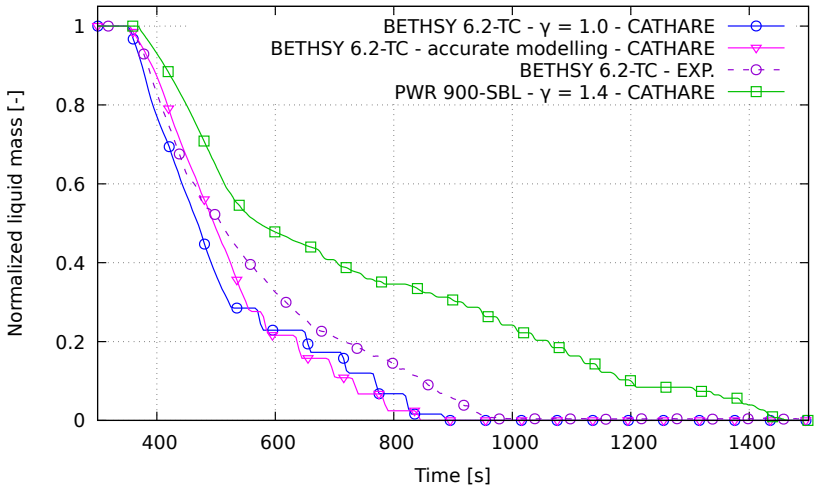

Figure 6.25: Investigation of accumulator liquid mass distortions of the 6% SB-LOCA counterpart test - CATHARE predictions

The two BETHSY accumulator modelling show the same trend, which is close to the experimental trend with several closure and opening of the valve not seen in BETHSY. The difference between BETHSY and the reactor is more significant and is attributed to the distorted parameters of the accumulators: increased metallic thermal capacity and increased ratio between the wall exchange surface to the volume. As a result, more heat is released from the wall to the nitrogen, the accumulator pressure drops more slowly, and the discharge flow rate is higher than in the reactor. As a result, the accumulator discharge is faster on the facilities.

6.3.8. Modification of PWR Pumps Behaviour and Core Power Decay Law

An analysis is performed here to validate previous hypothesis about the observed distortions between the PWR and the facilities. Since the facilities cannot handle the 100% power of the full-scale reactor during the initial moments of the transient, the PWR 900-SBL dataset is modified to reflect the conditions of the facilities. Figure 6.26 depicts significant evolutions influenced by these changes. Given that this is the reference reactor, a comparison is made between the original PWR 900-SBL dataset and the BETHSY 6.2-TC test. The parameters under consideration are:

- The core power decay laws of the facilities, which differs from the PWR at the first instants of the transient. This can be seen from the averaged core power ratio between the facilities and the PWR. In the SBD phase, these ratios are 1/706 and 1/242, respectively for BETHSY and LSTF, and drop to 1/64 and 1/22 in the NC phase. These cause different behaviours, most notably boiling in the core and the amount of vapour in the primary circuit. The JAERI conservative decay power curve is imposed on the PWR on the "Modif. power" curves. The initial power is also scaled to 10% of the original nominal value, just like the facilities.
- The impact of pump behaviour on PWR compared to facilities. The inertia of the PWR pumps alters the natural circulation phase, as seen in BETHSY and LSTF, where the pumps are stopped almost immediately. The transient is simulated on the PWR without pump inertia on the "Modif. pumps" curves in the same way than in the facilities.

Modifications of the PWR including the imposed core decay power curve as well as the immediate coastdown of the pumps are taken into account on the "Modif. power/pumps" curves. These changes have an impact on the main evolutions in the PWR transient, as shown in Figure 6.26.

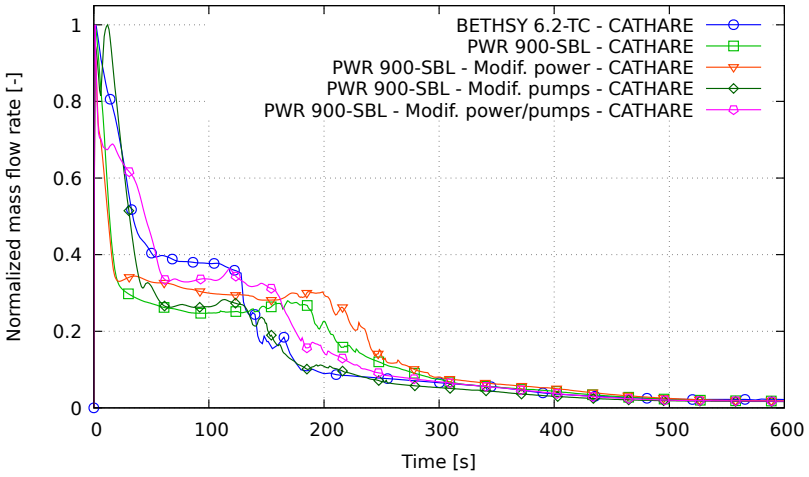

(a) Break mass flow rate

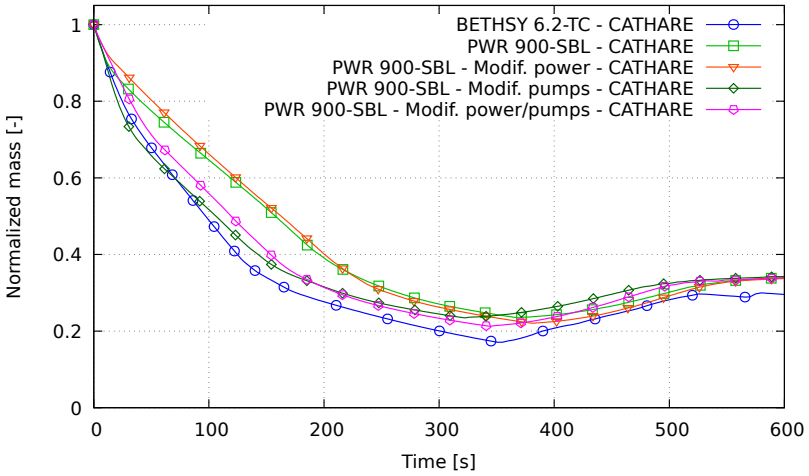

(b) Primary mass inventory

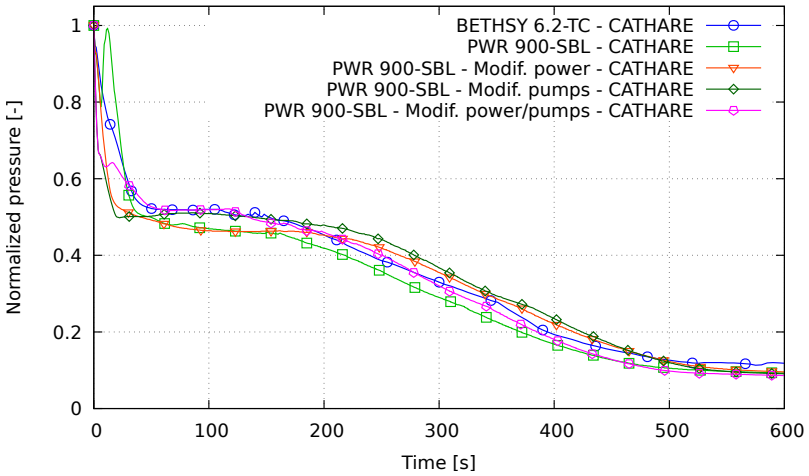

(c) Primary pressure

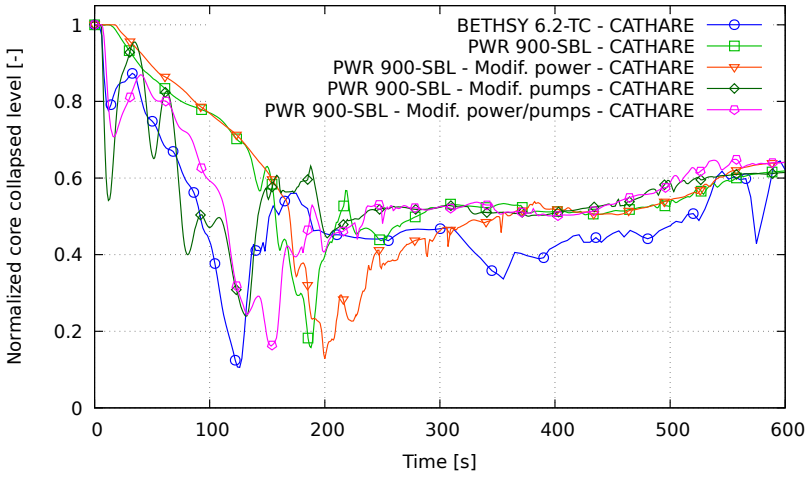

(d) Core-collapsed level

Figure 6.26: Comparison of major transient evolutions between the BETHSY 6.2-TC test and modifications of the PWR 900-SBL transient - CATHARE predictions

It is observed that:

- The power correction brings the evolutions of the PWR break mass flow rate (Figure 6.26a) and the primary pressure (Figure 6.26c) closer to BETHSY evolutions during the plateau in the NC and the RCM phases.
- The changes in the pumps behaviour bring the PWR evolutions significantly closer to the BETHSY evolutions during the SBD and the HQMD phases. The mass flow rate at the break (Figure 6.26a), primary mass inventory (Figure 6.26b) and primary pressure (Figure 6.26c) during the SBD are closer to BETHSY's behaviour. This correction also reduces the temporal shift that was observed on major transient phenomena, such as the first core uncovery in Figure 6.26d.

As demonstrated, the scaled power of the facilities in the early moments of the transient compared to the PWR causes discrepancies. This is illustrated by the integral of the power corresponding to the area n°1 in Figure 6.27. These investigations and the results obtained could be a starting point for suggestions regarding the design of future reduced-scale experiments.

However, a further analysis now aims to determine whether the additional power of the facilities (between 22 seconds and about 300 seconds) could have an impact on the transient results compared to the PWR. This difference is illustrated in the area n°2 in Figure 6.27. For this purpose, the power decay laws of the facilities are adapted to match the PWR power curve after 22s of transient. The new decay power laws of the facilities are referred as "Modified power decay":

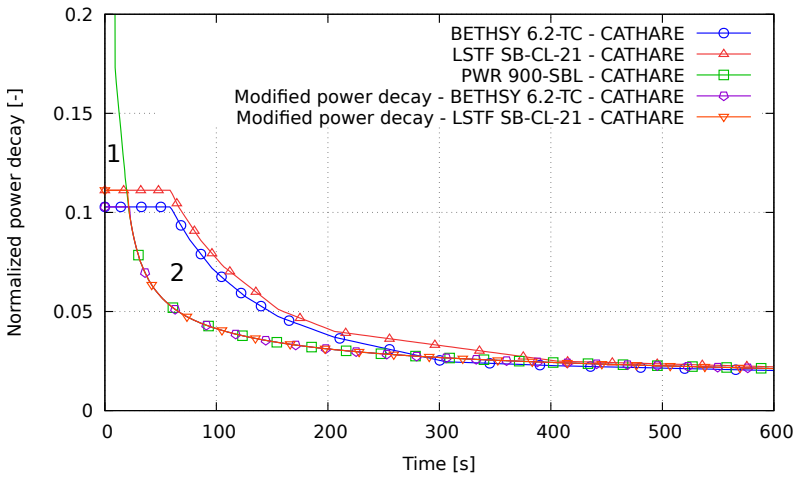

Figure 6.27: Modification of the core power decay law of the facilities of the 6% SB-LOCA counterpart test - CATHARE predictions

The predicted PoI evolutions of the BETHSY and LSTF tests with and without the power law matched to the PWR are shown in the Figure 6.28.

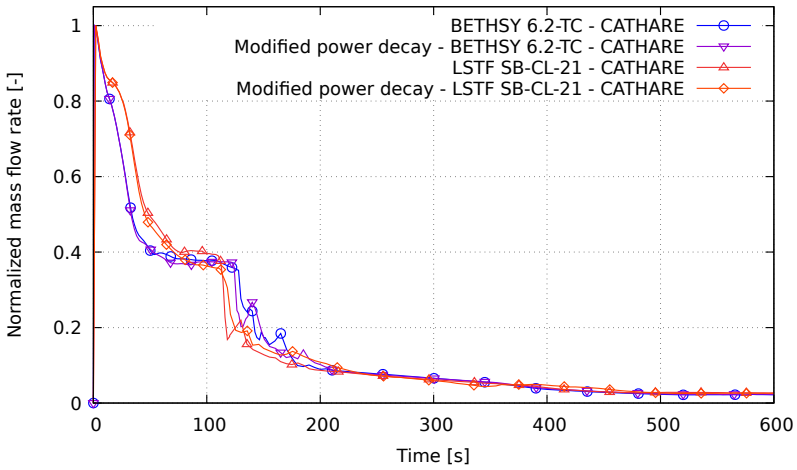

(a) Break mass flow rate

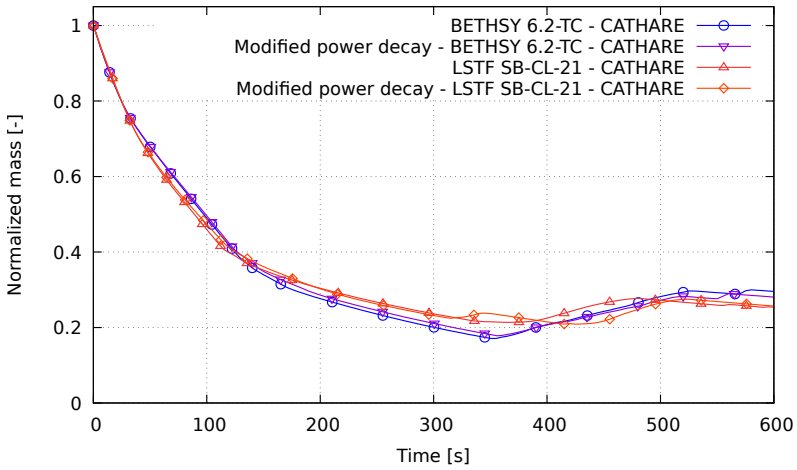

(b) Primary mass inventory

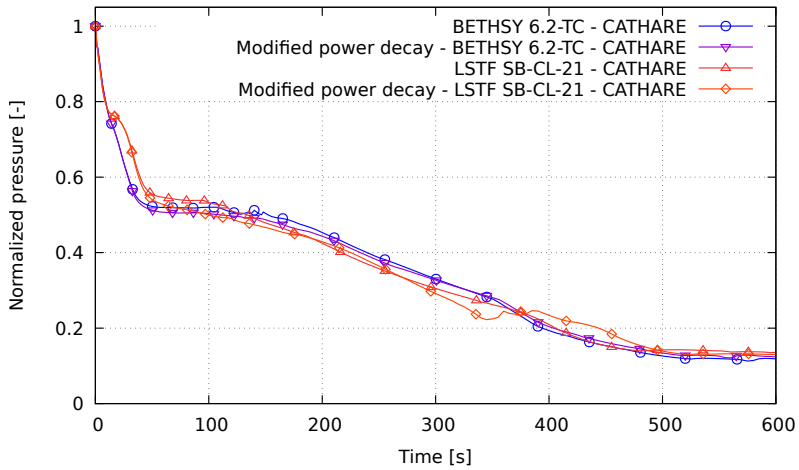

(c) Primary pressure

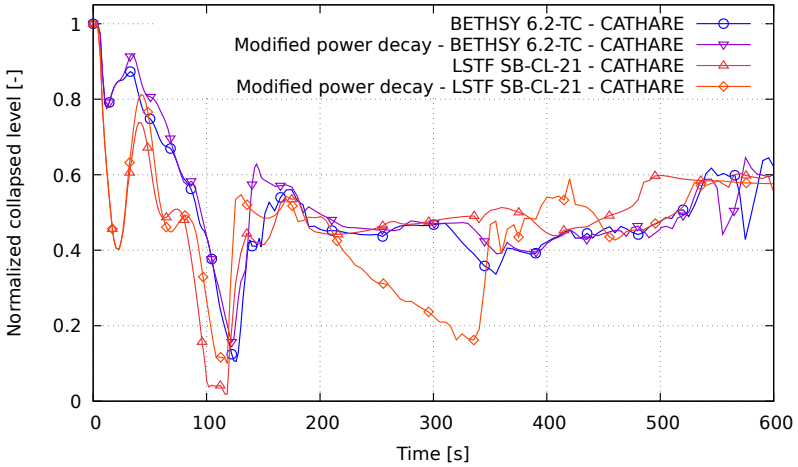

(d) Core-collapsed level

Figure 6.28: Comparison of major transient evolutions between the BETHSY 6.2-TC and LSTF SB-CL-21 tests with the modified core power decay law - CATHARE predictions

No significant difference in the BETHSY predicted results are observed. Only a second core uncovery is observed for the LSTF predicted results, which corresponds to a longer LSP phenomena (see Figure 6.28d). It can be supposed that this longer LSP is triggered by a cliff effect.

The distortions found in the facilities tests are then mostly attributable to discrepancies with the PWR power law in the early transient, as indicated by the lack of significant differences between the results of the facilities with and without the modified core power decay law.

6.4. Discussions

The main objective of this chapter was to investigate the FSA method capability to identify and quantify distortions at the system/component level. Furthermore, after demonstrating the applicability of this method on a single transient in chapter 5, another interest now lies in its application to a set of several tests. For this purpose, an a posteriori scaling analysis is here performed to a 6% cold leg SB-LOCA, comparing two IET of a counterpart test (D'Auria et al. 1992; Kumamaru et al. 1992) and a PWR simulation:

- The 6.2-TC test performed on the French BETHSY facility (Equipe BETHSY 1990).
- The SB-CL-21 test performed on the Japanese LSTF-ROSA-IV facility (The ROSA-V Group 1985).
- A full-scale model of a Framatome commercial reactor.

6.4.1. Summary of the Scaling Analysis Results

The FSA method is applied to primary mass and primary pressure by VRC equations. The term values for those equations are evaluated using the CATHARE code simulations of the two facilities and the PWR. The 6% SB-LOCA transient of the present study is divided into five phases that are applied to the primary system and pressurizer volumes. The scaling analysis results, along with the evolution and differences in the effect metrics of the three systems, provides an identification distortions and their sources:

- In the pressurizer emptying, the behaviour of the predicted LSTF pressurizer differs from the predicted BETHSY pressurizer due to its design difference (full height for BETHSY and a reduced height in LSTF).
- The facilities seem to be distorted since the predicted vapour volume flow rate leaving the pressurizer are smaller than in the PWR simulation. However this may be related to an oversimplified 0-D two-node pressurizer modelling with CATHARE, which cannot predict very precisely the void fraction entrained in the expansion line.
- During the subcooled blowdown phase, significant distortions between the facilities and the PWR are observed in the primary system due to pump behaviour and power evolution differences. Higher volume change by wall heat transfers in the PWR core and SG tubes are observed compared to the facilities just reflecting the fact that core power is truncated at 10% and 11% in experiments. The initial pump produces only 10% of nominal flow rate in experiments and pump speed rapidly decreases to zero. These two differences impact the loop flow rate and the break quality and flow rate.
- The natural circulation phase is temporally distorted because of the PWR pumps behaviour in comparison to the facilities. These distortions are transferred to the RCM, HQMD and RR phases of the transient.
- The reactor refilling phase also differs significantly between the facilities and the PWR. It is demonstrated that scaling effects on heat transfers between accumulator walls and nitrogen can drastically change the discharge duration. These results indicate that choices in the basic design of ITF can have a notable impact on phenomena behaviour throughout the transient.

- Some distortions are found in the wall heat transfers and the wall-boiling/condensation phenomena between the facilities and the PWR, but also between BETHSY and LSTF. These discrepancies are due to the overestimated wall thermal mass and thermal inertia, and overestimated wall heat transfer area in the scaled experiments (except for the fuel rods and SG tubes). These are unavoidable scale effect directly caused by the power-to-volume scaling method used in the design of these facilities.

- The LSP and LSC phenomena are still difficult to predict by the calculation codes. These phenomena appear to be sensitive to facilities design parameters as well as scale effects. Although the code predictions on BETHSY and LSTF yield asymmetric results, there is a significant difference in the phenomena behaviour between the facilities and the PWR.

  Perspectives for future work are intended to conduct scaling analyses at component/local scale in order to better understand these phenomena and the processes or scale effects influencing them.

6.4.2. Methodology Improvements

Beyond the results presented in the previous section, the work in this chapter contributes to the improvement of the a posteriori scaling analysis methodology developed in this thesis.

An important contribution of the study in this chapter is the conduct of the scaling analysis on a counterpart test. It allowed the identification of inter-system distortions as well as scale transposition when analysing the results between the IET and the PWR. The scaling analysis showed discrepancies that could be attributed to ITF design choices, code deficiencies, or scale effects. This demonstrates that confronting several system in a study is an effective tool for scaling analyses.

Compared to chapter 5, a major improvement in the methodology is the application of the FSA method to the general pressure by VRC equation, without saturation assumption. The formulation of this equation allows for a much more detailed analysis of the phenomena and processes than the equation with saturation assumption. This can be seen by comparing Figures 5.9 and 6.11 which summarize the effect metrics of both studies. The general equation thus provides more confidence in the scaling analysis results. This was demonstrated by the uncertainties in the saturation condition during the HQMD phase analysis in section 5.2.3. Because of the detailed hierarchy and precise identification of the important phenomena, the results obtained with this equation allow for the formulation of a structured PIRT at the system/component scale.

The analysis of the results of the a posteriori scaling analysis is however more complex, and the difficulty lies in a thorough understanding of the thermal-hydraulic of the transient processes. This is why the author suggests that a phenomenological analysis (allowed by the validated code) should be used to interpret the meaning of the effect metrics and the associated phenomena. For example, as it have been shown in the analyses, some phenomena can appear to be significant as a result of another upstream phenomenon (process chains), and it is sometimes required to have an expert judgement on the thermal-hydraulic of transients to distinguish the dominant phenomenon during each phase of the transient.

This phenomenological analysis would constitute an additional step to the scaling analysis methodology road map depicted in Figure 3.6. This step could be performed before the scaling analysis, as shown in section 6.2.2. In order to illustrate the good agreement between code predictions and experimental results, it would be useful to investigate the major evolutions of the transient prior to the scaling results. Furthermore, as shown in section 6.3, this step could also be performed systematically in support of the scaling analysis to establish the correlations between the scaling

criteria (here the effect metrics) and the phenomenology of the transient. Finally, as shown in section 6.3.8, additional phenomenological studies may be required to confirm the results of scaling analyses.

Sensitivity and boundary conditions analyses appear to be useful when combined with phenomenological and scaling analyses to study and understand complex phenomena. As it has been demonstrated in this chapter, it allows for the highlighting of scale effects and cliff edge phenomenon. Sensitivity analyses can also be used to assess the impact of parameters that are thought to be important in the behaviour of the studied phenomena. And they can be used in a counterpart test to understand inter-system distortions.

The author suggests that the user of scaling analyses could use the saturation equation if the expected results are relatively "simple" and "convenient to analyse" according to the application, and then select the general equation in a second step for a more accurate analysis.

This study also addresses another scaling analysis issue: the choice of the transient phase division which is an essential (see section 3.3.2.2 and Appendice E). Phenomenological analysis and expert judgement currently allow for the selection of bifurcating events, but it can be assumed that an improvement in the methodology would allow for the phases splitting, depending on the evolution of PoI and key phenomena. The use of the code is now commonly recognised in phase splitting because it allows certain bifurcating events to be accurately identified.

Using the FSA scaling method, it is possible to conclude that using a mature and extensively validated system code – here, the CATHARE code – reduces the impact of the assumptions made to evaluate the terms of the equations for the scaling analysis. Furthermore, as previously stated in the chapter 5, the code actually provides more precision by averaging the values of the equations rather than relying on estimates at the phase boundaries. As demonstrated, scaling tools such as equations at the system level can also support the improvement of code modelling by identifying code errors or sensitive phenomena.

The capability of the FSA method to identify inter-system distortions on a full transient is validated for this application.

CHAPTER 7

The A Posteriori Scaling Analysis Methodology

As the title of the thesis suggests, the main objective was to develop a methodology for scaling analyses. Especially, and as mentioned in section 3.4, the purpose was to provide guidelines for the application of a scaling methodology applied to nuclear transients with the support of calculation codes. This chapter summarizes the four steps of the methodology, developed through the studies of this thesis as well as based on a reinterpretation of the literature review. Guidelines on the methodology application are provided to the reader and an illustration is shown in Figure 7.4.

7.1. Preliminary Analysis

The preliminary analysis is the first part of the methodology. The first step is the **selection of the transient** to be studied. For example, if it is chosen to investigate a LOCA, the type of the break must be considered, and it is a priori required to have at least experimental data and/or prediction results from a calculation code. Therefore, selecting the transient occurs simultaneously with selecting the reduced-scale facility(ies) to be studied. The work in this thesis has only focused on ITF/IET, but analyses on SETF/SET could be considered.

If the purpose of the study is to conduct a comparative analysis of several systems, for example, to identify and quantify distortions and/or scale effects, a **counterpart test** must be defined. Several reduced-scale facilities or one/several facilities and a reference full-scale reactor can be selected, as in section 6.1. It is then necessary to ensure that the experimental conditions and/or the code modelling of the counterpart test are consistent, i.e. that the transient and test conditions are the same (see section 6.2.2). In general, the international nuclear industry agrees on counterpart tests under predetermined conditions. It should be noted that a counterpart test is not necessary if the expected outcome is only the establishment of a PIRT. However, this obviously allows for a better justification of the results on process hierarchy.

The most important step in this part of the methodology is the **phenomenological analysis**, which comes before the scaling analysis (see examples in sections 5.1.2 and 6.2.1). The author highlights the role of this step in defining the subsequent steps. This analysis is conducted simultaneously on each systems of the counterpart test and allows for:

- A thorough understanding of the transient, test parameters, and important evolutions and processes. It is, however, convenient to have an expert judgement regarding the observation of these key parameters.
- To have a first look at the processes that may be distorted by observing differences in the evolution of the transient key variables. An available counterpart test therefore makes sense

here.

The next step is to establish the **chronology of the transient events** using the phenomenological analysis. The occurrence of known and/or identified important phenomena and processes, as well as the trigger of safety systems, is taken into account (see Table 6.3). This step allows:

- To assess the boundary conditions of the counterpart test. It can also provide some indications on transient temporal distortions.
- The comparison of the code predictions with experimental results. It should be noted that the code V&V is usually done before the scaling analysis on known transients. However, the author suggests that a qualitative verification of the code predictions is a good practice in order to ensure the confidence given to the code, especially for the scaling analysis and identification of the sources of distortion.

Finally, the last step of the preliminary analysis is the establishment of the **transient scenario**, allowed by the phenomenological analysis, through its major evolutions and their behaviour throughout the transient. The preliminary analysis of the a posteriori scaling analysis methodology is illustrated in Figure 7.1.

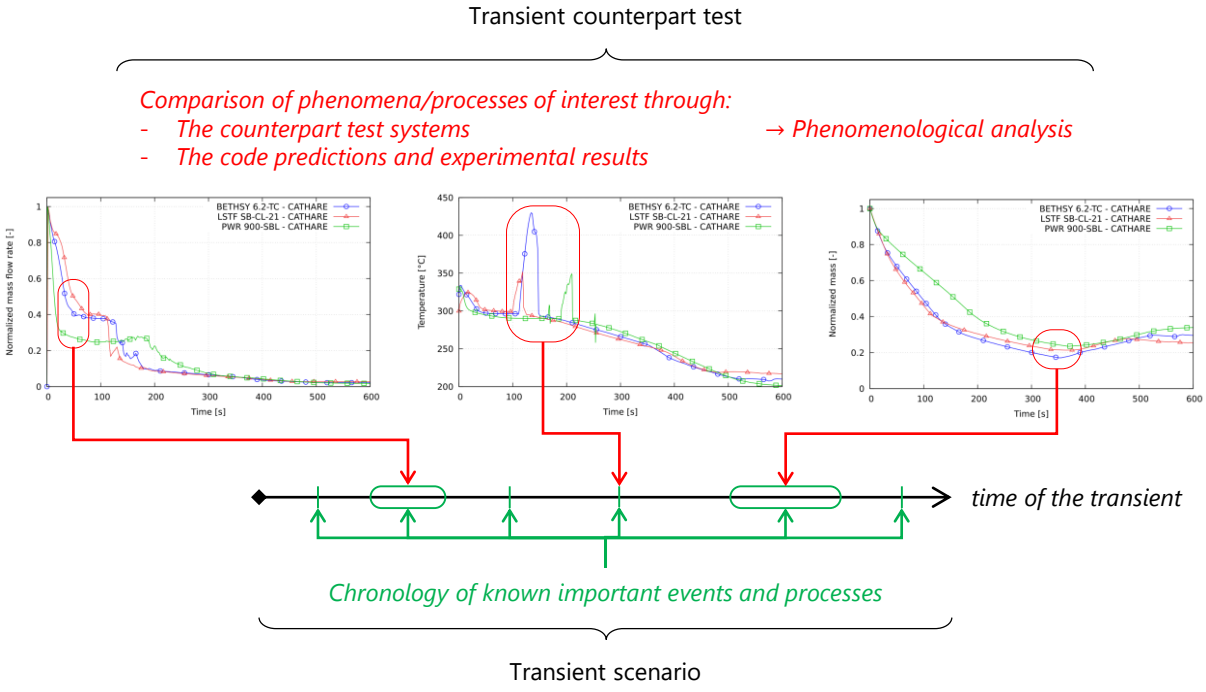

Figure 7.1: Schematic of the preliminary analysis of the a posteriori scaling analysis methodology

7.2. Reinterpretation of the Fractional Scaling Analysis (FSA) Method

The second part of the methodology is the reinterpretation of the Fractional Scaling Analysis (FSA) method. The following guidelines, based on the theory described in Zuber's work as well as its theoretical applications (see section 3.3.2.4), allow for a scaling analysis supported by calculation codes (which the FSA method was not initially conceived for).

The first step is to define the **Figure of Merit (FoM)** of the transient. It is a critical criterion of the transient, such as a safety criterion. This criterion is usually established by expert judgement and can be identified by the previous phenomenological analysis. In the case of standard nuclear transients, for example, the FoM is defined as the Peak Clad Temperature (PCT) or the core mixture level.

The **Parameters of Interest (PoI)** are then defined. These are the variables, parameters, or processes that have a significant impact on the FoM. They are also defined initially by expert judgement, but may be identified from the phenomenological analysis, existing PIRT, or extrapolated from known similar transients.

It is usually necessary to divide the transient into **temporal phases**. **Bifurcating events** are identified for this purpose using the phenomenological analysis on the one hand and PoI variations on the other (see Figures 5.2, 6.3 and Table 5.2). They can also be known points of interest of the transient identified by expert judgement, but may also correspond to safety triggers. Bifurcating events are then instant where the status of the system or the scenario of the transient changes more or less significantly. Theses changes in the transient behaviour are linked to changes in physics and local phenomena occurrence. Then, bifurcating events and the resulting phases must match in the case of a counterpart test in order to limit the uncertainties in the representativeness of the scaling analysis results.

The **scale of the analysis** should then be defined. Motivated by the top-down and bottom-up approaches (see section 3.3.2.1), the author suggests a three-scales approach, illustrated in Figure 7.2:

- The system scale, which takes into account the entire system in the analysis. For the study of a transient on an ITF or a nuclear reactor, the system scale analysis can be performed on the primary system. However, the system will be too complex to be understood as a whole. It will therefore be necessary to divide it into sub-systems thanks to the top-down approach.
- The component scale, which focuses on the intermediate volumes of the system. For example, the main components that can be studied for a transient from the perspective of the primary system are the core, the steam generators, or the pressurizer. The analysis at this scale will thus be able to consider the interactions between the various components while also accounting for the overall behaviour of the system as a whole thanks the bottom-up approach.
- The local scale, which is also allowed by the top-down approach whose purpose is to focus on specific phenomena and processes within or between components. The analysis at this scale can be linked to the component and system scales through the bottom-up approach.

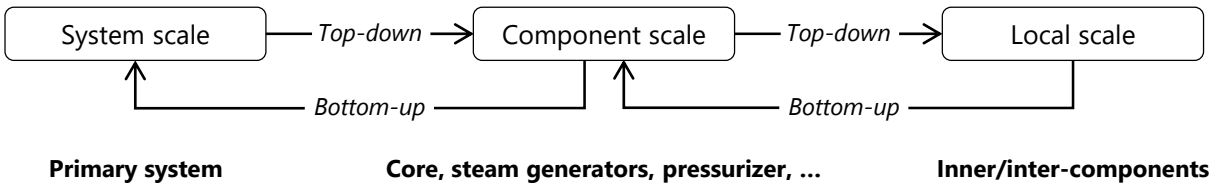

Figure 7.2: The three-scales approach the a posteriori scaling analysis methodology

It should be noted that a scaling analysis is generally performed on at least two scales in conjunction: system/component scale (like in the studies of chapters 5 and 6) or component/local scale. This step is significantly achieved by the availability of calculation codes that can predict both global and local behaviour. However, it is important to keep in mind the uncertainties that may remain in the codes predictions. It is reasonable to expect that a system code will not be able to fully account for local scale behaviour, or that a CFD code will not be suitable for system scale analysis.

Based on the scale(s) selected for the analysis, corresponding **control volume(s)** is/are defined. The volume of the primary system may be sufficient for the establishment of a transient PIRT. However, if one intends to go further and investigate in greater depth, for example, by studying inter-system distortions within specific components or the behaviour of specific processes, it may be necessary to add additional volumes to the study.

The following step is the selection of the **balance equations** that will be applied to the scaling analysis (see Eq. 5.4 and 5.14). They must be chosen to be solved using the available data, such as experimental results or code predictions. Thus, the author suggests using equations similar to those employed in the calculation code of the study. Furthermore, depending on the type of results expected or the type of data available, it may be decided to apply **simplifications and assumptions** to these equations (e.g. Eq. 5.15).

The balance equations are then applied to the previously selected control volume(s) giving the terms contributing to the evolution of the studied variables over the transient (see Eq. 5.5, 5.16, 5.17, 6.1 and 6.2). The equations are then solved according to the type of analysis and expected results:

- Through a **resolution at specific points in time**, such as bifurcating events, trigger points, or points of interest. The FSA method foresees for solving the equations from their maximum estimated values, which often correspond to their initial values in the case of monotonic evolution (refer to Eq. 3.20). However, this resolution remains limited and does not accurately reflect an entire transient. It can however satisfy studies where only experimental results or limited transient data are available (see Figure E.1a).
- Through a **phase averaged resolution**, with averaged calculation during the established phases of the transient allowed by the support of the code predictions (refer to Eq. 3.21 and 5.7). Because the phases have been defined to limit drastic behavioural changes, this resolution is more representative of the evolution of the transient. Nonetheless, this method of solving the equations might be unable to capture a possible brief intense process peak. However, this can be avoided through a qualitative phenomenological analysis. The author highlights that this option developed during the thesis is intended to take advantage of the calculation codes, for which the FSA method was not initially conceived (see Figure E.1b).
- Through **instantaneous resolution**, i.e. at each time step of the code calculation, thus taking full advantage of the code. This would allow each process of the balance equations to be followed in real time and to be fully representative of transient behaviour. However, this type of resolution could make the analysis of the results much more complex than with phase averaged resolution.

The equations being solved and each term quantified according to one of the three options, they must be **normalized**. Two approaches are proposed by the FSA method:

- The ***Time Scaling for Relative Importance of Agents***, which takes into account the impact of each term in the equation according to the most important one (refer to Eq. 3.25 to 3.32).

This procedure yields non-dimensional numbers ranging from -1 to 1, which quantify the relative importance of each process described in the balance equations.

- The ***Time Scaling for an Aggregate Response Time***, which takes into account the impact of each term of the equations according on the global response of all the terms combined (refer to Eq. 3.33 to 3.35). This procedure yields non-dimensional numbers that quantify the time-dependent response rate of each process described in the balance equations.

These two procedures provide **scaling criteria** (the non-dimensional numbers) (see effect metrics Tables from sections 5.2.3 and 6.3.3 to 6.3.7). The author emphasises their use for three purposes:

- The scaling criteria can be compared together and ranked for an independent system. They allow the impact of the processes described by the balance equations to be quantified. The highest scaling criteria will correspond to the most important transient processes and phenomena, while the intermediates ones will correspond to the influent processes. Finally, those with magnitudes close to 0 will correspond to negligible transient processes. A classification for the **scaling criteria hierarchy** is proposed in Figure 5.3.

  As a result of the hierarchy of scaling criteria, a **structured PIRT** that is both qualitative and quantitative can be established. The scaling criteria hierarchy can be established phase by phase using the second option of resolving the equations. They could also be established at each time step of the calculation time using the third option. This could allow a dynamic PIRT to be obtained through transient evolution. It should be noted that the PIRT is directly dependent on the balance equations established beforehand.

- For a counterpart test, the scaling criteria can be compared between several systems. This comparison achieves the **identification and quantification of inter-system distortions**. For example, it can be assessed whether processes are observed to be of similar significance between several reduced-scale facilities or between one/several facilities and a reference full-scale reactor. This amounts to compare and evaluate the PIRT of several systems. This work can also be done dynamically as in the establishment of the PIRT.

- A second **phenomenological analysis** (after the one conducted in the preliminary analysis) should be performed in parallel with the scaling analysis in order to correlate the scaling criteria and their meaning with the complex behaviour of the transients. This analysis provides a thorough understanding of the processes and their impacts on the transient as a whole (as part of the bottom-up approach). It can also help to understand process chain impacts, such as the influence of one process on another or the propagation of distortions from phase to phase (or throughout the transient).

An illustration of the reinterpretation of the FSA method is provided in Figure 7.3. The reader can refer to chapter 6 for more details.

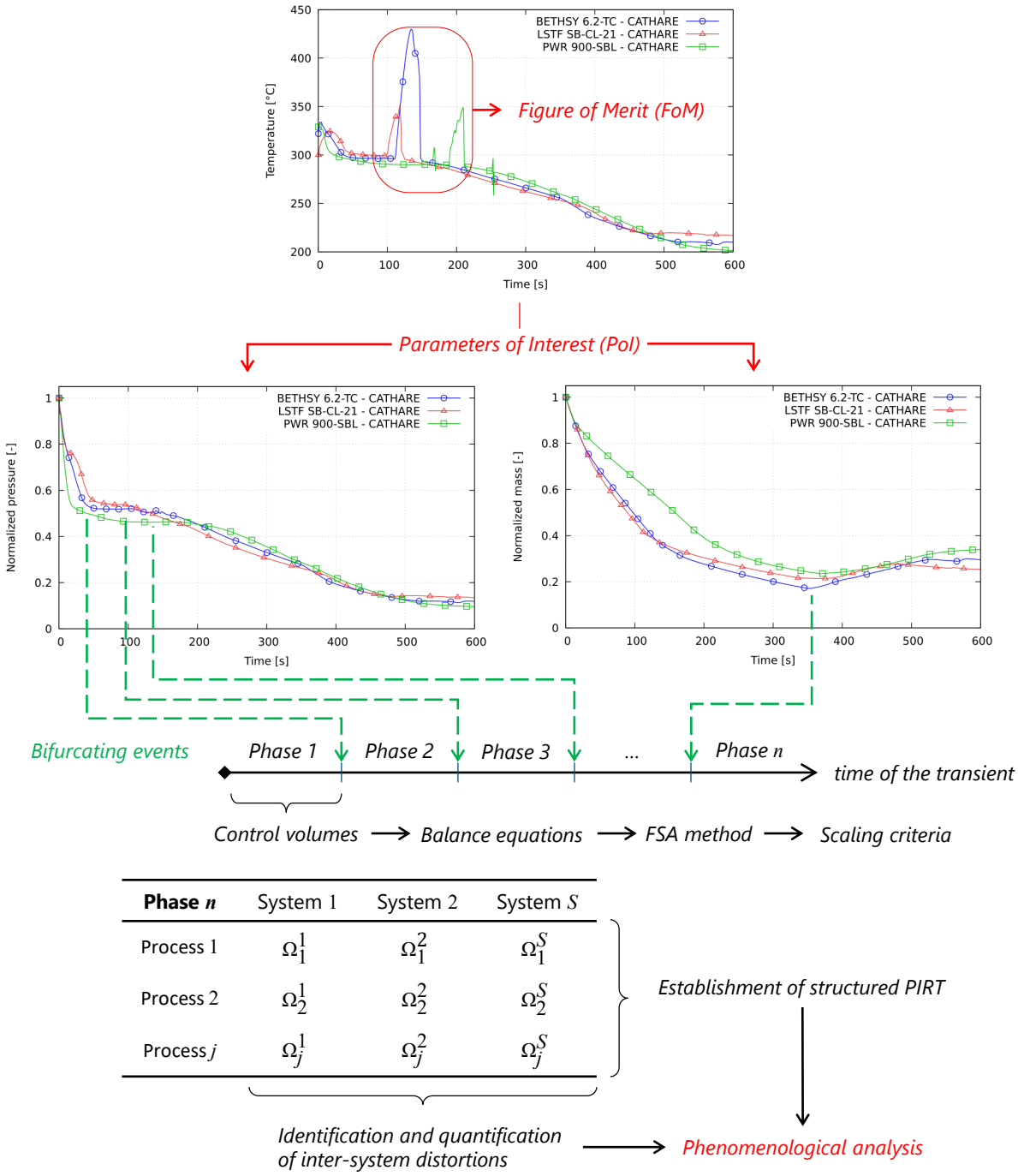

Figure 7.3: Schematic of the reinterpretation of the Fractional Scaling Analysis (FSA) Method of the a posteriori scaling analysis methodology

7.3. Distortions Sources Analysis Supported by the Code

The third part of the methodology is the analysis of the distortions supported by the code predictions. The purpose is to use the scaling analysis results, i.e. the scaling criteria and their analyses, to conclude on the inter-system representativeness (the scale transposition).

Using the results of the counterpart test, the identified discrepancies and the phenomenological

analysis, it is possible to investigate the **source of the inter-system distortions**. Obviously, no single method can identify all sources of distortion with certainty. The analysis of scaling criteria provides the most information about potential sources of distortion. They can at least provide some insight by narrowing the area in which the source of distortion may be found. For example:

- **Sensitivity analyses** of specific process parameters related to the distorted scaling criteria should then be considered. It is also important to explore the parameters known to be sensitive in the literature. Furthermore, sensitivity analyses on specific design parameters should be investigated.
- **Parameter modifications analyses** can be investigated based on the scaling analysis results and the previously identified inter-system design purpose difference. These parameters can be boundary conditions, geometric or ratio differences and may be a source of transient behaviour differences that affect the scale transposition. It is possible to conclude on the influence of the investigated parameters identified by the scaling analysis as the source of distortions by correcting these differences using the code (e.g. in section 6.3.8 and Appendice H).
- Finally, the **code modelling** and/or the code data set should be evaluated (e.g. in the analysis presented in Figure 6.25).

Relying on these analyses, three types of distortions can be defined:

- Distortions caused by **design purpose** made in the construction of a reduced-scale facility in comparison to its full-scale reference reactor. Currently, experimental facilities are designed using general and technical criteria, supported by design scaling methods. Some of these choices can have a significant impact on transient behaviour and thus be the source of these distortions.
- **Scale effects** may occur. They are unrelated to the design purpose of the facilities, but are linked to phenomena or processes that behave differently due to the scale reduction. These scale effects may be related to the facilities reduced volume or surface area (or volume and surface area ratio) compared to the full-scale reactor. They may also be correlated to other thermal-hydraulic parameters (flow rates, heat transfers, thermal inertia, ...).
- Finally, distortions in the scaling criteria could be induced by **code errors**. On the one hand, because the code is not totally validated, but also because some experimentally detected phenomena are difficult to reproduce numerically due to their sensitive nature. This is the case for example with cliff edge effect processes, or phenomena subject to experimental randomness.

The last step of this part of the methodology is achieved by concluding on the **scale transposition** of the counterpart test systems. For example, the representativeness of a reduced-scale facility in comparison to a reference full-scale reactor can be assessed by identifying and quantifying distortions and assessing their impact on transient behaviour. It should be noted that there is no single global criterion of scale transposition between two systems, but rather a set of distortions that provide a detailed overview of a system representativeness in comparison to another.

7.4. Distortions Sources Analysis Supported by Experimental Results

The fourth part of the methodology is the analysis of the distortions supported by **experimental results**. This part is optional and follows the step of comparing the code predictions and the experimental results of the preliminary analysis. It can take place if the code is not sufficiently predictive or accurate of a transient or local phenomenon.

The first step is devoted to the resolution of **simplified balance equations** (i.e. that can be solved using experimental data). As in the reinterpretation of the FSA method part, these equations are applied to a control volume of interest that corresponds to the one containing the phenomenon poorly predicted by the codes. This work is carried out in parallel with the **distorted code predictions**, using the same simplified equations. The two scaling analyses are conducted in order to obtain the scaling criteria.

The purpose is then to compare the scaling criteria of the two analyses - from the experimental results and - from the distorted code predictions, as if it were a counterpart test on two systems. The scaling criteria for the process under consideration are compared between the two systems. This comparison achieves the identification and quantification of inter-system distortions.

Because experimental results are non-distorted by definition, discrepancies from code predictions indicate which processes and models should be corrected. Conversely, scaling criteria for phenomena with no deviations from experimental results could participate in the **justification of the code**.

Once the **correction of the code** is completed, the methodology can be iterated by comparing the experimental results to the corrected code predictions.

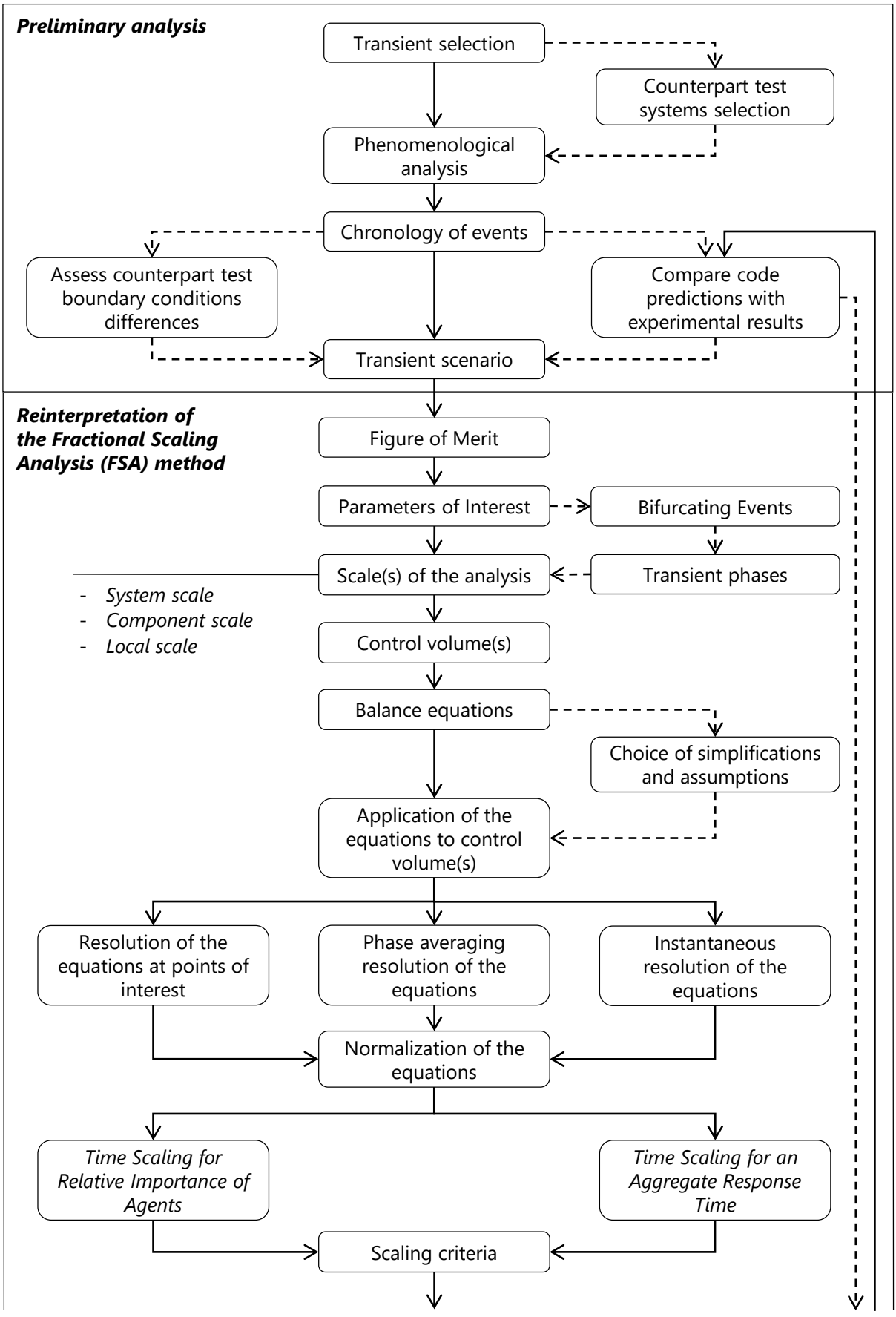

Continued on next page

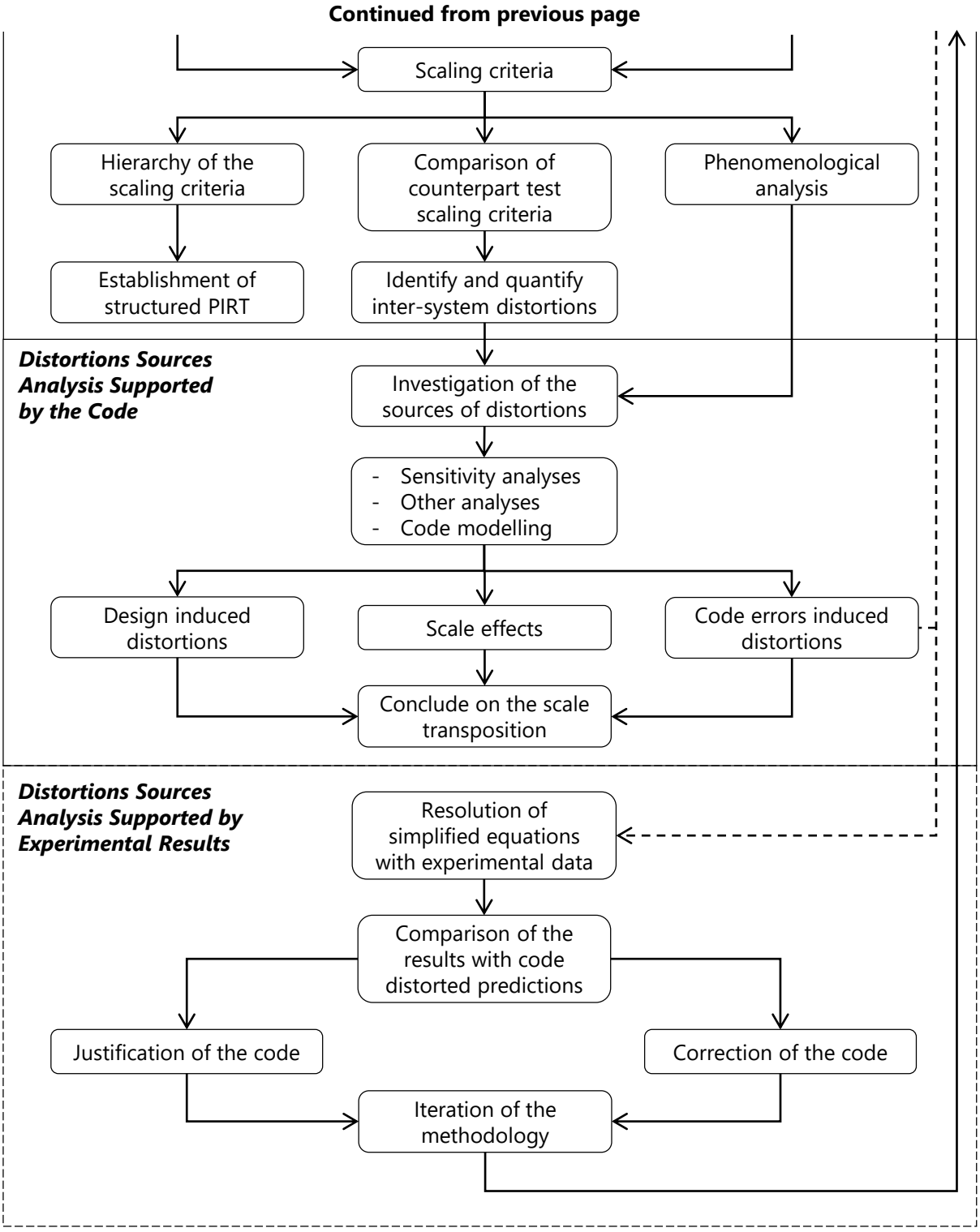

Figure 7.4: The a posteriori scaling analysis methodology

CHAPTER 8

Conclusions

This work is part of the nuclear safety activities encountered in accidental transients studies. Due to the operating complexity and cost of a full-scale experimental reactor, reduced-scale facilities are developed to simulate accidents. The aim of this thesis is to develop an improved scaling analysis methodology for the study of complex nuclear thermal-hydraulic transients and to evaluate the scale transposition between experimental facilities and full-scale reactors.

8.1. Main Results

A verification of the applicability of the Fractional Scaling Analysis (FSA) method (Wulff et al. 2005; Catton et al. 2005; Zuber et al. 2007) to a complex nuclear transient is firstly proposed. For this purpose, the results of this advanced scaling method applied to the 1% SB-LOCA transient performed on the LSTF ROSA 1.2 test (The ROSA-V Group 2003) are compared to results obtained with the Hierarchical Two-Tiered Scaling (H2TS) method (Muñoz-Cobo et al. 2018). The a posteriori scaling analysis is performed on two transient phases of interest: - the Subcooled Blowdown and - the High-Quality Mixture Discharge. Novel mass equation and pressure equation expressed with Volume Rate of Change (VRC) are established for the primary system and for the pressurizer control volumes assuming a saturated steam-water mixture. The CATHARE system code (Emonot et al. 2011) predictions is used for the first time to evaluate terms of these equations and to establish scaling criteria.

The comparative study showed consistency between the FSA method and the H2TS method results. This work demonstrated the applicability of an advanced scaling method with the support of a mature system code. The novel treatment of equations using averaged quantities during a transient phase duration rather than estimates at phase boundaries provides more precision in the scaling criteria evaluation. It has also been demonstrated that using both scaling methods and system codes can also support the improvement of the code modelling.

The capability of the FSA to identify and quantify distortions at the system/component scale is then further investigated. For this purpose, an a posteriori phenomenology and scaling analysis of a 6% SB-LOCA transient counterpart test is revisited (Kumamaru et al. 1992; D'Auria et al. 1992). A new application of the FSA to the BETHSY 6.2-TC and LSTF SB-CL-21 tests, as well as to a PWR simulation is conducted using CATHARE code simulations. The study is conducted on five phases of the transient: - the Subcooled Blowdown, - the Natural Circulation, - the Reflux Condenser Mode, - the High-Quality Mixture Discharge and - the Reactor Refilling. Primary mass equation and mean pressure equations are established for either the primary systems or only the pressurizer control volumes of the counterpart test. Each term of the pressure equation corresponds to a Volume Rate of Change (VRC).

The scaling analysis is performed using these mass and pressure equations for each transient phase, the terms of the equations being evaluated from the CATHARE code predictions. The study identified and quantified discrepancies between the facilities and the PWR results. Improvements to the methodology were made through this study. The formulation of a general pressure equation without saturation hypothesis allowed a more detailed and more reliable analysis. This application defines a detailed hierarchy of the influence of the phenomena and processes occurring during the different phases of the transient. In order to properly analyse the scaling criteria, the interest of performing a phenomenological analysis in parallel with the scaling analyses is demonstrated.

8.2. New Insights and Opportunities Highlighted

The a posteriori scaling analysis methodology is developed throughout the thesis. Clarifications of the potentialities of scaling methods are provided by a state of the art of the existing methods, as well as studies and applications. Improvements, conclusions and limitations are drawn and guidelines in how addressing the scaling issue are established. Furthermore, the process of reinterpreting an initial methodology allowed to answer several concerns raised by the state of the art.

- **Scaling analyses help to understand the phenomenology of transients with the use of advanced scaling methods.** The study of complex phenomena occurring within transients such as LOCA, can be supported by the application of these methods. It has been demonstrated that phenomenological analyses performed prior to scaling analyses can contribute in the determination of scaling method key parameters. The phenomenological analysis thus justifies the definition of Figures of Merit and Parameters of Interest and the study of their evolution along the transient.

- **The division of transients into successive phases allows a structured study of their behaviour.** It is therefore essential to identify the bifurcating events, which change the status of the system.

- **Top-down and bottom-up approaches bring depth, consistency and structure to analyse important phenomena identified by scaling analyses.** The applications carried out, as well as the methodology developed in this manuscript, have placed a strong emphasis on the steps that should be followed in order to carry out efficient scaling analyses. These approaches provided by advanced scaling methods should be considered, especially for multi-scale analyses.

- **The concept of normalization of the scaling criteria, based on the establishment of balance equations, is a significant contribution of advanced scaling methods, as in the FSA method.** As demonstrated in the studies of the manuscript, quantifying the relative magnitude of processes allows to consider their importance in terms of causality. When combined with the bottom-up approach, this allows for an understandable and traceable hierarchy of the contributing processes. The quantitative evaluation of each phenomenon provides the establishment of a structured PIRT.

- **Modifications and improvements have been made to the FSA method through reinterpretations and the development of the methodology presented in this manuscript.** The applications carried out illustrate the intention of the designers of the advanced scaling methods to make them flexible and adaptable tools. The parameters of the scaling analyses can be adapted to meet specific requirements, such as by selecting and formulating the balance equations and assumptions, applying to different physics of transients

(i.e. through different phases), and identifying the systems and components (i.e. through the control volumes).

- **The a posteriori scaling analysis applied to counterpart tests allows the identification of differences due to different reactor designs.** The scaling analysis based on system code simulations can help identifying differences in ITF counterpart tests due to differences in the design of the reference reactors and those due to distortions of IET with respect to their reference reactor.

- **Advanced scaling methods can be used with the support of system codes that have reached a reasonable level of maturity and confidence.** The CATHARE code is used to conduct the scaling analyses, thanks to the confidence in the predictions made at the system/component scale. When weaknesses of the system code capabilities are identified for some processes, they must be used with caution for scaling analysis of these processes (e.g. asymmetrical loop seal plugging and clearing are very difficult to predict).

- **Using a mature system code allows estimating more precisely the terms of equations of Parameters of Interest (e.g. the primary pressure equation) and can establish scaling criteria in a very detailed manner.** The basic scaling methods such as H2TS or FSA estimate only an order of magnitude of each term of the equations based on dimensional analysis performed for each phase of the transient. Using code simulations may provide an evaluation of the time evolution of these terms, which provides a much better evaluation of scaling distortions required for the establishment of scaling criteria.

- **The capability to follow the value of each term of the Parameters of Interest equation along time helps in identifying bifurcating events and the processes which control them** (e.g. when primary pressure crosses secondary pressure). The interpretation of the meaning of the scaling criteria is facilitated by the support of the code, thanks to a detailed phenomenological analysis performed in parallel of the scaling analyses. This make a link between the impact of the phenomena and processes observed as dominant/influent and the behaviour of the transients through the different phases studied. Thanks to the code predictions, these phases are defined in a precise and justifiable manner.

- Beyond the support of the code to conduct scaling analyses, **it is possible to use these results combined with sensitivity analyses and phenomenological analyses to support and propose improvements to the code modelling.**

Some limitations to scaling analyses and advanced methods for the study of nuclear transient have been identified.

- **Expert judgement is still required when analysing scaling criteria for the study of complex phenomena within nuclear transients.** This is due to the variety of thermal-hydraulic phenomena and to the multi-physics aspects encountered in reactor transients. Furthermore, although successive phases are identified along the transients, some distortions may be propagated from one to another, making the analysis of scaling criteria more difficult.

- **The code must be fully validated on representative experiments to perform reliable scaling analyses, and the scaling of representative experiments is necessary for code validation** This shows that the processes of scaling experiments and code validation are

somewhat iterative. One can perform a simple scaling without using codes, then design experiments, then revisit the scaling analysis using experimental results, then perform the code validation. When the code fails to predict a specific phenomenon, the modelling must be improved before using it for scaling analysis. Finally one can perform an a posteriori scaling analysis with the code for more accurate and more reliable identification and quantification of distortions.

CHAPTER 9

Perspectives

The methodology developed in this thesis has demonstrated many promising potentials, especially through applications and analyses of complex transients. Nonetheless, the author indicates that the methodology will be improved in the future.

9.1. Further Methodology Improvements

The capability of the Fractional Scaling Analysis (FSA) method to be applied to a full 6% SB-LOCA transient was demonstrated in chapter 6, through a scaling analysis performed on a counterpart test of two facilities and a full-scale PWR. This study showed that the FSA method could identify and quantify distortions at the system/component level for a complex nuclear transient while achieving consistent results.

A future objective will be the investigation of the FSA method capability to identify and quantify distortions at the component/local scale. For this purpose, a scaling analysis will be performed on the same counterpart test, with a focus on the Loop Seal Plugging (LSP) and Loop Seal Clearing (LSC) phenomena. These phenomena have been identified as key processes of SB-LOCA transients, but their behaviour remain unclear. This study will therefore aim to better understand these processes and their associated parameters especially through a comparison between:

- Results based on code predictions, which badly predicts the LSP phenomenon.
- Results using only experimental data, performed to complete this work and the development of the methodology.
- Sensitivity analyses on parameters suspected to be responsible for behaviour change of the LSP and LSC phenomena.

Future work will lead to the establishment of a momentum conservation equation to be applied to the FSA method. This will be added to the mass and pressure by volume change effect metrics. Thus, the analysis of transient processes and phenomenology will be more exhaustive, accounting for volume and surface forces such as pressure, gravity, and viscous forces.

In addition, the methodology will have to be applied in other studies, such as various counterpart tests, other types of transients, and different phenomenologies. The robustness of the methodology can thus be confirmed and improved.

Within the CATHARE code, the development of a post-processing module for the scaling analysis methodology should be of interest. Once the user would have specified the desired scaling analysis

parameters, this module should allow for the automation of the application of the methodology, in particular concerning the calculation of the effect metrics. For example, the user could have to choose the scale and control volumes on which the analysis should be performed, the type of equations to be used and whether or not to divide the transient into phases. The application of the methodology would always require some expert judgement, particularly in the analysis of the results and understanding of the phenomenology of the transients, as well as the investigation of distortions sources. However, the field of addressing scaling issues could be popularised even further thanks to this module.

9.2. A Posteriori Methodology in Support of the A Priori ITF Design

As explained in section 3.3.1, experimental facilities are currently designed on the basis of technical and general criteria and supported by design scaling methods. These methods have been shown to have limitations and weaknesses due the lack of link between deep transient phenomenology and design criteria.

Furthermore, the nuclear industry has now greater confidence in the predictions of the calculation codes than it had when these design methods were conceived. Added to the non-negligible cost of building and operating ITF, it appears compelling to consider any assistance that could help to reduce scaling issues. It is then proposed here to consider the a posteriori methodology developed during this thesis in support of the a priori ITF design phase.

9.2.1. From Scratch Design

The procedure proposed in Figure 9.1 could be considered from the theoretical standpoint that it would be necessary to design an ITF from scratch. Depending on the initial expectations in terms of cost-representativeness of the ITF results in comparison to the full-scale reactor, first general technical criteria could be established. A scaling method would then be used to develop and model a hypothetical ITF code dataset and its considered IET. The scaling method used could then be a design method (see section 3.3.1) or an advanced method (see section 3.3.2), as it was done with the H2TS. Because the design of the ITF reference reactor is initially known, its code dataset is also developed in parallel.

The a posteriori scaling analysis methodology (see section 7) would be applied to the counterpart test of the ITF and its reference reactor, through the predictions of the calculation code. As previously stated, complete trust in the code would be assumed here since there would be no experimental results. The methodology would provides results on the ITF representativeness in comparison to the full-scale reactor by identifying and quantifying distortions.

The satisfaction on the scale transposition could then be determined by evaluating these distortions. If the results are not satisfactory (i.e., the distortions are not small enough), either the general criteria or the cost-representativeness expectations must be revised. This procedure could thus be iterated until design parameters with sufficiently negligible distortions are validated.

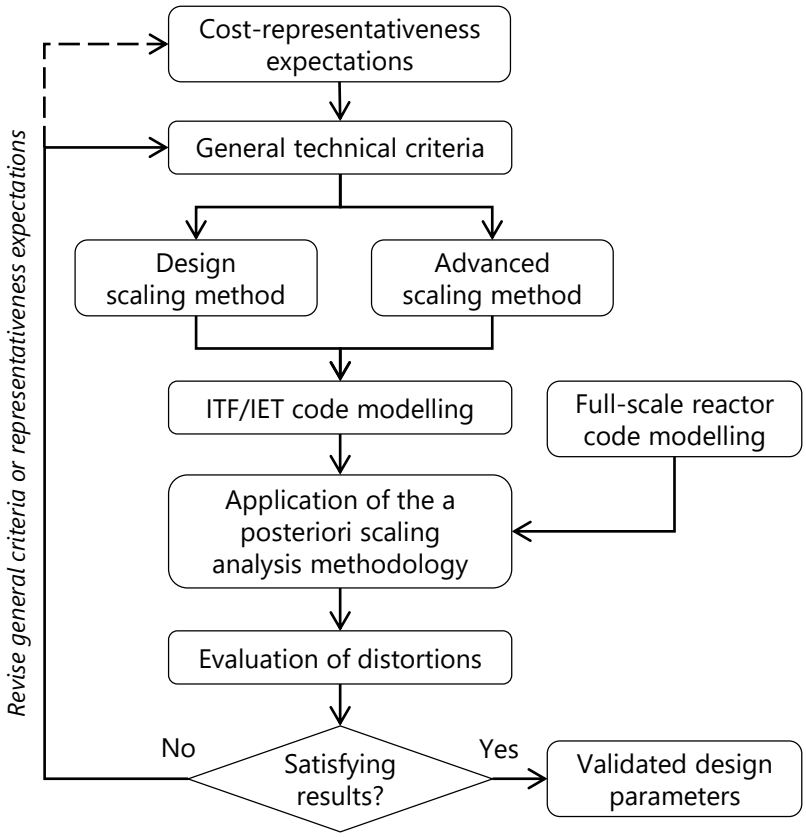

Figure 9.1: Proposed procedure for ITF design using scaling analyses and codes predictions

9.2.2. From Suggested Designs

When designing an ITF, a situation that could be envisaged is the competition between various designs suggested by several research teams. It would then be necessary to decide which design to keep. The procedure proposed in Figure 9.2 and derived from the one in Figure 9.1 would yield concrete results on the most suitable design.

The a posteriori scaling analysis methodology (see section 7) would be applied to the ITF in parallel and to the reference reactor, through the predictions of the calculation code. The distortions between the suggested ITF and the full-scale reactor would then be evaluated in order to assess the scale transposition of each design. The design with the least distortion could then be selected.

As with the procedure in Figure 9.1, it could be considered to optimize the design of the ITF by iterating the application of the methodology and revising the design criteria if necessary.

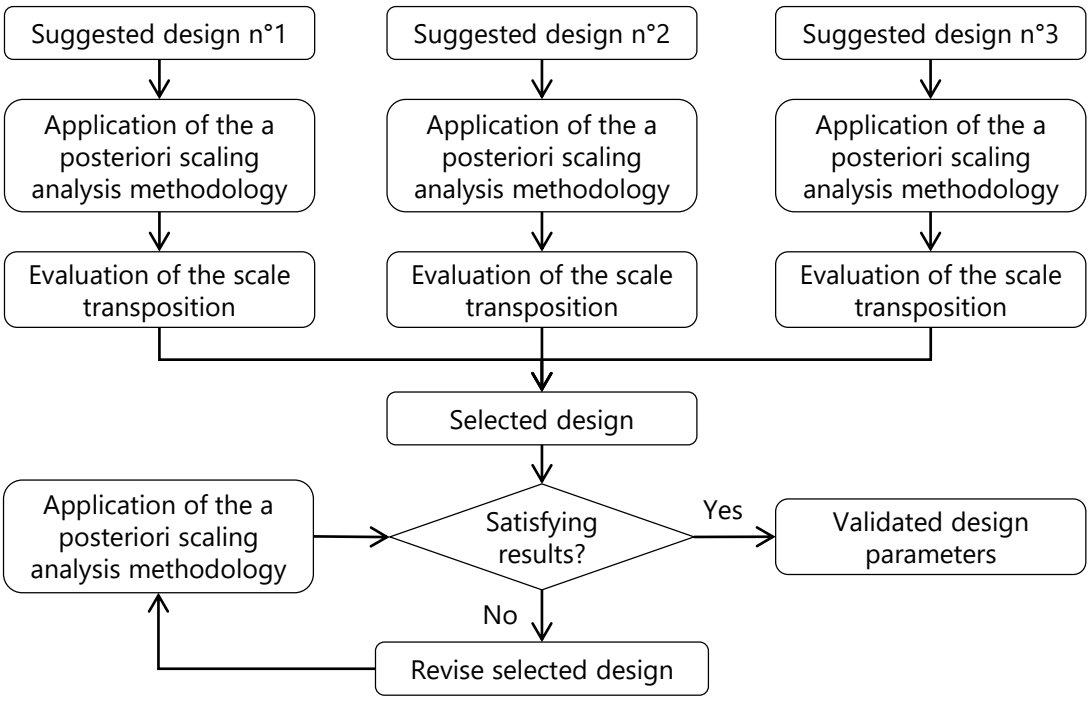

Figure 9.2: Proposed iterative sequential procedure for ITF design using scaling analyses and codes predictions

The advantage of these two procedures for the a priori design of ITF using the a posteriori scaling analysis methodology is that a test counterpart of several experimental reactors is not required. Prior to the construction and operation of ITF, the support of calculation codes and dataset modelling would allow for the identification of inter-system distortions.

Obviously, the uncertainty in the predictions of the codes for the evaluation of a phenomenology for which no experimental results exist a priori remains the perspective's limitation. As a result, no code V&V work can be undertaken. However, it should be noted that these proposed procedures would be, at best, a tool to quantitatively deciding between several suggested designs and, at worst, an additional validation to the methods already used for the design of ITF.

Finally, as illustrated in Figure 9.3 this demonstrates the interest in the effort to improve the calculation codes in order to perhaps allow for the optimization of experiments supported by scaling analyses in the future. Thus, the developed methodology could be used to define tests matrices that would assess the code limits and representativeness. The parameters of interest could then be verified and corrected when possible.

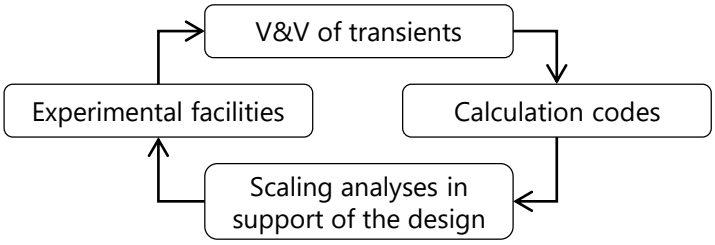

Figure 9.3: Interest in the effort to improve calculation codes for the scaling analyses supported design

References

[1] A. Achilli, C. Congiu, R. Ferri, F. Bianchi, P. Meloni, D. Grgić, and M. Dzodzo. "SPES3 Facility RELAP5 Sensitivity Analyses on the Containment System for Design Review". In: Science and Technology of Nuclear Installations 2012 (2012), pp. 1–19. ISSN: 1687-6075, 1687-6083. DOI: 10.1155/2012/173637.

[2] C. Addabbo and A. Annunziato. "The LOBI Integral System Test Facility Experimental Program". In: Journal of Nuclear Science and Technology (2012). DOI: 10.1155/2012/238019.

[3] ASN and IRNS. Qualification des outils de calcul scientifique utilisés dans la démonstration de sûreté nucléaire – 1re barrière. Guide n°28. 2017.

[4] ASN and IRSN. Guides de l'ASN. 2022. URL: https://www.asn.fr/l-asn-reglemente/guides-de-l-asn.

[5] C.-H. Bachelet. "Status of the Evaluation of the VINCI Rocket Engine Oxygen Chill-down with COMETE Thermal-Hydraulic Software". In: 69th International Astronautical Congress. Bremen, Germany, 2018.

[6] S. M. Bajorek, N. Petkov, K. Ohkawa, R. M. Kemper, and A. P. Ginsberg. "Realistic Small- and Intermediate-Break Loss-of-Coolant Accident Analysis Using WCOBRA/TRAC". In: Nuclear Technology 136.1 (Oct. 2001), pp. 50–62. ISSN: 0029-5450, 1943-7471. DOI: 10.13182/NT01-A3228.

[7] C. Berna, J. L. Muñoz-Cobo, and A. Escrivá. "Application of Fractional Scaling Analysis to a SBLOCA between the LSTF Facility and a Commercial Three Loop PWR Reactor". In: NURETH-19 1 (2022), p. 16. ISSN: 1886-4996, 1134-2196. DOI: 10.4995/ia.2014.3293.

[8] D. Bestion. "The Physical Closure Laws in the CATHARE Code". In: Nuclear Engineering and Design 124.3 (Dec. 1990), pp. 229–245. ISSN: 00295493. DOI: 10.1016/0029-5493(90)90294-8.

[9] D. Bestion. "About Phenomena Identification in a PIRT". In: NURETH-18. Portland, USA, 2020.

[10] D. Bestion, F. Barré, and B. Faydide. "Methodology, Status and Plans for Development and Assessment of CATHARE Code". In: NUREG/CP-0159, OECD-CSNI. Annapolis, USA, 1999.

[11] D. Bestion, F. D'Auria, P. Lien, and H. Nakamura. A State-of-the-Art Report on Scaling in System Thermal Hydraulics Applications to Nuclear Reactor Safety and Design. OECD/NEA/CSNI/R(2016)14, 2017.

[12] D. Bestion and F. D'Auria. "Identification of Thermalhydraulic Phenomena for PWR Transient Analysis and Simulation". In: NURETH-19 (2022), p. 16.

[13] D. Bestion, D. Lucas, H. Anglart, B. Niceno, and L. Vyskocil. "Multi-Scale Thermalhydraulic Analyses Performed in NURESIM and NURISP Projects". In: Volume 4: Codes, Standards, Licensing, and Regulatory Issues; Fuel Cycle, Radioactive Waste Management and Decommissioning; Computational Fluid Dynamics (CFD) and Coupled Codes; Instrumentation and Co. 2012 20th International Conference on Nuclear Engineering and the ASME 2012 Power Conference. Anaheim, California, USA: ASME, July 30, 2012, p. 581. ISBN: 978-0-7918-4498-4. DOI: 10.1115/ICONE20-POWER2012-54891.

[14] W. A. Carbiener and R. A. Cudnik. "Similitude Considerations for Modeling Nuclear Reactor Blowdown". In: Transactions of the American Nuclear Society 12 (1969).

[15] I. Catton, U. S. Rohatgi, W. Wulff, and N. Zuber. "Application of Fractional Scaling Analysis (FSA) to Loss of Coolant Accidents (LOCA) - Part 3. Component Level Scaling for Peak Clad Temperature". In: NURETH-11. Vol. 237. 2005, pp. 1593–1607. DOI: 10.1016/j.nucengdes.2007.01.017.

[16] CEA. CATHARE Thermal-hydraulic Simulation of Multiphase Flow Dynamics. 2021. URL: https://cathare.cea.fr/.

[17] CEA. CATHARE VV&Q. 2021. URL: https://cathare.cea.fr/Pages/CATHARE/VV_and_Q.aspx.

[18] K.-Y. Choi, K.-H. Kang, T.-S. Kwon, Y.-S. Kim, J.-R. Kim, S.-K. Moon, Y.-S. Park, H.-S. Park, B.-U. Bae, C.-H. Song, S.-J. Yi, S. Cho, and B.-J. Yun. Scaling Analysis Report of the ATLAS Facility. Korea Atomic Energy Research Institute, 2014.

[19] A. Ciechocki, S. Carnevali, D. Bestion, and L. Rossi. "Application of the FSA Scaling Method to the LSTF ROSA 1.2 Test and Comparison to an Application of the H2TS Method". In: NURETH-19. Bruxelles, Belgium, 2022. URL: hal-cea.archives-ouvertes.fr/cea-03818077.

[20] A. Ciechocki, S. Carnevali, D. Bestion, and L. Rossi. "Scaling Analyses of a SB-LOCA Counterpart Test between BETHSY and LSTF Facilities and a Three Loops PWR". In: Nuclear Engineering and Design 400 (2022). ISSN: 00295493. DOI: 10.1016/j.nucengdes.2022.112051.

[21] I. Clifford, O. Zerkak, A. Pautz, H. Yao, and J. Freixa. "System Code Validation Series Based on a Consistent Plant Nodalisation of the ROSA/LSTF Integral Test Facility Using TRACE v5.0 Patch 4". In: NUTHOS-11. Gyeongju, Korea, 2016.

[22] J. Couturier. Éléments de sûreté nucléaire: les réacteurs à eau sous pression. In collab. with IRNS. Série Éléments de sûreté nucléaire, de radioprotection et de sécurité. Les Ulis: EDP sciences, 2020. ISBN: 978-2-7598-2455-7.

[23] W. E. Cummins, M. M. Corletti, and T. L. Schulz. "Westinghouse AP1000 Advanced Passive Plant". In: Nuclear Engineering and Design 236.14-16 (2003), pp. 1547–1557. ISSN: 00295493. DOI: 10.1016/j.nucengdes.2006.03.049.

[24] F. D'Auria, N. Aksan, D. Bestion, G. M. Galassi, H. Glaeser, Y. Hassan, J. J. Jeong, P. L. Kirillov, C. Morel, H. Ninokata, F. Reventós, U. S. Rohatgi, R. R. Schultz, and K. Umminger. Thermal Hydraulics of Water Cooled Nuclear Reactors. 2017.

[25] F. D'Auria, R. Ferri, G. M. Galassi, and F. Sugaroni. "Evaluation of the Data Base from the Small Break LOCA Counterpart Tests Performed in LOBI, SPES, BETHSY and LSTF Facilities". In: Dipartimento Costruzioni Meccaniche E Nucleari, NT 193 (92) Rev.1 Università Di Pisa Applications of Sys. Th. Codes to Nuclear Reactor Design and Accident Analysis (1992), p. 250. DOI: 10.13140/RG.2.2.32181.22241.

[26] F. D'Auria and G. M. Galassi. "Code Validation and Uncertainties in System Thermalhydraulics". In: Progress in Nuclear Energy 33 (1998), pp. 175–216. ISSN: 0149-1970. DOI: 10.1016/S0149-1970(97)00097-8.

[27] F. D'Auria, W. Giznnotti, and A. Piagentini. "Consideration of Bifurcations within the Internal Assessment of Uncertainty". In: ICONE8 (2000).

[28] F. D'Auria, C. Camargo, and O. Mazzantini. "The Best Estimate Plus Uncertainty (BEPU) Approach in Licensing of Current Nuclear Reactors". In: Nuclear Engineering and Design 248 (July 2012), pp. 317–328. ISSN: 00295493. DOI: 10.1016/j.nucengdes.2012.04.002.

[29] F. D'Auria and G. M. Galassi. "Scaling in Nuclear Reactor System Thermal-Hydraulics". In: Nuclear Engineering and Design 240.10 (Oct. 2010), pp. 3267–3293. ISSN: 00295493. DOI: 10.1016/j.nucengdes.2010.06.010.

[30] W. J. M. de Kruijf, K. C. J. Ketelaar, G. Avakian, P. Gubernatis, D. Caruge, A. Manera, T. H. J. J Van der Hagen, G. Yadigaroglu, G. Dominicus, U. Rohde, H.-M. Prasser, F. Castrillo, M. Huggenberger, D. Hennig, J. L. Munoz-Cobo, and C. Aguirre. "Planned Experimental Studies on Natural-Circulation and Stability Performance of Boiling Water Reactors in Four Experimental Facilities and First Results (NACUSP)". In: Nuclear Engineering and Design 221.1-3 (Apr. 2003), pp. 241–250. ISSN: 00295493. DOI: 10.1016/S0029-5493(02)00338-2.

[31] J.-M. Delhaye. Thermohydraulique des réacteurs nucléaires. Génie atomique. Les Ulis: EDP sciences, 2008. ISBN: 978-2-86883-823-0.

[32] R. Deruaz and J. C. Megnln. The French Integral Loop, a Joint CEA-EDF-Framatome Project. Gaithersburg, USA: 10th Water Reactor Safety Research Information Meeting, 1982.

[33] M. B. Dzodzo. "EMDAP – Method for Scaling Analysis". In: (2009). DOI: 10.13140/RG.2.2.24313.98402.

[34] M. B. Dzodzo, F. Oriolo, W. Ambrosini, M. Ricotti, D. Grgic, R. Ferri, A. Achilli, F. Bianchi, and P. Meloni. "Application of Fractional Scaling Analysis for Development and Design of Integral Effects Test Facility". In: Journal of Nuclear Engineering and Radiation Science 5.4 (2019). ISSN: 2332-8983, 2332-8975. DOI: 10.1115/1.4042496.

[35] P. Emonot, A. Souyri, J. L. Gandrille, and F. Barré. "CATHARE-3: A New System Code for Thermal-Hydraulics in the Context of the NEPTUNE Project". In: Nuclear Engineering and Design (May 2011), S0029549311004018. ISSN: 00295493. DOI: 10.1016/j.nucengdes.2011.04.049.

[36] Equipe BETHSY. BETHSY General Description. Centre d'études nucléaires de Grenoble, 1990, p. 73.

[37] R. P. Forslund and W. M. Rohsenow. "Dispersed Flow Film Boiling". In: Journal of Heat Transfer (1968), pp. 399–407. DOI: 10.1115/1.3597531.

[38] C. Frepoli and J. P. Yurko. "Experimental Test Facility Data Synthesis with the Dynamical System Scaling Methodology". In: NURETH-16. 2015.

[39] A. Guelfi, D. Bestion, M. Boucker, P. Boudier, P. Fillion, M. Grandotto, J.-M. Hérard, E. Hervieu, and P. Péturaud. "NEPTUNE: A New Software Platform for Advanced Nuclear Thermal Hydraulics". In: Nuclear Science and Engineering 156.3 (July 2007), pp. 281–324. ISSN: 0029-5639, 1943-748X. DOI: 10.13182/NSE05-98.

[40] T Habib, C Koksal, T Moskal, G Rush, and J Gloudemans. Multiloop Integral System Test (MIST): MIST Facility Functional Specification. NUREG/CR-5670, EPRI-NP–7165, 5681659. Apr. 1, 1991, NUREG/CR–5670, EPRI-NP–7165, 5681659. DOI: 10.2172/5681659.

[41] T. Höhne, E. Krepper, and U. Rohde. "Application of CFD Codes in Nuclear Reactor Safety Analysis". In: Science and Technology of Nuclear Installations 2010 (2010), pp. 1–8. ISSN: 1687-6075, 1687-6083. DOI: 10.1155/2010/198758.

[42] M. Hwang, S. K. Sim, K.-Y. Choi, and K. W. Lee. "Investigation of the Loop Seal Clearing Phenomena for the ATLAS DVI Line and Cold Leg SBLOCA Tests Using MARS-KS and RELAP5/MOD3.3". In: Nuclear Regulatory Commission (2019).

[43] IAEA. World Electricity Final Consumption by Sector, 1974-2019. 2021. URL: https://www.iea.org/data-and-statistics/charts/world-electricity-final-consumption-by-sector-1974-2019.

[44] IAEA. World Electricity Generation Mix by Fuel, 1971-2019. 2021. URL: https://www.iea.org/data-and-statistics/charts/world-electricity-generation-mix-by-fuel-1971-2019.

[45] IAEA. In-Operation & Long-Term Shutdown Reactors. 2022. URL: https://pris.iaea.org/PRIS/WorldStatistics/OperationalReactorsByCountry.aspx.

[46] IAEA. In-Operation & Long-Term Shutdown Reactors. 2022. URL: https://pris.iaea.org/PRIS/WorldStatistics/OperationalReactorsByType.aspx.

[47] IAEA and AEN/NEA. The International Nuclear and Radiological Event Scale (INES). Vienna, Austria, 2009. ISBN: IAEA–INES–2009.

[48] M. Ishii. Thermo-Fluid Dynamic Theory of Two-Phase Flow. Eyrolles. 1975.

[49] M. Ishii and I. Kataoka. Similarity Analysis and Scaling Criteria for LWR's under Single-Phase and Two-Phase Natural Circulation. NUREG/CR–3267, ANL–83-32, 6312011. Nuclear Regulatory Commission, Mar. 1, 1983, NUREG/CR–3267, ANL–83-32, 6312011. DOI: 10.2172/6312011.

[50] M. Ishii, S.T. Ravankar, and R. Dowlati. Scientific Design of Purdue University Multi-Dimensional Integral Test Assembly (PUMA) for GE SBWR. NUREG/CR–6309, PU-NE–94/1, 220555. Apr. 1, 1996. DOI: 10.2172/220555.

[51] M. Ishii, S. T. Revankar, T. Leonardi, R. Dowlati, M.L. Bertodano, I. Babelli, W. Wang, H. Pokharna, V. H. Ransom, R. Viskanta, and J. T. Han. "The Three-Level Scaling Approach with Application to the Purdue University Multi-Dimensional Integral Test Assembly (PUMA)". In: Nuclear Engineering and Design 186.1-2 (Nov. 1998), pp. 177–211. ISSN: 00295493. DOI: 10.1016/S0029-5493(98)00222-2.

[52] O.-P. Kauppinen, V. Kouhia, V. Riikonen, J. Hyvärinen, and H. Sjövall. "Computer Analyses on Loop Seal Clearing Experiment at PWR PACTEL". In: Annals of Nuclear Energy 85 (Nov. 2015), pp. 47–57. ISSN: 03064549. DOI: 10.1016/j.anucene.2015.04.036.

[53] Y. S. Kim, K. Y. Choi, H. S. Park, S. Cho, B. D. Kim, N. H. Choi, and W. P. Baek. "Commissioning of the ATLAS Thermal-Hydraulic Integral Test Facility". In: Annals of Nuclear Energy 35 (2008).

[54] Y.-S. Kim and S. Cho. "An Experimental Investigation of Loop Seal Clearings in SBLOCA Tests". In: Annals of Nuclear Energy 63 (Jan. 2014), pp. 721–730. ISSN: 03064549. DOI: 10.1016/j.anucene.2013.09.014.

[55] G. Kocamustafaogullari and M. Ishii. "Scaling Criteria for Two-Phase Flow Natural- and Forced-Convection Loop and Their Application to Conceptual 2 x 4 Simulation-Loop Design. [PWR]". In: (1983).

[56] Y. Kukita, J. Katayama, H. Nakamura, and K. Tasaka. "Loop Seal Clearing and Refilling During a PWR Small-Break LOCA". In: Nuclear Engineering and Design (1989), p. 10.

[57] H. Kumamaru, G. Briday, Y. Kukita, D. Juhel, and R. Deruaz. "LSTF and BETHSY Counterpart Tests on PWR Small Break LOCA". In: ANS Proc. of the 1992 National Heat Transfer Conf. 1992, pp. 285–292.

[58] T. K. Larson, J. L. Anderson, and D. J. Shimeck. Scaling Criteria and an Assessment of Semiscale MOD-3 Scaling for Small Break LOCA Transients. Idaho Falls, USA: EGG/SEMI 5121, 1980.

[59] N. Lee. "Discussions on Loop Seal Behavior during Cold Leg Small Break LOCAs of a PWR". In: Nuclear Engineering and Design 99 (Feb. 1987), pp. 453–458. ISSN: 00295493. DOI: 10.1016/0029-5493(87)90141-5.

[60] J. Liao. "System Scaling Analysis for Modeling Small Break LOCA Using the FULL SPECTRUM LOCA Evaluation Model". In: Annals of Nuclear Energy 87 (Jan. 2016), pp. 443–453. ISSN: 03064549. DOI: 10.1016/j.anucene.2015.09.014.

[61] T.-J. Liu and C.-H. Lee. "Adequacy of Power-to-Mass Scaling in Simulating PWR Incident Transient for Reduced-Height, Reduced-Pressure and Full-Height, Full-Pressure Integral System Test Facilities". In: Nuclear Science and Engineering 146.3 (Mar. 2004), pp. 274–290. ISSN: 0029-5639, 1943-748X. DOI: 10.13182/NSE04-A2410.

[62] T.-J. Liu, C.-H. Lee, and C.-Y. Chang. "Power-Operated Relief Valve Stuck-Open Accident and Recovery Scenarios in the Institute of Nuclear Energy Research Integral System Test Facility". In: Nuclear Engineering and Design 186 (1998). DOI: 10.1016/S0029-5493(98)00221-0.

[63] T.-J. Liu, C.-H. Lee, and Y.-S. Way. "IIST and LSTF Counterpart Test on PWR Station Blackout Transient". In: Nuclear Engineering and Design 167 (1997).

[64] Z. Liu, T. Bai, C. Peng, H. Bao, and J. Lu. "A Method of Scaling Distortion Assessment Based on Dynamic Time Warping". In: Annals of Nuclear Energy 177 (Nov. 2022), p. 109304. ISSN: 03064549. DOI: 10.1016/j.anucene.2022.109304.

[65] M. Lorduy-Alós, S. Gallardo, and G. Verdú. Scaling Analysis of an IBLOCA Counterpart Test between the ATLAS and LSTF Facilities. Sept. 2020, p. 103460. URL: https://linkinghub.elsevier.com/retrieve/pii/S0149197020302122 (visited on 09/29/2020).

[66] K. V. Moore and W. H. Rettig. RELAP2 – a Digital Program for Reactor Blowdown and Power Excursion Analysis. Idaho Falls, USA, 1968.

[67] J. L. Muñoz-Cobo, C. Berna, and A. Escrivá. "Top-down Scaling Methodology from the LSTF Facility to a Three Loop PWR Plant Applied to a SBLOCA Event – The ROSA 1.2 Test". In: Nuclear Engineering and Design 327 (Feb. 2018), pp. 248–273. ISSN: 00295493. DOI: 10.1016/j.nucengdes.2017.12.011.

[68] A. N. Nahavandi, F. S. Castellana, and E. N. Moradkhanian. "Scaling Laws for Modeling Nuclear Reactor Systems". In: Nuclear Science and Engineering 72.1 (Oct. 1979), pp. 75–83. ISSN: 0029-5639, 1943-748X. DOI: 10.13182/NSE79-A19310.

[69] NEA. TMI-2 Analysis Exercise Final Report. OECD/NEA/CSNI/R(91)8, 1991.

[70] NEA. Progress Made in the Last Fifteen Years through Analyses of the TMI-2 Accident Performed in Member Countries. OECD/NEA/CSNI/R(2005)1, 2005.

[71] NEA Databank. CSNI Code Validation Matrix (CCVM), INTEGRAL TEST DATA. Nuclear Energy Agency. 2010. URL: https://www.oecd-nea.org/dbcps/ccvm/index.html.

[72] NEA Databank. CSNI Code Validation Matrix (CCVM), SEPARATE EFFECTS TEST DATA. Nuclear Energy Agency. 2015. URL: https://www.oecd-nea.org/dbcps/ccvm/indexset.html.

[73] NEA/CSNI. Thermohydraulics of Emergency Core Cooling in Light Water Reactors-A State of the Art Report. Paris, France: OECD/CSNI 161, 1989.

[74] NEA/CSNI. CSNI Integral Test Facility Validation Matrix For The Assessment Of Thermal-Hydraulic Codes For LWR LOCA and Transients. Paris, France: NEA/CSNI/R(96)17, 1996.

[75] I. Novozhilov. Fractional Analysis – Methods of Motion Decomposition. Birkhauser Publisher. Boston USA, 1997. URL: https://doi.org/10.1007/978-1-4612-4130-0.

[76] OECD/NEA. Final Integration Report of the OECD/NEA ROSA Project 2005-2009. 2013.

[77] OECD/NEA. Phenomena Identification and Ranking Table: R&D Priorities for Loss-of-Cooling and Loss-of-Coolant Accidents in Spent Nuclear Fuel Pools. OECD, 2018. DOI: 10.1787/6def40c2-en.

[78] OECD/NEA. The International Experimental Thermal HYdraulics Systems Database. TIETHYS. 2022. URL: https://www.oecd-nea.org/tiethysweb/.

[79] Y. Park, B.-U. Bae, J.-R. Kim, S. Cho, K.-H. Kang, and K.-Y. Choi. "Counterpart Test for LSTF 1% Cold-Leg Break LOCA (SB-CL-32) Utilizing ATLAS Test Facility". In: Nuclear Engineering and Design 370 (Dec. 2020), p. 110912. ISSN: 00295493. DOI: 10.1016/j.nucengdes.2020.110912.

[80] P. F. Peterson, V. E. Schrock, and R. Greif. "Scaling for Integral Simulation of Mixing in Large, Stratified Volumes". In: Nuclear Engineering and Design 186 (1998), pp. 213–224. DOI: 10.1016/S0029-5493(98)00223-4.

[81] R. Préa, P. Fillion, L. Matteo, G. Mauger, and A. Mekkas. "CATHARE-3 V2.1: The New Industrial Version of the CATHARE Code". In: Advances in Thermal Hydraulics (2020), p. 13. DOI: https://dx.doi.org/10.13182/ATH2020-31587.

[82] A. Prošek and O.-A. Berar. "Advanced Presentation of BETHSY 6.2TC Test Results Calculated by RELAP5 and TRACE". In: Science and Technology of Nuclear Installations 2012 (2012), pp. 1–15. ISSN: 1687-6075, 1687-6083. DOI: 10.1155/2012/812130.

[83] D. L. Reeder. LOFT System and Test Description (5.5-Ft Nuclear Core 1 LOCES). NUREG/CR-0247 (TRBE-1208). Idaho Falls (USA): USRNC, 1978.

[84] J. N. Reyes. "The Dynamical System Scaling Methodology". In: NURETH-16. 2015.

[85] J. N. Reyes and C. Frepoli. "The Dynamical System Scaling Methodology Compararing Dimensionless Governing Equations with the H2TS and FSA Methodologies". In: NURETH-16. 2015, p. 15.

[86] J. N. Reyes and L. Hochreiter. "Scaling Analysis for the OSU AP600 Test Facility (APEX)". In: Nuclear Engineering and Design 186.1-2 (Nov. 1998), pp. 53–109. ISSN: 00295493. DOI: 10.1016/S0029-5493(98)00218-0.

[87] M. Shockling, C. Frepoli, and K. Ohkawa. "Calculating LOCA System Effects". In: Nuclear Engineering International 57(670) (2012), pp. 24–28.

[88] H. A. Simon. "The Architecture of Complexity". In: Proceedings of the American Philosophical Society 106 (1962).

[89] C.-H. Song. "Scaling of Multi-Dimensional Thermal-Hydraulic Phenomena in Advanced Nuclear Reactor Systems". In: Fifth Korea-Japan Symposium on Nuclear Thermal Hydraulics and Safety (NTHAS5). Jeju, Korea, 2006.

[90] The ROSA-V Group. ROSA-IV Large Scale Test Facility (LSTF) System Description. Tokai-Mura, Japan: JAERI-M 84237, 1985.

[91] The ROSA-V Group. ROSA-V Large Scale Test Facility (LSTF) System For The Third And Fourth Simulated Fuel Assemblies. Tokai-Mura, Japan: JAERI-Tech 2003-037, 2003.

[92] K. Umminger, L. Dennhardt, S. Schollenberger, and B. Schoen. "Integral Test Facility PKL: Experimental PWR Accident Investigation". In: Science and Technology of Nuclear Installations 2012 (2012), pp. 1–16. ISSN: 1687-6075, 1687-6083. DOI: 10.1155/2012/891056.

[93] USNRC. Quantifying Reactor Safety Margins: Application of CSAU to a LBLOCA. Washington, USA: NUREG/CR-5249, 1989.

[94] USNRC. Combined License Applications for Nuclear Power Plants. Regulatory Guide 1.206, 1997.

[95] USNRC. Review of Analytical Computer Codes, of NUREG-0800, "Standard Review Plan for the Review of Safety Analysis Reports for Nuclear Power Plants, Washington, USA: USNRC, 2000.

[96] USNRC. Transient and Accident Analysis Methods. Washington, USA: RG 1.203, USNRC, 2005.

[97] USNRC. A Phenomena Identification and Ranking Table (PIRT) Exercise for Nuclear Power Plant Fire Modeling Applications. NUREG/CR-6978, 2008.

[98] G. B. Wallis. One-Dimensional Two-Phase Flow. New York, USA, 1969.

[99] G. E. Wilson and B. E. Boyack. CSAU (Code Scaling, Applicability and Uncertainty), a Tool to Prioritize Advanced Reactor Research. USNRC, 1990.

[100] G. E. Wilson and B. E. Boyack. "The Role of the PIRT Process in Experiments, Code Development and Code Applications Associated with Reactor Safety Analysis". In: Nuclear Engineering and Design 186.1-2 (Nov. 1998), pp. 23–37. ISSN: 00295493. DOI: 10.1016/S0029-5493(98)00216-7.

[101] W. Wulff. "Scaling of Thermohydraulic Systems". In: Nuclear Engineering and Design (1996), p. 37.

[102] W. Wulff and U. S. Rohatgi. "System Scaling for the Westinghouse AP600 Pressurized Water Reactor and Related Test Facilities Analysis and Results". In: NUREG/CR-5541, BNL-NUREG-52550. Washington, USA, 1999.

[103] W. Wulff, N. Zuber, U. S Rohatgi, and I. Catton. "Application of Fractional Scaling Analysis (FSA) to Loss of Coolant Accidents (LOCA) Part 2. System Level Scaling for System Depressurization". In: NURETH-11. 2005, p. 21.

[104] W. Wulff, N. Zuber, U. S. Rohatgi, and I. Catton. "Application of Fractional Scaling Analysis to Loss of Coolant Accidents, System Level Scaling for System Depressurization". In: Journal of Fluids Engineering 131.8 (2009), p. 081402. ISSN: 0098-2202, 1528-901X. DOI: 10.1115/1.3155994.

[105] L. J. Ybarrondo, S. Fabic, P. Griffith, and G. D. McPherson. Examination of LOFT Scaling. New York, USA: 74-WA/HT53, 95th Winter Annual Meeting of the ASME, 1974.

[106] B. J. Yun, H. K. Cho, D. J. Euh, C.-H. Song, and G. C. Park. "Scaling for the ECC Bypass Phenomena during the LBLOCA Reflood Phase". In: Nuclear Engineering and Design 231 (2004).

[107] J. P. Yurko, C. Frepoli, and J. N. Reyes. "Demonstration of Test Facility Design Optimization with the Dynamical System Scaling Methodology". In: NURETH-16. 2015, p. 17.

[108] N. Zuber. "A Hierarchical, Two-tiered Scaling Analysis, Appendix D of An Integrated Structure and Scaling Methodology for Severe Accident Technical Issue Resolution". In: NUREG/CR-5809. 1991, p. 688.

[109] N. Zuber. "The Effects of Complexity, of Simplicity and of Scaling in Thermal-Hydraulics". In: Nuclear Engineering and Design (2001).

[110] N. Zuber. Scaling a Nuclear Power Plant as a Complex System. Rockville, USA: Nuclear Energy for New Europe, 2005.

[111] N. Zuber and J. A. Findlay. "Average Volumetric Concentration in Two-Phase Flow Systems". In: Journal of Heat Transfer (1965), pp. 453–468. DOI: 10.1115/1.3689137.

[112] N. Zuber, U. S. Rohatgi, W. Wulff, and I. Catton. "Application of Fractional Scaling Analysis (FSA) to Loss of Coolant Accidents (LOCA)". In: Nuclear Engineering and Design 237.15-17 (2007), pp. 1593–1607. ISSN: 00295493. DOI: 10.1016/j.nucengdes.2007.01.017.

[113] N. Zuber, G. E. Wilson, M. Ishii, W. Wulff, B. E. Boyack, A. E. Dukler, P. Griffith, J. M. Healzer, R. E. Henry, J. R. Lehner, S. Levy, F. J. Moody, M. Pilch, B. R. Sehgal, B. W. Spencer, T. G. Theofanous, and J. Valente. "An Integrated Structure and Scaling Methodology for Severe Accident Technical Issue Resolution: Development of Methodology". In: Nuclear Engineering and Design 186.1-2 (1998), pp. 1–21. ISSN: 00295493. DOI: 10.1016/S0029-5493(98)00215-5.

Appendices

A. Code Scaling and Applicability and Uncertainty (CSAU)

Reference: Wilson et al. 1990

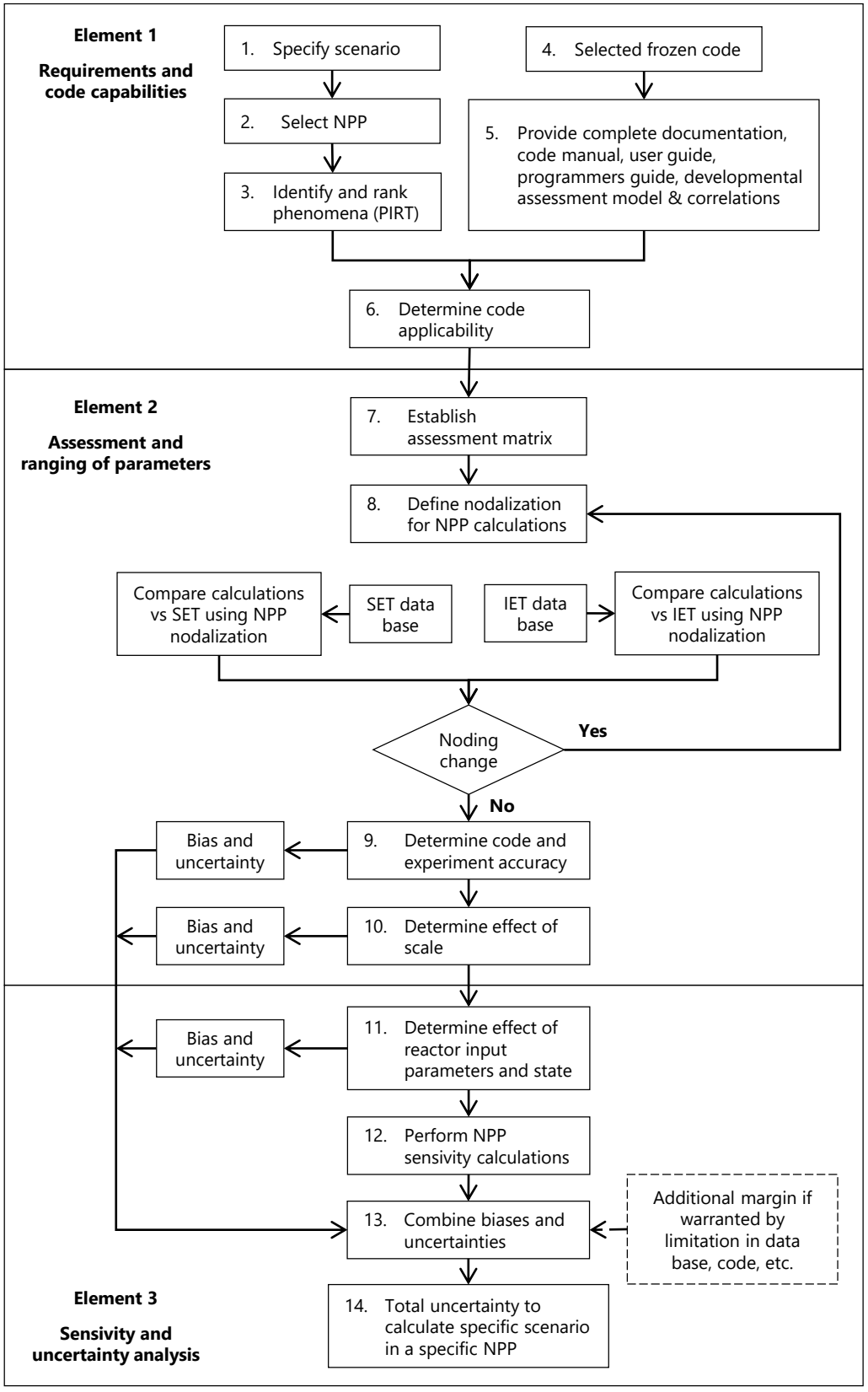

B. The Phenomena Identification and Ranking Table (PIRT)

Reference: D'Auria et al. 2017

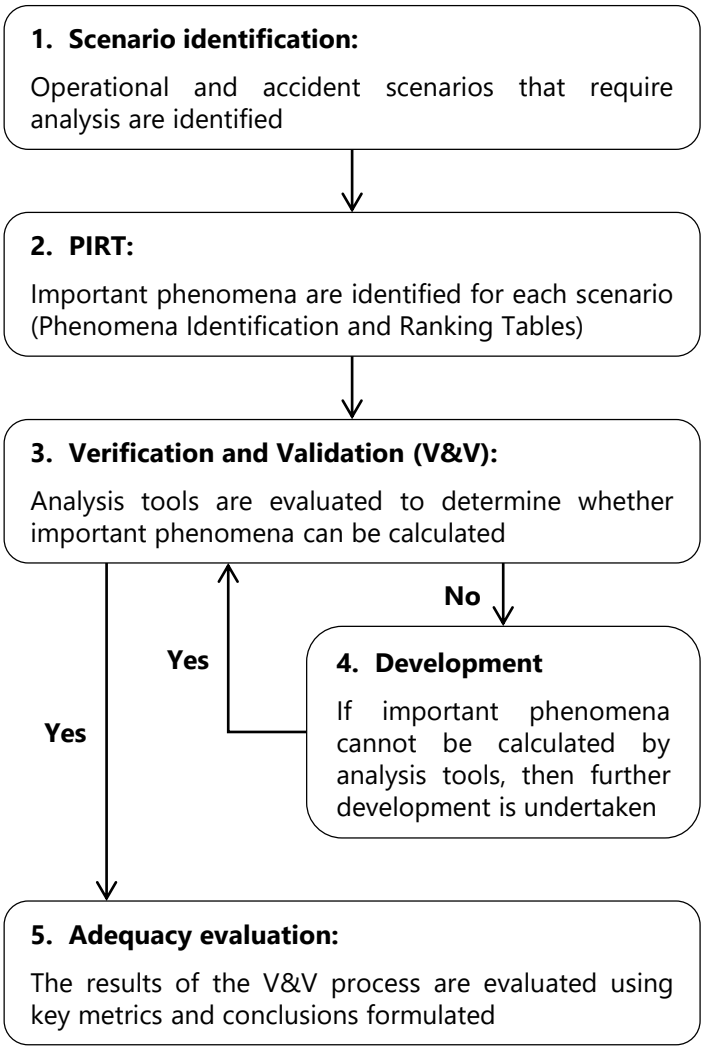

C. The Evaluation Model Development and Assessment Procedure (EMDAP)

Reference: USNRC 2005

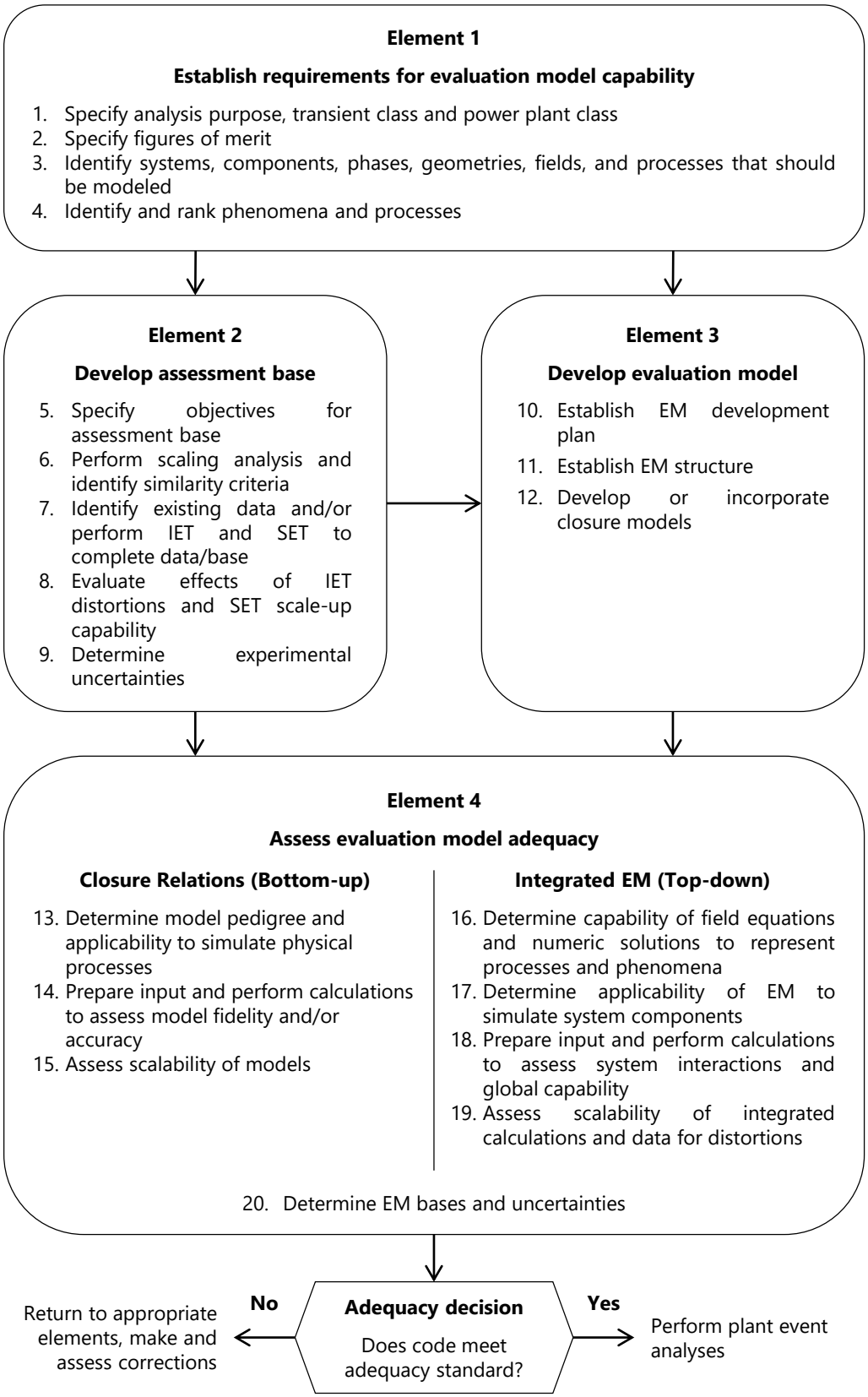

D. Organisations Represented in the International Panel of Experts

Reference: OECD/NEA 2018

Country/organisation	Participating organisations
Belgium	BEL V
Canada	CNL, CNSC
Czech Republic	UJV
European Commission	JRC
France	CEA, EDF, IRSN
Germany	GRS
Hungary	MTA-EK
Italy	NINE
Japan	IAE, JAEA, MNF, S/NRA/R*
Republic of Korea	KAERI
Russian Federation	NRCKI
Slovenia	JSI
Spain	CIEMAT, CSN
Sweden	QT
Switzerland	PSI
USA	U.S. NRC

* As for Japan, experts are selected from researcher organisations (JAEA, CRIEPI, IAE), PWR vendors (MHI, MNF), BWR vendors (Hitachi-GE, TOSHIBA, GNFJ) and regulatory body (S/NRA/R). JAEA, MNF, IAE and S/NRA/R are representatives of those organisations.

E. Considerations on Transients Phases Establishment

As discussed in step 2 of section 3.3.2.2, determining bifurcating events and identifying the temporal phases are decisive in the context of accidental transient studies coupled with scaling analyses.

Historically, expert judgements were used to select these bifurcating events from experimental results. Phenomenological considerations guided the division of these phases and the duration of each. For Small-Break Loss Of Coolant Accident (SB-LOCA) transients for example, the primary pressure evolution results showed the presence of three distinct regions with a first violent depressurization, a pressure plateau, and a second depressurization (Bestion et al. 2017). These variations in primary pressure were then linked to specific thermal-hydraulic phenomena that justified the phase splitting.

Other authors have also conducted studies that divide transients into four or five phases (Muñoz-Cobo et al. 2018). Their bifurcating events are caused by changes in system behaviour. This demonstrates that the study of a transient can be influenced by the user and the division of these phases.

Another way to define bifurcating events, particularly for uncertainty studies, have been identified. These points correspond to the safety system's triggering parameters (D'Auria et al. 2000). This method of identifying parameter values that trigger system actuation ensures that the reactor is in a well-known configuration (the triggers of safety systems being based on fixed pressure values).

Codes can now predict the behaviour of transients (Bestion et al. 2017). Although the reliability of the predictions remains questionable, they allow for the identification of phenomena, and thus of bifurcating events, which can lead to the selection of more accurate phases. Work to identify these phenomena may also help in scaling analysis, whether for the design of IET and SET for code validation or for a posteriori scaling studies (Bestion et al. 2022). Advanced scaling analyses then rely on code predictions to identify the bifurcating events that determine the different phases of the transients (Liao 2016; Muñoz-Cobo et al. 2018; Dzodzo et al. 2019; Lorduy-Alós et al. 2020), such as those performed in chapters 5 and 6 of the present manuscript. These studies also demonstrated that system codes could be used to support scaling studies by calculating the variables required to solve the conservation equations used with scaling methods such as Hierarchical Two-Tiered Scaling (H2TS) or Fractional Scaling Analysis (FSA).

Figure E.1 depicts the current approaches in the definition of the phases to evaluate the scaling criteria:

- Either calculated at specific times with safety trigger points with experimental results (see Figure E.1a).
- Or more recently, with averaged calculation during phases allowed with the support of the codes predictions (see Figure E.1b) as performed in chapters 5 and 6.

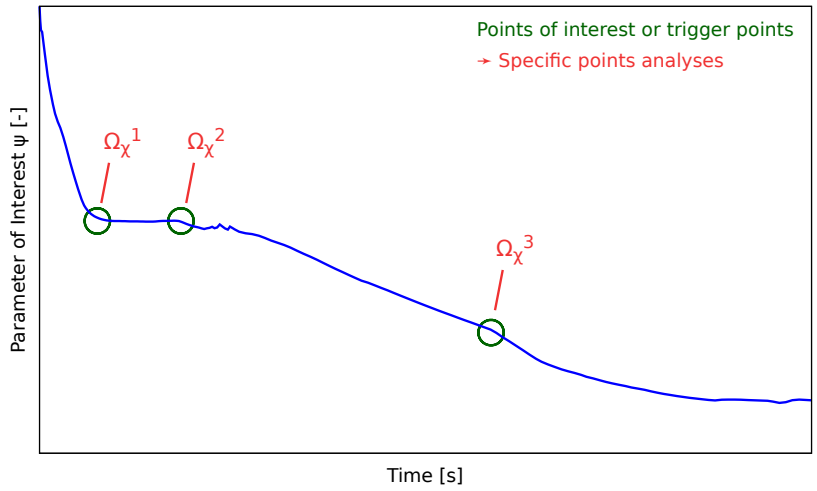

(a) Without code support

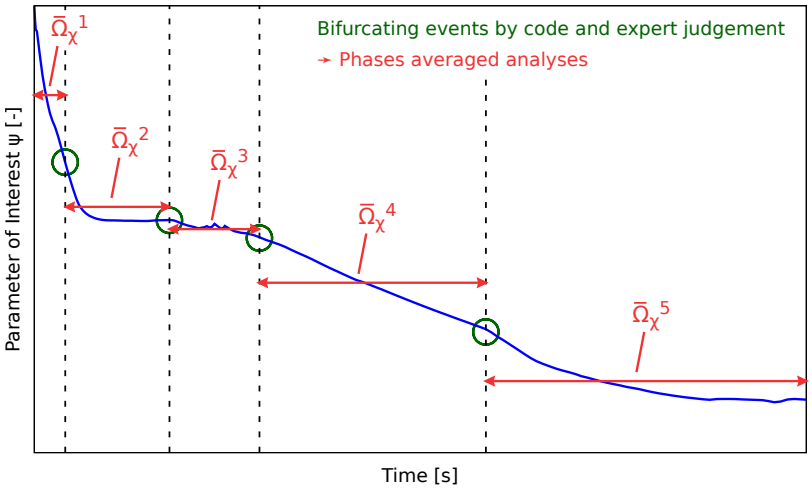

(b) With code support

Figure E.1: Current approaches in the evaluation of scaling criteria

F. CATHARE Code Strategy for Development VV&Q

Reference: Bestion et al. 1999

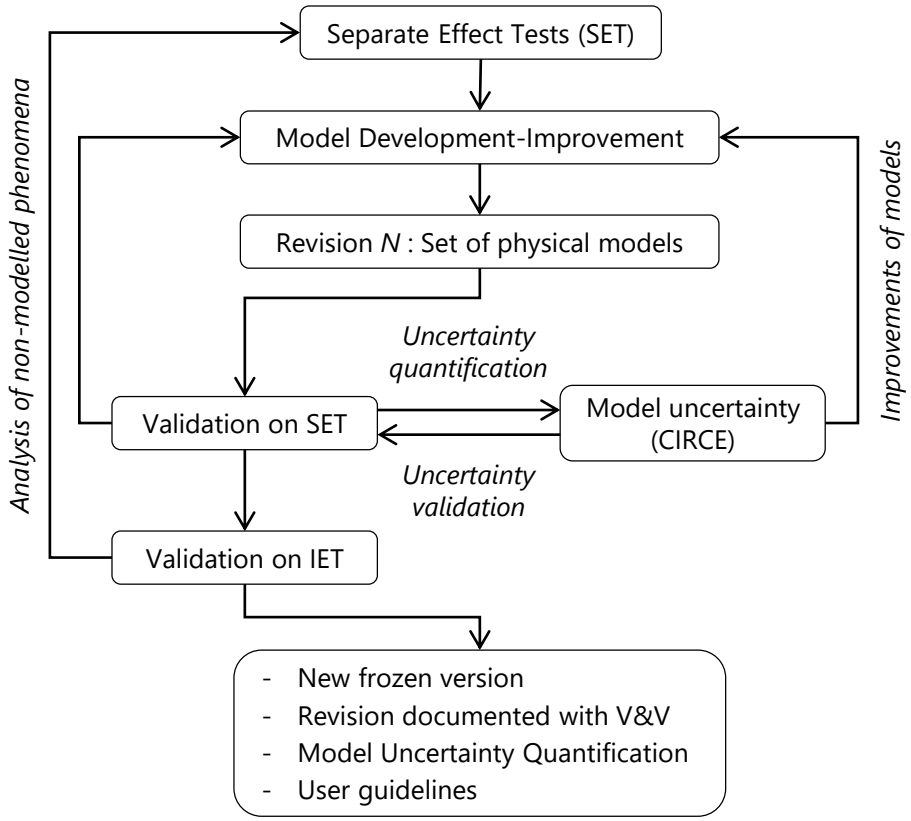

G. Validation of the Pressure by VRC Equation

A verification of the equation resolution is performed on the pressurizer results in order to validate the general pressure by VRC equation. For this purpose, an instantaneous calculation of the l.h.s terms of the Eq. 6.2 are compared to the r.h.s terms. As explained in section 6.3.2, the VRC corresponding to fluid isentropic expansion/contraction is equal to the sum of the depressurization/pressurization contributing terms. This yieds Eq. G.1 with the sum of the contributing terms to the pressure change by VRC Q_n.

$$K_{prz} \cdot \dot{P}_{prz} = \sum Q_{n,prz} \tag{G.1}$$

Figure G.1 shows the evolution of the l.h.s and r.h.s terms of Eq. G.1 applied to the pressurizer control volumes of the BETHSY 6.2-TC, LSTF SB-CL-21 and PWR 900-SBL tests.

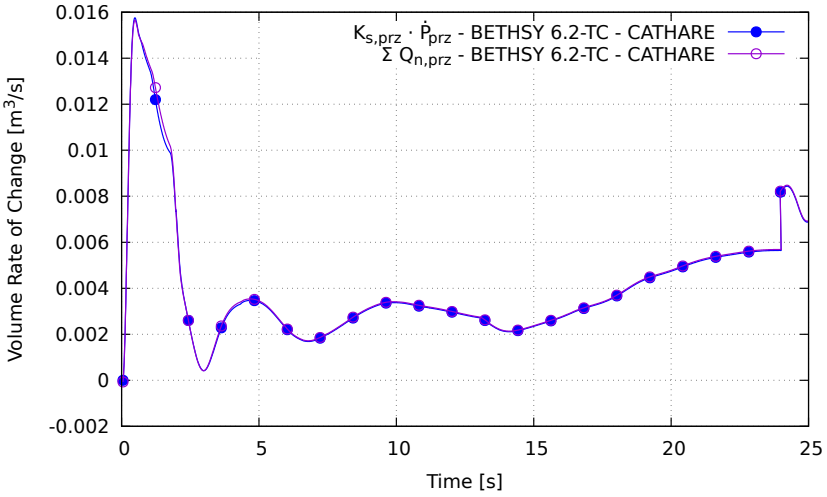

(a) BETHSY 6.2-TC pressurizer equation

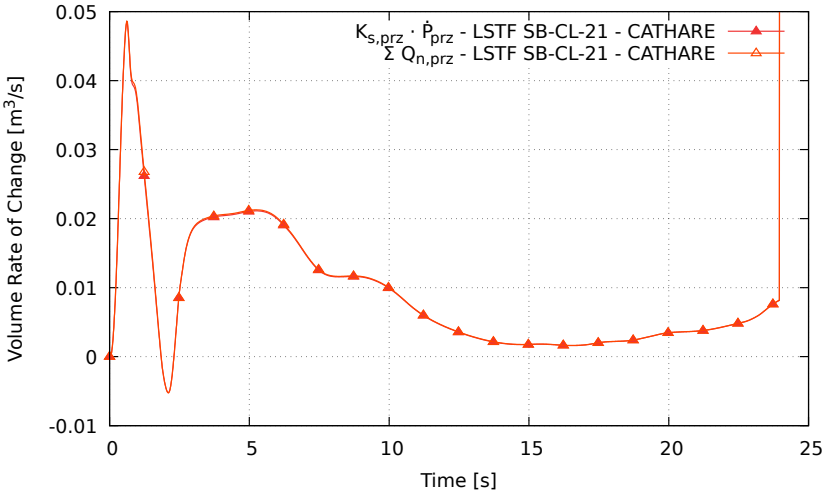

(b) LSTF SB-CL-21 pressurizer equation

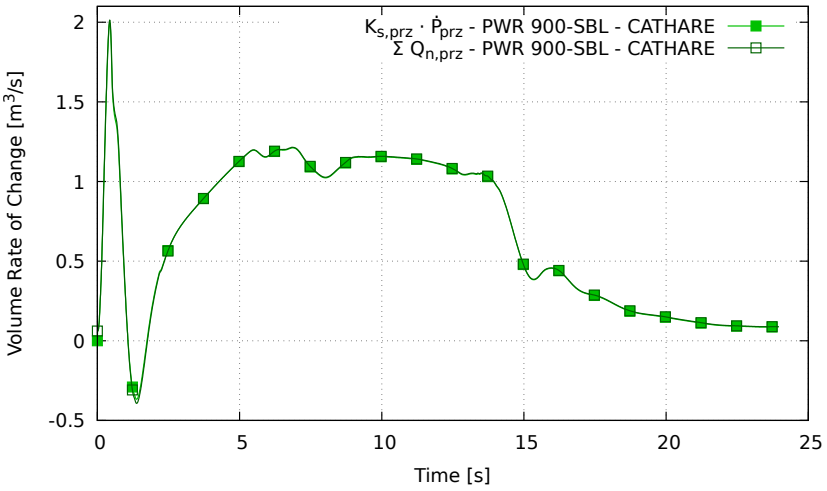

(c) PWR 900-SBL pressurizer equation

Figure G.1: Validation of the pressure by VRC equation applied to the pressurizer control volume - CATHARE predictions

As the two curves merge for the three transients, the pressure by VRC is equal to the sum of the depressurization/pressurization contributing terms. This analysis demonstrates the validation of the pressure by VRC equation, and can thus be extrapolated to the whole primary system control volume.

It can be noted on Figure G.1c the relative higher depressurization of the PWR (here in positive value) compared to the facilities, which is also observed on the resulting primary pressure in Figure 6.13a.

H. Impact of the BETHSY Secondary Pressure Adjustment

The 6.2-TC and SB-CL-21 tests were respectively performed on BETHSY and LSTF facilities. The designers intended to keep the FHFP criteria for these ITF. The two tests were thus intended to be studied alongside, between France and Japan. However, BETHSY is based on a 900 MWe reference reactor (three loops PWR), whereas LSTF is based on a 1100 MWe reactor design (four loops PWR). Some parameters, depending on the type of reference reactor, had to be revised in order to maintain some comparability between the BETHSY and LSTF tests. This is especially true for the BETHSY secondary system pressure, which had to be increased from 5.78 MPa to 6.85 MPa in order to match LSTF.

A CATHARE simulation is performed by adjusting the secondary pressure of BETHSY to that of its reference PWR at 5.78 MPa. Figure H.1 depicts the distortion caused on the BETHSY primary pressure. Figure H.2 depicts the distortion caused on pressurizer emptying. It is then found that changing the secondary pressure for BETHSY has a direct effect on the transposition of the results with its reference PWR.

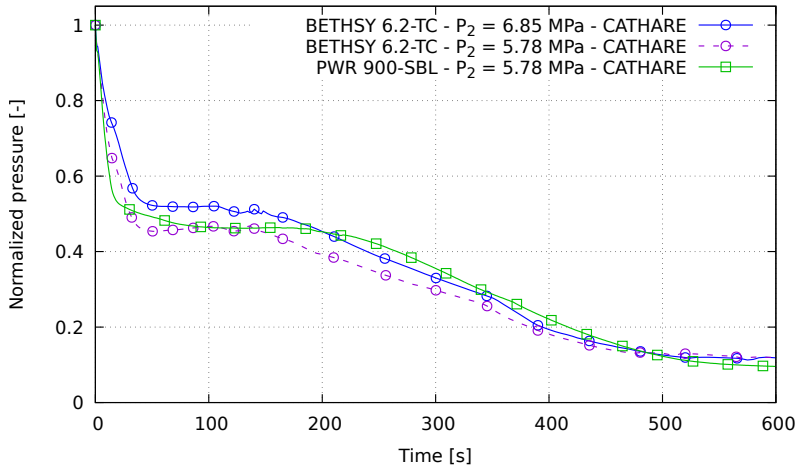

(a) CATHARE results on the global transient

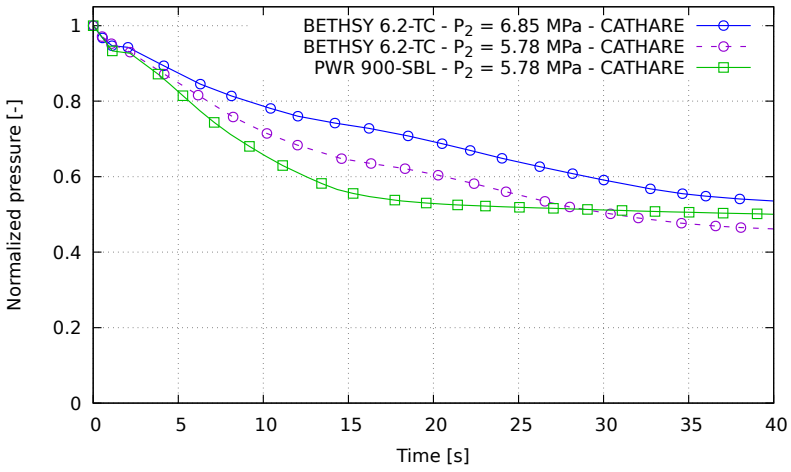

(b) CATHARE results on the SBD phase

Figure H.1: Comparison of the primary pressure on the BETHSY 6.2-TC and the PWR 900-SBL tests

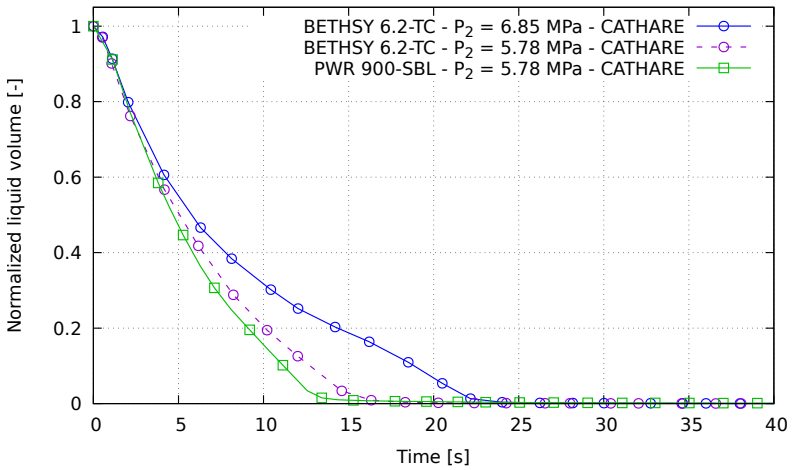

Figure H.2: Comparison of the pressurizer liquid volume on the BETHSY 6.2-TC and the PWR 900-SBL tests

Résumé en Français

Titre : Nouveaux développements d'une méthodologie d'analyse d'échelle pour des transitoires complexes de thermohydraulique de réacteurs nucléaires avec calcul de la distorsion associée à la transposition d'échelle.

Contexte

En France, le nucléaire est la première source de production et de consommation d'électricité. Avec une capacité 61,4 GWe fournie par 56 réacteurs à eau pressurisée, le parc nucléaire français est le deuxième plus important au monde, derrière celui des États-Unis. L'industrie nucléaire porte ainsi un intérêt particulier à l'étude du comportement des réacteurs, en situation nominale comme en situation accidentelle.

De par la complexité et le coût que représenteraient la mise en œuvre d'installations à échelle réelle pour l'analyse d'accidents nucléaires contrôlés, l'industrie nucléaire se dote de réacteurs expérimentaux à échelle réduite. Ces équipements sont privilégiés pour étudier les comportements en régime accidentel (également appelé transitoire) et permettent d'obtenir de précieuses données qui peuvent alimenter des codes de calculs. C'est finalement au travers de ces codes de calculs que sont simulés les hypothétiques accidents qui auraient lieu à échelle réelle : c'est la transposition d'échelle. Toutefois, la représentativité des résultats des expériences à échelle réduite par rapport à un réacteur réel est une question cruciale. Il est ainsi nécessaire de disposer d'une méthodologie qui permette l'évaluation de cette représentativité et de potentielles distorsions entraînées par la réduction d'échelle (« scaling down ») lors de la conception des réacteurs expérimentaux.

État de l'art et problématiques

Des méthodes destinées aux « analyses de scaling » ont été développées afin d'identifier et quantifier ces distorsions. Elles reposent notamment sur des analyses de nombres adimensionnalisés basés sur des équations de conservation. Les méthodes permettant l'obtention de ces nombres adimensionnalisés s'inspirent ainsi des exigences du PIRT (Process Identification and Ranking Table) qui vise à hiérarchiser les phénomènes d'intérêt au cours des transitoires nucléaires. Finalement, ces méthodes de scaling exploitent les concepts d'approche « top-down » et d'approche « bottom-up » qui consistent à diviser un système complexe en sous-systèmes plus simples à étudier.

Cependant, ces méthodes restent théoriques et ont peu été appliquées à des cas concrets. Ainsi, des améliorations voire des réinterprétations de ces méthodes sont nécessaires afin de les employer, en particulier avec le support des codes de calculs. C'est l'objectif principal de la thèse : développer une méthodologie d'analyse de scaling pour l'étude des comportements des transitoires nucléaires. Elle doit clarifier les potentialités de ces méthodes et comprendre comment elles peuvent contribuer aux études existantes. Afin de rendre cette méthodologie applicable par l'industrie nucléaire, des lignes directrices doivent également être établies.

Ainsi, ce manuscrit vise à répondre à un certain nombre de questions et problématiques soulevées par un état de l'art du scaling et des méthodes existantes :

- **Comment les analyses de scaling peuvent aider dans la compréhension phénoménologique des transitoires complexes ?** Et dans quelle mesure interviennent les approches top-down et bottom-up pour l'établissement d'un PIRT structuré ?

- **Comment les méthodes de scaling peuvent permettre l'identification et la quantification de distorsions inter-systèmes (i.e. entre un réacteur de référence et un réacteur à échelle réduite) ?** La pertinence de cette question découle de la nécessité d'évaluer l'impact des choix de conception des expériences à échelle réduite et des résultats des transitoires par rapport à ce qui est prédit par les codes pour les réacteurs à échelle réelle.
- **Comment les méthodes de scaling avancées peuvent-elles être utilisées en support des codes de calculs ?** Il s'agit d'une problématique importante, étant donné que les méthodes de scaling n'ont pas été initialement conçues à cette fin.
- **Quelles sont les limites actuelles des analyses et méthodes de scaling pour l'étude des transitoires nucléaires ?** Des suggestions d'améliorations et de perspectives sont proposées au travers des études présentées dans ce manuscrit.

Pour répondre à ces problématiques, la thèse est composée de trois parties. Dans la première partie, un état de l'art présente le contexte dans lequel les travaux de ce manuscrit interviennent. Cet état de l'art propose un aperçu général de la thermohydraulique nucléaire et de la contribution des codes calculs à ce domaine d'ingénierie et de recherche. L'état actuel des connaissances concernant les problématiques et préoccupations techniques liées au domaine du scaling est décrit, notamment au travers d'une présentation des méthodes existantes. Une brève présentation du code de calcul à l'échelle système CATHARE est également réalisée (Emonot et al. 2011).

Synthèse des résultats

La deuxième partie de la thèse consiste en deux chapitres d'études et d'analyses destinées au développement de la méthodologie de scaling :

- Une approche comparative de deux méthodes de scaling avancées est réalisée. L'objectif est de fournir une introduction et une base à la méthodologie au travers l'étude de l'applicabilité de la méthode de « Fractional Scaling Analysis » (FSA) (Wulff et al. 2005; Catton et al. 2005; Zuber et al. 2007) à un transitoire d'Accident de Perte de Réfrigérant Primaire (APRP) Petite Brèche (PB). Une analyse de scaling a posteriori est réalisée sur deux phases temporelles du test LSTF ROSA 1.2 (The ROSA-V Group 2003) : - la phase de « Subcooled Blowdown » et de - « High-Quality Mixture Discharge ». Des équations de masse et de pression par changement de volume à saturation sont établies pour les volumes du système primaire et du pressuriseur. Des prédictions du code CATHARE sont utilisées afin de résoudre les équations bilans et obtenir des « scaling criteria ». La méthode FSA, son application et ses résultats sont comparés à des travaux similaires réalisés avec la méthode de « Hierarchical Two-Tiered Scaling » (H2TS) par un autre groupe de recherche (Muñoz-Cobo et al. 2018).

  Cette étude comparative a révélé une cohérence entre les résultats obtenus avec les méthodes FSA et H2TS. Ce travail démontre de plus l'applicabilité d'une méthode de scaling avancée utilisée avec le support d'un code système. La résolution des équations, réalisée par estimation des termes moyennés au travers de chaque phase plutôt que calculés à leurs limites, est une amélioration permise par le code qui fournit davantage de précision dans l'évaluation des scaling criteria. Il est également démontré que les méthodes de scaling peuvent contribuer à l'amélioration de la modélisation du code.

- La capacité de la méthode FSA à identifier et quantifier des distorsions sur un transitoire d'APRP-PB à l'échelle système/composant est ensuite investiguée. Pour cela, la phénoménologie et le scaling a posteriori d'un test comparatif d'APRP-PB est revisité

(Kumamaru et al. 1992; D'Auria et al. 1992). La méthode FSA est appliquée aux tests expérimentaux BETHSY 6.2-TC et LSTF SB-CL-21 ainsi qu'à une simulation d'un réacteur à échelle réelle. L'analyse de scaling est réalisée sur cinq phases temporelles : les phases - de « Subcooled Blowdown », - de « Natural Circulation », - de « Reflux Condenser Mode », - de « High-Quality Mixture Discharge » et - de « Reactor Refilling ». Des équations de masse et de pression par changement de volume sont établies pour les volumes des systèmes primaires et des pressuriseurs du test comparatif.

En utilisant les prédictions du code CATHARE, l'analyse de scaling et l'étude des évolutions et des différences entre les scaling criteria des trois systèmes mettent en évidence des distorsions ainsi que leurs origines. Cette étude souligne des différences de comportement entre les tests à échelle réduite et le réacteur à échelle réelle. Des améliorations sont apportées à la méthodologie développée. La formulation d'une équation de pression par changement de volume générale sans hypothèse de saturation permet une analyse beaucoup plus détaillée et augmente la confiance dans les résultats des scaling criteria. Cette application démontre une hiérarchie détaillée de l'influence des phénomènes et procédés des différentes phases du transitoire. Afin d'analyser correctement les scaling criteria, un intérêt particulier est porté à la réalisation d'une analyse phénoménologique en parallèle des analyses de scaling.

Conclusions et perspectives

Dans la troisième partie de la thèse, la méthodologie d'analyse de scaling pour l'étude des distorsions dans le cadre des transitoires nucléaires développée au cours de la thèse est présentée dans son intégralité. Des conclusions sont tirées des deux études réalisées ainsi qu'au travers d'un bilan des réinterprétations et améliorations de la méthodologie initiale. Des réponses aux problématiques et aux objectifs évoqués en introduction sont fournies :

- **Les analyses de scaling aident à la compréhension de la phénoménologie des transitoires grâce à l'utilisation des méthodes de scaling avancées.** Les études de phénomènes complexes qui ont lieu lors de transitoires tels que des APRP peuvent être assistées par l'utilisation de ces méthodes. Il est démontré que les analyses phénoménologiques réalisées en amont des analyses de scaling peuvent contribuer à la détermination des paramètres clés nécessaires à leur application. Ces analyses phénoménologiques justifient ainsi la définition et l'étude des « Figures of Merit » et des « Parameters of Interest ».

- **La division des transitoires en phases temporelles permet de réaliser des analyses de scaling structurées.** Il est ainsi essentiel de sélectionner correctement les « bifurcating events », en fonction des changements de comportements des systèmes étudiés.

- **Les concepts d'approches top-down et bottom-up apportent cohérence et structure dans l'analyse des phénomènes importants identifiés par les analyses de scaling.** Les applications réalisées ainsi que la méthodologie développée dans ce manuscrit mettent l'accent sur les étapes à suivre afin de réaliser des analyses de scaling efficaces. Ces approches devraient être considérées, en particulier pour des analyses multi-échelles.

- **Le concept de normalisation des scaling criteria, basé sur l'établissement d'équations bilan est une contribution importante des méthodes de scaling avancées, telle que la méthode FSA.** La quantification de la magnitude (valeur normalisée) relative des scaling criteria permet de considérer l'importance des phénomènes en terme de causalité. Combinée aux approches top-down et bottom-up, la FSA permet d'établir une hiérarchie

claire des procédés d'importance. Cette évaluation quantitative de chaque phénomène permet l'établissement d'un PIRT structuré.

- **Des modifications et des améliorations ont été apportées à la méthode FSA au travers de réinterprétations et du développement de la méthodologie présentée dans ce manuscrit.** Les applications réalisées dans ce manuscrit illustrent l'intention des concepteurs des méthodes de scaling avancées d'en faire des outils flexibles et adaptables. Les paramètres des analyses de scaling peuvent être adaptés pour répondre à des exigences spécifiques, par exemple en sélectionnant et en formulant des équations bilan et des hypothèses, en les appliquant à différences physiques de transitoires (au travers de différentes phases temporelles) et en identifiant les systèmes et composants auxquels les appliquer.

- **Les analyses de scaling a posteriori permettent d'identifier et de quantifier des distorsions inter-systèmes.** Cela est observé dans ce manuscrit par l'étude d'un test comparatif basé sur l'étude d'un même transitoire. La transposition d'échelle peut être évaluée en comparant les scaling criteria (et donc les PIRT respectifs) des différents systèmes de l'étude. L'intérêt est particulièrement démontré par l'étude d'un test comparatif mêlant différentes conceptions d'installations expérimentales. La comparaison d'installations à échelle réduite et de réacteurs de référence à échelle réelle présente un intérêt particulier dans ce type d'application. Ainsi, les distorsions ou différences potentielles entre les systèmes peuvent être évaluées. Ces écarts peuvent être attribuées à des différences de conception, à des déficiences du code ou à des effets d'échelle.

- **Les méthodes de scaling avancées peuvent être appliquées avec le support des codes de calcul ayant atteint un niveau raisonnable de confiance.** Le code CATHARE a été utilisé afin de réaliser des analyses de scaling, grâce à la confiance accordée dans ses prédictions à l'échelle système/composant. Lorsque des faiblesses dans les capacités prédictives du code pour certains phénomènes sont identifiées, les analyses de scaling menées sur ces phénomènes doivent être utilisées avec prudence.

- **L'utilisation du code permet la résolution des équations (en particulier l'équation de pression générale) et l'établissement des scaling criteria de manière très détaillée.** Le code permet également d'évaluer les termes des équations moyennés à chaque pas de temps du calcul, ce qui conduit en une plus grande précision dans les résultats des analyses de scaling.

- **La possibilité de suivre la valeur de chaque terme des équations au cours du temps aide à identifier les bifurcating events et les procédés qui leur sont liés.** L'interprétation de la signification des scaling criteria est facilité par le support du code, grâce à l'analyse phénoménologique détaillée et réalisée en parallèle des analyses de scaling. Celle-ci établit un lien entre l'impact des phénomènes et procédés identifiés comme dominants/influents et le comportement des transitoires au travers des différentes phases temporelles étudiées. Grâce aux prédictions du code, ces phases sont définies de manière précise et justifiable.

- Au-delà de l'aide apportée par le code afin de réaliser des analyses de scaling, **il est possible d'utiliser ses résultats conjointement à des analyses de sensibilité et phénoménologiques afin de proposer des améliorations dans la modélisation du code.**

Certaines limites aux analyses de scaling et des méthodes de scaling avancées pour l'étude des transitoires nucléaires sont identifiées :

- **Un jugement d'expert est parfois requis lors de l'analyse des scaling criteria pour l'étude des phénomènes complexes des transitoires nucléaires.** Celà est dû aux nombreux phénomènes thermohydrauliques et aux aspects multi-physiques rencontrés dans l'étude des transitoires nucléaires. De plus, malgré les différentes phases temporelles identifiées au cours des transitoires, certaines distorsions peuvent se propager de phase en phase, rendant l'analyse des critères d'échelle plus difficile.

- **Le code devrait être entièrement validé sur des expériences représentatives pour effectuer des analyses de scaling fiables, tandis que et la conception d'expériences représentatives est nécessaire pour la validation du code.** Cela montre que les processus de conception des expériences et de validation du code sont quelque peu itératifs. Il est possible d'effectuer un design simplifié sans utiliser de code, puis concevoir les expériences, puis revoir l'analyse de scaling en utilisant les résultats expérimentaux, puis effectuer la validation du code. Lorsque le code ne parvient pas à prédire un phénomène spécifique, la modélisation doit être améliorée avant de l'utiliser pour les analyses de scaling. Enfin, on peut effectuer une analyse de scaling a posteriori en utilisant le code pour une identification et une quantification plus précises et plus fiables des distorsions.

Finalement, des perspectives d'améliorations et de potentielles utilisations de la méthodologie sont proposées :

- Une investigation de la capabilité de la méthode FSA à identifier et à quantifier des distorsions à l'échelle composant/locale devrait être réalisée. Pour cela, les phénomènes de création et de vidange de bouchons dans les branches intermédiaires du test comparatif d'APRP-PB seront étudiés. Grâce aux analyses réalisées au cours de la thèse, ces phénomènes ont été identifiés comme importants dans le comportement du transitoire. Cependant, ils restent mal prédits par le code. Ainsi, des analyses de scaling basées sur des résultats du code et sur des résultats expérimentaux devront permettent de mieux comprendre les procédés et paramètres associés à ces phénomènes.

- De futurs travaux devront conduire à l'établissement d'une équation de conservation de la quantité de mouvement qui sera appliqué à la méthode FSA. Cette équation sera ajoutée aux équations de masse et de pression par changement de volume et rendra la méthodologie d'analyse de scaling plus exhaustive.

- La méthodologie devrait être appliquée à d'autres cas d'études, tels qu'à divers tests comparatifs, d'autres types de transitoires, et différentes phénoménologies. La robustesse de la méthodologie pourra ainsi être confirmée et améliorée.

- Dans le cadre du code CATHARE, le développement d'un module de post-traitement pour l'application de la méthodologie d'analyse de scaling serait d'intérêt. Une fois que l'utilisateur aurait spécifié les paramètres d'analyse de scaling souhaités, ce module devrait permettre l'automatisation de l'application de la méthodologie, en particulier concernant le calcul des scaling criteria. Par exemple, l'utilisateur pourrait avoir à choisir l'échelle et les volumes de contrôle sur lesquels l'analyse devrait être effectuée, le type d'équations à utiliser et la division ou non du transitoire en phases temporelles. L'application de la méthodologie nécessiterait toujours un certain jugement d'expert, en particulier pour l'analyse des résultats et la compréhension de la phénoménologie des transitoires, ainsi que pour la recherche des sources de distorsion. Cependant, le domaine d'étude relatif aux problématiques de scaling pourrait être davantage popularisé grâce à ce module.

- L'état de l'art et les analyses de scaling réalisées dans ce manuscrit ont démontré des limites dans les méthodes utilisées dans la conception des installations expérimentales, quant à leur représentativité avec les réacteurs à échelle réelle. L'industrie nucléaire a aujourd'hui une plus grande confiance dans les codes de calcul qu'elle n'en avait lorsque les méthodes de conception d'expériences à échelle réduite ont été développées. Dû au coût non négligeable de la construction et de l'exploitation de ces installations, il semble essentiel d'envisager toute aide qui pourrait contribuer à réduire les distorsions liées à leur conception. Il est alors proposé de considérer la méthodologie a posteriori développée au cours de cette thèse, en soutien à la phase de conception a priori des installations expérimentales à échelle réduite.

université PARIS-SACLAY

ÉCOLE DOCTORALE
Sciences mécaniques et énergétiques, matériaux et géosciences (SMEMAG)

Titre: Nouveaux développements d'une méthodologie d'analyse d'échelle pour des transitoires complexes de thermohydraulique de réacteurs nucléaires avec calcul de la distorsion associée à la transposition d'échelle.

Mots clés: Analyses d'échelle, Transposition d'échelle, Thermohydraulique, Réacteurs nucléaires, Transitoires nucléaires, CATHARE

Résumé: Le coût et la complexité de la mise en œuvre et de la construction d'installations expérimentales à échelle réelle nous obligent à faire reposer les études sur des expériences à échelle réduite. Par conséquent les phénomènes, plus ou moins complexes, qui ont lieu à échelle réelle sont simulés par des codes de calculs validés par des expériences à échelle réduite. De ce fait, la question de la transposition de résultats d'une expérience à échelle réduite est un point crucial pour la validation des codes. Ceci est d'autant plus vrai que la physique en jeu est complexe. Il est donc indispensable de mettre au point une méthodologie d'analyse d'échelle : c'est l'objectif de la présente thèse. Un cas d'application typique de phénomènes complexes dépendant de l'échelle considérée est celui des situations accidentelles dans les réacteurs nucléaires.
La thèse vise à développer une méthodologie permettant l'identification et la quantification de distorsions entre des expériences à échelle réduite et des réacteurs à échelle réelle. Pour cela, la méthode de « Fractional Scaling Analysis (FSA) » est revisitée au travers de son application à des « Accidents de Perte de Réfrigérant Primaire (APRP) ». Les études présentées dans ce mémoire démontrent comment des analyses de scaling utilisant les concepts d'approches top-down et bottom-up, couplées au code de calcul CATHARE, peuvent contribuer dans la compréhension de la phénoménologie des transitoires nucléaires.

Title: New developments of a scaling analysis methodology for nuclear reactors complex thermal-hydraulic transients with calculation of the distortion associated with the full-scale transposition.

Keywords: Scaling analyses, Scale transposition, Thermal-hydraulic, Nuclear reactors, Nuclear transients, CATHARE

Abstract: The cost and complexity of implementing and constructing full-scale experimental facilities requires us to base the studies on small-scale experiments. Consequently, the more or less complex phenomena which take place on a real scale are simulated by computer codes validated by experiments on a reduced scale. Therefore, the question of transposing results of a small-scale experiment is a crucial point for the validation of codes. This is all the more true since the physics involved is complex. It is therefore essential to develop a scaling analysis methodology: this is the objective of this thesis. A typical application of complex phenomena depending on the scale under consideration is that of accidental situations in nuclear reactors.
The thesis aims to develop a methodology for identifying and quantifying distortions between reduced-scale facilities and full-scale reactors. For this purpose, the "Fractional Scaling Analysis (FSA)" method is revisited through its application to "Loss of Coolant Accidents (LOCA)". The studies presented in this thesis demonstrate how scaling analyses based on the top-down and bottom-up approaches, with the support of the CATHARE calculation code, can contribute in the understanding of nuclear transient phenomenology.